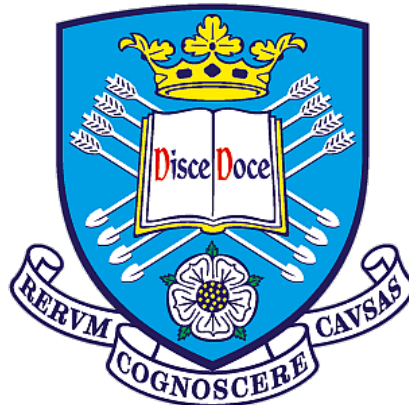# Detailed Characterisation and Comparison of the C9orf72 Bacterial Artificial Chromosome Mouse Model on Two FVB/N Lines

By

Sophie Elizabeth Badger

Sheffield Institute for Translational Neuroscience

University of Sheffield

Submitted for the degree of Doctor of Philosophy (PhD)

March 2023

Acknowledgements

"Have no fear of perfection; you'll never reach it."

– Marie Skłodowska–Curie

Abstract

Background: Amyotrophic lateral sclerosis (ALS) is a progressive and ultimately fatal neurodegenerative disease characterised by upper motor neurone loss in the brain and lower motor neurone loss in the spinal cord. The most common genetic cause is a hexanucleotide repeat expansion in the *C9ORF72* gene. Bacterial artificial chromosome transgenic mouse models of the expansion have been generated, yet only one reported decreased survival and progressive motor phenotypes. Subsequent reports of this model in several laboratories have revealed contradictory results regarding the nature of the phenotype. Determining the utility of the model is vital to advance preclinical studies investigating C9orf72 ALS.

Methods: Two colonies of transgenic C9orf72 mice were established. The first was generated with C9orf72 transgenic and FVB/N control animals from The Jackson Laboratory. The second colony was generated with C9orf72 transgenic mice donated from the University of Bern and FVB/N control animals from Janvier labs. Both colonies underwent an extensive range of behavioural and electrophysiological characterisations to assess survival, motor, and cognitive function up to 1 year of age. Immunohistochemical studies were also carried out.

Results: Over the course of 1 year, C9orf72 BAC mice displayed no discernible survival, motor, or cognitive abnormalities, despite production of dipeptide repeat proteins. Both transgenic and non-transgenic mice demonstrated a gradual decline over time in several behavioural/cognitive tests. No neurodegeneration was observed in the brain or spinal cord of either colony. The Janvier labs colony displayed possible neuronal abnormalities in the motor cortex revealed by Sholl analysis. Both colonies exhibited intermittent seizures consistent with previous reports of the FVB/N genetic background. Histopathology of mice seen to exhibit seizures demonstrated similar abnormalities to those reported in the initial report of this model.

Conclusions: Neither colony manifested a neurodegenerative phenotype attributable to the C9orf72 BAC insert. Background strain related abnormalities were observed. The data indicate that the model is not suitable for preclinical studies with the aim to measure phenotype.

Contents

List of Figures

List of Tables

List of Abbreviations

ALS	Amyotrophic lateral sclerosis
ALSFRS	ALS functional rating scale
ASO	Antisense oligonucleotide
BAC	Bacterial artificial chromosome
BOS	Base of support
C9orf72	Chromosome 9 open reading frame 72
CA	Cornu ammonis
CMAP	Compound muscle action potential
CNS	Central nervous system
CSF	Cerebrospinal fluid
DAPI	4',6-diamidino-2-phenylindole
DENN	Differentially expressed in normal cells and neoplasia
DG	Dentate gyrus
DIG	Digoxigenin
DPR	Dipeptide repeat protein
EMG	Electromyography
FDA	Food and drug administration
FTD	Frontotemporal dementia
FUS	Fused in sarcoma
FVB	Friend virus B
GFAP	Glial fibrillary acidic protein
hnRNP	Heterogeneous ribonucleoprotein
HRE	Hexanucleotide repeat expansion
Iba1	Ionised calcium binding adaptor molecule 1

JAX	Jackson laboratories
LMN	Lower motor neurone
MND	Motor neurone disease
MRI	Magnetic resonance imaging
MSD	Meso-scale discovery
NMJ	Neuromuscular junction
NT	Non-transgenic
RAN	Repeat-associated non-ATG translation
SCS	Space cadet syndrome
SOD1	Superoxide dismutase 1
SPF	Specified pathogen free
TA	Tibialis anterior
TARDBP	Transactivating response DNA binding protein 43
UMN	Upper motor neurone

1 Introduction

1.1 Amyotrophic Lateral Sclerosis

Amyotrophic lateral sclerosis (ALS), also known as motor neurone disease, is a progressive and ultimately fatal neurodegenerative disease characterised by upper motor neurone (UMN) loss in the brain and lower motor neurone (LMN) loss in the spinal cord. This causes extensive muscle weakness and atrophy as denervation of the voluntary muscles progresses, leading to eventual paralysis and death.

1.1.1 Epidemiology

The incidence of ALS is approximately 2 in 100,000 individuals with a prevalence of 4-5 in 100,000 individuals, although this varies with geographical region (Xu et al., 2020; Longinetti and Fang, 2019). The lifetime risk is 1 in 350 for men and 1 in 400 for women (Kiernan et al., 2011). Some studies show a stable incidence (Ryan et al., 2019), while others show an increase in recent years (Xu et al., 2020; Feigin et al., 2021), perhaps resulting from diagnostic improvements. However, it is anticipated to increase due to ageing populations (Arthur et al., 2016). The average age of onset is 55-60 years, and survival is approximately 2-3 years from diagnosis (Hoppitt et al., 2011; Hobson et al., 2016), however the age of onset and disease progression can vary considerably between patients.

1.1.2 Clinical Presentation

Pathologically, ALS displays a combination of UMN and LMN features. However, onset often occurs focally and can present in a number of different ways. Limb onset is the most common, presenting in approximately 60% of patients, and usually occurs asymmetrically in either the upper or lower limbs causing spasticity, weakness, and fasciculations in the affected limb. Bulbar onset occurs in approximately 30% of patients and is primarily characterised by progressive dysarthria (speech problems) and dysphagia (swallowing difficulties) before progressing to limb features. The least common presentation is respiratory onset, resulting in breathing difficulties (Kiernan et al., 2011; Hardiman et al., 2017).

Over the past decade, it has been accepted that there is an overlap between ALS and frontotemporal dementia (FTD); a degenerative condition caused by neuronal pathology within the frontal and temporal lobes of the brain that results in cognitive deficits and behavioural, personality, and language changes. Up to 50% of ALS patients can exhibit signs of FTD (Phukan et al., 2012; Cividini et al., 2021), and up to 30% FTD patients can exhibit motor dysfunction (Burrell et al., 2011).

1.1.3 Biomarkers and Treatment

Diagnosis of ALS is challenging due to the non-specific nature of symptoms that can mimic other neuromuscular disorders. Patients will often undergo several tests such as imaging of the brain and spinal cord and electrophysiological examinations before ALS is diagnosed. Clinicians use various diagnostic criteria including the revised El Escorial criteria (Brooks et al., 2000), Awaji Shima criteria (de Carvalho et al., 2008), and Gold Coast criteria (Shefner et al., 2020) to make a diagnosis. However, this can take time, due to the lack of a valid diagnostic biomarker and the requirement to show symptom progression. As a result, an average delay of 12 months between symptom onset and diagnosis is common (Mitchell et al., 2010; Longinetti and Fang, 2019). This delay may have a negative impact on prognosis as the early stages of disease are missed. A diagnostic biomarker for ALS would not only reduce this delay but also improve disease progression monitoring and prognosis, as well as patient stratification and the detection of early treatment effects in clinical trials.

Various potential biomarkers have been identified, such as neurofilament levels in blood and cerebrospinal fluid (CSF) as an indicator of neurodegeneration and neuroinflammation (Lu et al., 2015; De Schaepdryver et al., 2019), electrophysiological measurements to reflect motor unit loss and thus disease progression (Neuwirth et al., 2015), and neuroimaging such as magnetic resonance imaging (MRI) to track pathological changes *in vivo* (Turner et al., 2013). Despite great effort in developing a robust and replicable biomarker for diagnostic and prognostic applications, none have been approved for clinical use.

There is no cure for ALS and current treatments are limited, focusing primarily on managing symptoms and providing supportive care to improve quality of life. Drug development

remains focused on disease-modifying therapies, and to date, only four have been approved by the Food and Drug Administration (FDA) in the US: riluzole, edaravone, AMX0035, and most recently, Tofersen. Riluzole reduces glutamate excitotoxicity (Benoit and Escande, 1991) and was the first drug to be approved by the FDA for ALS in 1995. However, its benefit is limited, extending survival by approximately 3 months (Bensimon et al., 1994).

Edaravone was approved by the FDA in 2017. It reduces oxidative stress and was shown to slow disease progression in a trial in Japan (Writing Group and Edaravone, 2017) and prolong survival by 6 months in a trial in the US (Brooks et al., 2022). However, two other trials in Italy and Germany showed no effect on progression or survival (Lunetta et al., 2020; Witzel et al., 2022). Due to this inconsistency, edaravone has yet to be approved in Europe.

AMX0035 is a combination therapy of sodium phenylbutyrate and taurursodiol that targets multiple pathophysiological mechanisms. It was approved by the FDA in September 2022 after a phase II clinical trial suggested it confers functional and survival benefits in ALS (Paganoni et al., 2021), although there are criticisms of the trial (Mullard, 2022). A phase III trial is now underway to evaluate the efficacy of AMX0035.

Tofersen is an antisense oligonucleotide (ASO) therapy specifically for patients harbouring a *SOD1* mutation. It targets and degrades the *SOD1* mRNA thus reducing the synthesis of the abnormal SOD1 protein. It was approved by the FDA in April 2023 after a phase III clinical trial demonstrated a reduction of SOD1 protein level in the CSF and patients with early administration of the drug showed a decrease in the decline of respiratory function, strength, and quality of life (Miller et al., 2022).

Historically, ALS clinical trials have a high failure rate, highlighted by the fact that only four drugs have been approved in the past 30 years; all of which confer only very modest benefits or are specific to a particular causal mutation. There are several reasons, ranging from trials treating ALS as a homogeneous disease rather than a heterogeneous one; an over-reliance on the SOD1^{G93A} mouse model (which only represents 2% of patients and lacks the TDP-43 proteinopathy present in 97% of ALS cases); to pharmacology and trial design (Mead et al., 2022). However, a major issue is the lack of a biomarker of disease progression which could

provide a more accurate survival measure than the revised ALS functional rating scale (ALSFRS-R) currently used. As mentioned earlier, significant research is underway and identifying biomarkers that can be translated from preclinical models into clinical trials would significantly improve the detection of treatment effects and monitor disease progression.

1.2 Causes of ALS

Approximately 90% of ALS cases are sporadic (sALS), seemingly presenting at random with no family history of the disease, while the remaining 10% are classed as familial ALS (fALS). fALS cases have a family history of the disease and show a typical mendelian autosomal dominant pattern of inheritance (Ranganathan et al., 2020). There are over 30 known genes that have been identified as being causative or conferring an increased risk of developing ALS (Table 1.1). The most common are *C9ORF72*, *SOD1*, *TARDBP*, and *FUS*, and together they account for the majority of fALS cases in European and Asian populations; although in Asian populations the *SOD1* mutation is most common, followed by *FUS*, *C9ORF72*, and *TARDBP* (Zou et al., 2017). About 10% of sALS cases harbour known ALS genetic mutations yet do not have a family history of the disease (Feldman et al., 2022). Identification of these genes has led to the identification of various pathophysiological mechanisms underlying ALS, including protein aggregation, excitotoxicity, oxidative stress, mitochondrial dysfunction, neuroinflammation, RNA processing, and impaired axonal and nucleocytoplasmic transport. There is also emerging evidence regarding environmental risk factors, such as smoking, educational attainment, and intensive physical activity (Harwood et al., 2009; Bandres-Ciga et al., 2019). As such, ALS is considered to be a genetically complex and multifactorial disease resulting from a complex interaction of genetic and environmental influences (Zheng et al., 2023).

Table 1.1: Causal mutations identified in ALS.

Adapted from Mead et al. (2022). ALS-new denote potential ALS genes requiring further validation; ALS-putative denote potential ALS risk factors; FTD-ALS denote mutations associated with both ALS and FTD.

ALS locus number	Gene	Protein	Locus	Protein Function
ALS1	SOD1	Cu-Zn superoxide dismutase	21q22.11	Dismutates superoxide free radicals: oxidative stress; protein aggregation; mitochondrial dysfunction; axonal transport defects; proteasome impairment; glial dysfunction
ALS2	ALS2	Alsin	2q33.1	Intracellular trafficking
ALS4	SETX	Senataxin	9q34.13	RNA processing
ALS5	SPG11	Spatacsin	15q21.1	Vesicle trafficking; axonal defects
ALS6	FUS	Fused in sarcoma RNA binding protein (component of the hnRNP complex)	16p11.2	RNA processing; DNA damage repair defects; nucleocytoplasmic transport defects; stress granule function; protein aggregation
ALS8	VAPB	Vesicle-associated membrane protein	20q13. 32	Proteasome impairment; intracellular trafficking
ALS9	ANG	Angiogenin	14q11.2	RNA processing
ALS10	TARDBP	TDP-43	1p36.22	RNA processing; nucleocytoplasmic transport defects; stress granule function; protein aggregation
ALS11	FIG4	Polyphosphoinositide phosphatase	6q21	Intracellular trafficking
ALS12	OPTN	Optineurin	10p13	Autophagy; protein aggregation; inflammation; NF-κB regulation; membrane trafficking; exocytosis; vesicle transport; reorganization of actin and microtubules; cell cycle control
ALS13	ATXN2	Ataxin 2	12q24.12	RNA processing
ALS14	VCP	Valosin-containing protein/Transitional endoplasmic reticulum ATPase	9p13.3	Autophagy; proteasome impairment; defects in stress granules; protein aggregation; mitochondrial dysfunction; endoplasmic reticulum dysfunction

ALS15	UBQLN2	Ubiquilin 2	Xp11.21	Proteasome impairment; autophagy; protein aggregation; oxidative stress; axonal defects
ALS16	SIGMAR1	Sigma non-opioid intracellular receptor 1	9p13.3	Proteasome impairment; intracellular trafficking
ALS17	CHMP2B	Charged multivesicular body protein 2b	3p11.2	Autophagy; protein aggregation
ALS18	PFN1	Profilin-1	17p13.2k	Axonal defects
ALS19	ERBB4	Receptor tyrosine-protein kinase erbB-4	2q34	Neuronal development
ALS20	hnRNPA1	Heterogeneous nuclear ribonucleoprotein A1	12q13.13	RNA processing
ALS21	MATR3	Matrin-3	5q31.2	RNA processing
ALS22	TUBA4A	Tubulin α4A chain	2q35	Cytoskeleton
ALS23	ANXA11	Annexin A11	10q22.2	Intracellular trafficking
ALS24	NEK1	Serine–threonine protein kinase Nek1	4q33	Intracellular trafficking; DNA-damage response; microtubule stability
ALS25	KIF5A	Kinesin heavy chain isoform 5A	12q13.3	Axonal defects; intracellular trafficking
ALS-new	GLT8D1	Glycosyltransferase 8 domain-containing protein 1	3p21.1	Ganglioside synthesis
ALS-new	TIA1	Cytotoxic granule-associated-RNA binding protein	2p13.3	Delayed stress granule disassembly; stress granule accumulation
ALS-new	C21orf2	Cilia and flagella-associated protein 410	21q22.3	Microtubule assembly; DNA damage response and repair; mitochondrial function; interacts with NEK1
ALS-new	DNAJC7	DnaJ heat shock protein family (Hsp40) member C7	17q21.2	Protein homeostasis; protein folding and clearance of degraded proteins; protein aggregation
ALS-new	LGALSL	Galectin-related protein	2p14	Protein function is largely unknown
ALS-new	KANK1	KN motif and ankyrin repeat domain-containing protein 1	9p24.3	Cytoskeleton; axonopathy
ALS-new	CAV1	Caveolin 1	7q31.2	Intracellular and neurotrophic signalling
ALS-new	SPTLC1	Serine palmitoyltransferase, long-chain base subunit 1	9q22.31	Excess sphingolipid biosynthesis

ALS-new	ACSL5	Long-chain fatty acid coenzyme A ligase 5	10q25.2	Long-chain fatty acid metabolism
ALS-putative	ELP3	Elongator protein 3	8p21	Ribostasis; cytoskeletal integrity
ALS-putative	DCTN1	Dynactin	2p13	Axonal transport
ALS-putative	PARK9	Probable cation-transporting ATPase 13A2	1p36.13	Lysosome function
FTD-ALS1	C9orf72	Chromosome 9 open reading frame 72	9p21.2	RNA processing; nucleocytoplasmic transport defects; proteasome impairment; autophagy; inflammation; protein aggregation (DPRs)
FTD-ALS2	CHCHD10	Coiled-coil–helix-coiled–coil-helix domain-containing protein 10	22q11.23	Mitochondrial function; synaptic dysfunction
FTD-ALS3	SQSTM1	Sequestosome-1	5q35.3	Proteasome impairment; autophagy; protein aggregation; axonal defects; oxidative stress
FTD-ALS4	TBK1	Serine–threonine protein kinase	12q14.2	Autophagy; inflammation; mitochondrial dysfunction
FTD-ALS5	CCNF	Cyclin F	16p13.3	Autophagy; axonal defects; protein aggregation

1.2.1 SOD1

Superoxide dismutase 1 (*SOD1*) was the first gene to be linked to ALS (Rosen et al., 1993). It codes for a homodimeric Cu/Zn-binding enzyme that is involved in reducing oxidative stress in cells, and over 150 mutations have been identified so far (Kaur et al., 2016). There is considerable phenotypic heterogeneity between *SOD1* mutations, however cognitive impairments are rarely seen (Renton et al., 2014; Rosenfeld and Strong, 2015). This variability has made investigating the pathogenesis of SOD1 ALS challenging, although the consensus is that *SOD1* mutations lead to ALS through toxic gain-of-function mechanisms.

SOD1 mutations account for 12-23% of fALS and 1-2% of sALS cases, and result in the formation of neuronal cytoplasmic inclusions in the spinal cord that contain misfolded SOD1 protein (Kaur et al., 2016; Renton et al., 2014). This is a unique pathology in ALS as it lacks the TDP-43 proteinopathy found in most other, non-SOD1 related ALS cases. Initially, it was thought the *SOD1* mutation led to loss-of-function and the lack of dismutase activity led to increased superoxide radicals (Deng et al., 1993), however it is now accepted that the mutation causes a toxic gain-of-function which leads to multiple downstream effects, such as oxidative stress, protein instability, and mitochondrial dysfunction (Barber and Shaw, 2010; Ferraiuolo et al., 2011; Bozzo et al., 2017).

1.2.2 TARDBP

The *TARDBP* gene encodes the TAR DNA-binding protein 43 (TDP-43), a primarily nuclear DNA/RNA-binding protein that plays a vital role in many cellular processes including transcription, splicing regulation, microRNA processing, and mRNA stability, transport and translation (Buratti and Baralle, 2012). The discovery that TDP-43 is present in the neuronal inclusions found in ALS and FTD (Neumann et al., 2006) not only placed both diseases on a clinical spectrum, but was key to the discovery of mutations in the *TARDBP* gene in fALS and FTD cases (Sreedharan et al., 2008; Chio et al., 2010). Consequently, over 50 mutations in the *TARDBP* gene have now been identified and they account for approximately 4% of fALS cases (Chio et al., 2012).

The presence of TDP-43 in neuronal aggregates and inclusions is a pathological hallmark of ALS due to their presence in 97% of cases (Ling et al., 2013). These inclusions contain ubiquitinated and hyperphosphorylated TDP-43 and occur both in the presence and absence of *TARDBP* mutations (Mackenzie et al., 2007). In cells with cytoplasmic TDP-43 aggregates, there is a concurrent loss of nuclear TDP-43 which has been suggested to cause disease via a loss-of-function mechanism (Chiang et al., 2010; Iguchi et al., 2013; Mitra et al., 2019). However, cytoplasmic aggregation suggests a toxic gain-of-function mechanism (Chou et al., 2018). Moreover, whether these cytoplasmic TDP-43 aggregates actively cause neurodegeneration or are simply a result of it is unclear, although evidence suggests it may be the latter as TDP-43 mouse models have displayed neurodegeneration in the absence of aggregates (Arnold et al., 2013; Ricketts et al., 2014). Therefore, it seems likely that both loss-of-function and toxic gain-of-function mechanisms play a role in the TDP-43 pathophysiology of ALS and FTD (Brown et al., 2022; Mehta et al., 2023).

1.2.3   C9ORF72

The most common cause of fALS is a mutation in chromosome 9 open reading frame 72 (*C9ORF72*). It accounts for approximately 40% of fALS and 25% of familial FTD cases, further strengthening the association of these two diseases on a clinical spectrum, and 7% of sALS cases (Majounie et al., 2012). The mutation was discovered by two independent groups simultaneously and was identified as a hexanucleotide repeat expansion (HRE) of G_4C_2 in intron 1 of the *C9ORF72* gene (DeJesus-Hernandez et al., 2011; Renton et al., 2011).

1.2.3.1   C9ORF72 Function

Little was known about the C9ORF72 protein prior to discovery of the HRE, but in the years following there was significant progress in revealing its function and how it pertains to *C9ORF72*-associated ALS/FTD (hereby referred to as C9ALS/FTD). The *C9ORF72* gene is made up of two non-coding exons, 1a and 1b, and 10 coding exons that result in three transcript variants and two protein isoforms through alternative splicing (Figure 1.1). Variant 1 is made up of exon 1a and exons 2-5, resulting in a 228 amino acid isoform and 24 kDa protein. Variants 2 and 3 are made up of exons 1b and 1a, respectively, and exons 2-11. These result in 481 amino acid isoforms and a 54 kDa protein (DeJesus-Hernandez et al., 2011; Renton et

al., 2011). The *C9orf72* gene is very highly conserved in many species, including apes, monkeys, rodents, and zebrafish, which indicates the protein has a critical function (Iyer et al., 2018).
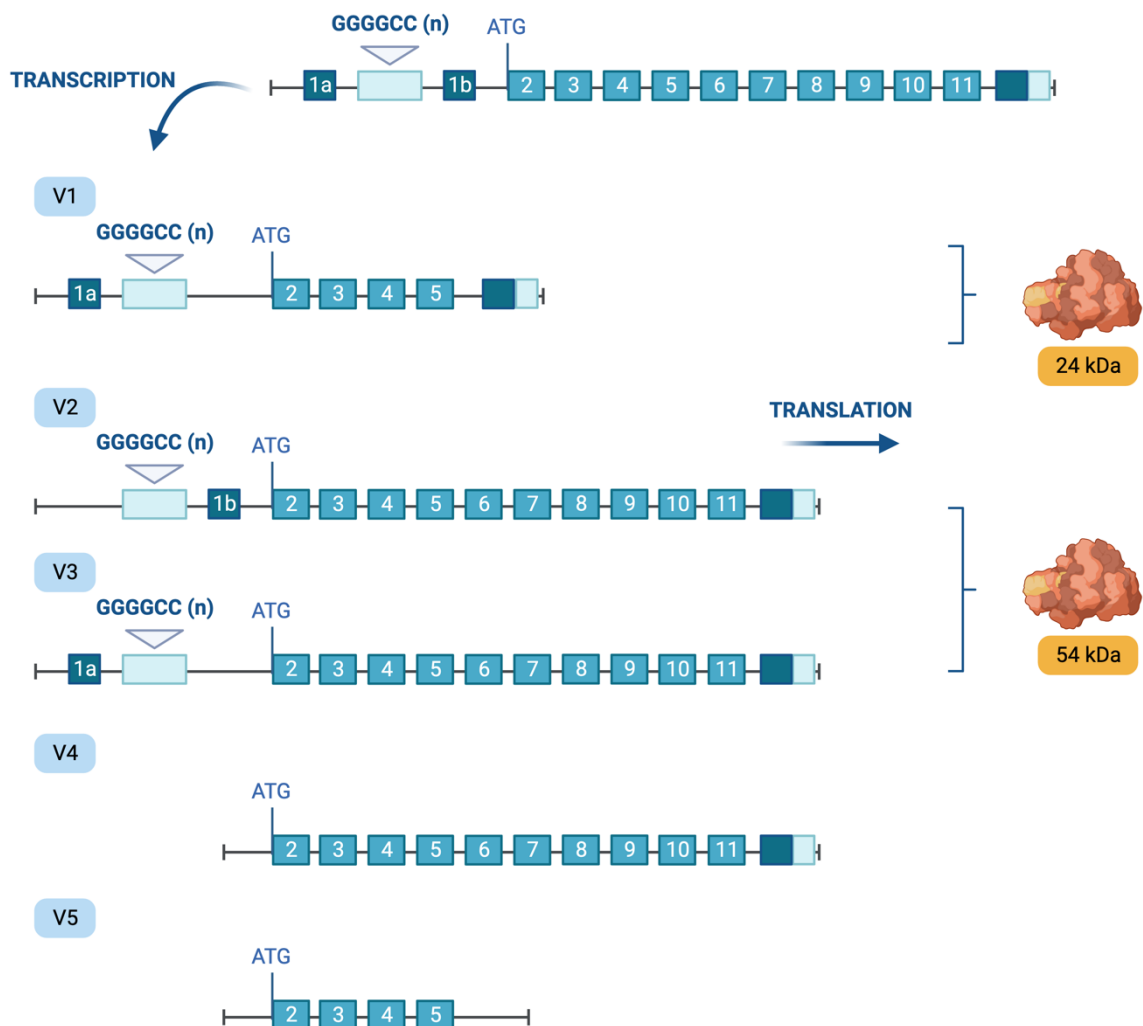
Figure 1.1: C9ORF72 transcripts and protein isoforms.

The *C9ORF72* gene is made up of two non-coding exons, 1a and 1b, and 10 coding exons that result in three transcript variants and two protein isoforms through alternative splicing. Variant 1 is made up of exon 1a and exons 2-5, resulting in a 228 amino acid isoform and 24 kDa protein. Variants 2 and 3 are made up of exons 1b and 1a, respectively, and exons 2-11. These result in 481 amino acid isoforms and a 54 kDa protein. Variants 4 and 5 are non-coding transcripts. Created with Biorender.com.

Expression of the C9ORF72 protein has been detected in several tissues throughout the body, but the highest levels are found in the brain, spinal cord, and immune system. C9ORF72 has been shown to have a wide range of functions, including involvement in membrane trafficking, the endolysosomal pathway, nucleocytoplasmic transport, stress granule

formation and degradation, and immune system regulation. Structurally, C9ORF72 is similar to the differentially expressed in normal and neoplastic cells (DENN) protein family (Marat et al., 2011; Levine et al., 2013), which suggests a role in activation of Rab-GTPases. These proteins regulate membrane trafficking and co-localise with C9ORF72 (Farg et al., 2014), indicating C9ORF72 is involved in the endolysosomal trafficking and autophagy pathways. Furthermore, in human cell lines, a knockdown of C9ORF72 results in inhibition of the autophagy pathway and accumulation of p62, an important protein involved in autophagy regulation (Sellier et al., 2016; Webster et al., 2016). These same results have been replicated in *C9orf72* knockout mouse models (O'Rourke et al., 2016; Sullivan et al., 2016).

Homozygous *C9orf72* knockout mouse models also display striking immune system dysregulation, including enlarged lymph nodes, splenomegaly, glomerulonephropathy, and excessive release of inflammatory cytokines and autoantibodies (Atanasio et al., 2016; Burberry et al., 2016; Sudria-Lopez et al., 2016). This indicates C9ORF72 has an important function in immune regulation, primarily in macrophages and microglia as a mouse model with *C9orf72* depletion in myeloid cells displayed the same immune deficits as global *C9orf72* knockout mouse models (McCauley et al., 2020), and microglia lacking C9ORF72 cannot clear protein aggregates (O'Rourke et al., 2016).

1.2.3.2 C9orf72 Pathological Mechanisms in ALS and FTD

Since discovery of the HRE, there has been much debate concerning the disease mechanisms that lead to C9ALS/FTD. Most of the healthy population have less than 10 repeats while a repeat length above 30 is considered pathological. However, this cut-off is an arbitrary number as there have been reports of individuals with pathological length repeats that do not develop disease (Xi et al., 2015). The vast majority of C9ALS/FTD patients harbour repeat lengths ranging from hundreds to thousands (van Blitterswijk et al., 2013); although there have been cases of C9ALS/FTD in individuals with very short repeats (Iacoangeli et al., 2019). This has made it challenging to determine to what extent repeat length drives disease. In addition to this variability, the HRE exhibits somatic heterogeneity within the same patient, with expansions in the central nervous system (CNS) differing from that in the blood (Nordin et al., 2015; Gijselinck et al., 2016). To further complicate matters, repeat length also appears to differ between brain regions in the same patient (van Blitterswijk et al., 2013). This

instability could account for the clinical heterogeneity in symptom presentation and age of onset seen in C9ALS/FTD patients, but evidence is still inconclusive.

Three disease mechanisms are currently hypothesised to lead to C9ALS/FTD. The first is a loss-of-function mechanism that results in C9orf72 haploinsufficiency. Exactly how this occurs was the focus of several studies and is thought to be due to hypermethylation of the repeat and the CpG island upstream of it (Gijselinck et al., 2016; Jackson et al., 2020). This causes a reduction in C9ORF72 protein levels, and several knockdown and knockout models have been created to investigate the physiological effects (Jiang et al., 2016; Sudria-Lopez et al., 2016; Burberry et al., 2016; Atanasio et al., 2016). As mentioned in the previous section, knockout mouse models develop striking immune system dysregulation, but crucially, none of them develop neurodegeneration. This implies that *C9ORF72* haploinsufficiency alone is insufficient to cause disease and may instead be contributory in combination with other disease mechanisms.

The second mechanism is a toxic gain-of-function mechanism that results from sense and antisense transcription of the HRE. This results in the formation of RNA foci; very stable DNA and RNA structures. They are found in the spinal cord and several brain regions, such as the motor cortex, hippocampus, and cerebellum, and predominantly form in neurones (Mizielinska et al., 2013). Toxicity is thought to come from the interaction of these structures with several RNA-binding proteins, sequestering them in aggregates and inducing RNA metabolism dysfunction (Xu et al., 2013). In particular, the heterogeneous nuclear ribonucleoproteins (hnRNPs) are affected, and have been shown to directly bind to the RNA repeat and colocalise with RNA foci, leading to potent neurotoxicity (Lee et al., 2013). Primary cortical and motor neurone cultures have been used to model RNA toxicity and show reduced survival in the presence of nuclear RNA foci (Wen et al., 2014). A *Drosophila* model also suggests RNA toxicity causes eye and motor neurone degeneration (Zhang et al., 2015). However, another *Drosophila* model expressing repeat lengths similar to patients, found no motor neurone degeneration in adult neurones (Moens et al., 2018). This could indicate that RNA foci have a more limited role in disease pathogenesis than previously thought.

The third mechanism is another toxic gain-of-function mechanism and results from repeat-associated non-ATG (RAN) translation of transcripts containing the HRE (Ash et al., 2013). These transcripts are translated in both sense and antisense directions in all three frames, producing five dipeptide repeat proteins (DPRs): poly-glycine-alanine (poly-GA) and poly-glycine-arginine (poly-GR) in the sense direction, poly-glycine-proline (poly-GP) in both sense and antisense directions, and poly-proline-arginine (poly-PR) and poly-proline-alanine (poly-PA) in the antisense direction. These DPRs form cytoplasmic aggregates positive for p62 and ubiquitin, but negative for TDP-43. They are found in several areas of the brain, and to a lesser extent in the spinal cord, and do not appear to correlate with areas of neuronal loss (Cooper-Knock et al., 2012; Schipper et al., 2016).

The most toxic of the five DPR species are the arginine-containing DPRs, poly-GR and poly-PR. In a zebrafish model, poly-GR primarily affected motor activity and survival (Swaminathan et al., 2018). In *Drosophila*, poly-GR and poly-PR were found to be the most toxic in the eyes and motor neurones, while poly-PA and poly-GP were found to not be toxic at all and poly-GA only caused a slight decrease in survival (Wen et al., 2014; Mizielinska et al., 2014; Freibaum et al., 2015). Overexpression of poly-GA has been shown to lead to toxicity in various model systems from cell cultures to mice (May et al., 2014; Zhang et al., 2014; Zhang et al., 2016; Swaminathan et al., 2018), however these levels of poly-GA are unlikely to accurately represent physiological levels. Poly-GA is the most prone of the DPR species to aggregate, forming fibrils similar to those seen in amyloid-beta in Alzheimer's disease (Chang et al., 2016) and is thought to indirectly result in toxicity through sequestration of proteins, particularly Unc119 (May et al., 2014).

1.3 Animal Modelling C9orf72 ALS

The use of animal models is an important step to uncover the pathophysiological mechanisms of C9ALS/FTD and develop therapeutics. Many different types of models have been developed on a range of species, some of which are briefly covered here.

1.3.1 Non-Murine Models of C9orf72

While rodent models, and particularly mice, are some of the most popular model systems to use, lower order organisms have been important in elucidating the mechanisms of C9ALS/FTD and enabling modelling *in vivo* in organisms with lower neurophysiological sensitivity which is attractive for ethical reasons.

1.3.1.1 *Caenorhabditis elegans*

C. elegans is an attractive model organism as it is cheap, small, and has a short lifespan, which allows for easy manipulation and study. Approximately 38% of its genes have a human ortholog, including *tau* and *C9orf72* (Alexander et al., 2014), which make it a good candidate for studying neurodegenerative diseases. The first model of C9ALS/FTD following the discovery of the HRE was a null mutation of the *C9orf72* ortholog in *C. elegans* (Therrien et al., 2013). It resulted in motility defects and degeneration of motor neurones as a result of TDP-43 toxicity and was one of the first studies to suggest a combination of loss-of-function and gain-of-function mechanisms in C9ALS/FTD. However, *C. elegans* is an invertebrate and lacks a spinal cord so is unlikely to holistically replicate such a complex disease as C9ALS/FTD.

1.3.1.2 *Drosophila melanogaster*

Drosophila have been used to model several neurodegenerative diseases, including Parkinson's (West et al., 2015) and Alzheimer's (Chakraborty et al., 2011), and are an attractive organism due to their low cost, short generation time and lifespan, and ease of genetic manipulation. Approximately 75% of human genes have an ortholog in *Drosophila*, however *C9orf72* is not one of them (Sharpe et al., 2021). While this means *Drosophila* cannot be used for loss-of-function studies, they are widely used to investigate gain-of-function mechanisms and as overexpression models. As such, studies in *Drosophila* were the first to suggest purely gain-of-function mechanisms could lead to toxicity (Xu et al., 2013; Mizielinska et al., 2014). *Drosophila* are also useful for high-throughput genetic screens and have been used in this way to identify genes involved in gain-of-function toxicity (Freibaum et al., 2015).

1.3.1.3   Zebrafish

Zebrafish are a useful alternative to other model organisms such as *C. elegans* and *Drosophila* as they are vertebrates, have a similar CNS to humans, are easy to genetically manipulate, and have high conservation of genes (Babin et al., 2014). Zebrafish models of C9ALS/FTD have provided evidence for both loss-of-function and gain-of-function mechanisms (Ciura et al., 2013; Swaminathan et al., 2018). However, their usefulness is limited as they are not mammals and they lack a corticospinal tract (Babin et al., 2014), which makes it difficult to fully recapitulate ALS.

1.3.2   Murine Models of C9orf72

Rat and mouse models are the most popular animal model systems as they are mammals, share 98% of genes with humans, are relatively easily to genetically manipulate, and have relatively short lifespans. Their use also has fewer ethical concerns than a more closely related model organism such as a non-human primate.

1.3.2.1   Rat

While rats are larger than mice, which makes imaging studies and surgery much easier, they are also more expensive to keep and more challenging to genetically manipulate (Bryda, 2013). Rat models have been created for various fALS mutations including *SOD1* (Aoki et al., 2005) and *TARDBP* (Zhou et al., 2010). Two rat models of C9ALS/FTD have been created. The first was a knock-in model of 80 repeats in the endogenous rat *C9orf72* locus that resulted in reduced *C9orf72* expression, motor deficits, and neurodegeneration in the spinal cord that ultimately led to hindlimb paralysis (Dong et al., 2020). The second was a rat model with a deletion mutation in the endogenous rat *C9orf72* gene, resulting in haploinsufficiency (Dong et al., 2021). This alone did not cause a phenotype, but when the rats were treated with kainic acid to induce excitotoxicity, they developed motor deficits and neurodegeneration that was not seen in the treated wild-type group. These results suggest that while loss-of-function may not be sufficient to cause C9ALS/FTD alone, it may sensitise motor neurones to other insults such as excitotoxicity, TDP-43, or DPRs.

1.3.2.2   Mouse

Mouse models are the most popular animal model for *in vivo* studies. Since discovery of the *C9ORF72* HRE, many mouse models have been developed to model different aspects of C9ALS/FTD (Table 1.2). Loss-of-function models were among some of the earliest mouse models to be generated and have demonstrated that *C9orf72* knockouts, both global and cell-specific, were not sufficient to trigger disease (Koppers et al., 2015; O'Rourke et al., 2016; Atanasio et al., 2016). Instead, they develop widespread immune dysfunction (as mentioned in section 1.2.3.1) and reduced survival (O'Rourke et al., 2016; Atanasio et al., 2016; Burberry et al., 2016; Sudria-Lopez et al., 2016). Initially, there was confusion regarding the immune phenotypes observed and why some studies reported premature death in heterozygous and homozygous knockouts, while others only observed it in the latter. It was not until one study investigated environmental effects on *C9orf72* knockouts, and very elegantly demonstrated that the gut microbiome can have a dramatic effect on the phenotype observed, that this discrepancy was resolved (Burberry et al., 2020). While these studies support the hypothesis that C9ALS/FTD is primarily a toxic gain-of-function disease, it is still possible that prolonged loss-of-function of the *C9orf72* gene may influence disease pathogenesis by sensitising the CNS to further insults. For example, recent studies have demonstrated that loss-of-function of C9ORF72 exacerbates toxic gain-of-function disease phenotypes (Shao et al., 2019; Zhu et al., 2020).

Table 1.2: Current mouse models of the C9ALS/FTD HRE

Study	Strain	Generation of mouse model and G4C2 repeat size	Pathology	Behavioural Phenotype
Chew et al. (2015)	C57BL/6J	AAV2/9 vector with CBA promoter driving transcription of 2 or 66 repeats with 119 bp 5' and 100 bp 3' flanking regions of the human *C9ORF72* gene	Sense RNA foci cortex, cerebellum, CA1 to CA3 and dentate gyrus regions of the hippocampus, thalamus, ventral horns of the spinal cord, and amygdala of 66-repeat mice; sense DPR inclusions in cortex, hippocampus, cerebellum, and the ventral horn of the spinal cord of 66-repeat mice; nuclear, and occasionally cytoplasmic, pTDP-43 inclusions in cortex and hippocampus of 66-repeat mice; neurodegeneration in cortex, motor cortex, and cerebellum; astrogliosis in cortex.	Increased anxiety-like behaviour in open field test; decreased social interaction score, indicative of social deficits; motor deficits present in open field and rotarod at 6 months.
O'Rourke et al. (2015)	C57BL/6J	Bacterial artificial chromosome (BAC) containing complete human *C9ORF72* gene with a mix of 100 to 1000 repeats and 110 kb 5' upstream and 20 kb 3' downstream flanking regions	Sense and antisense RNA foci throughout CNS at 3 months; poly-GP in cortex, hippocampus, cerebellum, and spinal cord at 6 months; evidence of nucleolar stress	No abnormalities in body weight, grip strength, rotarod, open field, 3-chamber test, or Y-maze test

Peters et al. (2015)	SJL/BL6	BAC containing partial human *C9ORF72* gene with a mix of 500/300 repeats and 141 kb 5' upstream flanking region; Transgene expression equivalent to endogenous mouse *C9orf72* expression	Sense RNA foci detected throughout CNS at 3 months; antisense RNA foci detected throughout CNS at 10 months; poly-GP throughout brain at 4 months	No abnormalities in rotarod, grip strength, or sociability
Jiang et al. (2016)	C57BL6/C3H	BAC containing partial human *C9ORF72* gene with 450 repeats and 140 kb 5' upstream flanking region; three lines generated and labelled 450A, 450B, and 450C with expressions levels at 1x, 3x and 4.5x endogenous mouse *C9orf72* expression	Sense and antisense RNA foci throughout CNS by 2 months in 450B mice; soluble poly-GP found in cerebellum, cortex, and spinal cord of 450B and 450C mice; sense DPR aggregates found frontal cortex, in retrosplenial cortex, and hippocampus in 450C mice at 3 months; increased pTDP-43 in CA1 and dentate gyrus hippocampal regions at 12 months in 450C mice; mild neuronal loss in CA1 and dentate gyrus hippocampal regions of 450B and 450C mice at 12 months	450B and 450C mice exhibited spatial learning deficits and increased anxiety
Liu et al. (2016)	FVB/NJ	BAC containing complete human *C9ORF72* gene, and 2 kb of the nearby *Mps one binder kinase activator 3B* gene, with a mix of 500,	**Acute-progress mice**: sense RNA foci in cortex, hippocampus, cerebellum, and spinal cord; antisense RNA only found in motor cortex, hippocampus, and cerebellar Purkinje cells at 2 months; C9-36/29 mice did not develop RNA foci; poly-GA and poly-GP found	**Acute-progress mice**: 30% of female C9-500 and C9-500/32 mice developed sudden weight loss, gait abnormalities, reduced grip strength, hindlimb paralysis,

			throughout the brain; nuclear and cytoplasmic TDP-43 inclusions found in degenerating neurones in the brain, but not in asymptomatic mice of the same line; neurodegeneration in layer II/III and V of motor cortex, CA and dentate gyrus hippocampal regions, cerebellar Purkinje cell layer, and posterior horn on the spinal cord; extensive neuromuscular denervation in diaphragm and tibialis anterior **Slow-progress mice**: sense and antisense RNA foci; mild neurodegeneration in neocortex, cerebellum, and lumber spinal; subtle neuromuscular junction abnormalities	and early death beginning at 3 months; this was also seen in C9-36/29 mice, but onset was later at 6 months **Slow-progress mice**: 50% of male and female C9-500 and C9-500/32 mice, and 30% of C9-36/29 mice, developed a slower phenotype of kyphosis, reduced activity, clasping, intermittent seizures, and increased anxiety at 12 months
		500/32, and 36/29 repeats and 52 kb upstream and 19 kb downstream flanking regions; four founder lines generated and labelled C9-500, C9-500/32, C9-36/29, and C9-37 with expression levels at 1x, 2x, 2.5x, and 0.5x endogenous mouse *C9orf72*		
Herranz-Martin et al. (2017)	C57BL/6J	AAV9 vector with CMV promoter driving transcription of 10 or 102 repeats with intervening TCGAG linker sequence to create mixed dipeptide proteins	Nuclear and cytoplasmic poly-GA in cerebellum and brain stem; enhanced p62 expression in cerebellum; increased expression of proteins involved in apoptosis in cerebellar Purkinje cells; pathological neuromuscular junctions at 12 months	Gait abnormalities and hindlimb splay defect in the right hindlimb at 12 months; memory deficit in object recognition test at 12 months
Chew et al. (2019)	C57BL/6J	AAV2/9 vector with CBA promoter driving transcription of 2 or 149	Astrogliosis in the cortex at 3 and 6 months with neurodegeneration present at 6 months; sense and antisense RNA foci in the motor cortex, hippocampus,	Hyperactivity in open field test at 3 and 6 months; motor deficits in hanging wire test and cognitive

		repeats with 119 bp 5' and 100 bp 3' flanking regions of the human *C9ORF72* gene	cerebellar Purkinje cells, thalamus, and ventral horn of the spinal cord; sense DPR inclusions in the cortex, CA regions of the hippocampus, cerebellum, and the spinal cord from 3 months; poly-PR and poly-PA inclusions occasionally observed in hippocampus at 12 months; cytoplasmic pTDP-43 inclusions in cortex and hippocampus by 3 months; aggregation of stress granule-associated proteins and nucleocytoplasmic transport defects at 3 months.	dysfunction in contextual fear conditioning test at 6 months.
(Zhu et al., 2020)	C57BL/6J	BAC containing partial human *C9ORF72* gene with 450 repeats and 140 kb 5' upstream flanking region with one or two alleles of endogenous mouse *C9orf72* inactivated; transgene expression at 4x endogenous mouse *C9orf72* expression*;*	Loss of *C9orf72* in 450 repeat mice did not affect RNA foci levels; *C9orf72* knockdown and knockout increased accumulation of poly-GP and poly-GA in the cortex in a dose-dependent manner in 450 repeat mice; *C9orf72* knockout mice developed immune dysfunction regardless of 450 repeat presence; neurone loss in CA1 and dentate gyrus hippocampal regions and activation of microglia and astrocytes in 450 repeat mice were exacerbated by *C9orf72* knockout; reduction of C9ORF72 protein levels decreased autophagy	Decreased survival in knockout mice both with and without 450 repeats; 450 repeat mice developed learning and memory deficits at 12 months that were exacerbated by *C9orf72* knockdown and knockout; knockdown and knockout 450 repeat mice developed motor deficits at 6 months; knockout 450 repeat mice developed abnormal stride length and reduced activity

| (Riemslagh et al., 2021) | C57BL/6J | Inducible Tet-on promoter system with 36 repeats, 118 bp upstream and 115 bp downstream human flanking regions, a TRE promoter and a GFP gene | No RNA foci detected; sense DPRs in several organs and extensor digitorum muscle; muscular dystrophy and neuromuscular junction abnormalities in extensor digitorum longus muscle 4 weeks after induction of transgene expression | Reduced survival; decline in body weight; locomotor deficit on Erasmus ladder test 2 weeks after induction of transgene expression |

Four bacterial artificial chromosome (BAC) mouse models have also been generated. Using a BAC allows the full length of the human *C9ORF72* gene to be inserted into the mouse genome, plus flanking regions that may contain necessary regulatory sequences. However, insertion location of the BAC in the genome is random and may interrupt coding genes that have phenotypic consequences (Goodwin et al., 2019). The model created by O'Rourke et al. (2015) contained the full coding region (exons 1 to 11) of the C9orf72 gene and a range of repeat lengths from 100-1000, including a 110 kb 5' upstream and 20 kb 3' downstream flanking region on a C57BL/6J genetic background. The two lines chosen for analysis expressed sense and antisense RNA foci throughout the CNS by 3 months of age. Soluble poly-GP was highest in the cerebellum and the cortex and lowest in the spinal cord, while poly-GP aggregates were not detected. However, poly-GP aggregates were found in several brain regions including the hippocampus, cortex, and cerebellum at 20 months of age. TDP-43 pathology, motor unit pathology and neuronal loss were investigated, but no abnormalities were found. Behavioural tests analysing motor function, anxiety, sociability, and memory also found no deficits at any age.

The Peters et al. (2015) model contained a partial coding region (exons 1 to 6) of the *C9ORF72* gene and a mix of 500/300 repeats, including a 141 kb 5' upstream flanking region on an SJL/B6 genetic background. Transgene expression was equivalent to endogenous mouse *C9orf72* expression. Sense RNA foci were detected in abundance in the CNS from 3 months, while antisense RNA foci were detected from 10 months, although at lower levels compared to sense foci. Distribution of soluble poly-GP was similar to the O'Rourke et al. (2015) model, with the highest levels in the cerebellum, followed by the cortex, hippocampus and midbrain, and the lowest levels in the spinal cord. Poly-GP aggregates were also detected in the brain with an increase in number and size at 24 months of age compared to 10 months. TDP-43 pathology, motor unit pathology and neuronal loss were investigated, but no abnormalities were found. Dendritic spine density and electrophysiology of cortical neurones were also examined, but no abnormalities were found. Behavioural tests examining motor function were performed throughout the study, and sociability was tested from 18 months, however no deficits were observed.

The Jiang et al. (2016) model contained a partial coding region (exons 1 to 5) of the *C9ORF72* gene and 450 repeats, including a 140 kb 5' upstream flanking region, on a C57BL6/C3H genetic background. They generated three lines with 450 repeats that were labelled 450A, 450B and 450C, with expression levels at 1x, 3x and 4.5x that of endogenous *C9orf72* expression in the cortex, respectively. They also generated a 110-repeat line with 2.5x expression, and a homozygous 450C line. Sense and antisense RNA foci were detected throughout the CNS from 2 months in 450B mice, but not in 110-repeat mice, indicating a repeat length-dependent effect on RNA foci formation. Distribution of soluble poly-GP at 6 months was similar to the O'Rourke et al. (2015) and Peters et al. (2015) models, with levels of soluble poly-GP in 450C mice highest in the cortex, followed by the cerebellum and the spinal cord. Homozygous 450C mice displayed increased levels of soluble poly-GP in the same regions. Aggregates of all three sense-strand DPRs (poly-GP, poly-GA, and poly-GR) were detected in the frontal cortex, retrosplenial cortex, and hippocampus in heterozygous 450C mice at 3 months, with poly-GA increasing in number and size with age. TDP-43 aggregates were not detected; however, levels of phosphorylated TDP-43 were increased in the cortex at 22 months in 450C mice. Additionally, mild neuronal loss was observed in the hippocampal DG and CA1 regions of 450B and 450C mice at 12 months, which correlated with spatial learning and memory deficits. They also exhibited increased anxiety, but had no deficits in sociability, fear conditioning or serial reverse learning. No motor unit abnormalities were found in any of the lines.

The Liu et al. (2016) model contained the full coding region (exons 1 to 11) of the *C9ORF72* gene, including a 52 kb 5' upstream and 19 kb 3' downstream flanking region, and 2 kb of the nearby *Mps one binder kinase activator 3B* gene. The FVB/NJ genetic background was used. They generated four founder lines with varying repeat lengths and copy numbers: C9-500, C9-500/32, C9-36/29, and C9-37, which displayed expression 1x, 2x, 2.5, and 0.5x that of the mouse endogenous *C9orf72*, respectively. Approximately 30% of female C9-500 and C9-500/32 mice developed phenotypes characterised by sudden weight loss, inactivity, hindlimb paralysis, and death beginning at 3 months and were subsequently labelled "acute". This acute phenotype was also seen in the C9-36/29 mice, although onset was later at approximately 6 months. Acute mice in the C9-500 and C9-500/32 groups displayed sense and antisense RNA foci throughout the CNS, although the antisense foci were only found in

the degenerating regions of the hippocampus, motor cortex, cerebellar Purkinje layer, and lumbar spinal cord. The acute C9-36/29 mice did not display sense or antisense foci, perhaps suggesting the presence of foci is not associated with neurotoxicity. Poly-GA aggregates were observed in several brain regions, increasing in size with age, as well as poly-GP. TDP-43 pathology was found only in degenerating regions of the brain. Interestingly, some mice in the C9-500 and C9-500/32 groups remained asymptomatic and did not display the pathology observed in the acute mice. Substantial neurodegeneration was found in the hippocampal DG and CA regions, layer II/III and V of the motor cortex, the cerebellum, and the ventral horns of the lumbar spinal cord in acute mice at end-stage. Survival was also reduced, with 35% of C9-500 and C9-500/32 and 28% of C9-36/29 mice having died by 12 months. Axonal degeneration and NMJ denervation were observed in the diaphragm and TA of acute mice. Hindlimb gait abnormalities developed from 4 months of age and progressed to reduced grip strength, open field abnormalities, and eventually hindlimb paralysis. Approximately half of male and female C9-500 and C9-500/32 mice, and a third of C9-36/29 mice, developed a slower phenotype that was termed "slow progressive". In these mice, sense and antisense RNA foci, mild neuronal loss in the neocortex, cerebellum, and lumbar spinal cord, as well as mild NMJ and axonal abnormalities, were all observed. These mice developed a milder phenotype characterised by kyphosis, reduced activity, hyperactivity when provoked, clasping, and seizures at 12 months of age and beyond.

While expression of the HRE occurred in all models, only two developed neurodegenerative and behavioural phenotypes associated with C9ALS/FTD. Taken together, the models make it unclear exactly which aspects of HRE pathology are required to develop a phenotype. However, there does appear to be repeat- and expression-dependent effects. In Jiang et al. (2016), the 110-repeat and 450-repeat mice exhibited similar expression levels yet only the 450-repeat mice developed a phenotype. The same pattern was seen in Liu et al. (2016)'s 37- and 500-repeat mice. Additionally, low levels of HRE expression did not appear to be sufficient to trigger disease. In Jiang et al. (2016), the 450A line displayed no phenotype, however the higher expressing 450B and 450C lines developed cognitive deficits. Since O'Rourke et al. (2015) and Peters et al. (2015) only expressed the HRE at 1x and 2x endogenous mouse *C9orf72* levels, it is possible that this low level of expression could be responsible for the lack of phenotype. Although conversely, Liu et al. (2016)'s C9-500 mice displayed HRE expression

at 1x expression of the mouse endogenous *C9orf72* and yet developed acute phenotypes. It was the only model generated on an FVB/NJ background and was also the only one to display marked sex differences.

While initially promising, several groups, including an internal study from The Jackson Laboratory, have since been unable to reproduce the results of Liu et al. (2016). In a recent study, two independent colonies of C9ALS/FTD BAC mice displayed no motor, behavioural, or survival deficits in both males and females despite expression of the BAC transgene and production of poly-GP (Mordes et al., 2020). They also reported no evidence of neurodegeneration or inflammation in the brain or spinal cord. Chronic inactivity and occasional seizures were observed; however, these were present in both C9ALS/FTD BAC and non-transgenic littermates and so are likely to be an artefact of the background strain. These findings concur with the initial reports of C9ALS/FTD BAC mouse models that failed to develop motor or survival deficits (Peters et al., 2015; O'Rourke et al., 2015) and brings into question whether C9ALS/FTD is indeed a primarily gain-of-function disease. In contrast, Liu et al. (2016) and colleagues repeated their study in collaboration with the University of Rochester Medical Center and Prof. Smita Saxena's research group at the University of Bern, with all groups demonstrating the same "acute" phenotype as previously reported (Nguyen et al., 2020a).

One explanation for these contradictory results is differing environmental conditions between facilities which may influence phenotype presentation. As mentioned previously, it has been shown that the gut microbiome can have a striking effect on phenotype severity in *C9orf72* knockout models, which has also been demonstrated in a SOD1 ALS mouse model (Blacher et al., 2019). Therefore, it is possible a similar effect could be occurring here.

Another reason for the discrepancy could be due to the background strain the model is generated on. Out of all the BAC models, the Liu et al. (2016) model was the only one to be generated on the FVB/NJ background strain; the other three were generated on C57BL/6 or SJL strains. Furthermore, despite Jiang et al. (2016) and Liu et al. (2016) reporting similar repeat lengths in their C9 BAC mice, the former had increased levels of expression yet developed a much milder phenotype and no motor deficits. Therefore, it is possible the background strains used in these studies may have influenced phenotype. The effect of

background strain on phenotypes is discussed in more detail in section 1.3.3. Further investigations to identify which factors are responsible for the varying phenotypes across facilities are needed, of which this thesis is one.

Overall, these findings across the C9ALS/FTD BAC mouse models suggest that purely gain-of-function mechanisms may not be enough to cause neurodegeneration. While behavioural deficits and histopathology were present, the models are overexpression models and are not physiologically accurate. Rather, it is likely that more insults are needed to reach a threshold to trigger disease, perhaps in combination with *C9ORF72* haploinsufficiency and/or environmental factors (Chio et al., 2018).

1.3.3 Effect of Mouse Background Strain

Since the advent of genetic technology, a wide array of mouse models have been generated that exhibit a variety of genetic modifications such as gene knockouts, transgene insertions, and gene or base deletions to replicate human diseases. After the creation of mutant mouse founders, they must be crossed with an inbred strain for approximately 20 generations of brother-sister mating to ensure that 98.6% of the genome is homozygous between mice (Beck et al., 2000). This reduces the effects of genetic and phenotypic variability in subsequent studies.

Disease models of ALS/FTD are designed to recapitulate the disease to uncover the underlying pathophysiology and develop therapeutic interventions. As described in previous sections, a vast number of mouse models have been developed carrying mutations known to be implicated in ALS/FTD, such as *C9ORF72*, *SOD1*, and *TARDBP*. However, ALS/FTD is a heterogeneous disease, with age of onset and disease severity varying between patients and even between those with the same mutation (Regal et al., 2006). Surprisingly, harbouring a known ALS/FTD mutation does not guarantee that disease will develop. This heterogeneity suggests the presence of genetic modifiers or epigenetic differences in the genetic background of patients that can influence phenotype, alongside environmental and lifestyle effects. Increasing evidence supports the idea that ALS/FTD results via a combination of disease-associated genetic variants and environmental influences that synergise to cause

disease (Cirulli et al., 2015; Nguyen et al., 2018). Therefore, the natural genetic variability between patients may be responsible for the phenotypic variation observed.

Mouse models of ALS/FTD also demonstrate phenotypic heterogeneity due to genetic background and sex (Heiman-Patterson et al., 2011; Fisher and Bannerman, 2019), as do different wild-type strains when tested with a number of behavioural tests commonly used in animal research (Voikar et al., 2001). Therefore, the choice of background strain when generating a disease model must be carefully considered, as the differing genetics between strains can influence results and lead to possible misinterpretation of results.

The C9ALS/FTD BAC mouse model generated by Liu et al. (2016) is the focus of this thesis. As mentioned previously, the phenotype of this model is currently under debate due to conflicting results. The genetic background used to generate this model was an FVB/N line from The Jackson Laboratory (FVB/NJ). The FVB/N strain is a Swiss strain and was developed in the 1970s. It is a popular strain for transgenesis due to their large pronuclei, high breeding success, and large litter sizes (Taketo et al., 1991). They are functionally blind by 30 days due to retinal degeneration caused by the *Pde6b^{rd1}* gene, and perform poorly in tests that require vision, such as the Morris water maze (Pugh et al., 2004). FVB/N mice also exhibit an abnormal circadian rhythm and activity patterns compared to C57BL6/J mice (Pugh et al., 2004), likely because of their inability to sense light. They are also susceptible to spontaneous seizures (Goelz et al., 1998; Silva-Fernandes et al., 2010) and kainic acid-induced seizures (Royle et al., 1999; McCord et al., 2008). These seizures can develop into chronic, repetitive seizure activity that leads to a condition termed Space Cadet Syndrome (SCS). The first suggestion of SCS was from a study reporting 20% of female FVB/N mice between 4 to 12 months of age had been found dead following prior seizure activity (Mahler et al., 1996). The first description of a spontaneous seizure disorder in FVB/N mice was reported two years later, wherein 17.6% of mice over four years exhibited seizures, and over 90% of those mice were female (Goelz et al., 1998). SCS is a poorly characterised syndrome with very little information in the literature regarding its behavioural and neuropathological phenotypes and its impact on the use of FVB/N mice in research. What has been published suggests that SCS leads to withdrawal from social interaction, sudden death, neurodegeneration in the thalamus, cerebral cortex, and hippocampus, astrocytosis, reduced fertility, aggression, and infanticide (Hennemann, 2007).

Mordes et al. (2020) has suggested that SCS may have been responsible for the "acute" ALS/FTD phenotype reported by Liu et al. (2016) due to their striking phenotypic similarities. Nguyen et al. (2020a) dismissed the possibility and suggested methodological differences and a smaller number of non-transgenic animals used by Mordes et al. (2020) could be responsible for their lack of phenotype. They also suggested that the rederivation of the model at Jackson Laboratories following model deposition may have caused the loss of phenotype in groups that obtained the model from that source. While one of Mordes et al. (2020)'s colonies was indeed obtained from Jackson Laboratories, the other colony was obtained directly from Liu et al. (2016) at the University of Florida. However, both studies used FVB/N NT mice from The Jackson Laboratory, whereas the group at the University of Bern in Nguyen et al. (2020a) obtained their FVB/N non-transgenic mice from Janvier Labs. The Jackson Laboratory and Janvier Labs imported the FVB/N mice in 1988 and 1996, respectively. Exactly how these two groups now differ from each other is unknown, and it is possible that sufficient genetic drift may have occurred between the two to influence the ALS/FTD phenotype in the Liu et al. (2016) model (Uchimura et al., 2015; Chebib et al., 2021). Environmental influences could be at play and characterising both groups in the same facility eliminates this. Therefore, the first direct comparison of the model on the two FVB/N strains is performed in this thesis.

1.4 Aims and Objectives

The aims of the project were:

- To deeply characterise C9orf72 BAC mice obtained from Jackson laboratories.
- To deeply characterise C9orf72 BAC mice obtained from the University of Bern.
- To evaluate the utility of the C9orf72 BAC mouse model as a tool for preclinical research.

The objectives of the project were:

- To assess the motor, coordination, and cognitive abilities of C9orf72 BAC mice obtained from Jackson laboratories using a battery of behavioural and neurophysiological tests to explore the phenotype of the model.
- To assess the motor, coordination, and cognitive abilities of C9orf72 BAC mice obtained from Janvier laboratories using a battery of behavioural and neurophysiological tests to explore the phenotype of the model.

- To explore the effects of two FVB/N mouse strains on model phenotype and behavioural tests.
- To investigate neurodegeneration in the hippocampus, motor cortex, and spinal cord of transgenic C9orf72 BAC mice from Jackson and Janvier laboratories.

2   Methods

2.1   Ethics Statement

All mouse experiments were carried out in accordance with the Animals (Scientific Procedures) Act 1986 under a UK Home Office project licence. Mice were housed and cared for following the Home Office Code of Practice for Housing and Care of Animals Used in Scientific Procedures. All procedures were carried out under an appropriate UK Project Licence by personal licence holders.

2.2   C9orf72 Transgenic Mice

The C9orf72 transgenic mice used in this project were originally generated on an FVB/NJ background by pronuclear injection of a BAC containing the full-length human *C9ORF72* gene with ~500 hexanucleotide repeat expansions in intron 1a (Liu et al., 2016). Mice were subsequently deposited at The Jackson Laboratory (stock number 029099).

For the first study (chapter 3), transgenic males and non-transgenic females were obtained from The Jackson Laboratory and used for breeding (stock numbers 029099 and 001800, respectively). For the second study (chapter 4), four transgenic males were obtained directly from Prof. Smita Saxena's laboratory at the University of Bern, Switzerland, after reports of an acute ALS phenotype (Nguyen et al., 2020a) and were mated with non-transgenic FVB/N females from Janvier Labs (stock number SC-FVBN-F). Both the Jax and Janvier colonies did not interbreed and were kept separate. Only female mice were used in both studies as they exhibited the most severe phenotype in the initial report (Liu et al., 2016).

2.3   Animal Housing

Mice were bred in a specified pathogen free (SPF) facility and then transferred to a conventional facility for the studies described hereafter. Mice were housed in a 12-hour light/dark cycle, room temperature at 21°C and 45-55% humidity. All mice were housed in cages lined with sawdust, changed once or twice weekly, with a plastic house and shredded paper bedding. Some cages had metal rings attached to the cage lid or clear plastic tubes for enrichment. Mice were fed 2018 Teklad Global Rodent Diet (Envigo) and water *ad libitum*.

All mice were housed with same-sex littermates with 3-5 mice per cage. However, some mice were singly housed during the studies due to fighting or cagemate death.

2.4   Genotyping

The presence or absence of the BAC human *C9ORF72* transgene was determined by touchdown polymerase chain reaction (PCR). DNA was extracted from ear clips used for identification by incubating in 20 μl QuickExtract™ DNA Extraction Solution (Lucigen) at 60°C for 30 minutes. 1 μl of DNA was added to 2 μl of 5x Firepol Master Mix (Solis Biodyne), 4.5 μl of water, 0.25 μm of each C9BAC primer (forward: 5'-TCG AAA TGC AGA GAG TGG TG-3'; reverse: 5'-CTT CCT TTC CGG ATT ATA TGT G-3') and 1 μm of mouse beta actin control primer (forward: 5'-CTG TCC CTG TAT GCC TCT GG-3'; reverse: 5'-AGA TGG AGA AAG GAC TAG GCT ACA-3').

The following PCR protocol was run on a thermocycler (G-Storm, UK): initial denaturation period of 2 minutes at 94°C, followed by 10 cycles of 94°C for 20 seconds, 65°C for 15 seconds and 68°C for 10 seconds, with a 0.5°C decrease per cycle. This was followed by 28 cycles of 94°C for 15 seconds, 60°C for 15 seconds and 72°C for 15 seconds. Following this was a 2-minute elongation period at 72°C. Samples were stored at 10°C before removal from the machine.

Results were imaged by gel electrophoresis. A 1% w/vol agarose/1x TAE gel solution was heated until fully dissolved. 1% ethidium bromide was added and the solution poured into a gel mould. Once set, the gel was placed into a gel tank and submerged in 1X TAE solution. 5 μl of 100bp hyperladder (Bioline, UK) was loaded into the first well and then 10 μl of PCR product was loaded into each subsequent well. The gel was run at 100 V for 30 minutes and then imaged under UV light in a G:BOX (Syngene, UK).

Transgenic samples were identified by the presence of the BAC transgene indicated by PCR product at ~300 bp and the control PCR product at ~450 bp. Non-transgenic (NT) samples were identified by a single PCR product at ~450 bp.

2.4.1 Southern Blot

A Digoxigenin (DIG) Southern Blot protocol kindly provided by Ludo Van Den Bosch (KU Leuven) was optimised to size the *C9ORF72* repeat expansion in all transgenic mice.

DNA was extracted from brain tissue using a Qiagen DNeasy Blood & Tissue Kit (Cat. No.: 69504) following manufacturer's instructions. Following extraction, ~10 µg DNA was digested with AluI and DdeI restriction enzymes (New England Biolabs) at 37°C for 16 hours in a thermocycler (G-Storm, UK). A 1% w/vol agarose/1x TAE gel solution was heated until dissolved and poured into a gel mould until set. Once set, the gel was placed into a gel tank and submerged in 1X TAE solution. 5 µl of DIG-labelled molecular weight marker III (Roche) was loaded into the first and last wells, and then all digested DNA was loaded into the remaining wells. The gel was run for 2h at 80V. Following electrophoresis, the gel was submerged in denaturation solution (1.5M NaCl, 0.5M NaOH) followed by neutralisation solution (3M NaCl, 0.5M Tris, pH 7.5) for 45 minutes each time with gentle rocking at room temperature (RT).

DNA was transferred to a positively charged nylon membrane (Amersham Hybond N+) by capillary blotting overnight. The gel was place on a bridge of 2 layers of 3mm Whatman Chromatography paper (Cytiva) saturated with 20X SSC transfer buffer (0.3M sodium citrate, 3M NaCl, pH 7). A positively charged nylon membrane was cut to the size of the gel, saturated in 5X SSC transfer buffer and placed on top, followed by 2 layers of Whatman paper saturated in 5X SSC transfer buffer, 2 layers of dry Whatman paper, 8 layers of dry Grade GB005 blotting paper (Merck), 4 inches of tissue paper and two 500 g weights. Following transfer, the membrane was washed with 2X SSC for 5 minutes at RT on a rocker before UV crosslinking at 210,000 µJ on a transilluminator (UVP, TL-2000). The membrane was washed again in 2X SSC for 5 minutes at RT on a rocker.

For pre-hybridisation, the membrane was transferred into a glass hybridisation tube with 30 ml of pre-warmed DIG Easy Hyb™ solution (Sigma-Aldrich) and rotated in a hybridisation oven for 4 hours at 48°C. Following this, the membrane was hybridised with 100ng/ml DIG-labelled

oligonucleotide probe 5' [DIG]-(GGGGCC)x5-[DIG] 3') in a hybridisation oven overnight (16 hours) at 48°C.

The membrane was washed with pre-warmed 2X SSC 0.1% SDS for 10 minutes while ramping the temperature from 48 - 65°C, then washed again with 2X SSC 0.1% SDS for 10 minutes, 0.5X SSC 0.1% SDS for 15 minutes, and 0.2X SSC 0.1% SDS for 15 minutes, all at 65°C. The membrane was transferred to a plastic tray and washed using the DIG Wash and Block Buffer Set (Sigma-Aldrich) following manufacturer's instructions. In summary, the membrane was washed with 200 ml wash buffer for 5 minutes, blocked with 200 ml blocking solution for 60 minutes, then incubated with Anti-DIG antibody (11093274910, Sigma-Aldrich) at 1:20,000 dilution in blocking solution for 30 minutes. This was followed by three washes in 100 ml of wash buffer for 10 minutes each, followed by equilibration in 50 ml of detection buffer for 5 minutes. All wash steps were done with vigorous rocking, blocking and antibody incubation with gentle rocking, and equilibration done on the bench. All steps were done at RT.

The membrane was placed on a plastic sheet and ~50 drops of CSPD ready-to-use chemiluminescent substrate (Roche) were added. After incubating for 5 minutes at RT the plastic sheet was sealed and excess CSPD pressed out. The membrane was incubated at 37°C in the dark for 10 minutes. The membrane was exposed to chemiluminescent film (Amersham, Cat No. 28906837) for 3 hours in a dark room. Signal was visualised by submerging the film in developer solution (Ilford Multigrade) for 5 minutes, followed by fixative solution (Ilford Multigrade) for 5 minutes, before rinsing in water and leaving to dry.

2.5   Behavioural Tests

All mice underwent behavioural testing from 12 weeks of age to 52 weeks of age. Unless otherwise specified, all the following behavioural tests were performed at monthly intervals.

2.5.1   Distress Scoring

Mice were distressed scored weekly using a scoring system adapted from previous studies (Mead et al., 2011)(Table 2.1). Seizures observed were timed at onset or from time of discovery and scored according to the scale in Table 2.2.

Table 2.1: Scoring system for animal welfare.

Animals with a cumulative score of 10–16 or a maximum score in three categories were considered to have reached humane endpoint and were euthanised. Weight loss was calculated by comparison with weight recorded at 12 weeks of age.

Parameter	Description	Score
Weight loss	0–10%	0
	10–19%	1
	>20%	3
Appearance	Normal	0
	Lack of grooming (dusty coat)	1
	Lack of grooming and hunched	2
Behaviour	Normal, bright, inquisitive	0
	Stereotypic behaviour (circling)	1
	Mostly inactive, responds if provoked	2
	Inactive, does not respond if provoked	4
Clasping	Both hind limbs splay normally	0
	One hind limb splays normally	1
	Both hind limbs close to abdomen	2
	Both hind limbs tightly clasped	4
Neurologic	Normal	0
	Immobile and staring	1
	Seizure (<5 seconds) with recovery **or** hindlimb paralysis	2
	Seizure (>10 seconds) **or** any seizure plus hind limb paralysis	4

Table 2.2: Seizure scoring system.

Taken from Van Erum et al. (2019). Severe or repetitive seizures, or failure to recover from seizure, resulted in euthanasia.

Severity	Score	Phenotype
Mild	1	Whisker trembling
	2	Sudden behavioural arrest
	3	Facial jerking
Moderate	4	Neck jerks
	5	Clonic seizure (sitting)
	6	Clonic, clonic-tonic seizure (lying on belly)
Severe	7	Clonic, clonic-tonic seizure (lying on side) & wild jumping
	8	Tonic extension, possibly leading to respiratory arrest and death

2.5.2 Open Field Test

Mice were placed in a 45 cm x 45 cm x 45 cm grey acrylic chamber under white light. Their behaviour was video-recorded and analysed using Smart Video Tracking Software V3.0 (Panlab, Harvard Apparatus) for 10 minutes. Distance travelled and time spent in the centre zone (25 cm x 25 cm) and periphery zone of the chamber were examined to measure locomotion and levels of anxiety, respectively (Elston et al., 2014).

2.5.3 Accelerating Rotarod Test

Mice were placed on an accelerating rotarod (Ugo Basile 47600) which gradually rotated from 4 rpm to 40 rpm over a period of 300 seconds. The test was carried out at a similar time and on the same day of the week. Mice were initially trained on the rotarod over 3 consecutive days at 12 weeks of age before the first test, then tested monthly thereafter. During these tests each animal underwent two trials with at least five minutes between each trial and the best performance was used for analysis.

2.5.4 Burrowing Test

Burrowing tubes (7 cm x 7 cm x 20 cm) were made from plastic piping and sealed at one end. The open end of the burrowing tube was elevated by approximately 1 cm using machine screws (5 cm) inserted 1 cm from the opening (Figure 2.1) (Deacon, 2012).

Individual mice were placed into a cage (42.5 cm x 26.6 cm x 18.5 cm) lined with sawdust (~1 cm) and access to food and water ad libitum. A burrowing tube was filled with 200 g of food pellets (2018 teklad global rodent diet, Envigo) and placed into the cage. After two hours, a baseline measurement was taken. The burrow was emptied and the food pellets weighed before being replaced into the burrow and returned to the cage. This weighing procedure was completed even if no pellets had been burrowed out of the tube to provide a consistent environment. The weight burrowed was calculated by subtracting from 200 g. The final reading was taken the following morning.

Figure 2.1: Burrowing test cage layout pre-test.

The burrow was filled with 200 g food pellets and left overnight. The following morning, the remaining food pellets inside the burrow were weighed to calculate the amount burrowed out.

2.5.5 Marble Burying Test

Individual mice were placed in a cage (42.5 cm x 26.6 cm x 18.5 cm) filled with 5 cm of sawdust. 10 glass marbles (1 cm diameter) were placed in two columns of 5 marbles at evenly spaced intervals on the surface of the sawdust (Figure 2.2) (White et al., 2018). Mice were left undisturbed for 30 minutes under white light before being removed and the number of marbles buried counted. A marble was classed as buried when 2/3 covered by sawdust.
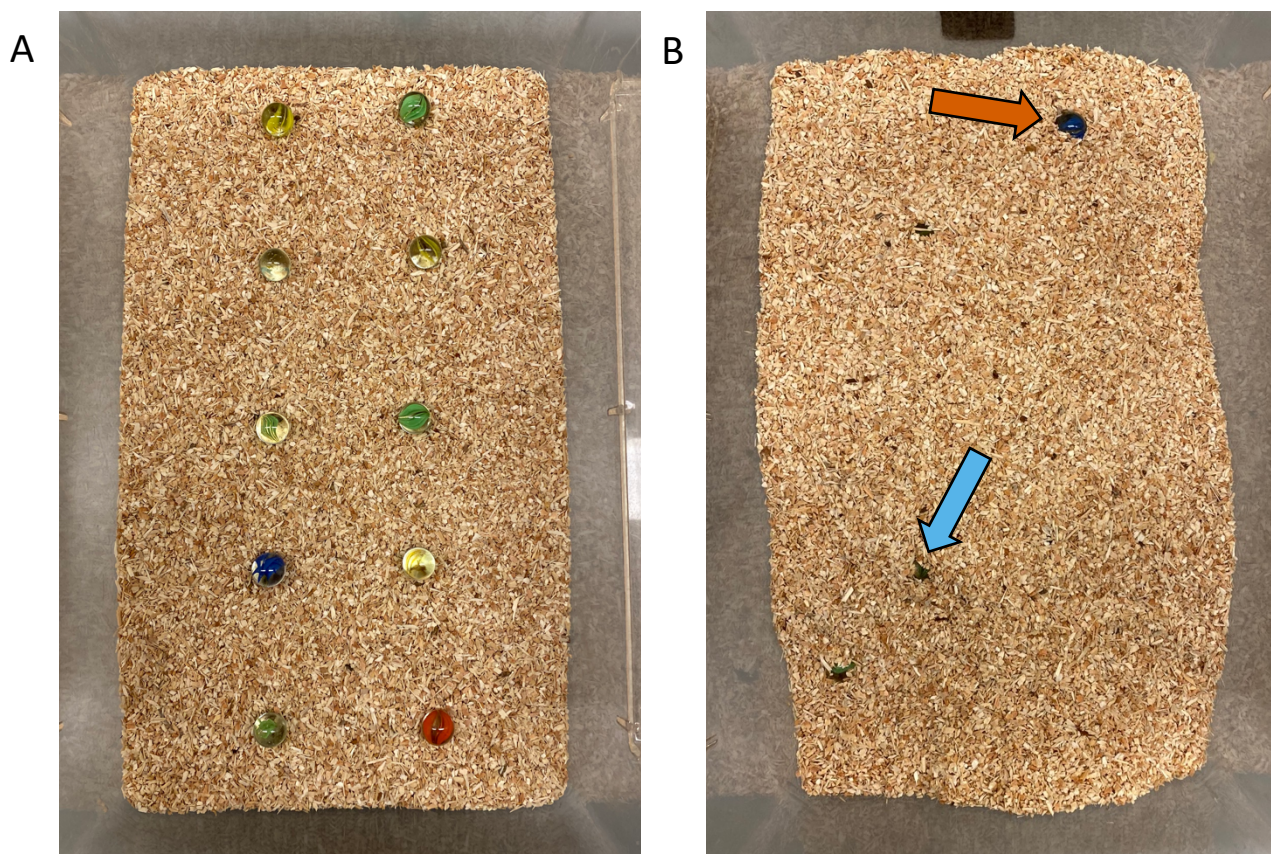
Figure 2.2: Marble burying pre-test (A) and post-test (B).

(A) Marbles were placed in a 2x5 grid. After the test (B), marbles buried were counted. Marbles were classed as not buried if <2/3 covered by sawdust (orange arrow) and buried if >2/3 covered by sawdust (blue arrow).

2.5.6 Nesting Behaviour Test

Individual mice were placed in a cage (42.5 cm x 26.6 cm x 18.5 cm) filled with a thin layer (~1 cm) of sawdust and access to food and water ad libitum. A 'nestlet' (2 inches x 2 inches, Ancare) was weighed and placed in the centre of each cage (Figure 2.3) (Deacon, 2012;

Warmus et al., 2014). The following morning, the nest was scored using the following 6-point scale and the amount of untorn nestlet weighed:

0. The nestlet is almost entirely untouched (>99% intact).
1. The nestlet is mostly intact (>90% intact).
2. The nestlet is partially torn up (50-90% intact).
3. The nestlet is mostly torn up (10-50% intact).
4. The nestlet is almost entirely torn up (<10% intact) with nest walls higher than the mouse body on <50% of its circumference.
5. The nestlet is almost entirely torn up (<10% intact) with nest walls higher than the mouse body on >50% of its circumference.

For scores 1-3, 0.5 was added if there was an identifiable nest site.

Figure 2.3: Nesting cage layout pre-test (A) and post-test (B).

Nestlets were weighed and placed in the centre of the cage (A) and left overnight. The following morning the nest was scored using a 6-point scale and the amount of untorn nestlet (B).

2.5.7 Food Intake

During the nesting behaviour test, food pellets were weighed before being placed in the hopper. The following morning the remaining food pellets were weighed and the weight eaten was calculated.

2.5.8 Balance Beam Test

Mice were placed on a cage ledge and observed walking along it (Guyenet et al., 2010). Each mouse was scored using the following criteria:

0. The mouse walks along the ledge without losing balance and easily lowers itself back into the cage.
1. The mouse loses its footing while walking along the ledge but looks otherwise coordinated.
2. The mouse does not effectively use its hind legs or lands on its head rather than its paws when descending into the cage.
3. The mouse falls off the ledge, or nearly so, while walking or attempting to lower itself, or shakes and refuses to move despite encouragement.

Each mouse underwent three trials and the median score from the trials was taken for analysis.

2.5.9 Limb Hang Test

A metal grid was placed 35 cm above a cage (42.5 cm x 26.6 cm x 18.5 cm) filled with approximately 5 cm of sawdust to provide a soft landing (Carlson, 2011). Each mouse was placed on the grid for 3–5 seconds before the grid was inverted over the cage. The hang period began with all four paws grasping the grid. The hang time was then measured from when the grid was inverted to when the mouse fell.

Any mouse that jumped off the grid was immediately re-tested. Each mouse underwent two trials, with at least 5 minutes between each trial, and the average time and the longest time

were used for analyses. Each mouse was weighed immediately prior to or following the test to account for the effect of weight on hang time.

2.5.10 Catwalk Gait Analysis

The catwalk gait analysis system 7.1 (Noldus Information Technology B.V., Netherlands) was used to capture gait parameters. Mice were placed onto the catwalk and allowed to walk freely in total darkness. 6 straight, continuous runs were recorded, and the 3 best runs were chosen for analysis. The Catwalk Software 7.1 was used to manually label each paw print of a run to analyse the gait of each mouse. Data were collated using Microsoft Excel and informative parameters chosen for analysis (Table 2.3).

Table 2.3: Descriptions of catwalk gait analysis parameters chosen for analysis.

Parameter	Description
Stride Length	Distance between successive placements of the same paw.
Base of Support	Average width between either the front or hind paws.
Swing Time	Duration of no contact with the glass plate in a step cycle.
Swing Speed	Speed of the paw during swing.
Print Length	Length of a complete paw print on the glass plate.
Print Width	Width of a complete paw print on the glass plate.
Regularity	A measure of inter-paw coordination by calculating the number of normal step sequence patterns relative to the total number of paw placements. 100% is perfectly coordinated.
Intensity	A measure of weight supported on the paws. Higher intensity = more weight on the paws.
Support	The percentage of time any number of paws is on the glass plate at any time during each run. Zero = no paws, single = one paw, diagonal = two diagonally opposite paws (e.g. left front paw and right hind paw), lateral = two vertically opposite paws (e.g. left front paw and left hind paw), girdle = two horizontally opposite paws (e.g. left front paw and right front paw).
Duty Cycle	A measure of stance duration expressed as a percentage of the duration of each stride.

2.5.11 Social Recognition Test

Adult mice were placed into a 45 cm x 45 cm x 45 cm grey acrylic chamber under white light with an empty mesh cage in the centre immediately prior to testing and allowed to habituate to the environment for 10 minutes. The adult mouse was removed from the chamber and a juvenile NT female mouse was placed into the mesh cage in the centre. The adult mouse was returned to the chamber for the initial interaction trial of 2 minutes. The trial was repeated with the same juvenile female mouse 3 days later (recall session), followed by a trial with an unfamiliar juvenile NT female mouse (novel session) (Kogan et al., 2000; Jacobs et al., 2016).

Each trial was video-recorded and analysed using Smart Video Tracking Software V3.0 (Panlab, Harvard Apparatus). Time spent investigating the juvenile mouse was calculated and used for analysis. Investigation was defined as any contact exceeding 1 second. Recognition index was calculated as time spent investigating in recall session relative to time spent investigating in initial session.

2.5.12 Running Wheel Test

A short running wheel study was added at the end of the 12-month behavioural study of the Janvier mice (chapter 4) to assess the effect of voluntary exercise on ALS phenotype.

All mice were housed separately in a large cage (42.5 cm x 26.6 cm x 18.5 cm) lined with sawdust. A 37.8 cm circumference running wheel at a 25 ° angle was attached to a mount and placed in the corner of the cage. A neodymium magnet was attached to the edge of the running wheel and a bike computer (Cateye Velo, Japan) with a reed switch was fixed to the outside of the cage. Food and water were available *ad libitum*. Time spent running, distance travelled, max speed, and average speed were taken daily.

2.5.13 Electrophysiological Tests

Electrophysiology of the hindlimb was carried out at 3, 6, 9 and 12 months of age in all NT and C9orf72 mice. Mice were anaesthetised (1-2% isoflurane, flow rate 0.5L/min oxygen through a nose cone). The left hindlimb was shaved and depilatory cream used to remove all fur.

Recordings were made using a Dantec Keypoint Focus EMG System (Optima, UK). Ring electrodes (Natus Neurology) were coated with Ten20 nerve conductive paste (Pulse Medical Ltd, UK) and placed around the distal hindlimb muscles, and a grounding electrode (Ambu Neuroline, UK) was placed in the tail (Figure 2.4). For compound muscle action potential (CMAP) and repetitive nerve stimulation readings, stimuli were applied using a twisted pair of electrodes placed on the skin over the sciatic notch (Ambu Neuroline, UK).
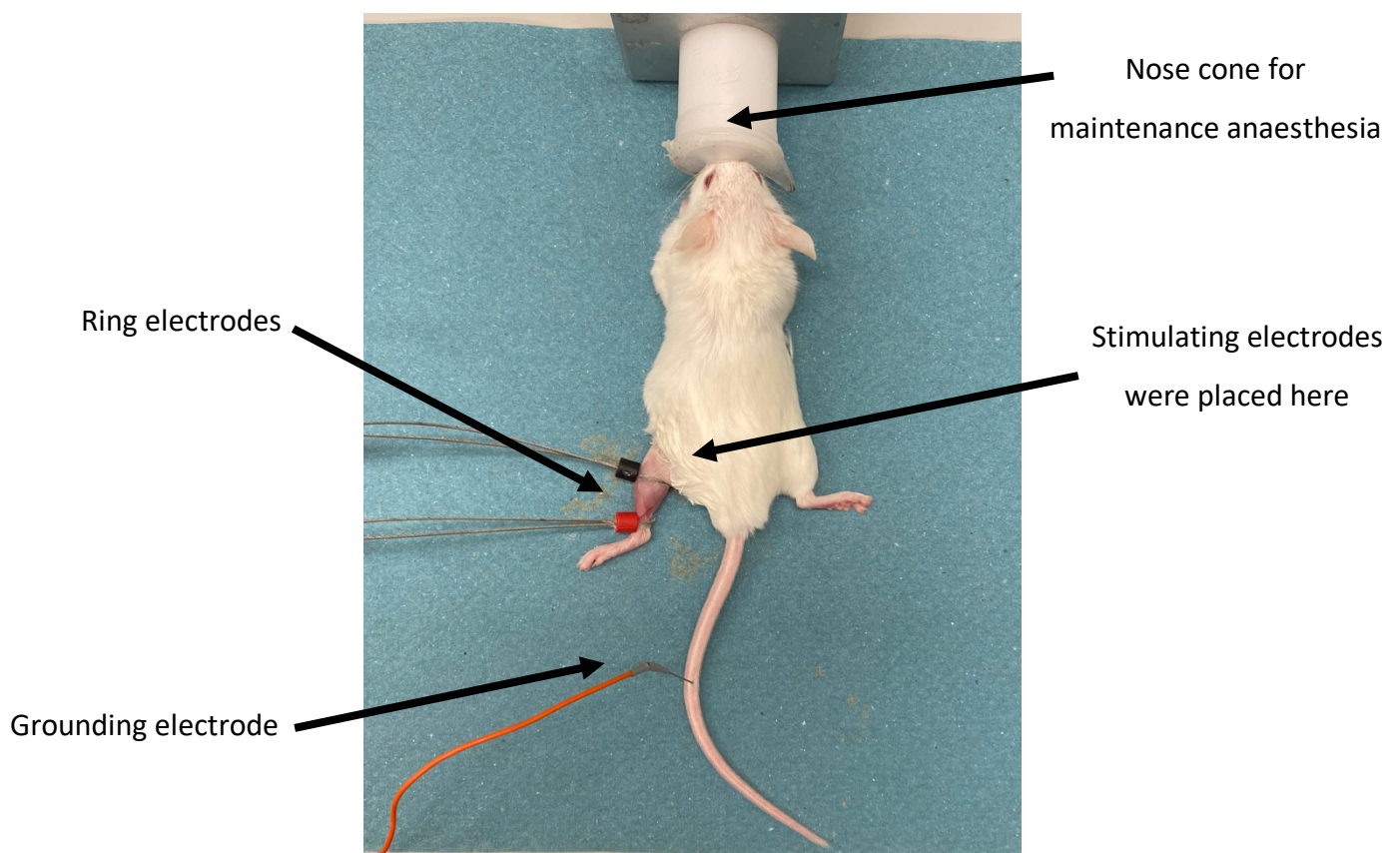
Figure 2.4: Electrophysiology of the hindlimb.

Mice were anaesthetised and maintained through a nose cone. Fur was removed from the hind limb with depilatory cream and ring electrodes placed around the distal hindlimb. A grounding electrode was placed in the tail and stimulating electrodes placed at the sciatic notch (not pictured).

CMAPs were acquired by applying a series of single, square-wave electrical impulses of 0.1ms to the sciatic notch. Stimulation intensity was then increased incrementally until no further increase in amplitude was seen (i.e. a supramaximal response was obtained). This amplitude was taken for analysis. For repetitive nerve stimulation, the stimulating electrodes were held in the same place and 10 supramaximal stimuli were delivered at 10Hz. The change in CMAP amplitudes relative to the 1st CMAP were used for analysis. A steady response is indicative of a healthy NMJ, while a response decrement of >10% is considered abnormal.

At 52 weeks of age, plantar interosseous muscle CMAPs and F wave recordings were also taken. A twisted pair of subdermal needles (Ambu Neuroine, UK) were inserted subdermally into the 2nd interosseous space and along the tibial nerve above the ankle. Stimuli were applied using a twisted pair of electrodes (Ambu Neuroline, UK) placed on the skin over the lateral aspect of the gastrocnemius muscle to stimulate the tibial nerve. A plantar interosseous CMAP was acquired and taken for analysis. For F wave recordings, 30 consecutive stimulations at 1 Hz were applied and examined for F waves. If present, F wave latencies and persistence were calculated and taken for analysis.

Lastly, EMG recordings of the gastrocnemius muscle were undertaken by my supervisor, Dr James Alix, to examine for spontaneous EMG activity (fibrillation potentials, positive sharp waves, and fasciculation potentials) using a 30-gauge concentric cable electrode (Ambu Neuroline, UK).

2.5.14 Blood Collection

Blood samples were collected at 6 and 12 months of age for neurofilament analyses. Approximately 200 µl of blood was taken from the tail vein and collected in a 1.5 ml Eppendorf containing 4 µl 0.5M EDTA to prevent clotting. The sample was immediately centrifuged at 10,000 xg for 5 minutes and the plasma pipetted into a fresh 1.5 ml Eppendorf and immediately frozen in liquid nitrogen. At 12 months of age, the blood sample was collected during tissue collection and was taken via the heart using a 27-gauge needle syringe.

2.5.15 Faeces Collection

Faeces were collected at 6 and 12 months of age for microbiome analyses. Mice were individually placed in a sterile chamber and several pellets of faeces were collected in a 1.5 ml Eppendorf and immediately snap frozen in liquid nitrogen.

2.5.16 Tissue Collection

Mice were sacrificed at 12 months of age by an overdose of pentobarbitone delivered intraperitoneally, followed by transcardial perfusion with sterile 1x phosphate buffered saline (PBS). Once deeply anaesthetised (assessed by the absence of the pedal reflex) but prior to cardiac cessation, a thoracotomy was performed to expose the heart. The left ventricle was cannulated with a syringe containing PBS and the right atrium was cut. The mouse was then perfused with PBS.

A lobe of the liver and 1 cm of tail were dissected and immediately frozen in liquid nitrogen. The tibialis anterior (TA), and the gastrocnemius from half of the mice in each group, were extracted and frozen in OCT embedding matrix (CellPath, UK) by submersion in isopentane cooled in liquid nitrogen, then stored at -80°C. The remaining gastrocnemius muscles were immediately frozen in liquid nitrogen following dissection.

Spinal cords were extracted and placed in 4% paraformaldehyde (PFA) in PBS overnight before being transferred to PBS and stored at 4°C. In half of the mice in each group, the cervical portion of the spinal cord was dissected prior to fixation and frozen in liquid nitrogen.

Brains were extracted from the skull and separated into two hemispheres. The left hemisphere was snap frozen in liquid nitrogen, and the right hemisphere was placed in 4% PFA in PBS overnight before being transferred to PBS and stored at 4°C.

2.6   Tissue Pathology

2.6.1   Tissue Preparation

For lumbar spinal cord sectioning, the centre of the lumbar enlargement was located and the cord cut 6 mm either side. After processing, the 12 mm piece was cut in half and embedded in paraffin wax. Lumbar sections were sectioned at 10 μm using a microtome (Leica Biosystems, RM2245) and mounted on charged slides (Starfrost, Germany). Sections were mounted serially over series' of 5 slides, with 4 sections per slide for a total of 20 slides.

For brain sectioning, the fixed tissue was sliced on a mouse brain matrix (Agnthos, Sweden) to isolate either the motor cortex or the hippocampus. The tissues were processed and embedded in paraffin wax. The motor cortex and hippocampus were sectioned coronally and sagittally, respectively, at 5 μm on a microtome and mounted onto charged slides. Sections were mounted continuously, with 3 sections per slide for a total of 16 slides.

2.6.2   H&E Staining

Slides were deparaffinised in two changes of xylene and rehydrated through graded ethanol. The slides were submerged in Harris' haematoxylin for 2 minutes and washed in water before differentiation in acid alcohol. The slides were washed in water again before 'blueing' in Scott's Tap Water. Next, the slides were submerged in eosin for 5 minutes, briefly washed in water, dehydrated through graded ethanol, and then cleared in xylene. The sections were coverslipped using DPX mounting media and left to dry overnight at 37°C. Slides were visualised using a digital slide scanner (NanoZoomer XR, Hamamatsu).

2.6.3   Nissl Staining

Slides were deparaffinised in two changes of xylene and rehydrated through graded ethanol. The slides were submerged in 0.25% cresyl violet for 2 minutes and differentiated in 0.25% acetic acid in alcohol for 10 seconds. Slides were then briefly immersed in 100% ethanol, cleared in xylene, and coverslipped using DPX mounting media and left to dry overnight at 37°C. Slides were visualised using a digital slide scanner (NanoZoomer XR, Hamamatsu).

2.6.4 Immunohistochemical Staining

2.6.4.1 GFAP and Iba1

Slides were deparaffinised in two changes of xylene and rehydrated through graded ethanol. Slides were then placed in an antigen access unit and submerged in access revelation buffer pH 9 (Biocare Medical) for a 30-minute cycle at 125 °C with a pressure of 20 pounds per square inch (psi).

Slides were washed with 125 mM glycine 0.4% Triton X-100 in PBS for 10 minutes on a shaker at RT and then washed in 1x PBS on a shaker at RT for 5 minutes. Sections were blocked with 5% bovine serine albumin (BSA) 0.25% Triton X-100 in PBS for 20 minutes at RT, then incubated with primary GFAP (abcam, Ab4674) and Iba1 (GeneTex, GTX100042) antibodies diluted in 1% BSA 0.25% Triton X-100 in PBS overnight at 4°C.

After 3 x 8-minute washes in PBS on a shaker, sections were blocked with 5% BSA for 10 minutes at RT. Next, they were incubated with secondary antibodies (A11039, A27039) diluted in 1% BSA for 90 minutes in the dark at RT.

After 4 x 8-minute washes in PBS on a shaker in the dark, the slides were submerged in distilled water and washed on a shaker for 5 minutes in the dark. Sections were coverslipped using Hardset Vectashield with 4',6-diamidino-2-phenylindole (DAPI) mounting medium (Vectorlabs) and left to dry at RT in the dark overnight. Slides were stored at 4°C and imaged using an IN-Cell Analyzer 2000 (GE Healthcare).

To assess astrocytosis and microgliosis in the hippocampus and motor cortex, fluorescence staining using GFAP and Iba1 antibodies was performed. Images were taken at 20x magnification and quantitative analysis was performed using ImageJ software. Parameters taken for analysis were percentage area staining and integrated density (a measure of staining intensity) when staining for GFAP. Increases in these parameters are indicative of GFAP immunoreactivity and astrogliosis (Hausmann, 2003). The same parameters were analysed for Iba1 staining, as well as an additional parameter of circularity. This is a measure of the shape of microglia, with a more rounded shape indicating hyper-ramified microglia which,

along with increased area and intensity of staining, is suggestive of microglial activation and neuroinflammation (Cao et al., 2021).

2.6.4.2   NeuN Staining

NeuN staining was done by DAB staining using a Vectastain Elite ABC-HRP peroxidase (Rabbit IgG) kit (PK6101) and a DAB substrate kit (Vectorlab SK-4100).

Slides were deparaffinised in two changes of xylene and rehydrated through graded ethanol. Slides were then placed in an antigen access unit and submerged in access revelation buffer pH 6 (Biocare Medical) for a 30-minute cycle at 125 °C with a pressure of 20 psi. Endogenous peroxidase activity was blocked by incubating the slides in 3% H_2O_2 in methanol for 20 minutes at RT, followed by a wash in PBS for 5 minutes on a shaker. Sections were blocked with 5% normal goat serum in 1% BSA/PBS for 30 minutes at RT, then incubated for 1 hour at RT with primary NeuN antibody (Cell signalling, 12943) diluted to 1 in 500 in 5% normal goat serum in 1% BSA/PBS.

After 3 x 5-minute washes in PBS on a shaker, sections were incubated with secondary antibody diluted to 1 in 200 in 5% normal goat serum in 1% BSA/PBS for 30 minutes at RT. After 3 x 5-minute washes in PBS on a shaker, sections were incubated with ABC-HRP reagent for 30 minutes at RT. After 3 x 5-minute washes in PBS on a shaker, sections were incubated with DAB substrate for 1.5 minutes before quenching in dH_2O for 1 minute. Sections were counterstained in haematoxylin for 2 minutes, rinsed in tap water, immersed in Scott's Tap Water for 30 seconds, dehydrated through graded ethanol, and cleared in xylene. Sections were coverslipped with DPX mounting media and left to dry overnight at 37°C. Slides were visualised using a digital slide scanner (NanoZoomer XR, Hamamatsu).

2.6.5 Motor Neurone Counting in the Spinal Cord

Motor neurone counting was performed blinded. QuPath open-source software was used to count motor neurones in the ventral horns of nissl-stained lumbar spinal cord tissue. 4 slides per mouse, with 8 sections per slide, were counted. Sections on each slide were separated by 50 μm to prevent double counting. Motor neurones were identified only if they had a clearly

visible, nissl-stained nucleolus and a soma size larger than 25 µm. Motor neurones per ventral horn were analysed on Graphpad Prism 9 using a nested t-test.

2.6.6 Neurone Counting in the Brain

Neurone counting was performed blinded. QuPath open-source software was used to count neurones in the cornu ammonis (CA) and dentate gyrus (DG) regions of the hippocampus and Layer V of the motor cortex of NeuN-stained tissue using the built-in positive cell detection algorithm. 4 slides per mouse, with 3 sections per slide, were counted. Slides were separated by 40 µm to prevent double counting. Neurones per mm^2 were analysed on Graphpad Prism 9 using a nested t-test.

2.6.7 Meso Scale Discovery (MSD) Assay

Quantification of DPR protein in the frontal cortex and gastrocnemius muscle of C9orf72 and age-matched NT littermates was done using an MSD Elisa assay performed by Ms Ergita Balli and Dr Adrian Higginbottom. Sample preparation and protein extraction were done by me. An approximate 3 mm x 3 mm piece of tissue was placed into screw top 1.5 ml tubes with ~20 Zirconium Oxide beads (1.4 mm, Precellys P000927-LYSK0-A.0). A working solution of 1x reporter lysis buffer was prepared (5x reporter lysis buffer, 20 µl/ml protease inhibitor cocktail, and 20 µl/ml PMSF) and 400 µl added to each sample. The samples were homogenised at 5500 rpm for 2 x 30 seconds, placed on ice for 10 minutes, and homogenised again at 5500 rpm for 2 x 30 seconds. The samples were then centrifuged at x17,000 g for 10 minutes at 4°C. The supernatant was transferred into a fresh 1.5 ml Eppendorf and protein concentration determined using a Bradford Assay. Samples were diluted with 1x reporter lysis buffer to 1 mg/ml or 2 mg/ml for cortex and muscle samples, respectively. Samples were loaded into a 96-well plate and given to Ms Ergita Balli or Dr Adrian Higginbottom.

2.6.8 Golgi Staining and Sholl Analysis

Mice were sacrificed as described in section 2.5.16 and one brain hemisphere stained using the FD Rapid GolgiStain™ Kit (FD NeuroTechnologies) following manufacturer's instructions. The motor cortex was isolated using a mouse brain matrix (Agnthos, Sweden) and sectioned coronally at 100 µm on a cryostat (Leica CM3050 S) before staining. Mr Daniel Fillingham

performed the impregnation, sectioning, and staining of brain tissue following manufacturer's instructions.

For analysis, Z-stacked images were taken using a Nikon ECLIPSE Ti Series Microscope with DS-Fi3 Colour Camera at 20x magnification. Five pyramidal neurones in Layer V of the motor cortex were selected randomly per mouse using the following criteria: 1) visible soma, 2) no overlap with other cells. Images were analysed using ImageJ. Images were converted to eight-bit files and a threshold applied to isolate the cell and corresponding processes. The Neuroanatomy Simple Neurite Tracer plugin (Arshadi et al., 2021) was used to manually trace all processes from the soma and the primary paths were merged into a shared root. The centre of the Sholl analysis was placed at this shared root and concentric circles placed at 1 µm apart to detect the number of intersections. Number of branch points and terminal tips were also taken for analysis. Data was analysed using a mixed effects model and corrected for multiple comparisons by controlling the false discovery rate (Wilson et al., 2017).

2.6.9 Statistics

Graphpad Prism 9 and RStudio were used for all statistical analyses. Repeated Measures Two-Way ANOVA with post-hoc Tukey was used for analysis unless otherwise stated. All data are presented as mean and standard deviation, unless otherwise stated, to display data variability.

To identify possible latent subsets within the data, a method was devised to assess the performance of each mouse in each behavioural test. A scoring system was created to describe nine different data patterns, detailed in Table 2.4 and Figure 2.5. Some of those scores represent potential ALS-compatible phenotypic changes, which are defined in Table 2.5, and represent consistent dysfunction or a deterioration in function without improvement. The remaining scores represent normal function expected in a healthy mouse. To perform the analysis, the median and interquartile ranges were calculated for each behavioural test. The performance of each mouse in each test was manually checked at each timepoint against these values and a score assigned using the criteria detailed in Table 2.4. The number of times each score was assigned per test was tallied for C9orf72 and NT groups.

The number of times each ALS-like score and normal score was assigned per test was then tallied for C9orf72 and NT groups in a contingency table. Graphpad Prism 9 was used to perform a Fisher's exact test.

Table 2.4: Subset analysis scoring criteria.

Code	Code description
1	Stable – in the same quartile throughout
2	Stable poor – consistently in the bottom quartile
3	Stable good – consistently in the top quartile
4	Increase (change quartile) then stable
5	Increase (change quartile) then increase (change quartile)
6	Increase (change quartile) then decrease (change quartile)
7	Decrease (change quartile) then stable
8	Decrease (change quartile) then increase (change quartile)
9	Decrease (change quartile) then decrease (change quartile)
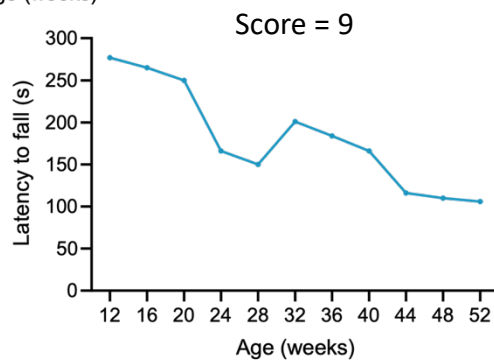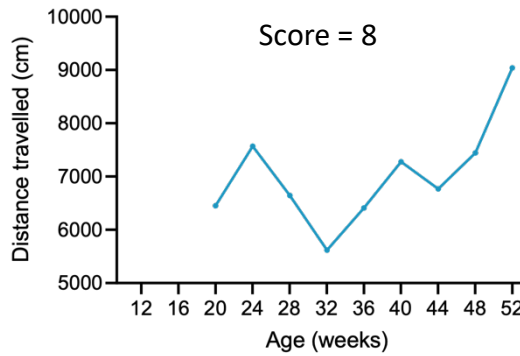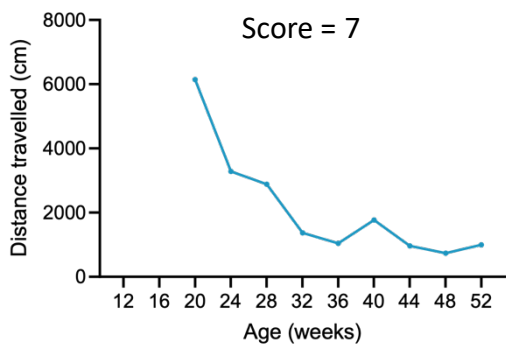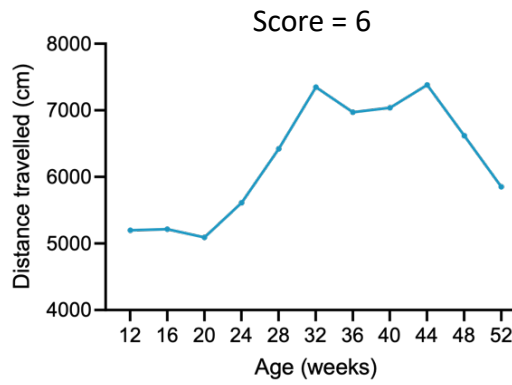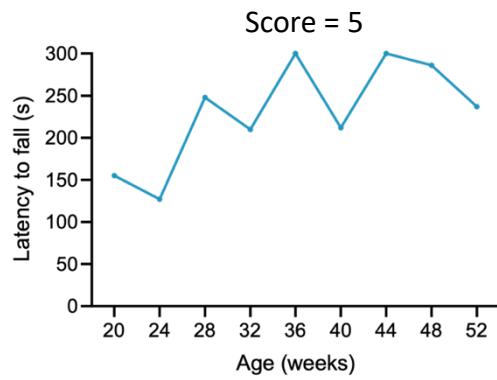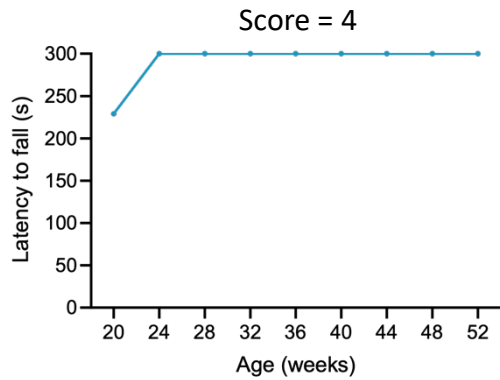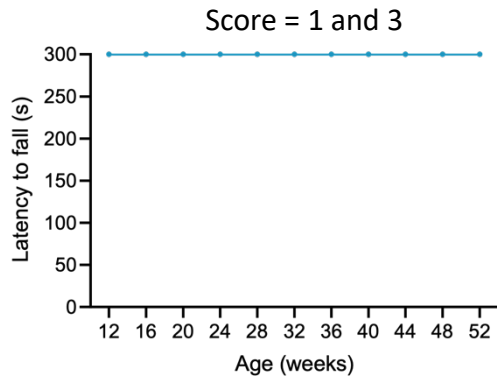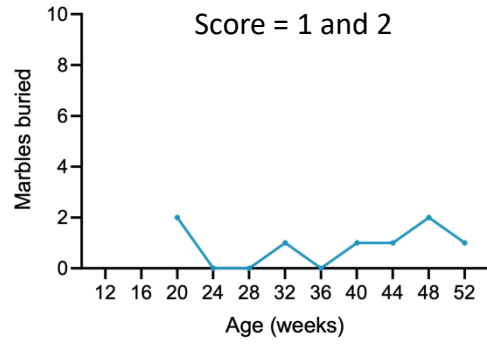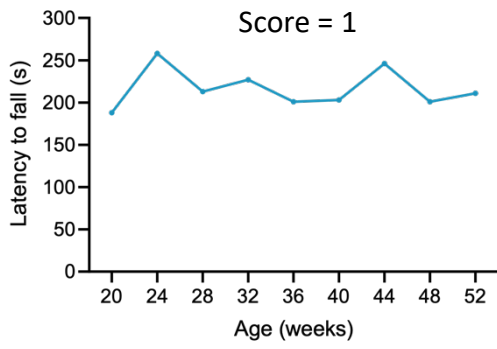
Figure 2.5: Representative examples of data patterns.

Examples of the data patterns described in the subset analysis.

Table 2.5: ALS-like scores and normal scores assigned from behavioural test performance.

	ALS-compatible scores			Normal scores
2	Stable poor – consistently in the bottom quartile		**3**	Stable good – consistently in the top quartile
6	Increase (change quartile) then decrease (change quartile)		**4**	Increase (change quartile) then stable
7	Decrease (change quartile) then stable		**5**	Increase (change quartile) then increase (change quartile)
9	Decrease (change quartile) then decrease (change quartile)		**8**	Decrease (change quartile) then increase (change quartile)

3   Phenotypic Characterisation of the Jax Mouse

3.1   Results

Due to laboratory and animal facility closures in response to the COVID-19 pandemic, the beginning of this study was delayed by 3 months. As a result, the first group of mice in this study began behavioural testing at 20 weeks of age and resulted in reduced n numbers at the 12- and 16-week timepoints. Additionally, because of this delay, the end of this study overlapped with the beginning of the second behavioural study (chapter 4). As such, several tests were removed to accommodate this, resulting in some tests having lower n numbers at the 40-week timepoint onwards in this study.

3.1.1   Confirmation of *C9ORF72* Repeat Expansion Size

Due to challenges associated with sizing the expansion in each mouse prior to study recruitment, southern blots were performed on post-mortem frontal cortex tissue to ensure all C9orf72 mice recruited to the study carried approximately 500 repeats of the G4C2 expansion. Blots demonstrated C9orf72 mice with repeat sizes ranging from 650-950 (Figure 3.1 and Fig. S 1). Only two of the mice recruited to the study dropped the expansion, these were removed from data analysis which follows.
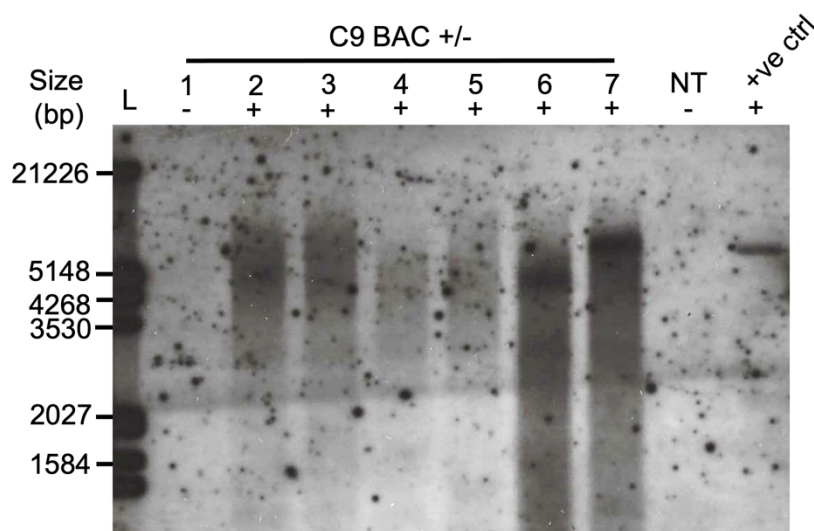
Figure 3.1: Confirmation of transgene with G4C2 repeat expansion in C9orf72 mice.
Southern blot of female C9orf72 mice showing repeat expansion size. Repeat size varied from 650-950 repeats. L, DNA ladder; +, transgene present; -, transgene absent; NT, non-transgenic control; +ve ctrl, pcDNA3.1/G4C2x45-3xV5 plasmid with a size of 5,927 bp when linearised.

3.1.2 Behavioural Tests

3.1.2.1 Accelerating Rotarod Test

C9orf72 mice showed no significantly decreased latency to fall compared to NT littermates at all timepoints (Figure 3.2). At 52 weeks of age, C9orf72 mice displayed a significantly decreased latency to fall compared to 12 weeks (n = 14-28, 270.9 ± 36.4 vs 199.3 ± 94.6, p = 0.01) (Figure 3.2). This was not present in NT littermates.
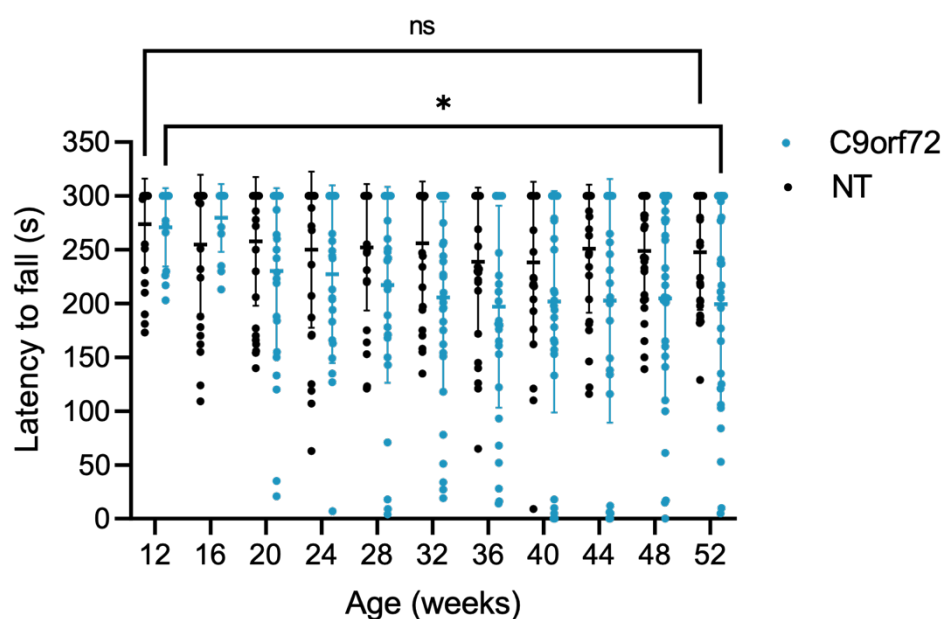
Figure 3.2: Mean latency to fall (± SD) in C9orf72 and non-transgenic (NT) mice.

Female C9orf72 mice showed no significantly decreased latency to fall compared to NT mice at any timepoint. At 52 weeks of age C9orf72 mice had significantly decreased latency to fall compared to 12 weeks. *$p < 0.05$, two-way ANOVA with repeated measures and Tukey's post-hoc test (C9orf72 n = 14-32, NT n = 27-33).

As weight may impact rotarod performance, mean weight and mean rotarod performance were correlated (Figure 3.3). There was a highly significant correlation between weight and rotarod performance in C9orf72 mice (r = -0.8727, p<0.001). This correlation was also present in NT mice, although at a lower significance (r = -0.7364, p<0.05). Following this, rotarod performance was normalised to weight by division of latency to fall by weight (Figure 3.4). A two-way ANOVA with Tukey's post-hoc test revealed no significant differences in rotarod performance between C9orf72 and NT mice once weight was accounted for. However, there

was a significant decrease in performance at 52 weeks of age compared to 12 weeks in both groups.
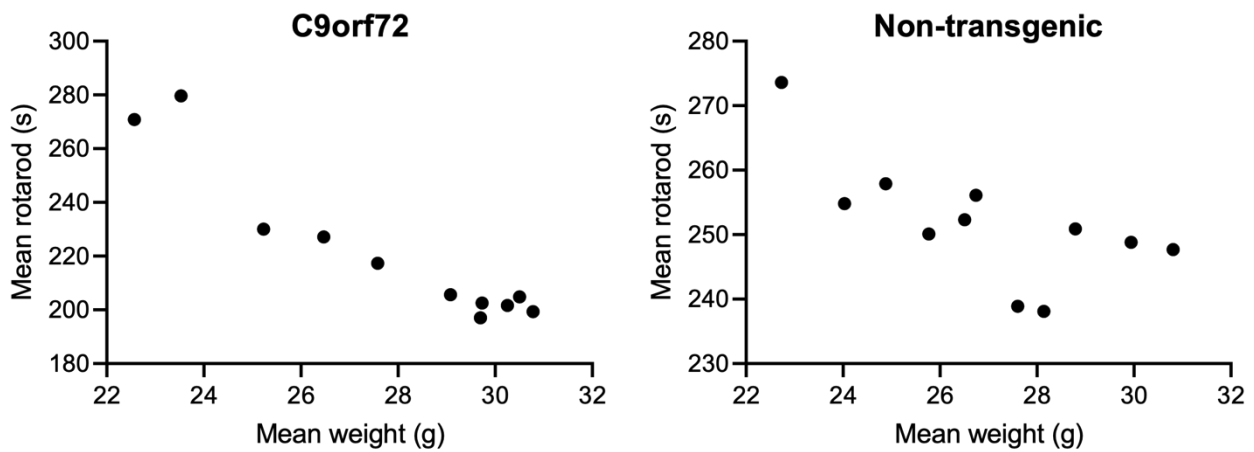
Figure 3.3: Spearman correlation of rotarod performance vs weight.

Spearman correlation of mean weight and mean rotarod performance of female C9orf72 and non-transgenic mice (C9orf72 r = -0.8727, p<0.001, NT r = -0.7364, p<0.05).
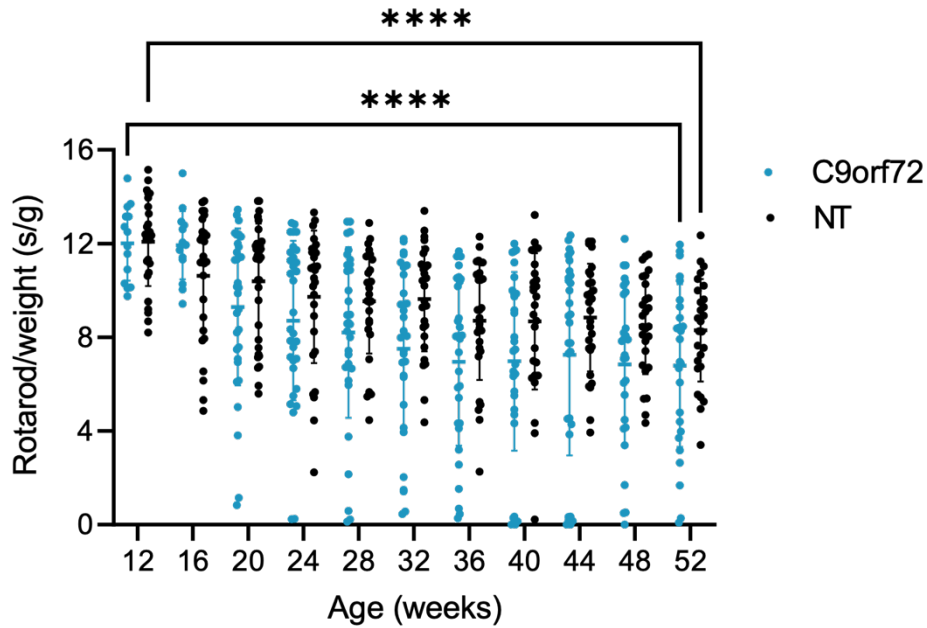
Figure 3.4: Rotarod performance/weight in C9orf72 and non-transgenic (NT) mice.

Mean latency to fall normalised to weight (± SD) showed no significant decreases between female C9orf72 and NT mice. At 52 weeks of age, both groups showed a significant decrease in latency to fall/weight ratio compared to 12 weeks. **** $p < 0.0001$, two-way ANOVA with repeated measures and Tukey's post-hoc test (C9orf72 n = 14-32, NT n = 27-33).

3.1.2.2   Catwalk Gait Analysis

Gait analysis was performed at monthly intervals from 12 weeks of age. Descriptions of parameters are detailed in Table 2.3. There was no significant difference in stride length between groups over time (Figure 3.5 A). Hindlimb base of support (BOS) tended to increase with age in both groups, however there was no significant difference between the two groups at any timepoint (Figure 3.5 B). Hindlimb swing time remained stable with age with no significant difference between the two groups (Figure 3.5 C). There was no significant difference in hindlimb swing speed between the two groups at any timepoint (Figure 3.5 D).
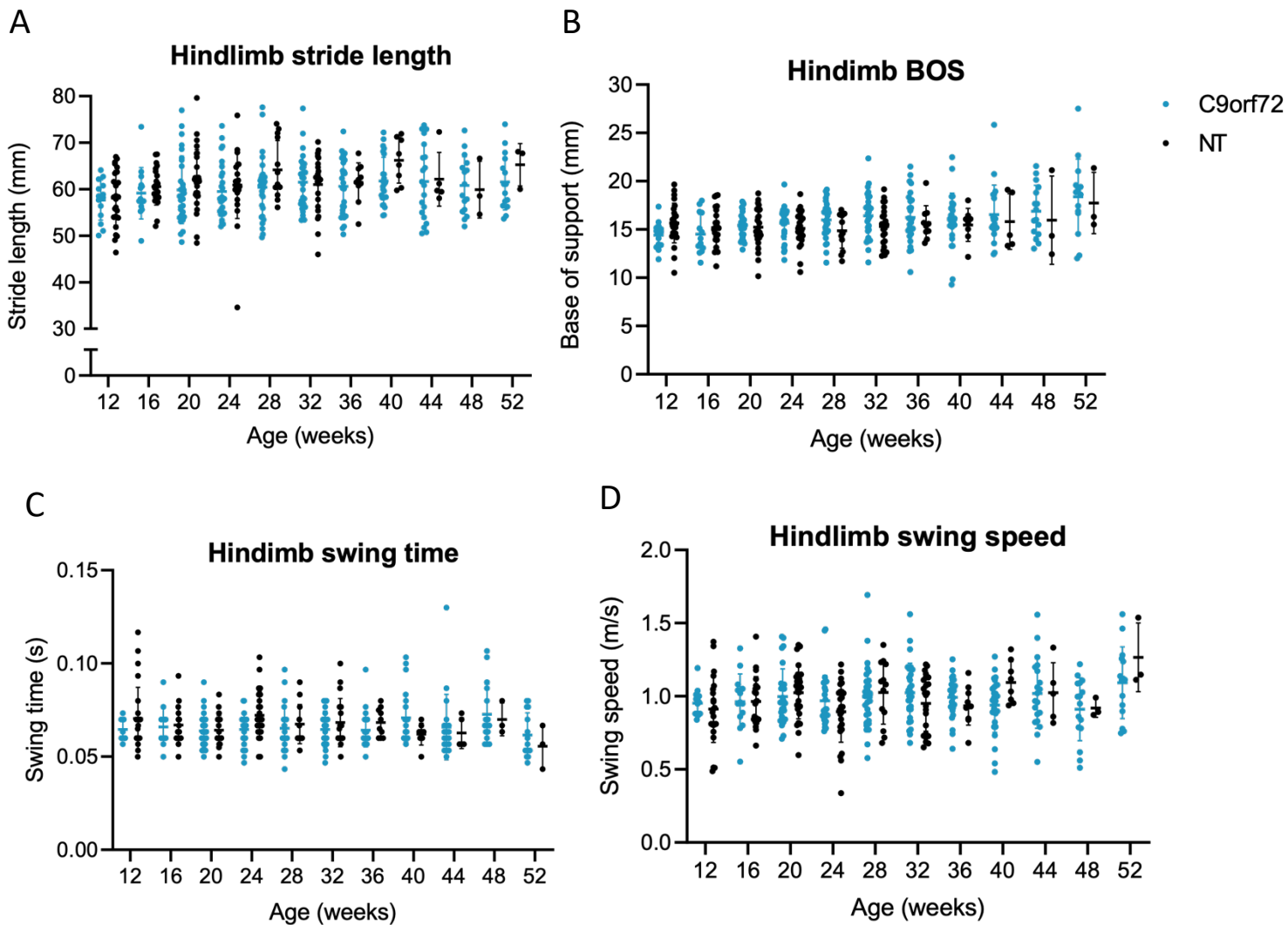
Figure 3.5: Catwalk gait analysis of C9orf72 and non-transgenic (NT) hindlimb stride length (A), base of support (B), hindlimb swing time (C), and swing speed (D).

Values are presented as the mean (± SD) of the left and right paws of each mouse. There were no significant differences between female C9orf72 and non-transgenic mice in any of the parameters (two-way ANOVA with repeated measures, C9orf72 n = 14-30, NT = 3-28).

Hindlimb print length remained stable with age, with no significant differences between the two groups. There was a slight increase in print length in NT mice at 52 weeks, however this is likely due to the small n number and one outlier at that timepoint (Figure 3.6 A). There was no significant difference in print width between the two groups at any timepoint (Figure 3.6 B). Most mice in both groups were well-coordinated, with no significant differences in regularity between them at any timepoint (Figure 3.6 C). Hindlimb intensity varied slightly

with age in both groups, however there were no significant differences between the two groups at any timepoint (Figure 3.6 D).
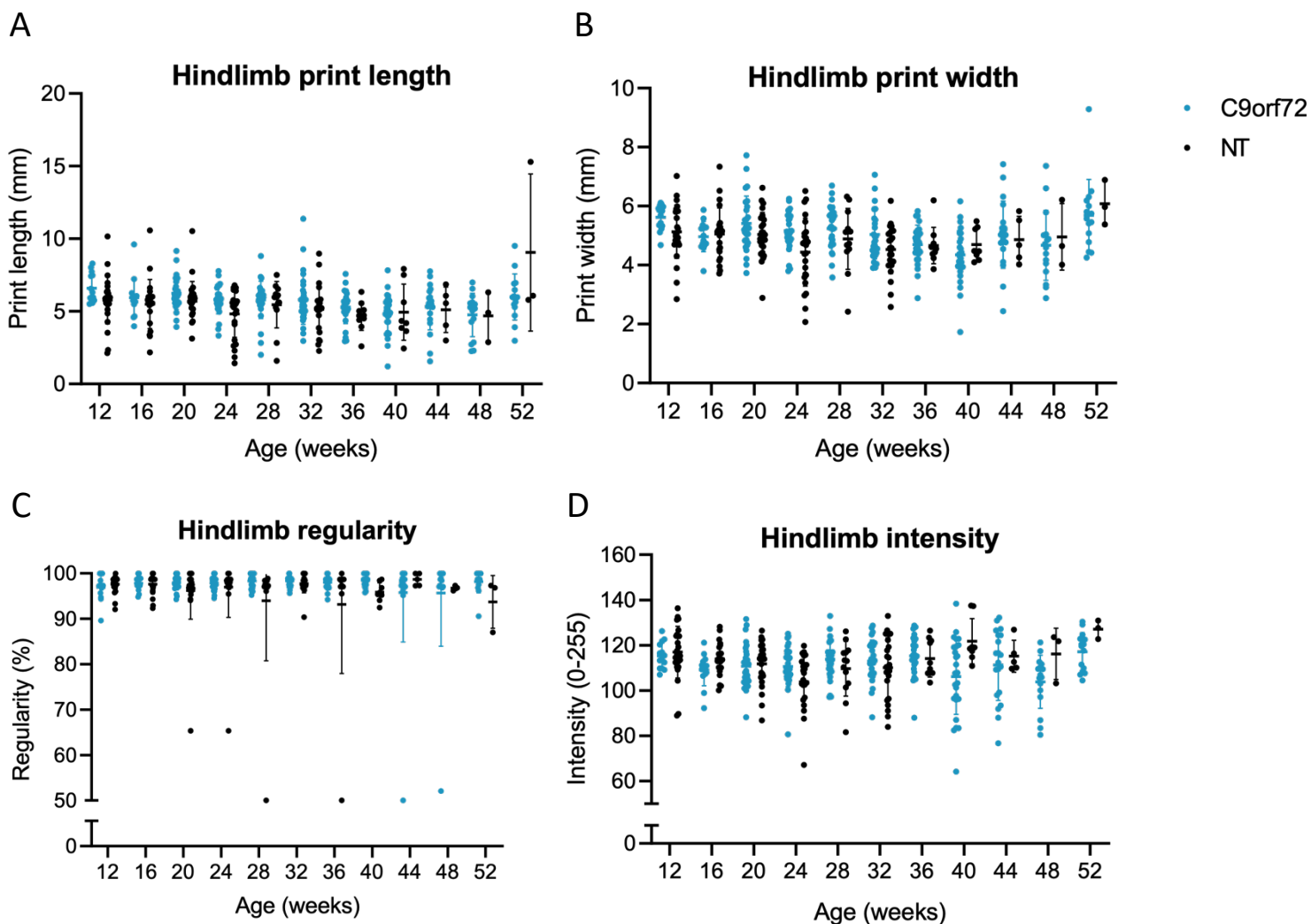
Figure 3.6: Catwalk gait analysis of C9orf72 and non-transgenic (NT) hindlimb print length (A), print width (B), regularity (C), and intensity (D).

Values are presented as the mean (± SD) of the left and right paws of each mouse. There were no significant differences between female C9orf72 and non-transgenic mice in any of the parameters (two-way ANOVA with repeated measures, C9orf72 n = 14-30, NT = 3-28).

Both groups spent most of the time on diagonal paws at all ages (Figure 3.7 A). The hindlimb duty cycle did not change with time and there were no significant differences between the two groups at any timepoint (Figure 3.7 B).
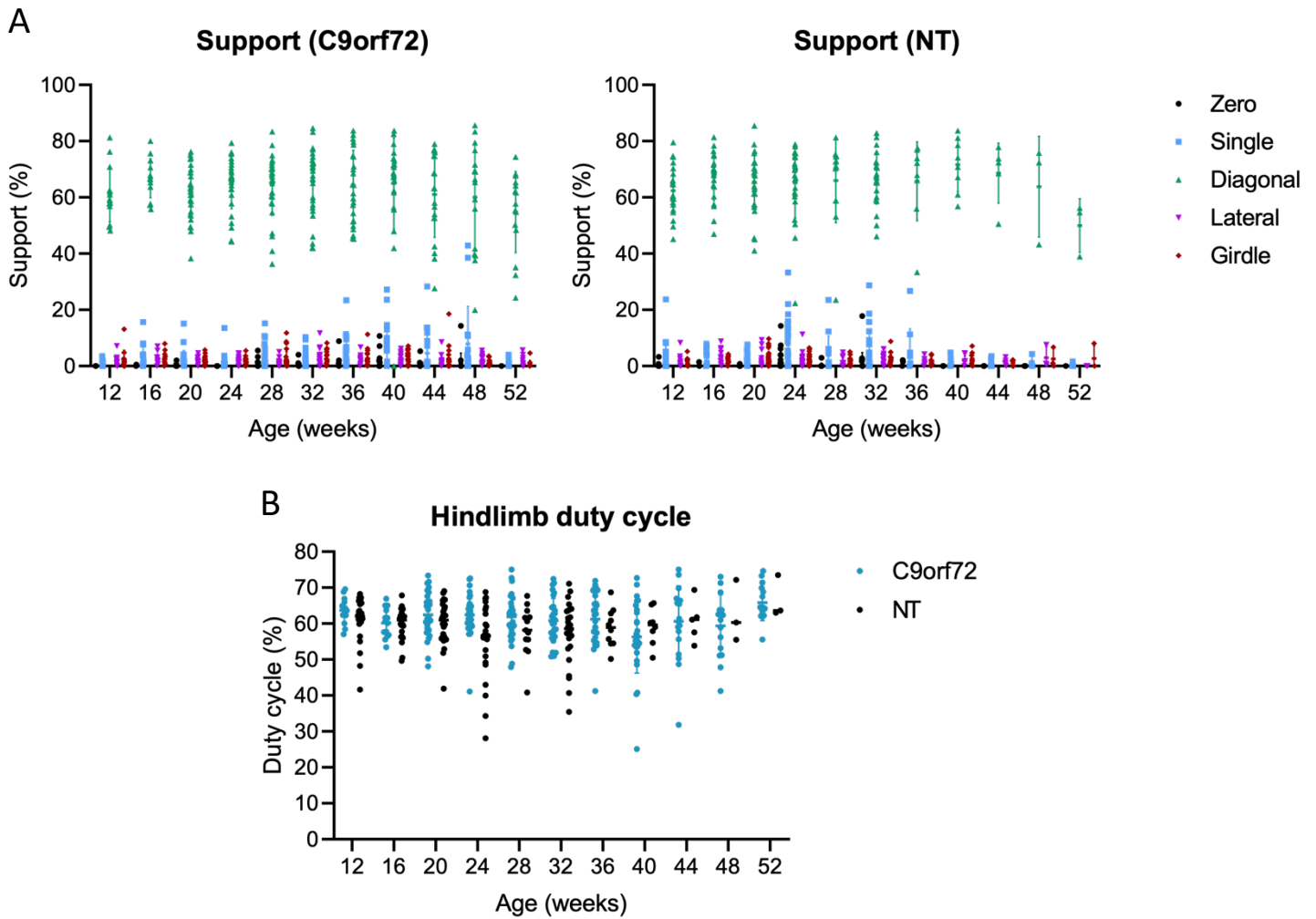
Figure 3.7: Catwalk gait analysis of percentage time spent on paws (A) and hindlimb duty cycle (B) C9orf72 and non-transgenic (NT) mice.

Values are presented as the mean (± SD) of the left and right paws of each mouse. There were no significant differences between female C9orf72 and non-transgenic mice in any of the parameters (two-way ANOVA with repeated measures, C9orf72 n = 14-30, NT = 3-28).

3.1.2.3   Open Field

The open field test is used as a measure of locomotion, anxiety, and willingness to explore a novel environment. C9orf72 mice did not show a significant decrease in total distance travelled in the open field chamber at any timepoint (Figure 3.8 A, B), indicating no motor deficit. Several C9orf72 and NT mice displayed a larger total distance travelled (>10,000 cm) compared to all other mice, which slightly increased over time. This was attributed to the development of stereotypic behaviour in this subset of mice (Figure 3.8 C).

The open field chamber was virtually split into centre and periphery zones to analyse exploratory behaviour and anxiety. C9orf72 mice did not spend any more or less time in the centre of the open field chamber compared to NT mice at any timepoint (Figure 3.9).
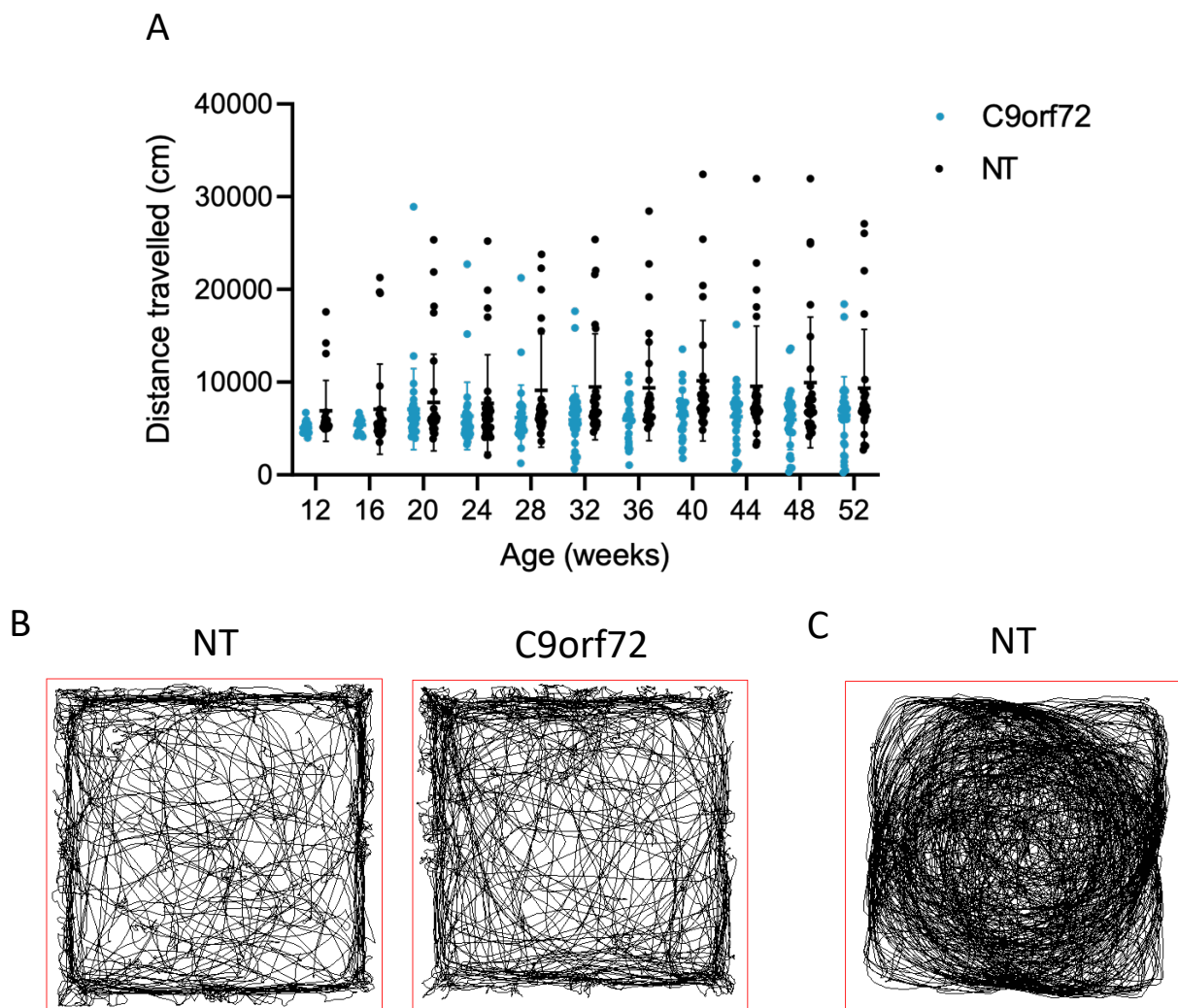
Figure 3.8: Mean distance travelled (± SD) in C9orf72 mice and non-transgenic (NT) mice.
(A) Female C9orf72 mice displayed no significantly decreased mobility compared to NT mice (two-way ANOVA with repeated measures, C9orf72 n = 14-32, NT n = 27-33). (B) Representative traces showing movement pattern in open field chamber after 10 minutes (52 weeks of age). (C) Representative example of stereotypic circling behaviour observed in both C9orf72 and NT mice.
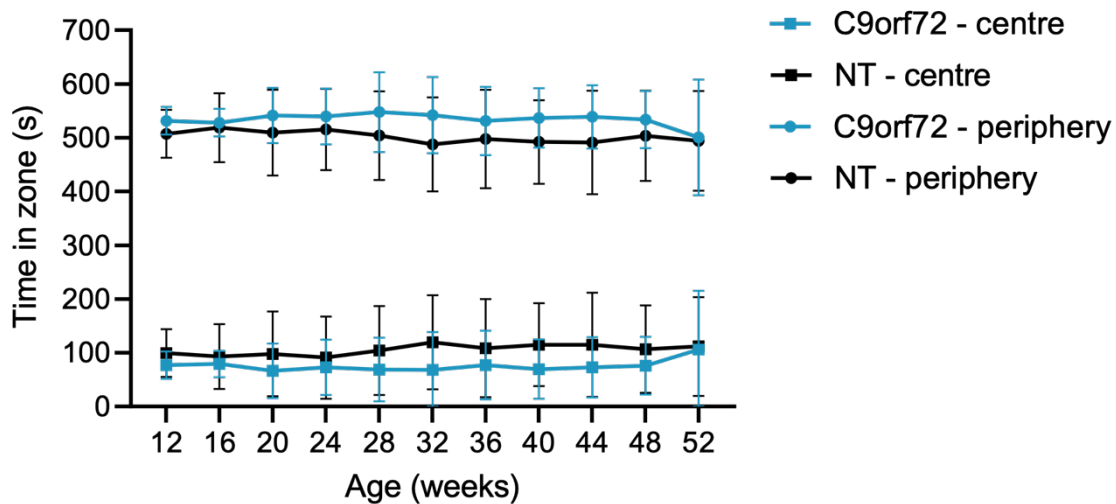
Figure 3.9: Mean time (± SD) in centre and periphery zones of open field chamber in C9orf72 mice and non-transgenic (NT) mice.

Female C9orf72 mice spent equivalent time (± SD) in the centre and periphery zones of the open field chamber as NT mice at every timepoint (two-way ANOVA with repeated measures, C9orf72 n = 29-32, NT n = 27-33).

3.1.2.4 Social Recognition Test

The social recognition test analyses social memory and relies on the fact that mice spend less time investigating a familiar mouse compared to a novel mouse. C9orf72 mice showed no significantly reduced investigation time in the recall session compared to the initial session when compared to NT, indicating no impaired social memory (Figure 3.10). However, both groups showed no significantly decreased investigation time in the recall session compared to the initial session and spent a similar amount of time investigating novel and familiar individuals, indicating both groups may have impaired social memory.

Recognition index (the ratio of recall investigation time relative to initial investigation time) also showed no differences in ability to recognise a familiar individual between C9orf72 and NT mice. It revealed that at most timepoints both groups spent equal or more time investigating the familiar mouse than the novel mouse (Figure 3.11), indicating impaired social memory.
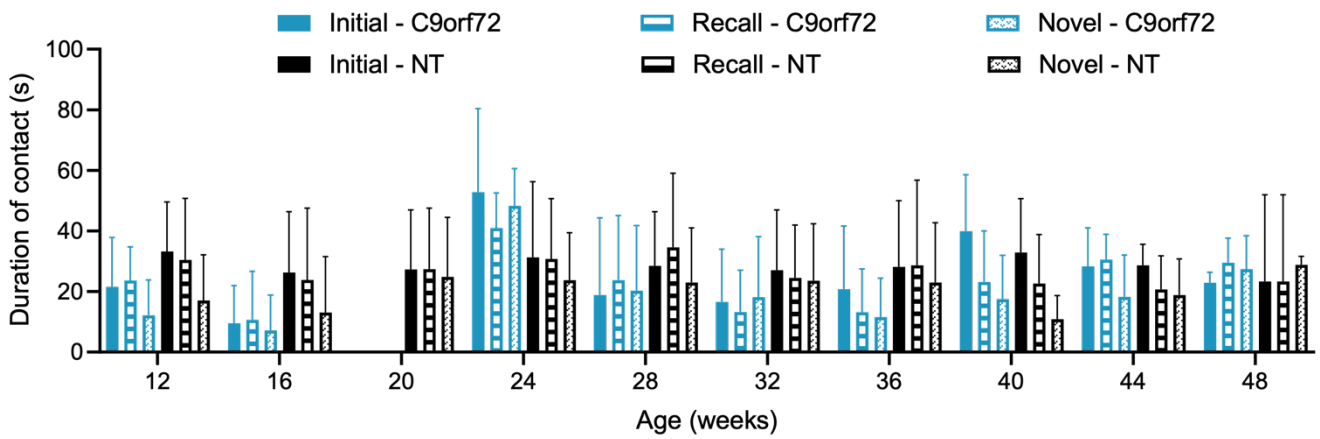
Figure 3.10: Mean duration of contact (± SD) with juvenile female mouse in C9orf72 mice and non-transgenic (NT) mice.

The same female juvenile mouse was used in the initial and recall sessions. Both female C9orf72 and non-transgenic mice showed no significantly decreased investigation time in the recall session compared to the initial session at any timepoint (two-way ANOVA with repeated measures, C9orf72 n = 2-31, NT n = 2-28).
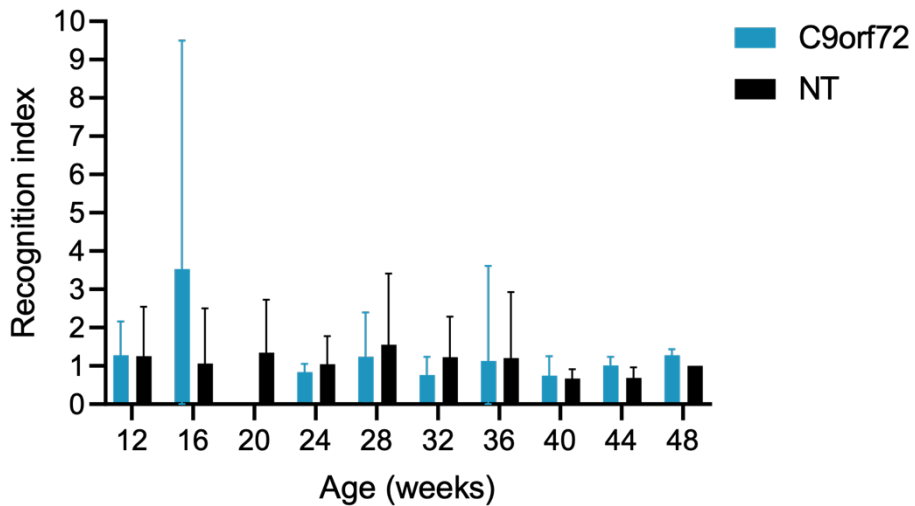
Figure 3.11: Recognition index of C9orf72 and non-transgenic (NT) mice.

Recognition index (the ratio of recall investigation time relative to initial investigation time, mean ± SD) showed no differences in ability to recognise a familiar individual between female C9orf72 and NT mice (two-way ANOVA with repeated measures, C9orf72 n = 2-31, NT n = 2-28). Both groups spent equal or more time investigating the familiar mouse than the novel mouse (index = 1: equal time spent investigating familiar and novel mouse, index > 1: more time spent investigating familiar mouse compared to novel mouse, index < 1: more time spent investigating novel mouse compared to familiar mouse).

3.1.2.5   Marble Burying

Marble burying is a measure of motor ability, motivation, and the presence of natural digging behaviour in mice. C9orf72 mice did not bury significantly fewer marbles than NT mice (Figure 3.12), however both groups showed a within-group significant decrease at 52 weeks of age compared to 12 weeks (C9orf72 n = 14-32, 9.7 ± 0.61 vs 5.0 ± 3.1, p<0.01; NT n = 27-33, 8.4 ± 2.64 vs 4.5 ± 3.01, p<0.001).
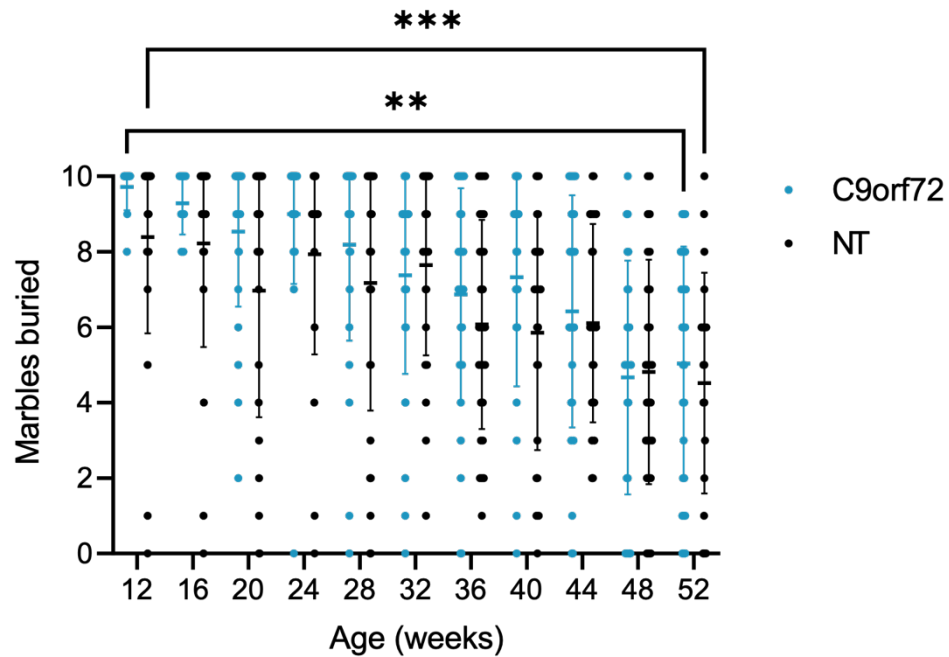
Figure 3.12: Mean number of marbles buried (± SD) by C9orf72 and non-transgenic (NT) mice.
There was no significant difference in number of marbles buried between female C9orf72 and NT mice at any timepoint, however both groups showed significantly reduced marble burying at 52 weeks of age compared to 12 weeks. ** <0.01, *** <0.001, two-way ANOVA with repeated measures and Tukey's post-hoc test (C9orf72 n = 14-32, NT n = 27-33).

3.1.2.6 Balance Beam

Median scores on the balance beam showed no difference in balance ability between C9orf72 and NT groups (Figure 3.13). However, a longitudinal analysis revealed a general non-significant increase in 'unbalanced' scores in both groups with age that is more pronounced in C9orf72 mice (Figure 3.14).
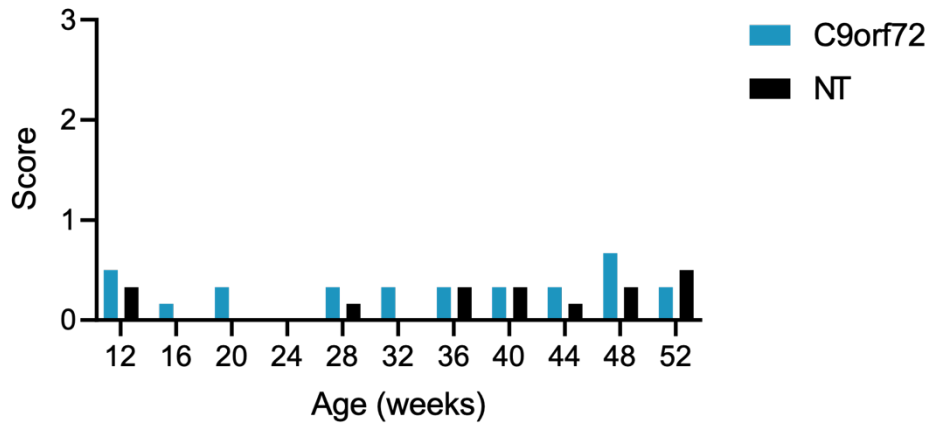
Figure 3.13: Median balance beam score of C9orf72 mice and non-transgenic (NT) mice.

Female C9orf72 mice displayed no significantly impaired coordination compared to NT mice at any timepoint (C9orf72 n = 14-32, NT n = 27-33).
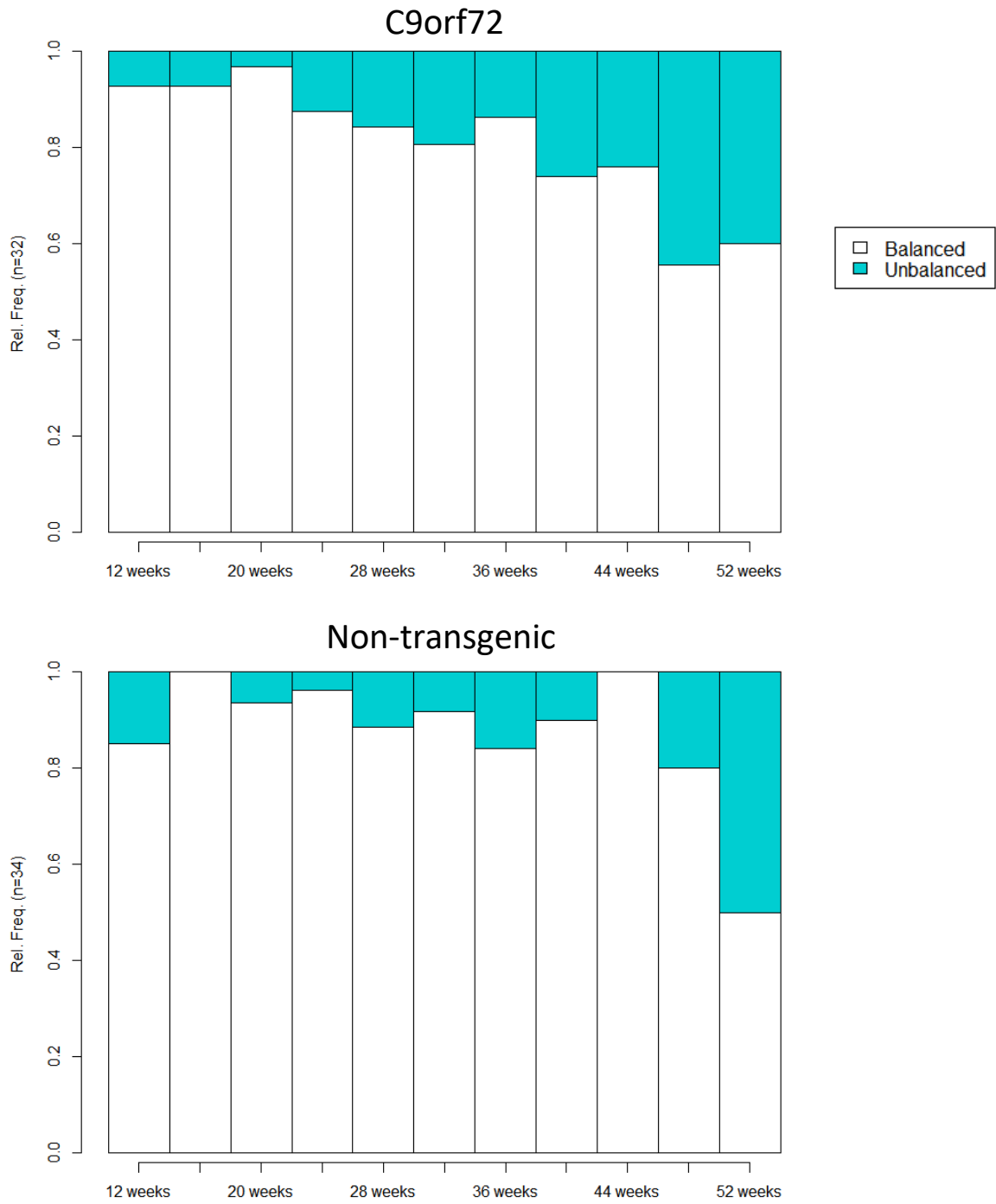
Figure 3.14: Longitudinal changes in balance beam scores in C9orf72 and non-transgenic (NT) mice. Longitudinal changes in the proportion of 'balanced' and 'unbalanced' scores in female C9orf72 and NT mice showed a general non-significant increase in 'unbalanced' scores with age.

3.1.2.7 Limb Hang Test

There was no significant difference in latency to fall between C9orf72 and NT mice (Figure 3.15). To eliminate the influence of weight on ability to hang, limb hang performance was normalised to weight by division of mean hang time by weight (Figure 3.16). A two-way ANOVA with repeated measures and Tukey's post-hoc test revealed no significant differences in the ratio of hang time/weight between C9orf72 and NT mice.
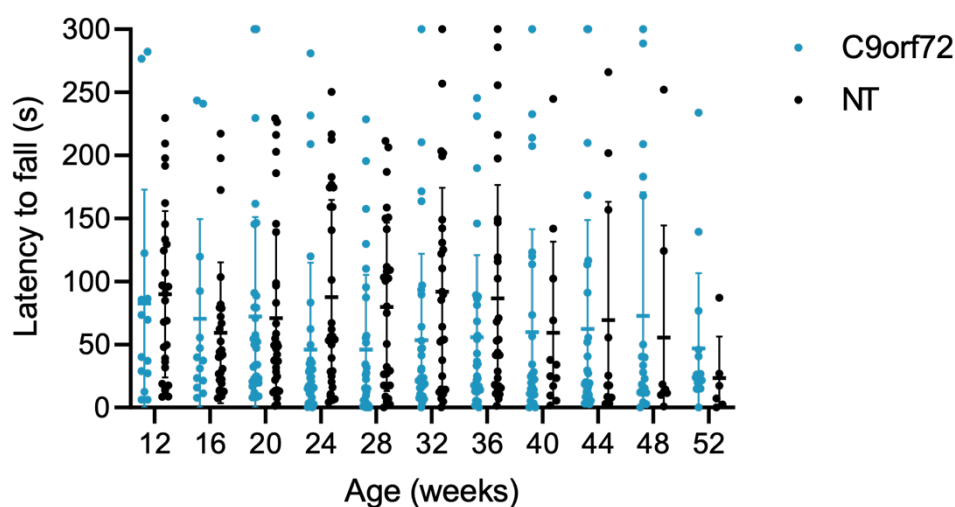
Figure 3.15: Mean hang time (± SD) of C9orf72 mice and non-transgenic (NT) mice.
Female C9orf72 mice showed no reduced hanging ability compared to NT mice at any timepoint (two-way ANOVA with repeated measures and Tukey's post-hoc test, C9orf72 n = 14-32, NT n = 27-33).
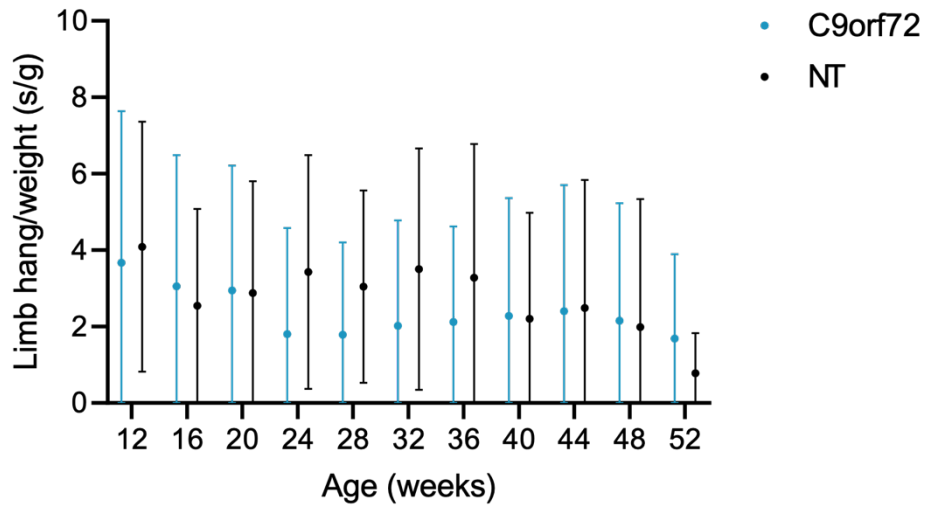
Figure 3.16: Limb hang/weight in C9orf72 and non-transgenic (NT) mice.

Mean latency to fall normalised to weight (± SD) showed no significant differences between female C9orf72 and NT mice (two-way ANOVA with repeated measures and Tukey's post-hoc test, C9orf72 n = 14-32, NT n = 27-33).

3.1.2.8   Burrowing

Burrowing is a measure of natural digging and burrowing behaviour. There was no significant difference in weight burrowed between C9orf72 and NT mice, however there was a general non-significant decrease in both groups with age (Figure 3.17).
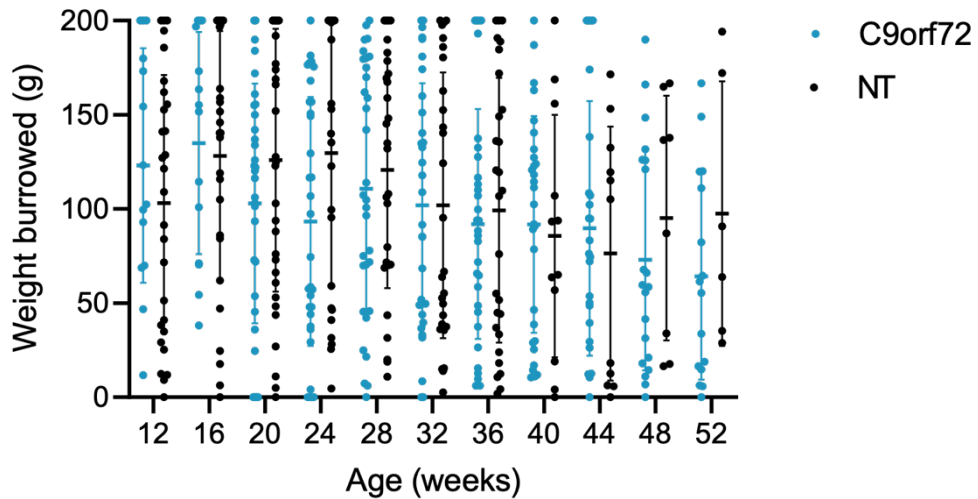
Figure 3.17: Mean weight burrowed (± SD) by C9orf72 and non-transgenic (NT) mice.

There was no significant difference in weight burrowed (± SD) between female C9orf72 and NT mice at any timepoint (two-way ANOVA with repeated measures, C9orf72 n = 14-32, NT n = 27-33).

3.1.2.9 Nesting

Median nesting scores showed no difference in nest building ability between C9orf72 and NT groups (Figure 3.18). However, a longitudinal analysis showed a general non-significant reduction in nest quality in both groups with age (Figure 3.19).
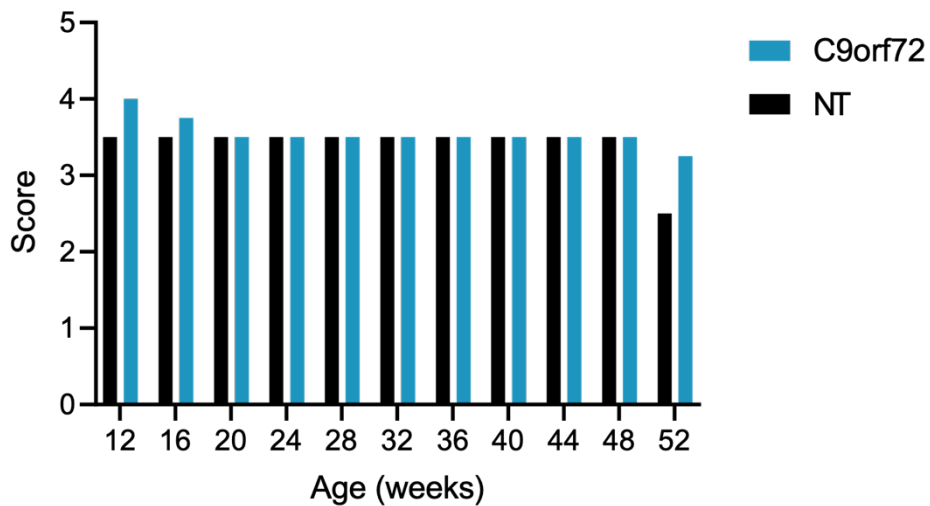
Figure 3.18: Median nesting score of C9orf72 mice and non-transgenic (NT) mice.

Female C9orf72 mice displayed no significantly impaired nesting behaviour compared to NT mice at any timepoint (C9orf72 n = 14-32, NT n = 27-33).
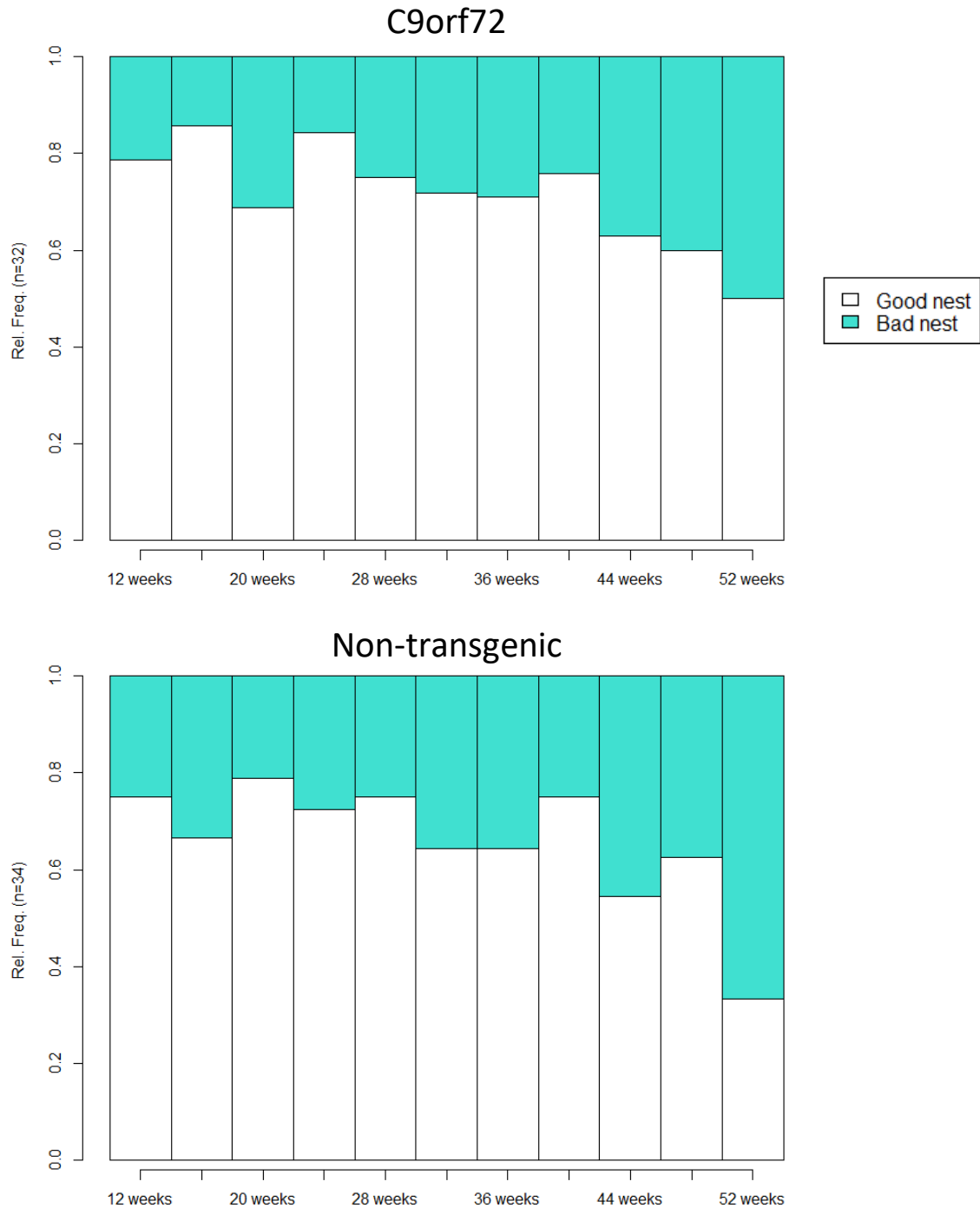
Figure 3.19: Longitudinal changes in nesting scores in C9orf72 and non-transgenic (NT) mice.
Longitudinal changes in the proportion of 'good nest' and 'bad nest' scores showed a general non-significant reduction in nest quality with age in female C9orf72 and non-transgenic mice.

3.1.2.10 Food Intake

The test was performed overnight (16 hours) once a month alongside the nesting test. There was no significant difference in food intake between C9orf72 and NT mice at any timepoint on a two-way repeated measures ANOVA (Figure 3.20).
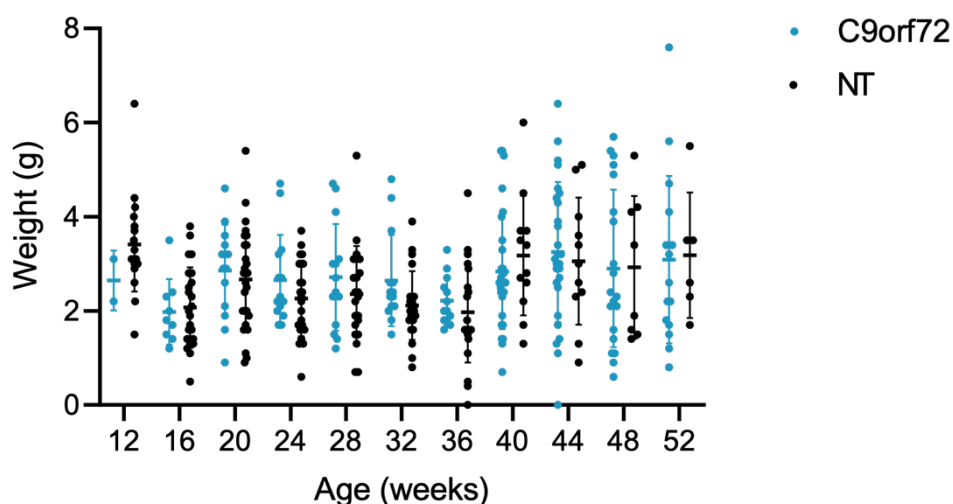
Figure 3.20: Mean food intake (± SD) overnight by C9orf72 and non-transgenic (NT) mice.
Test was performed alongside nesting behaviour test over a 16-hour period. There was no significant difference in food intake between female C9orf72 and non-transgenic mice at any timepoint (two-way ANOVA with repeated measures, C9orf72 n = 2-29, NT n = 21-28).

3.1.2.11 Weight

Both groups showed an increase in body weight with age (Figure 3.21). There was no significant difference between C9orf72 and NT mice at any timepoint on a two-way repeated measures ANOVA. Weight was monitored weekly, and no mouse required euthanasia due to progressive weight loss.
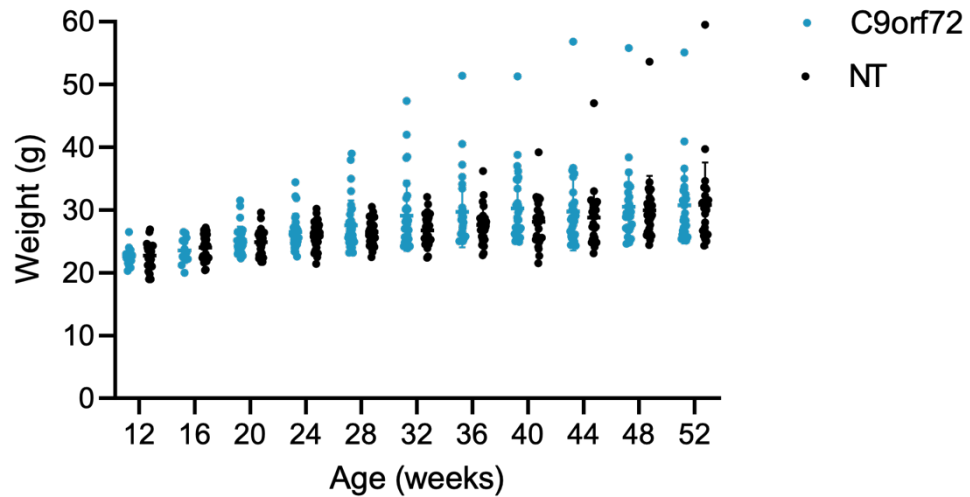
Figure 3.21: Mean body weight (± SD) of C9orf72 and non-transgenic (NT) mice.

Both groups increased body weight from 12-52 weeks of age. There was no significant difference between female C9orf72 and non-transgenic mice at any timepoint (two-way ANOVA with repeated measures, C9orf72 n = 14-32, NT n = 27-33).

3.1.2.12 Subset Data Analysis

An analysis method to identify possible subsets hidden within the data was described in the methods section 2.6.9. Results of this analysis are detailed in Table 3.1. Chi-Square analysis was performed between C9orf72 and NT groups for each test detailed, with none found to be significantly different (Table 3.1).

Table 3.1: Contingency table counts of C9orf72 and non-transgenic (NT) mice.

Each number is the number of times a score was given in each test. Chi-Square analysis was performed between female C9orf72 and NT groups. None were found to be significantly different. MND-like phenotype = motor neurone disease-compatible score expected in diseased mice, Normal = normal score expected in healthy mice.

Test	C9orf72		Non-transgenic		p-value
	MND-like phenotype	Normal	MND-like phenotype	Normal	
Rotarod	14	18	11	23	0.45
Open field	10	22	9	25	0.79
Marble burying	21	11	18	16	0.33
Balance beam	17	15	18	16	>0.99
Limb hang	14	18	13	21	0.80
Burrowing	16	16	14	20	0.62
Nesting	12	20	15	19	0.62
CMAP	11	21	12	22	>0.99

3.1.2.13 Electrophysiology

CMAP amplitude is a measure of the motor unit pool of a muscle and was measured in the hindlimb muscle every 3 months from 12 weeks of age. There was no significant change in CMAP amplitude in or between either group over time, indicating no loss of motor axons (Figure 3.23 A).

Repetitive nerve stimulation is a measure of neuromuscular junction (NMJ) function. There was no significant decrement in response between repetition 1 and 10 in C9orf72 mice, suggesting a healthy NMJ at all timepoints, as well as no significant difference in response between C9orf72 and NT mice (Figure 3.23 A).

EMG recordings were taken from the gastrocnemius muscle in a small group of mice (C9orf72 n = 3, NT n = 5) at 52 weeks of age by Dr James Alix to examine for spontaneous EMG activity. No fibrillation potentials, positive sharp waves, or fasciculation potentials were observed in either group (data not shown).
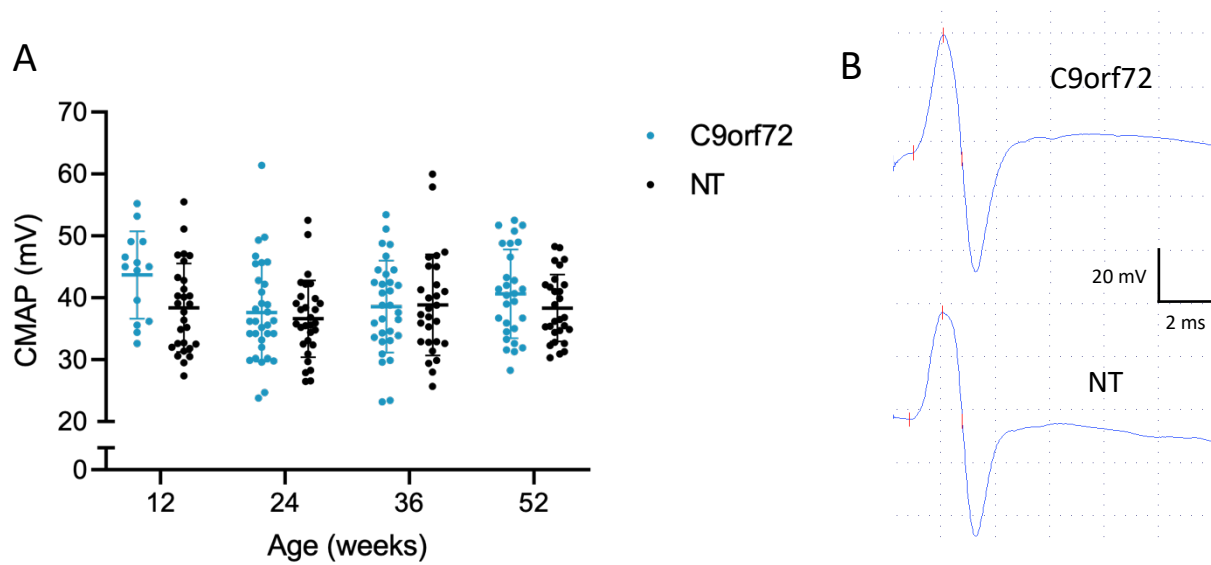
Figure 3.22: CMAP of the hindlimb muscles.

(A) There was no significant decrease in CMAP amplitude in female C9orf72 mice compared to non-transgenic (NT) mice at any timepoint, indicating no loss of motor axons. (B) Representative CMAP traces at 52 weeks of age (C9orf72 n = 14-32, NT n = 28-30).
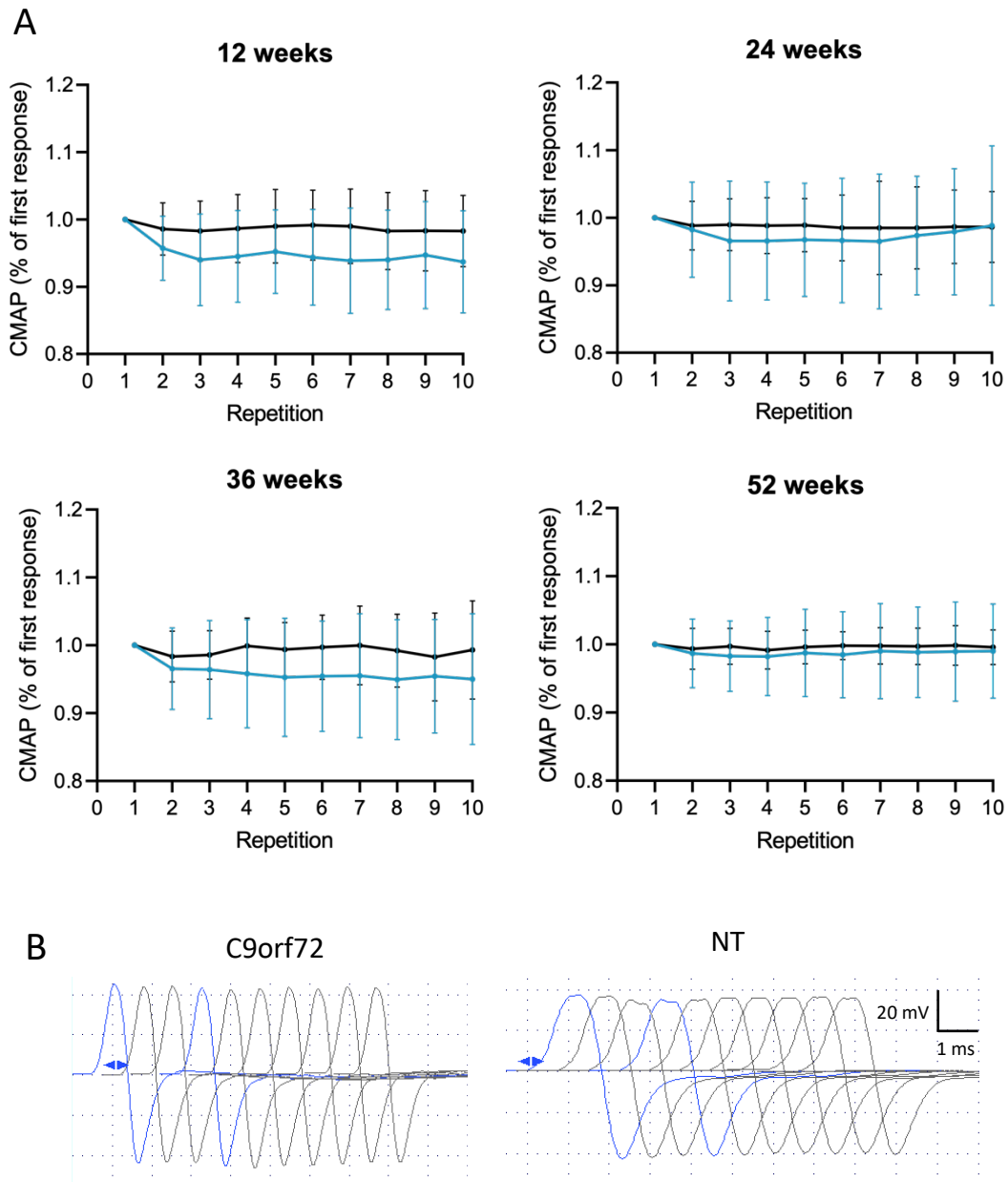
Figure 3.23: Repetitive stimulation of the hindlimb muscles.

(A) Repetitive nerve stimulation tests revealed no significant decrement in response (represented as percentage of the first response) in female C9orf72 mice compared to NT mice at any timepoint (two-way ANOVA with repeated measures and Sidak's post-hoc test, C9orf72 n = 14-32, NT n = 28-30). (B) Representative repetitive stimulation traces at 52 weeks of age.

At 52 weeks of age prior to end of study, a small group of C9orf72 and NT mice underwent additional electrophysiological tests. There was no decrease in plantar interossei CMAP amplitudes in C9orf72 compared to NT mice (Figure 3.24 A, B). There was also no prolonged F wave latencies and no reduced persistence in C9orf72 mice compared to NT mice (Figure 3.24 C-E).
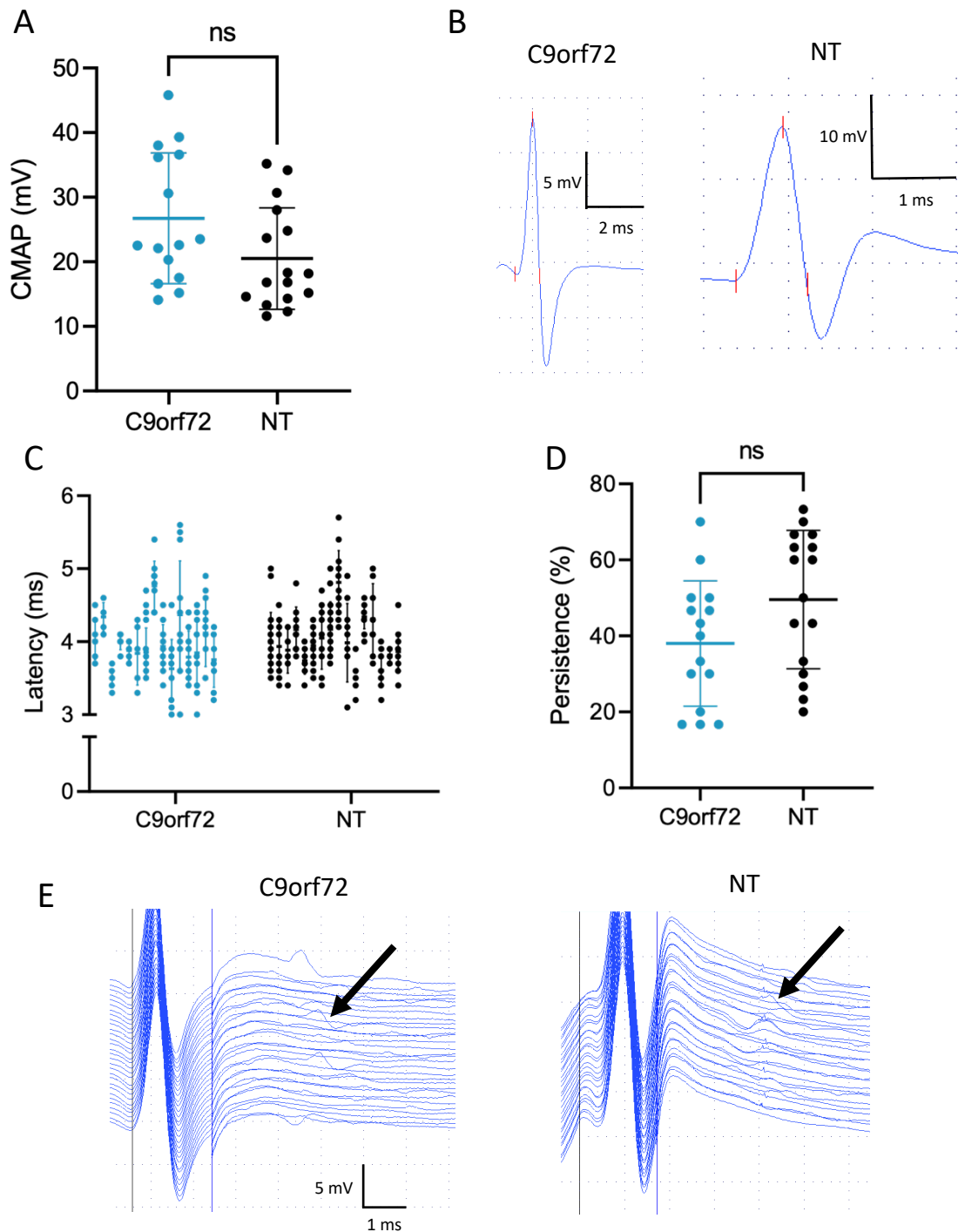
Figure 3.24: Plantar interossei CMAP and F wave recordings.

Plantar interossei CMAPs and F wave recordings were taken from a subgroup of female C9orf72 and non-transgenic (NT) mice at 52 weeks of age prior to end of study (C9orf72 n = 15, NT n = 16). (A) There was no reduction in plantar interossei CMAP amplitude in C9orf72 mice compared to NT (unpaired t-test). (B) Representative plantar interossei CMAP traces. (C) F wave latencies were not significantly prolonged in C9orf72 mice (nested t-test). (D) F wave persistence was unchanged in C9orf72 mice. (E) Representative F wave traces, arrows indicate individual F waves.

3.1.2.14 Survival

There was no reduction in survival in C9orf72 mice compared to NT (Figure 3.25). Of the six C9orf72 mice that died during the study, two were found dead in their home cages, two were euthanised due to a severe generalised seizure and a series of repetitive mild seizures respectively, and two were euthanised due to substantial distress, the reason for which was unknown. Of the six NT mice that died, four were found dead in their home cages, one was euthanised due to substantial distress of unknown cause, and one was euthanised on advice of the resident veterinarian due to a prolapse.

When possible, post-mortems were performed on mice found dead to ascertain cause of death. However, no cause was found. The only characteristic of note was a wet ventral neck present on all C9orf72 and NT mice found dead.
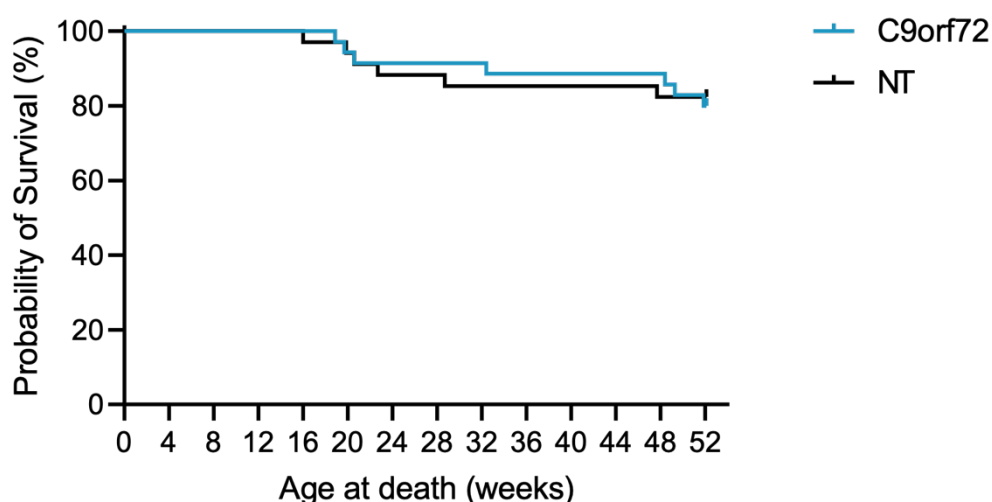
Figure 3.25: Survival curve of C9orf72 and non-transgenic (NT) mice.

Kaplan-Meier survival curve of female C9orf72 mice shows no decreased survival compared to NT mice (Gehan-Breslow-Wilcoxon test, p = 0.8951, C9orf72 n = 35, NT n = 34).

Hindlimb clasping is a common measure of disease progression in mouse models of neurodegeneration (Guyenet et al., 2010). Representative examples of clasping scores are shown in Figure 3.26 A and the proportions of each score given at each timepoint for both groups are shown in Figure 3.26 B.
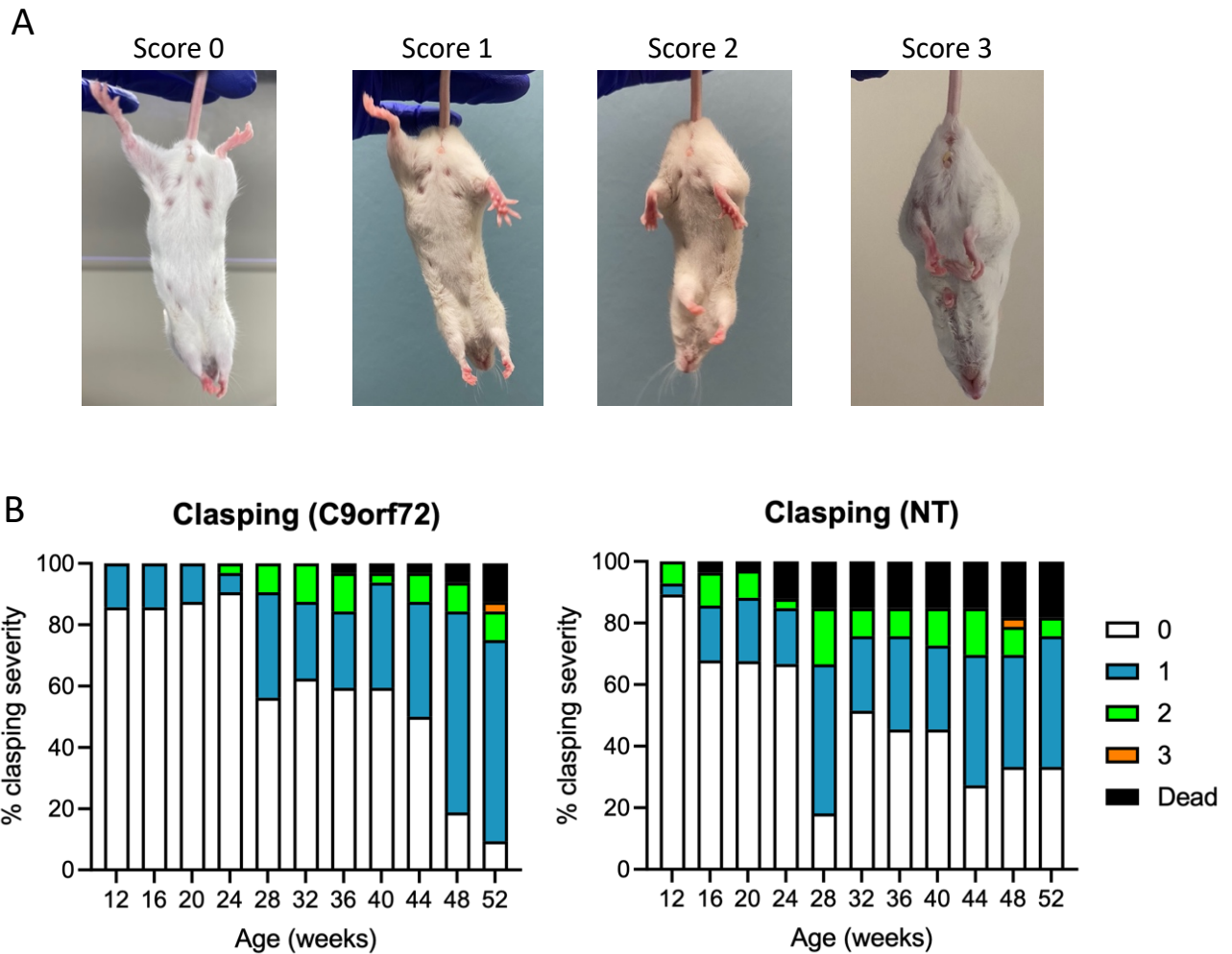
Figure 3.26: Clasping phenotypes of C9orf72 and non-transgenic (NT) mice.

(A) Representative images of clasping phenotypes. (B) Graphical depiction of female C9orf72 and NT mice displaying clasping phenotypes from 12-52 weeks of age (C9orf72 n = 35, NT n = 34).

3.1.2.15 Seizure Observations

Seizure susceptibility is a well-known phenotype in the FVB/N background strain used in this study (Goelz et al., 1998; Hennemann, 2007; Silva-Fernandes et al., 2010; Kohnken and Schwahn, 2016). Seizures were observed in C9orf72 and non-transgenic mice throughout the study. Seizures were timed at onset or from time of discovery and scored according to the scale from Van Erum et al. (2019). Severe or repetitive seizures, or failure to recover from seizure, resulted in euthanasia. Six mice were observed seizing in this study, two of which required euthanasia (Table 3.2).

Table 3.2: Seizures observed in C9orf72 and non-transgenic (NT) mice.

Seizures were scored according to Van Erum et al. (2019). Scores 1 to 3 were classed as mild (1, whisker trembling; 2, sudden behavioural arrest; 3, facial jerking). Scores 4 to 6 were classed as moderate (4, neck jerks; 5, clonic seizure (sitting); 6, clonic, clonic-tonic seizure (lying on belly)), 7 and 8 were classed as severe (7, clonic, clonic-tonic seizure (lying on side) and wild jumping; 8, tonic extension, possibly leading to respiratory arrest and death).

Genotype	Age	Score	Euthanasia
C9orf72	20 weeks	7	Yes
C9orf72	24 weeks	2	No
C9orf72	52 weeks	5	Yes (repetitive seizures)
C9orf72	36 weeks	2	No
NT	28 weeks	5	No
NT	20 weeks	3	No

3.1.2.16 Stereotypic Behaviour

Stereotypic circling behaviour was observed in both C9orf72 and NT groups of mice. Incidence increased over time but was generally more prevalent in the NT group (Figure 3.27).
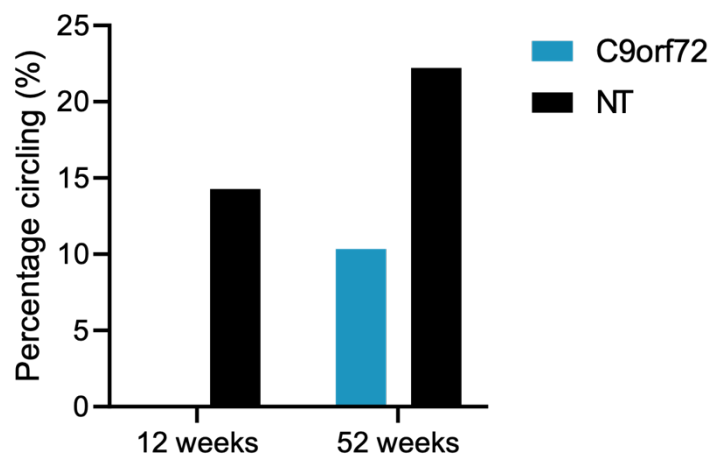
Figure 3.27: Proportion of stereotypic circling behaviour in C9orf72 and non-transgenic (NT) mice.
Stereotypic behaviour was observed in a small proportion of female non-transgenic mice at 12 weeks of age. Incidence increased over time and by 52 weeks both groups displayed stereotypic behaviour.

3.1.2.17 Variability of Behavioural Tests

Many of the behavioural tests show substantial variability. To investigate this, the coefficient of variability was calculated for C9orf72 and NT mice in each test and compared (Figure 3.28). As expected, the behavioural tests showed the largest variability, with the balance beam, limb hang, and burrowing tests showing the most. Neither group demonstrated more variability than the other. The electrophysiological tests showed the least variability as they were not reliant on mouse behaviour and demonstrate that the technique has a high level of reproducibility.
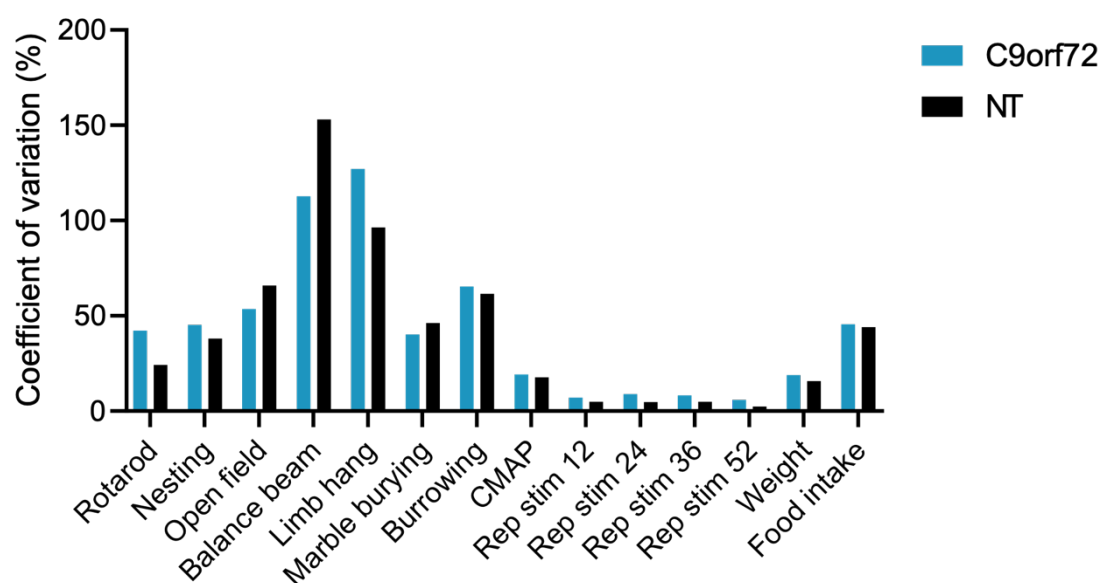
Figure 3.28: Variability of behavioural tests.

Coefficient of variation showed both female C9orf72 and non-transgenic mice were equally variable within each test. Balance beam, limb hang, and burrowing show the largest amount of variability.

3.1.3 Tissue Pathology

3.1.3.1 Dipeptide Repeat Protein Quantification

Detection of dipeptide repeat proteins (DPRs) was performed by Meso Scale Discovery (MSD) immunoassay on frontal cortex and gastrocnemius muscle tissue taken at 52 weeks of age. Poly-GP and poly-GA DPRs were both detected in the frontal cortex tissue at significantly elevated levels compared to NT controls (Figure 3.29 A), indicating expression of the *C9ORF72* transgene. The remaining DPRs, poly-GR, poly-PA, and poly-PR, were not detected (data not shown). Only poly-GP was detected in the gastrocnemius muscle (Figure 3.29 B).

Figure 3.29: Dipeptide repeat proteins detected in brain and muscle tissue of C9orf72 mice.

Meso scale discovery (MSD) immunoassay for poly-GP and poly-GA dipeptide repeat proteins in (A) frontal cortex and (B) gastrocnemius muscle tissue in female C9orf72 mice compared to non-transgenic controls (unpaired t-test, **** $p<0.0001$, *** $p<0.001$, ** $p<0.01$, cortex: C9orf72 n = 27, NT n = 11, muscle: C9orf72 n = 13, NT n = 14, mean ± SD).

3.1.3.2 Neurone Counts

Motor neurone counts were performed in the indicated regions of the ventral horns of the L4-5 region of the spinal cord in 52-week-old mice (Figure 3.30 A). There was no significant
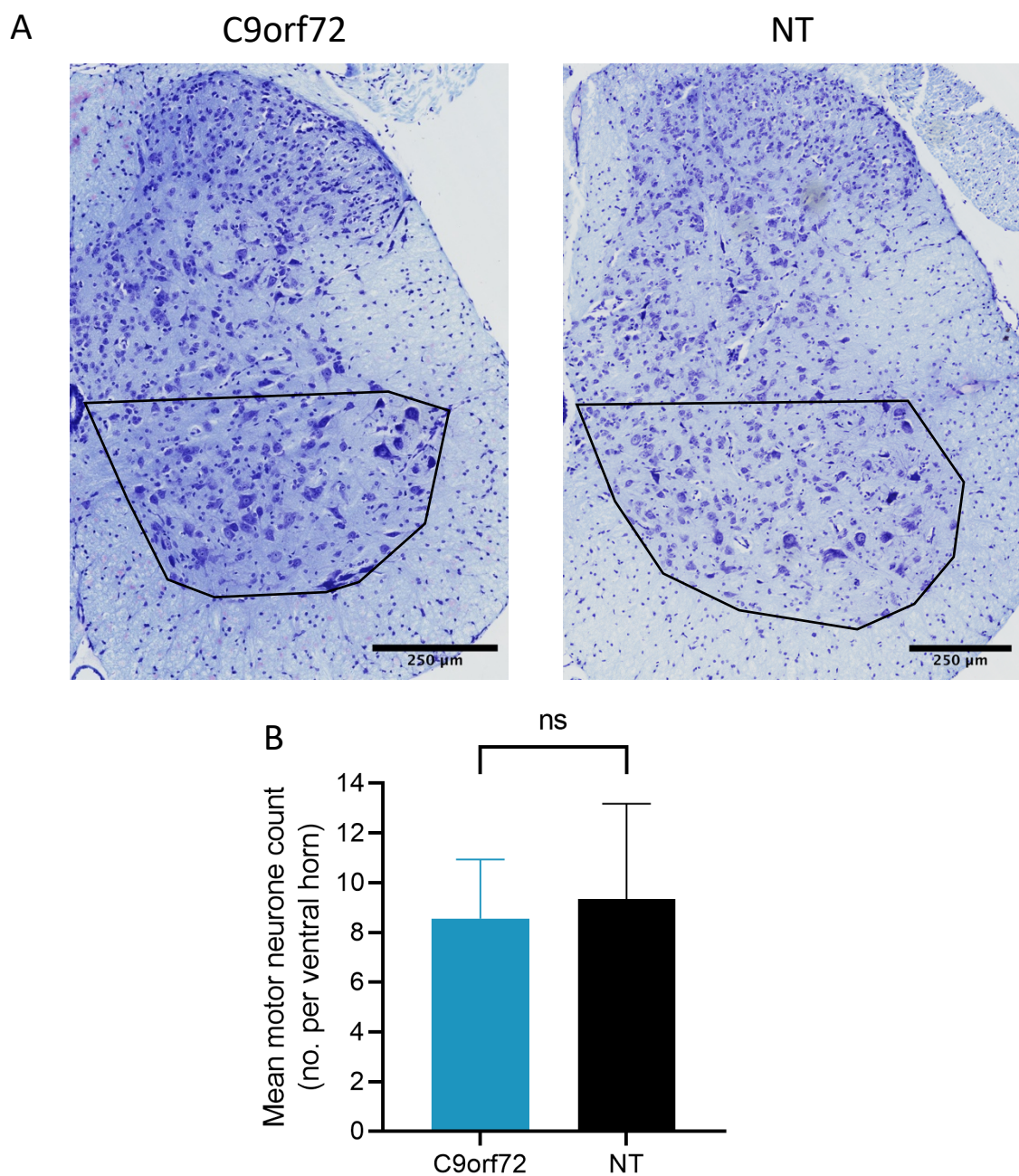
difference in the number of motor neurones in this region between C9orf72 and NT mice (Figure 3.30 B).

Figure 3.30: Motor neurone counts in L4 region of the lumbar spinal cord.

(A) Nissl staining of motor neurones in the lumbar spinal cord. (B) No significant motor neurone loss in the lumbar spinal cord of female C9orf72 mice compared to non-transgenic controls (mean ± SD, nested t-test, n = 5 per group).

Neuronal counts were performed in the CA and DG regions of the hippocampus (Figure 3.31) and layer V of the motor cortex (Figure 3.32) in 52-week-old mice. There was no significant difference in the number of neurones between C9orf72 and NT mice in any of the hippocampal regions or layer V of the motor cortex.
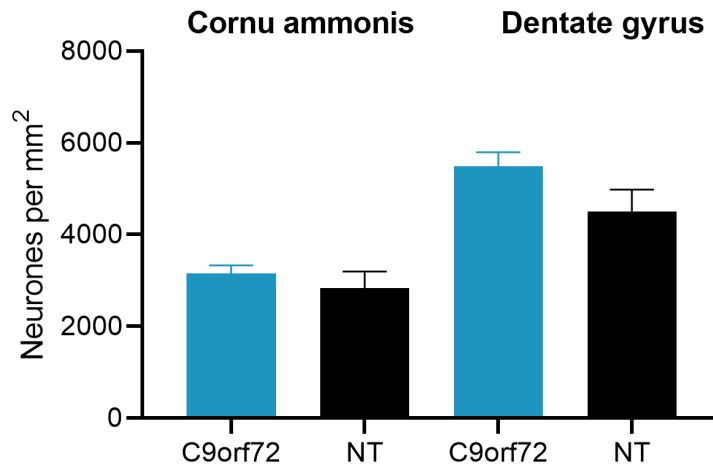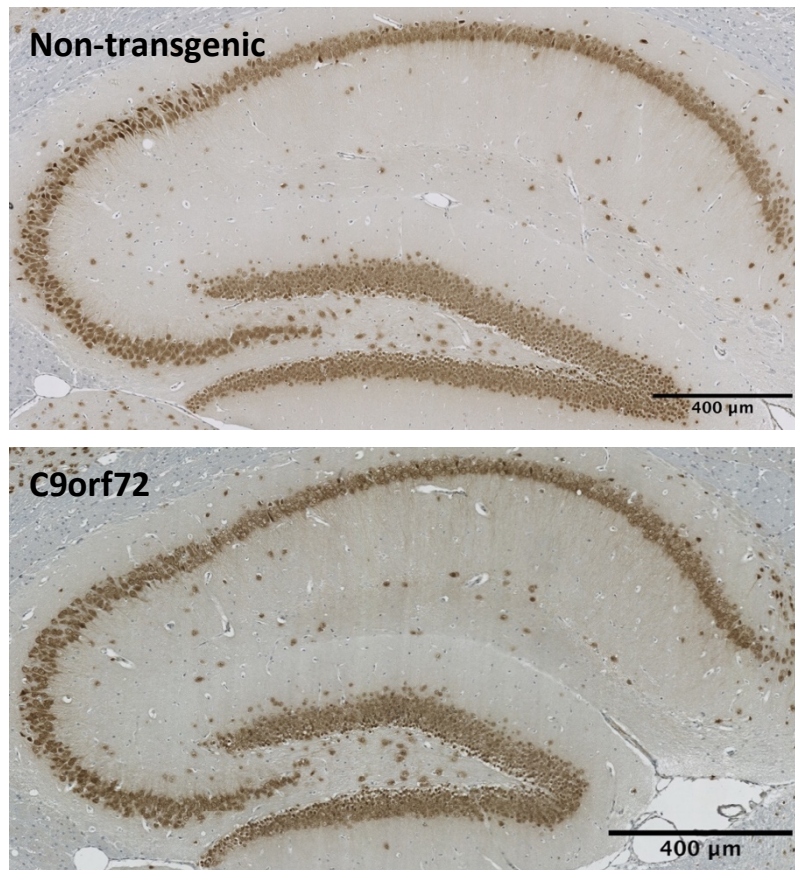
Figure 3.31: Neuronal counts in the hippocampus of C9orf72 and non-transgenic (NT) mice.

Neuronal counts in the cornu ammonis (CA) and the dentate gyrus (DG) of the hippocampus showed no significant difference between female C9orf72 and NT mice (mean ± SD, nested one-way ANOVA with Bonferroni's multiple comparisons, C9orf72 n = 5, NT n = 4).

NT **C9orf72**

Motor Cortex Layer V
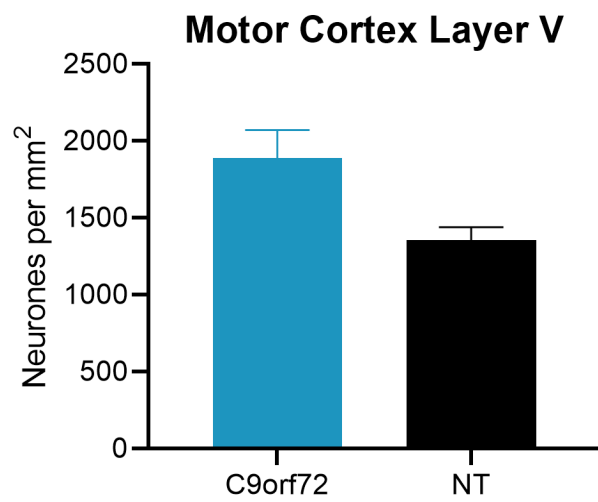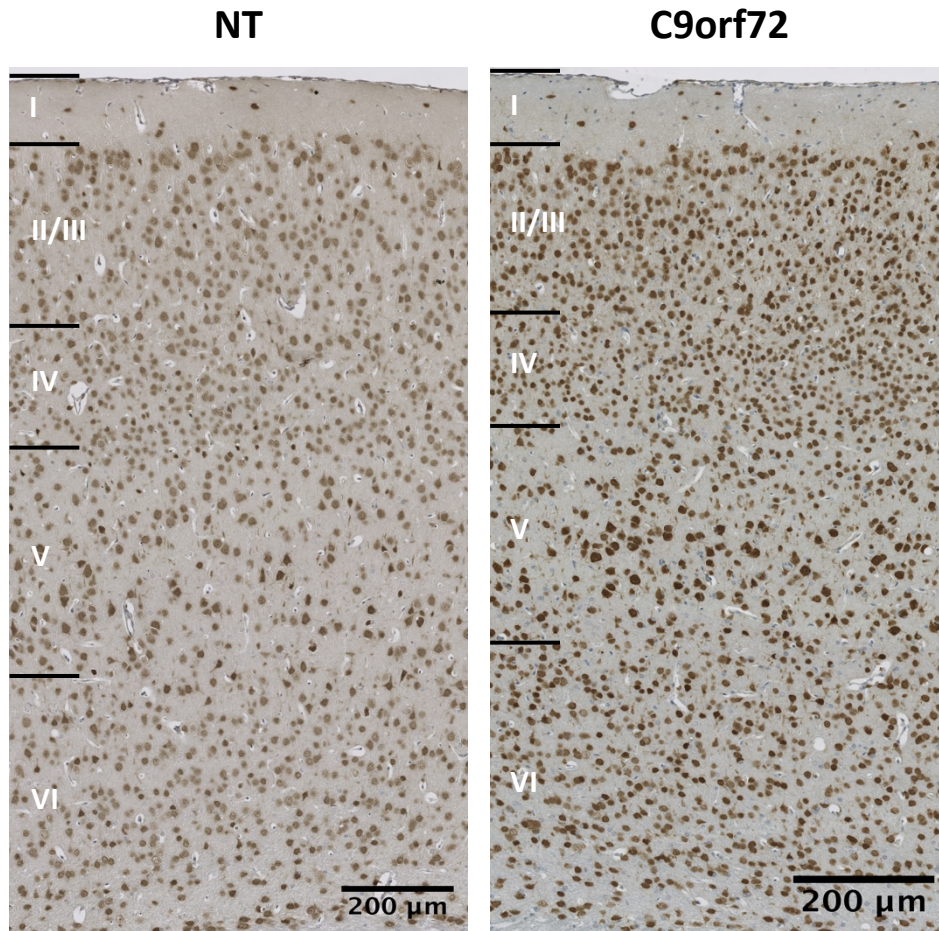
Figure 3.32: Neuronal count in layer V of the motor cortex of C9orf72 and non-transgenic (NT) mice.

There was no significant difference in neurones counted between female C9orf72 and NT mice (mean ± SD, nested t-test, n = 4 per group).

3.1.3.3   Immunohistochemical Analysis of Astrogliosis

Hippocampal sections from 52-week-old mice were stained for GFAP and analysed for increased area and intensity of staining, both of which are indicative of astrogliosis. No increased area or intensity of GFAP staining was found in C9orf72 mice compared to NT on a nested t-test (Figure 3.33). Increased GFAP staining area and intensity was seen in one C9orf72 mouse, which had previously been observed seizing at 24 weeks of age.
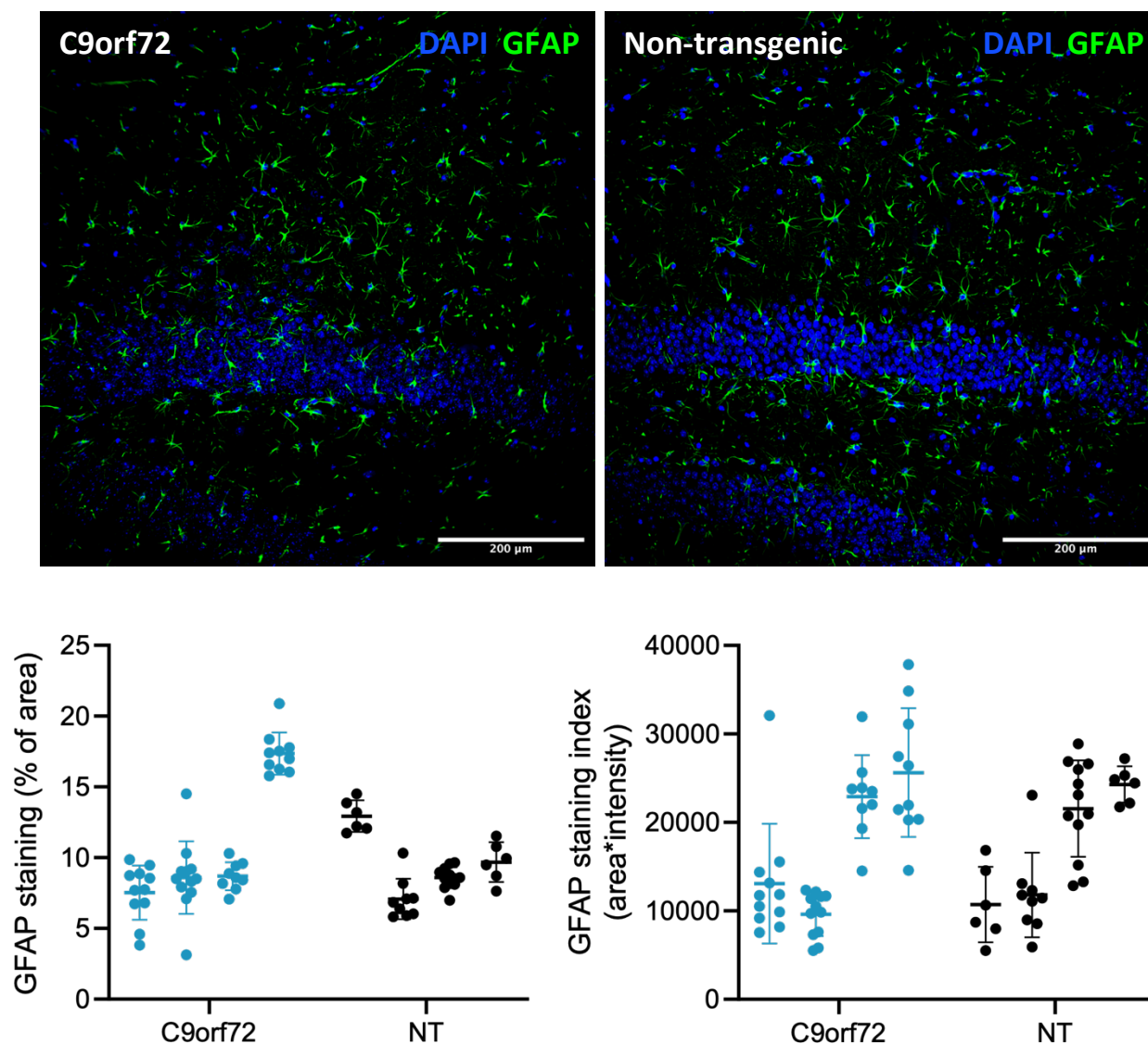
Figure 3.33: Dentate gyrus GFAP staining.

Quantification of GFAP staining in the dentate gyrus of female C9orf72 and non-transgenic mice (n = 4 per group). No significant difference in staining area or staining index (nested t-test).

Motor cortex sections from 52-week-old mice were stained for GFAP and analysed for increased area and intensity of staining. No increased area or intensity of GFAP staining was

found in C9orf72 mice compared to NT on a nested t-test (Figure 3.34). GFAP staining and intensity was variable in both groups.
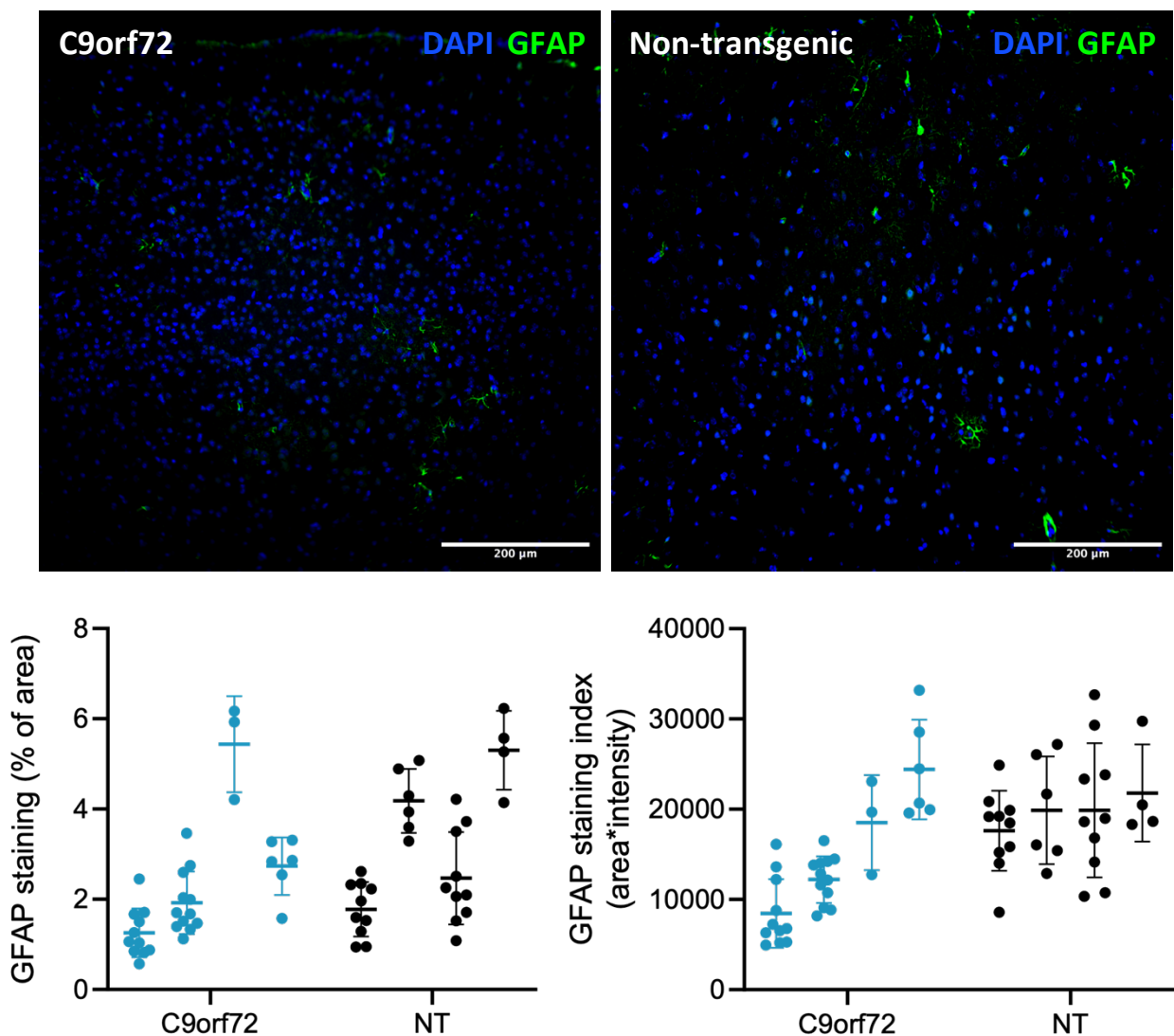
Figure 3.34: GFAP staining of the motor cortex.

Quantification of GFAP staining in the motor cortex of female C9orf72 and non-transgenic mice (n = 4 per group). No significant difference in staining area or staining index (nested t-test).

3.1.3.4   Immunohistochemical Analysis of Microgliosis

Hippocampal sections from 52-week-old mice were stained for Iba1 and analysed for increased area, intensity of staining, and circularity, all of which are indicative of

neuroinflammation. No increased area, intensity of Iba1 staining, or increased circularity was found in C9orf72 mice compared to NT on a nested t-test (Figure 3.35).
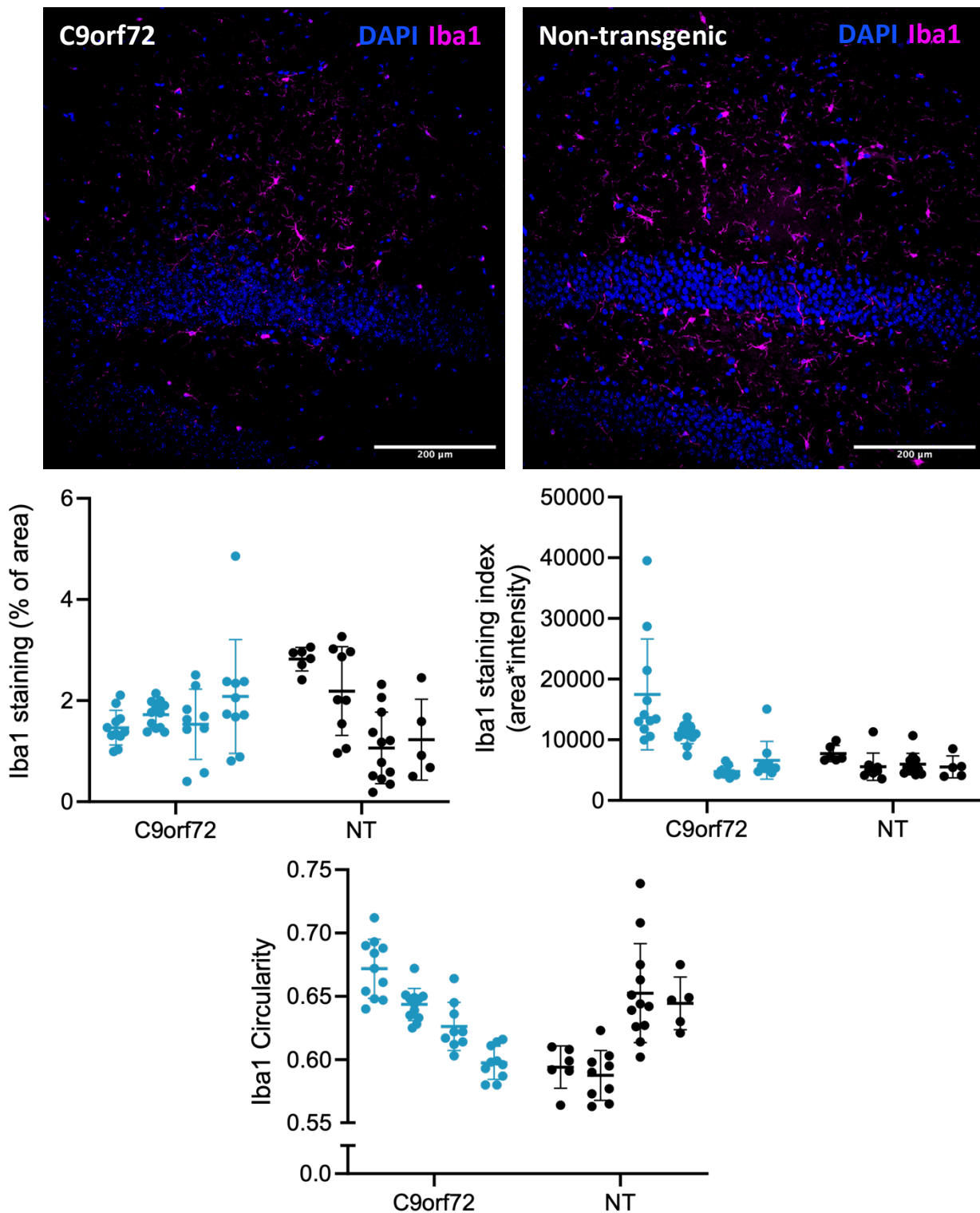
Figure 3.35: Dentate gyrus Iba1 staining.

Quantification of Iba1 staining in the dentate gyrus of female C9orf72 and non-transgenic mice (n = 4 per group). No significant difference on a nested t-test.

Motor cortex sections from 52-week-old mice were stained for Iba1 and analysed for increased area, intensity of staining, and circularity, all of which are indicative of microgliosis. No increased area, intensity of Iba1 staining, or increased circularity was found in C9orf72 mice compared to NT on a nested t-test (Figure 3.36).
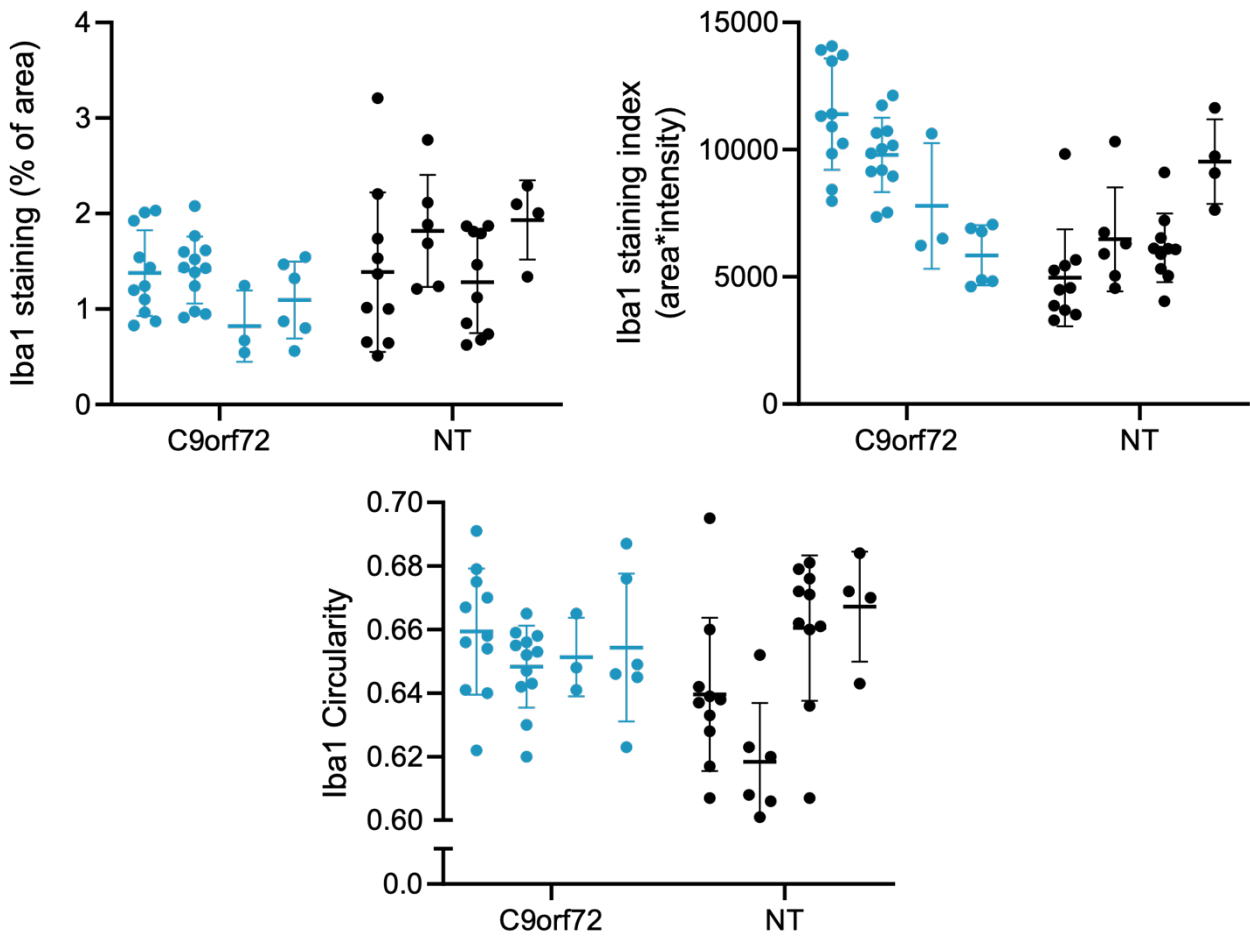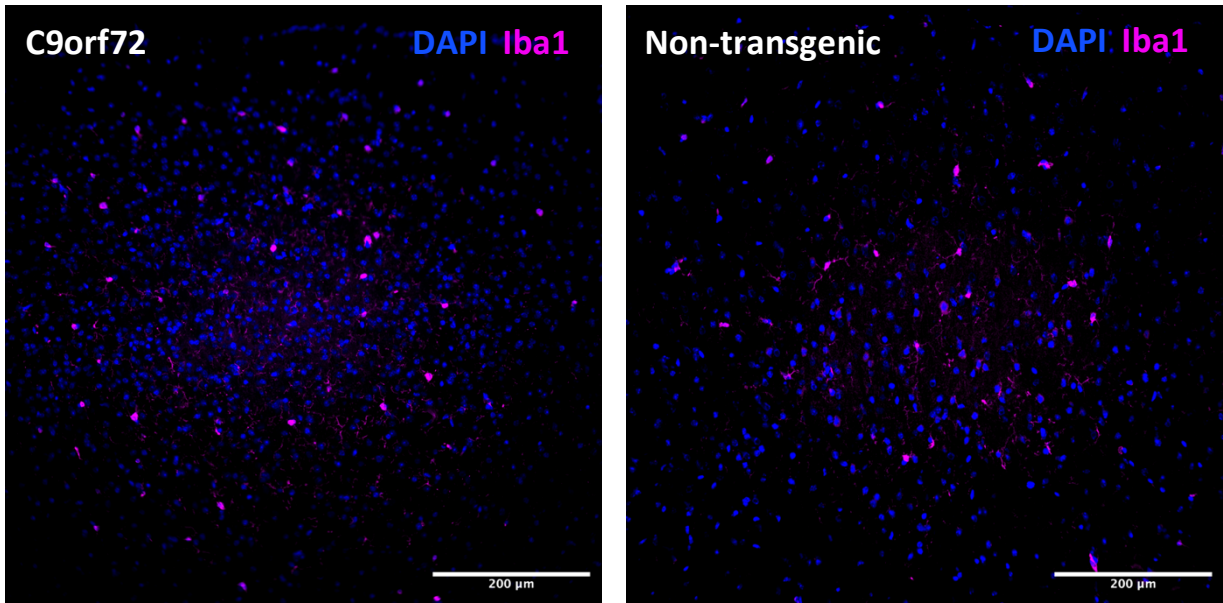
Figure 3.36: Iba1 staining of the motor cortex.

Quantification of Iba1 staining in the motor cortex of female C9orf72 and non-transgenic mice (n = 4 per group). No significant difference on a nested t-test.

4 Phenotypic Characterisation of the Janvier Mouse

4.1 Results

4.1.1 Confirmation of the *C9ORF72* Repeat Expansion Size

As in the JAX study, southern blots were undertaken on post-mortem frontal cortex tissue to ensure all C9orf72 mice recruited to the study carried approximately 500 repeats of the G4C2 expansion. Blots showed C9orf72 mice with repeat sizes ranging from 650-950 (see Figure 4.1 and Fig. S 2). In the study, one mouse had a contraction of the expansion to ~230 repeats (Fig. S 2 A) and was subsequently removed from data analysis.
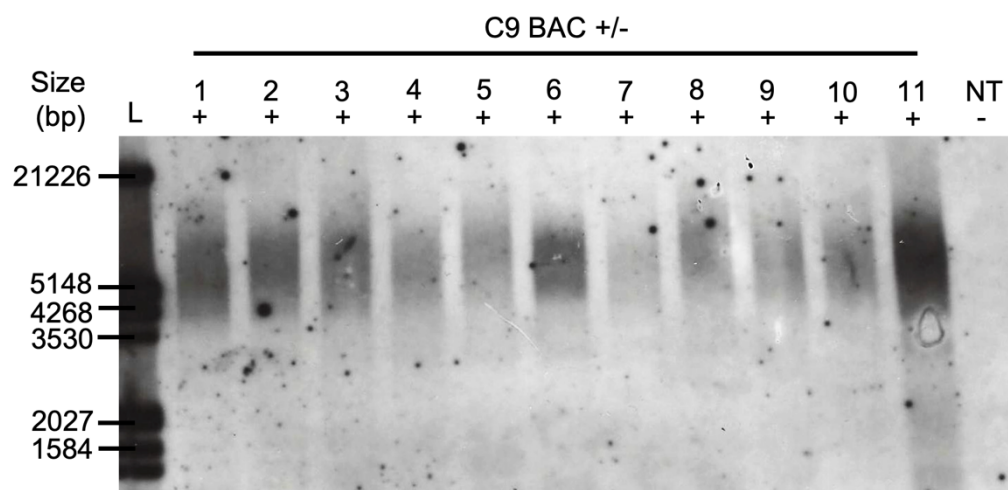
Figure 4.1: Confirmation of transgene with G4C2 repeat expansion in C9orf72 mice.

Southern blot of female C9orf72 mice showing repeat expansion size. Repeat size varied from 650-950 repeats. L, DNA ladder; +, transgene present; -, transgene absent; NT, non-transgenic control.

4.1.2 Behavioural Tests

4.1.2.1 Accelerating Rotarod Test

C9orf72 mice showed no significantly decreased latency to fall compared to NT littermates at all timepoints (Figure 4.2). At 52 weeks of age, C9orf72 and NT mice displayed a significantly decreased latency to fall compared to 12 weeks (C9orf72 n = 29-32, 290.7 ± 36.8 vs 218.1 ± 95.2, p = 0.01; NT = 28-35, 287.3 ± 33.5 vs 242.3 ± 63.6, p = 0.02).
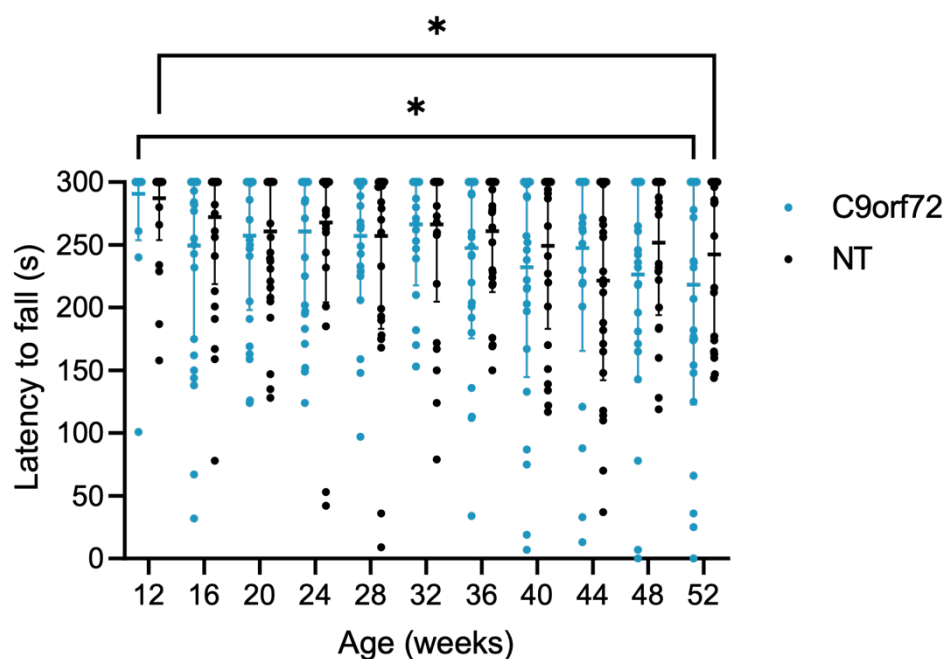
Figure 4.2: Mean latency to fall (± SD) of C9orf72 mice and non-transgenic (NT) mice.
Female C9orf72 mice showed no significantly decreased latency to fall (± SD) compared to NT mice at any timepoint. At 52 weeks of age both groups had significantly decreased latency to fall compared to 12 weeks. *p<0.05, two-way ANOVA with repeated measures and Tukey's post-hoc test (C9orf72 n = 29-32, NT n = 28-35).

As weight may impact rotarod performance, mean weight and mean rotarod performance were correlated (Figure 4.3). There was a highly significant correlation between weight and rotarod performance in C9orf72 mice (r = -0.8292, p<0.01) and NT mice (r = -0.8364, p<0.01). Following this, rotarod performance was normalised to weight by division of latency to fall by weight (Figure 4.4). A two-way ANOVA with Tukey's post-hoc test revealed no significant differences in rotarod performance between C9orf72 and NT mice once weight was accounted for. However, there was a significant decrease in performance at 52 weeks of age compared to 12 weeks in both groups.
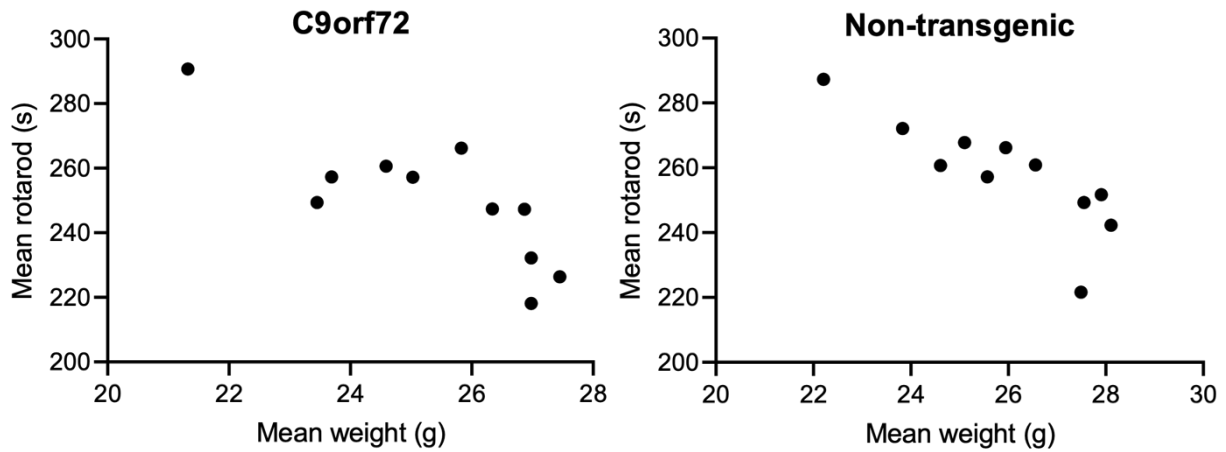
Figure 4.3: Spearman correlation of rotarod performance vs weight.

Spearman correlation of mean weight and mean rotarod performance of female C9orf72 and non-transgenic mice (C9orf72 r = -0.8292, p<0.01, NT r = -0.8364, p<0.01).
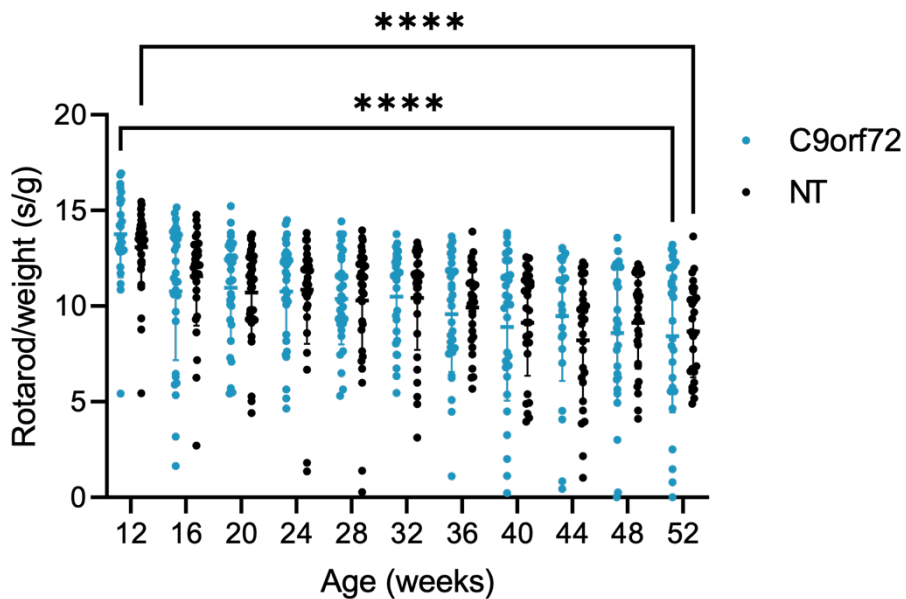
Figure 4.4: Rotarod performance/weight in C9orf72 and non-transgenic (NT) mice.

Mean latency to fall normalised to weight (± SD) showed no significant decreases between female C9orf72 and NT mice. At 52 weeks of age, both groups showed a significant decrease in latency to fall/weight ratio compared to 12 weeks. **** p<0.0001, two-way ANOVA with repeated measures and Tukey's post-hoc test (C9orf72 n = 29-32, NT n = 28-35).

4.1.2.2 Catwalk Gait Analysis

Gait analysis was performed at monthly intervals from 12 weeks of age. Descriptions of parameters are detailed in Table 2.3. There was no significant difference in stride length between groups over time (Figure 4.5A). There was no significant in hindlimb BOS between the two groups at any timepoint (Figure 4.5B). Hindlimb swing time remained stable with age with no significant difference between the two groups (Figure 4.5C). There was no significant difference in swing speed between the two groups at any timepoint (Figure 4.5D).
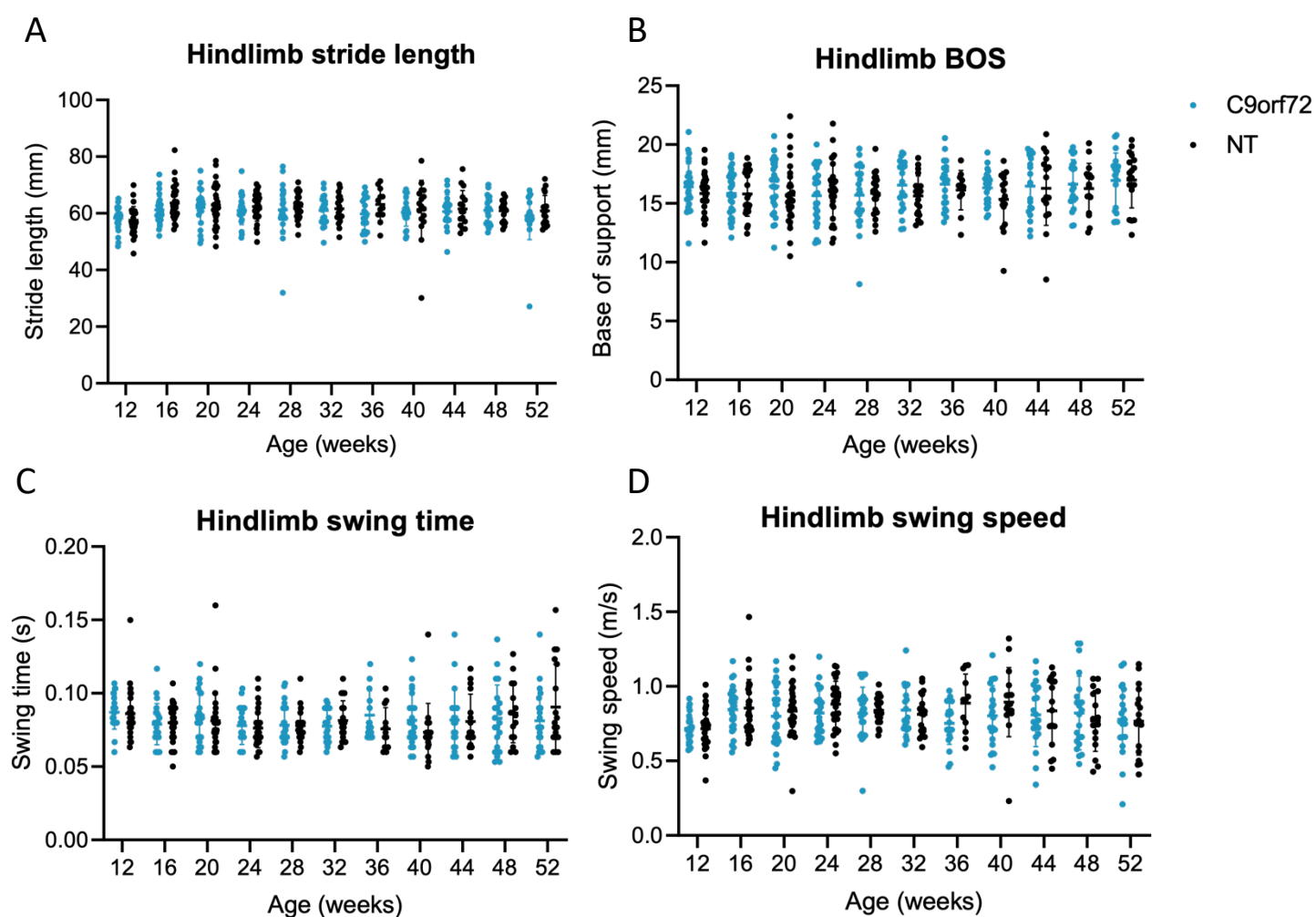
Figure 4.5: Catwalk gait analysis of C9orf72 and non-transgenic (NT) hindlimb stride length (A), base of support (B), hindlimb swing time (C), and swing speed (D).

Values are presented as the mean (± SD) of the left and right paws of each mouse. There were no significant differences between female C9orf72 and non-transgenic mice in any of the parameters (two-way ANOVA with repeated measures, C9orf72 n = 21-28, NT = 12-33).

Hindlimb print length remained stable with age, with no significant differences between the two groups (Figure 4.6 A). There was a slight decrease in width with age in both groups, but there was no significant difference between them at any timepoint (Figure 4.6 B). Most mice in both groups were well-coordinated, with no significant differences between them at any timepoint (Figure 4.6 C). Hindlimb intensity remained steady with age in both groups, and there were no significant differences between them at any timepoint (Figure 4.6 D).
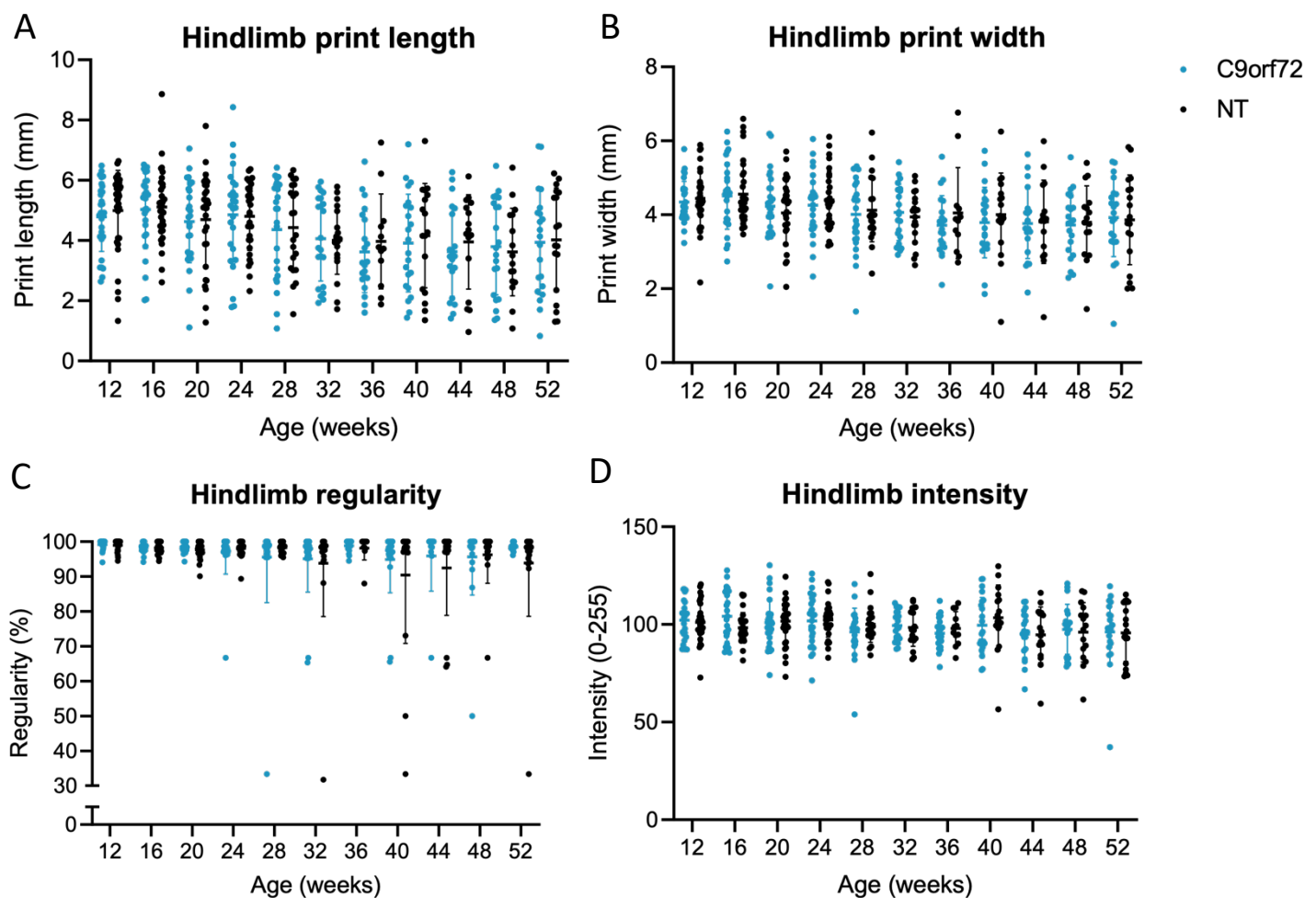
Figure 4.6: Catwalk gait analysis of C9orf72 and non-transgenic (NT) hindlimb print length (A), print width (B), regularity (C), and intensity (D).

Values are presented as the mean (± SD) of the left and right paws of each mouse. There were no significant differences between female C9orf72 and non-transgenic mice in any of the parameters (two-way ANOVA with repeated measures, C9orf72 n = 21-28, NT = 12-33).

Both groups spent most of the time on diagonal paws at all ages (Figure 4.7 A). The hindlimb duty cycle did not change with time and there were no significant differences between the two groups at any timepoint (Figure 4.7 B).

A

B
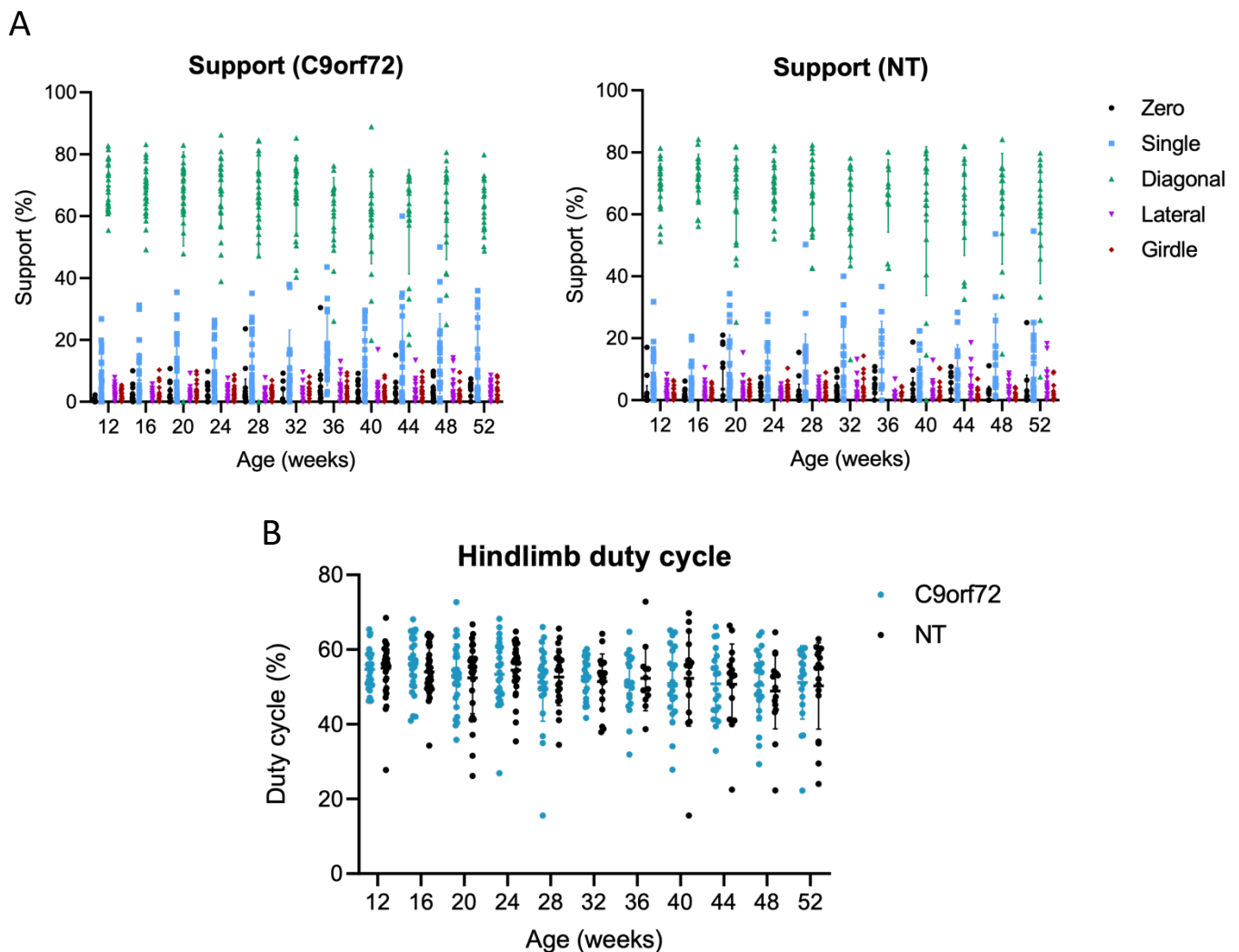
Figure 4.7: Catwalk gait analysis of percentage time spent on paws (B) and hindlimb duty cycle (A) in C9orf72 and non-transgenic (NT) mice.

Values are presented as the mean (± SD) of the left and right paws of each mouse. There were no significant differences between female C9orf72 and non-transgenic mice in any of the parameters (two-way ANOVA with repeated measures, C9orf72 n = 21-28, NT = 12-33).

4.1.2.3 Open Field

C9orf72 mice did not show a significant decrease in total distance travelled in the open field chamber at any timepoint (Figure 4.8 A, B), indicating no motor deficit. Quite a large proportion of mice from both groups displayed a larger total distance travelled (>15,000 cm). This was attributed to the high level of stereotypic behaviour observed in this study (Figure 4.8 C). When the chamber was virtually split into centre and periphery zones, C9orf72 mice did not spend any significantly more or less time in the centre of the open field chamber compared to NT mice at any timepoint (Figure 4.9).
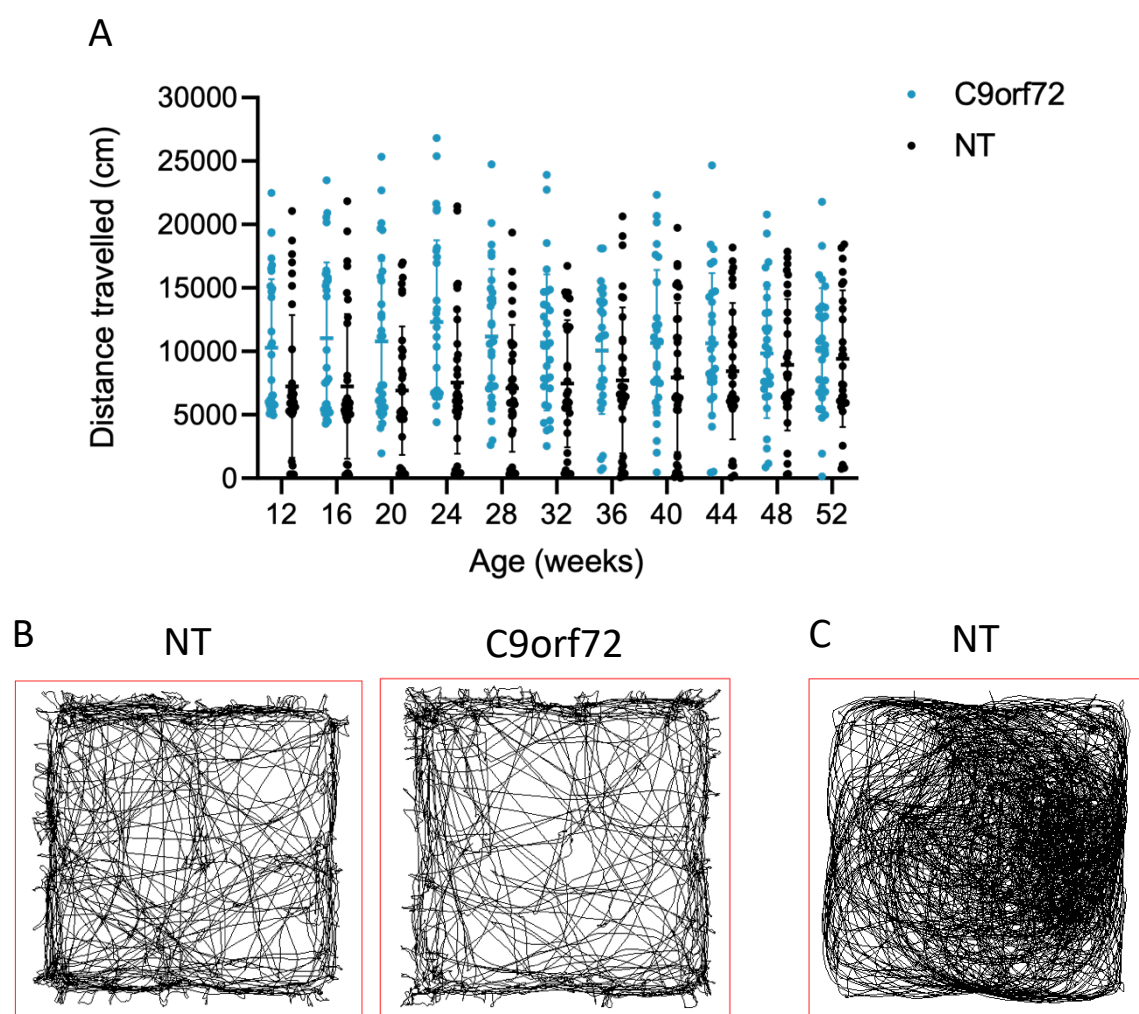
Figure 4.8: Mean distance travelled (± SD) of C9orf72 mice and non-transgenic (NT) mice.
(A) Female C9orf72 mice displayed no significantly decreased mobility compared to NT mice (two-way ANOVA with repeated measures, C9orf72 n = 29-32, NT n = 30-35). (B) Representative traces showing movement pattern in open field chamber after 10 minutes (52 weeks of age). (C) Representative example of stereotypic circling behaviour observed in both C9orf72 and NT mice.
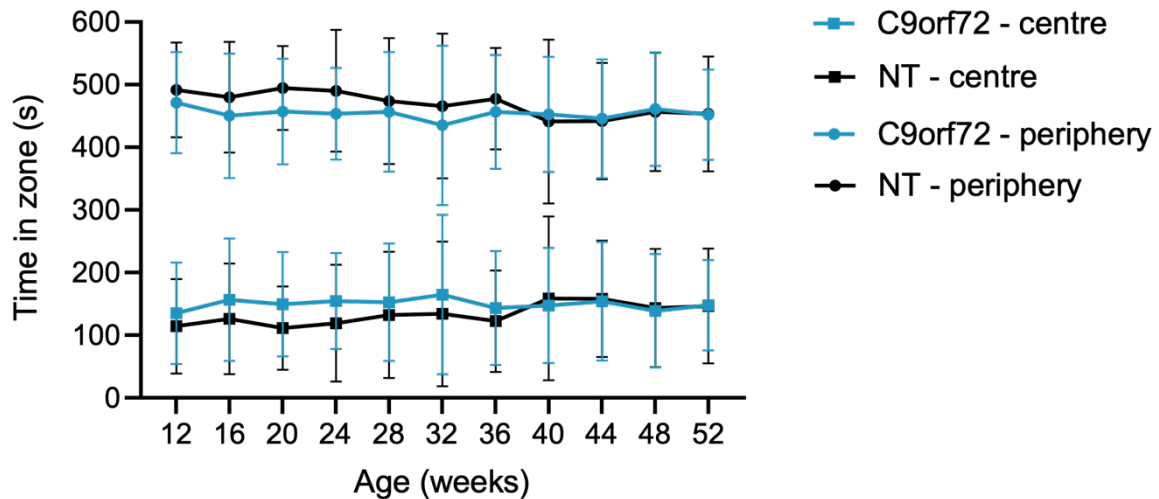
Figure 4.9: Mean time (± SD) in centre and periphery zones of open field chamber of C9orf72 mice and non-transgenic (NT) mice.

Female C9orf72 mice spent equivalent time (± SD) in the centre and periphery zones of the open field chamber as NT mice at every timepoint (two-way ANOVA with repeated measures, C9orf72 n = 29-32, NT n = 26-35).

4.1.2.4   Social Recognition Test

C9orf72 mice showed no significantly reduced investigation time in the recall session compared to the initial session when compared to NT, indicating no impaired social memory (Figure 4.10). However, both groups showed no significantly decreased investigation time in the recall session compared to the initial session and spent a similar amount of time investigating novel and familiar individuals, indicating both groups may have impaired social memory.

Recognition index (the ratio of recall investigation time relative to initial investigation time) also showed no differences in ability to recognise a familiar individual between C9orf72 and NT mice. It revealed that at most timepoints both groups spent equal or more time investigating the familiar mouse than the novel mouse (Figure 4.11), indicating impaired social memory.
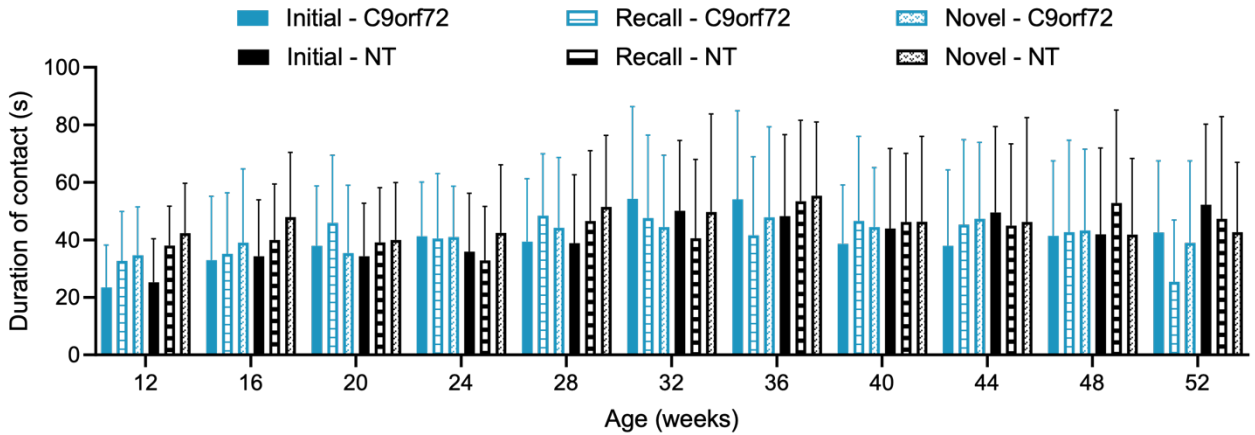
Figure 4.10: Mean duration of contact (± SD) with juvenile female mouse in C9orf72 mice and non-transgenic (NT) mice.

The same female juvenile mouse was used in the initial and recall sessions. Both female C9orf72 and non-transgenic mice showed no significantly decreased investigation time (± SD) in the recall session compared to the initial session at any timepoint (two-way ANOVA with repeated measures, C9orf72 n = 19-30, NT n = 14-28).
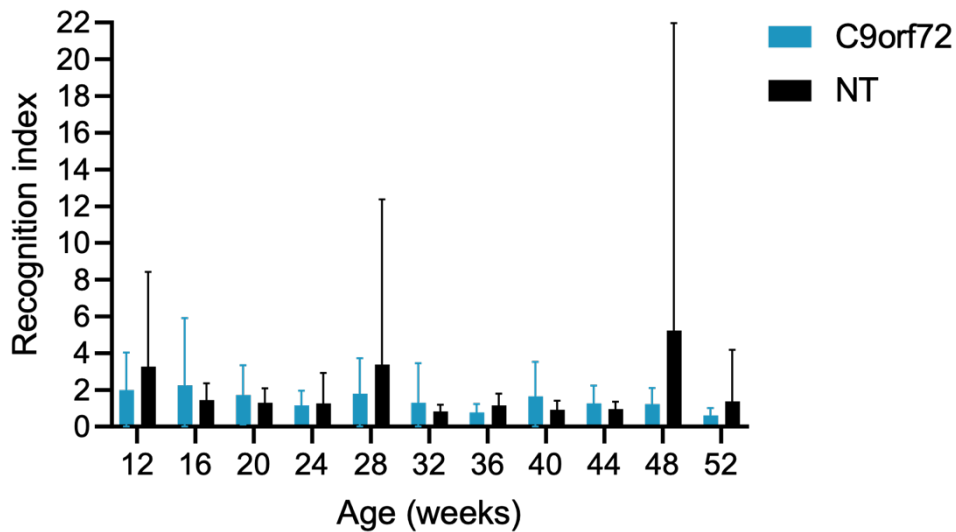
Figure 4.11: Recognition index of C9orf72 and non-transgenic (NT) mice.

Recognition index (the ratio of recall investigation time relative to initial investigation time, mean ± SD) showed no differences in ability to recognise a familiar individual between female C9orf72 and NT mice (two-way ANOVA with repeated measures, C9orf72 n = 19-30, NT = 14-28). Both groups spent equal or more time investigating the familiar mouse than the novel mouse (index = 1: equal time spent investigating familiar and novel mouse, index > 1: more time spent investigating familiar mouse compared to novel mouse, index < 1: more time spent investigating novel mouse compared to familiar mouse).

4.1.2.5 Marble Burying

C9orf72 mice did not bury significantly fewer marbles than NT mice, however NT mice showed a significant decrease in number of marbles buried at 52 weeks of age compared to 12 weeks (NT n = 30-35, 7.2 ± 2.9 vs 4.0 ± 3.2, p<0.01) (Figure 4.12).
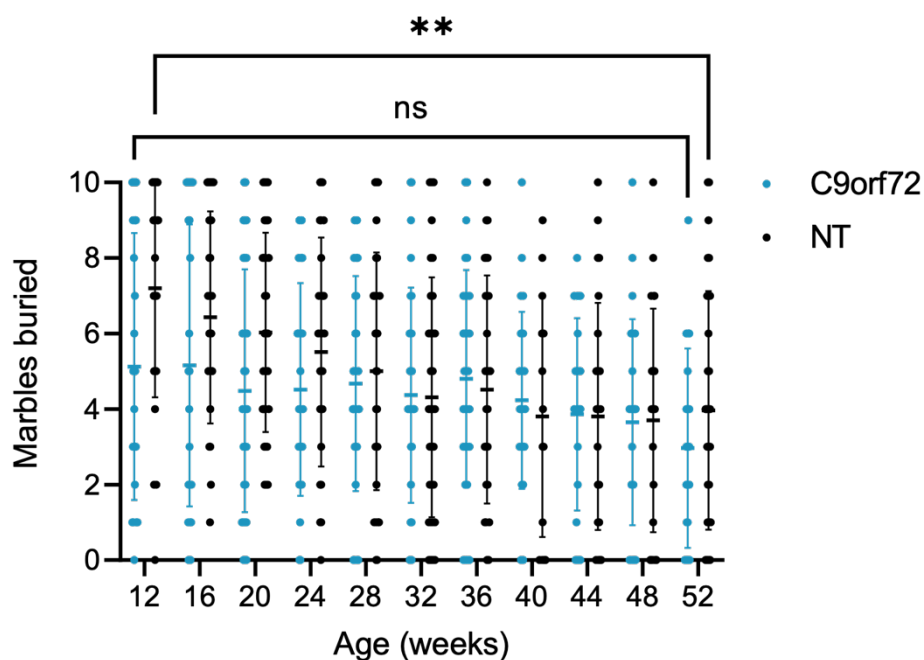
Figure 4.12: Mean number of marbles buried (± SD) by C9orf72 and non-transgenic (NT) mice.
There was no significant difference in number of marbles buried between female C9orf72 and NT mice at any timepoint. NT mice buried significantly fewer marbles at 52 weeks of age compared to 12 weeks. **p<0.01, two-way ANOVA with repeated measures, C9orf72 n = 29-32, NT n = 30-35.

4.1.2.6 Balance Beam

Median scores on the balance beam showed no difference in balance ability between C9orf72 and NT groups (Figure 4.13). A longitudinal analysis showed a slight decrease in balance ability from 44 weeks of age in both groups (Figure 4.14).
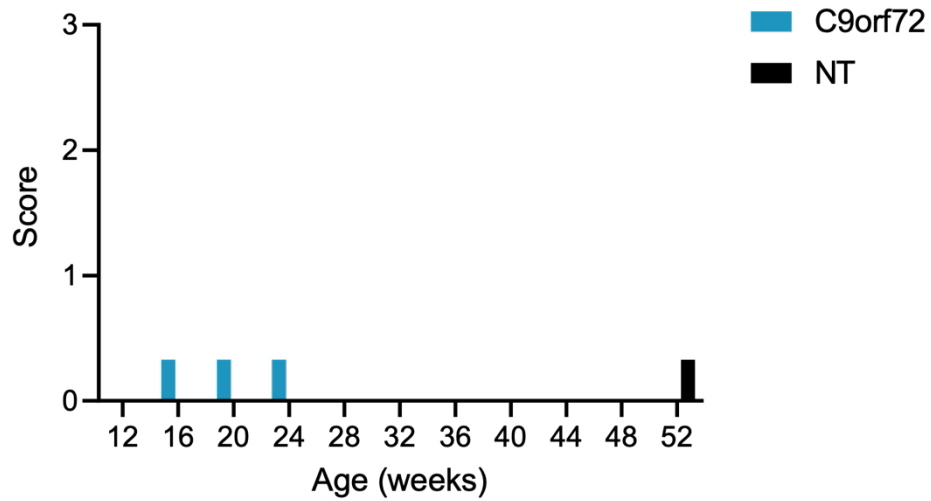
Figure 4.13: Median balance beam score of C9orf72 mice and non-transgenic (NT) mice.

Female C9orf72 mice displayed no significantly impaired coordination compared to NT mice at any timepoint (C9orf72 n = 29-32, NT n = 26-35).
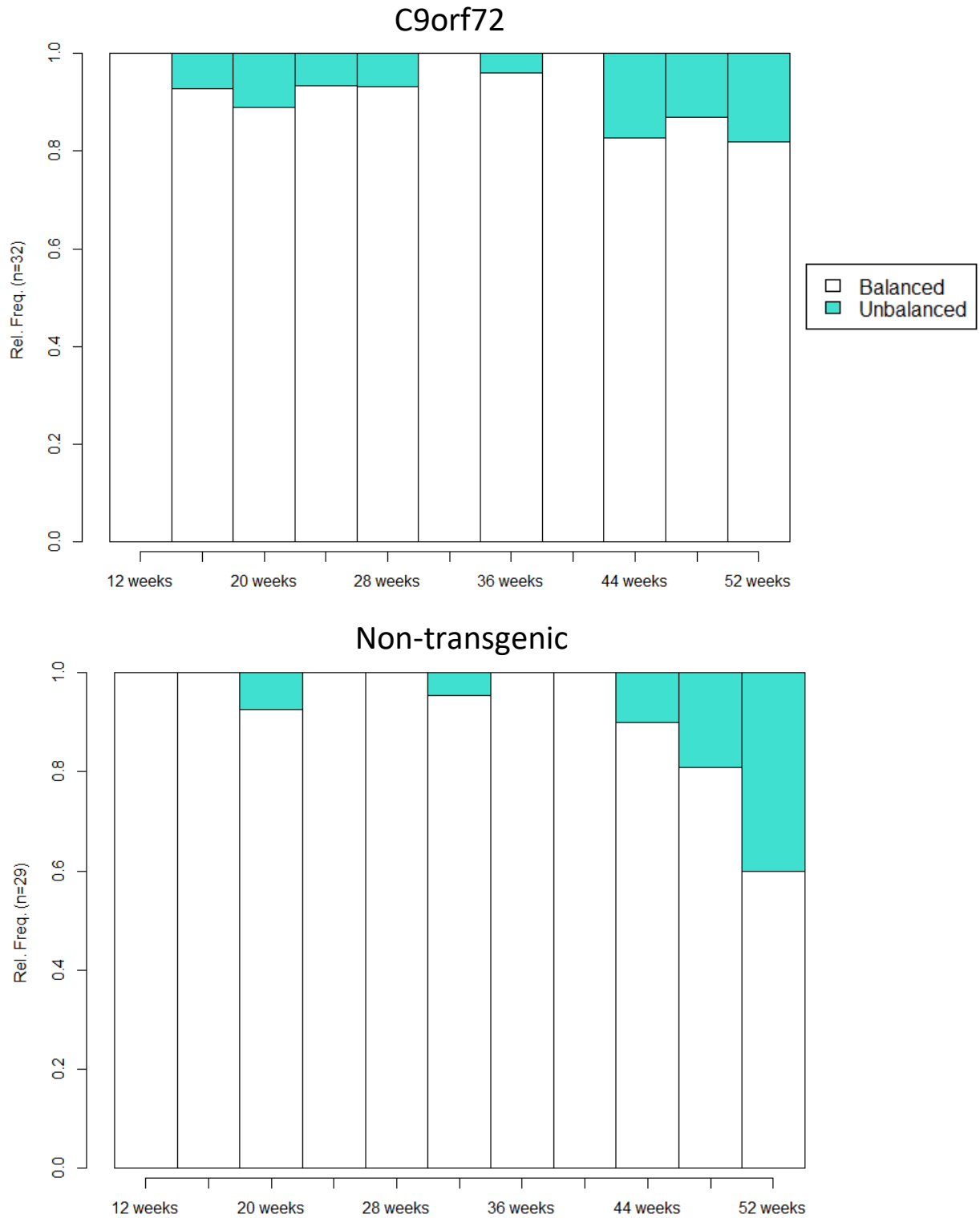
Figure 4.14: Longitudinal changes in balance beam scores in C9orf72 and non-transgenic (NT) mice. Longitudinal changes in the proportion of 'balanced' and 'unbalanced' scores in female C9orf72 and NT mice showed no change in balance ability in either group, with a slight increase in 'unbalanced' scores from 44 weeks of age.

4.1.2.7   Limb Hang Test

There was no significant difference in latency to fall between C9orf72 and NT mice (Figure 4.15). Within both groups, latency to fall was significantly decreased at 52 weeks of age compared to 12 weeks (C9orf72 n =29-32, 101.4 ± 74.6 vs 40.7 ± 38.9, p = 0.004; NT n = 23-35, 97.2 ± 86.1 vs 40.6 ± 42.5, p = 0.02).
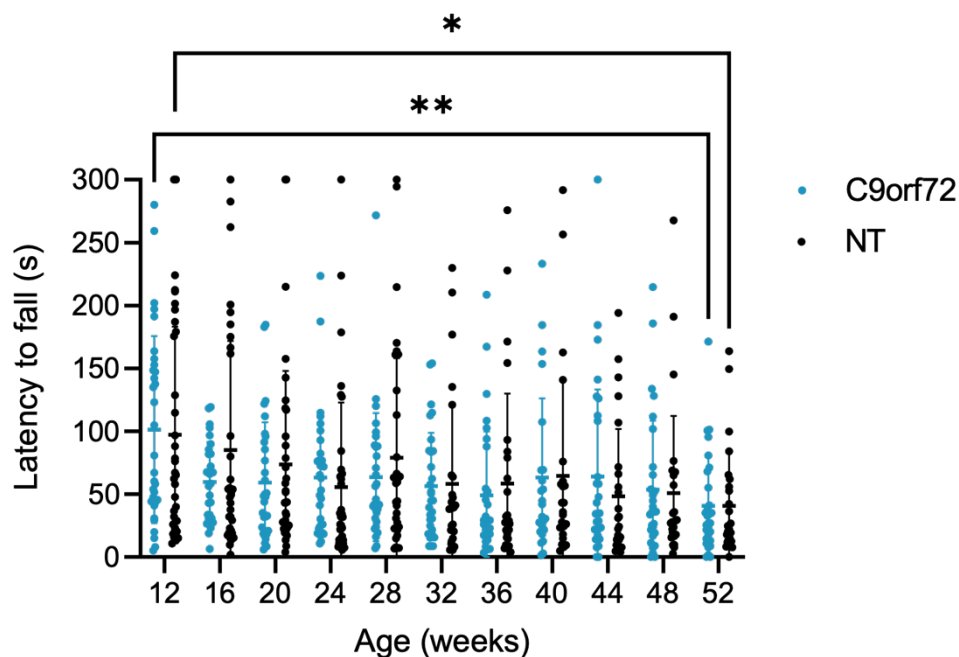
Figure 4.15: Mean hang time (± SD) of C9orf72 mice and non-transgenic (NT) mice.
Female C9orf72 mice showed no reduced hanging ability compared to NT mice at any timepoint. At 52 weeks of age, both groups showed significantly reduced hanging ability compared to 12 weeks. *p<0.05, ** p<0.01, two-way ANOVA with repeated measures and Tukey's post-hoc test (C9orf72 n = 29-32, NT n = 23-35).

To eliminate the influence of weight on ability to hang, limb hang performance was normalised to weight by division of mean hang time by weight (Figure 4.16). A two-way ANOVA with repeated measures and Tukey's post-hoc test revealed no significant differences in the ratio of hang time/weight between C9orf72 and NT mice, however there was a significant decrease in hang time/weight at 52 weeks of age compared to 12 weeks in both groups.
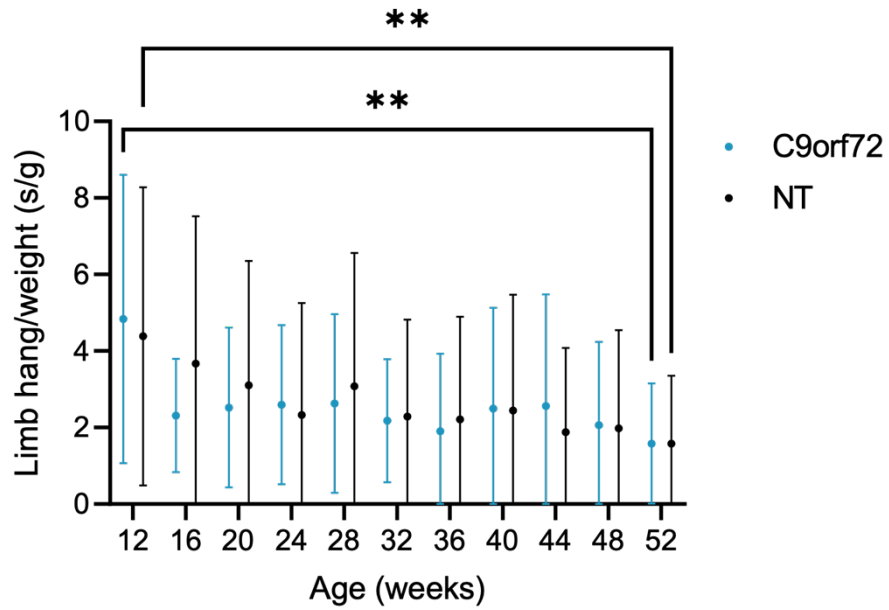
Figure 4.16: Limb hang/weight in C9orf72 and non-transgenic (NT) mice.

Mean latency to fall normalised to weight (± SD) showed no significant differences between female C9orf72 and NT mice. At 52 weeks of age, both groups showed a significant decrease in hang time/weight ratio compared to 12 weeks. ** p<0.01, two-way ANOVA with repeated measures and Tukey's post-hoc test (C9orf72 n = 29-32, NT n = 23-35).

4.1.2.8   Burrowing

There was no significant difference in weight burrowed between C9orf72 and NT mice, however there was a general non-significant decrease in both groups with age (Figure 4.17).
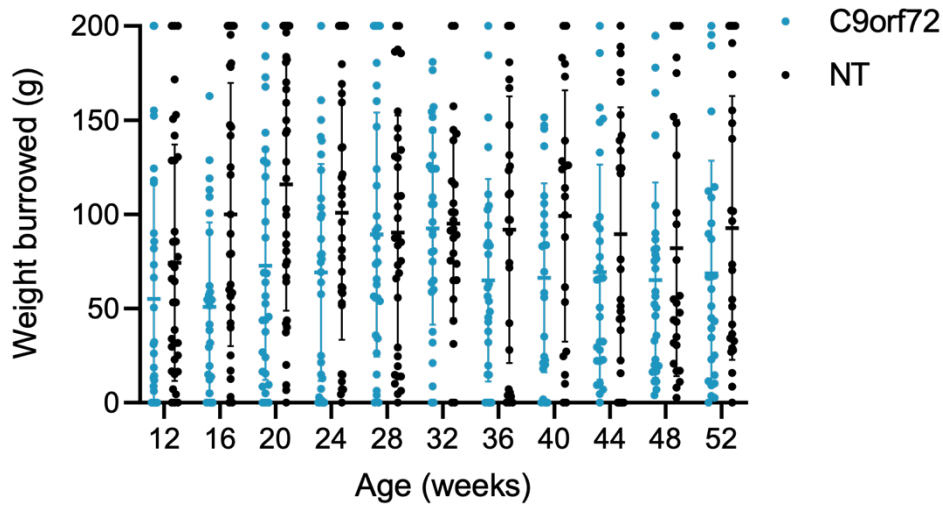
Figure 4.17: Mean weight burrowed (± SD) by C9orf72 and non-transgenic (NT) mice.

There was no significant difference in weight burrowed (± SD) between female C9orf72 and NT mice at any timepoint (two-way ANOVA with repeated measures, C9orf72 n = 29-32, NT n = 22-35).

4.1.2.9   Nesting

Median nesting scores showed no difference in nest building ability between C9orf72 and NT groups (Figure 4.18). However, a longitudinal analysis showed a general non-significant reduction in nest quality in both groups with age (Figure 4.19).
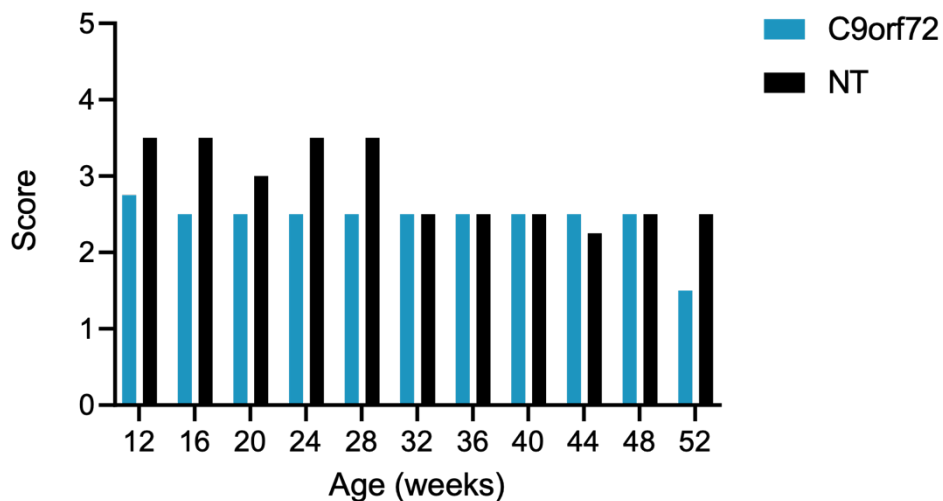
Figure 4.18: Median nesting score of C9orf72 mice and non-transgenic (NT) mice.

Female C9orf72 mice displayed no significantly impaired nesting behaviour compared to NT mice at any timepoint (C9orf72 n = 29-32, NT n = 26-35).
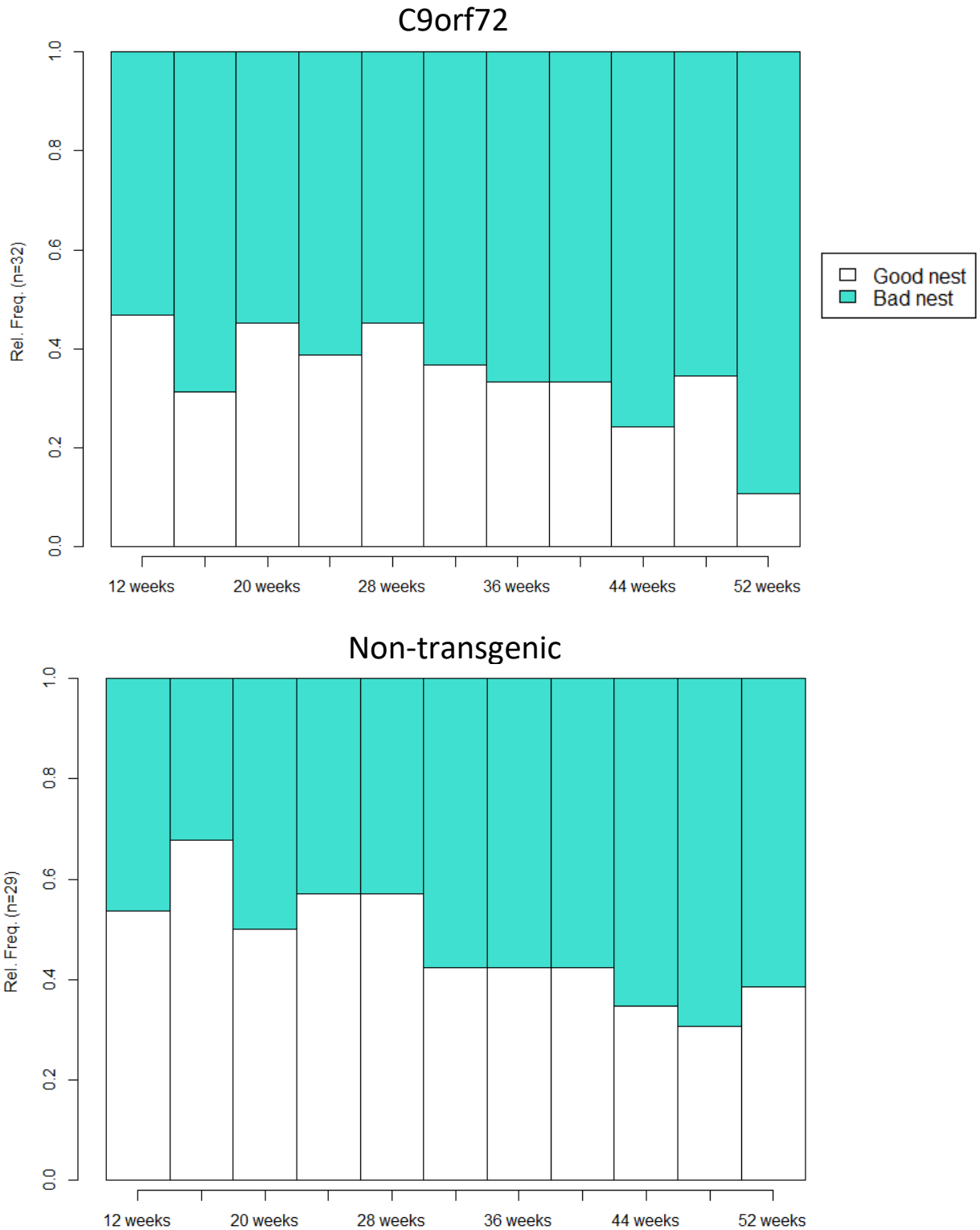
Figure 4.19: Longitudinal changes in nesting scores in C9orf72 and non-transgenic (NT) mice.

Longitudinal changes in the proportion of 'good nest' and 'bad nest' scores showed a general non-significant reduction in nest quality with age in both female C9orf72 and non-transgenic mice.

4.1.2.10 Food Intake

The test was performed overnight (16 hours) once a month alongside the nesting test. There was no significant difference in food intake between C9orf72 and NT mice at any timepoint on a two-way repeated measures ANOVA (Figure 4.20).
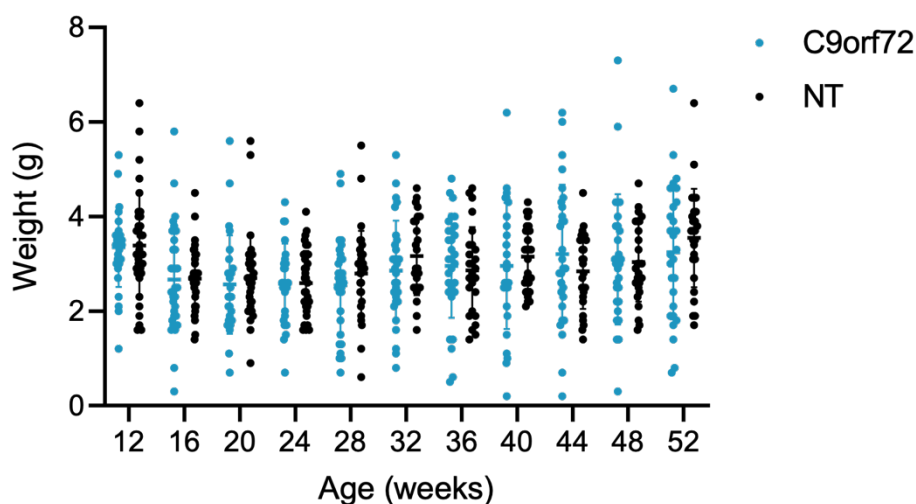
Figure 4.20: Mean weight (± SD) of food eaten overnight by C9orf72 and non-transgenic (NT) mice. Test was performed alongside nesting behaviour test. There was no significant difference in weight (± SD) of food eaten between female C9orf72 and non-transgenic mice at any timepoint (two-way ANOVA with repeated measures, C9orf72 n = 28-32, NT n = 26-35).

4.1.2.11 Weight

Both groups showed an increase in body weight with age (Figure 4.21). There was no significant difference between C9orf72 and NT mice at any timepoint on a two-way repeated measures ANOVA. Weight was monitored weekly, and no mouse required euthanasia due to progressive weight loss.
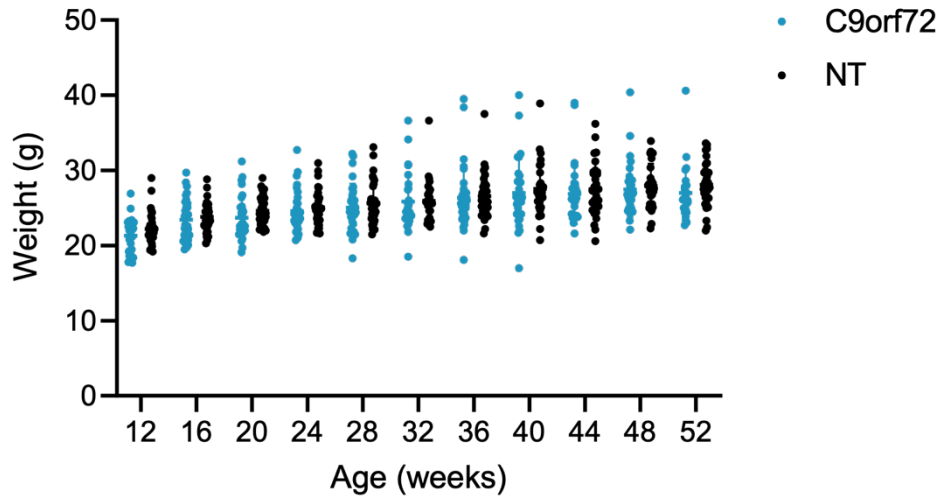
Figure 4.21: Mean body weight (± SD) of C9orf72 and non-transgenic (NT) mice.

Both groups increased body weight (± SD) from 12-52 weeks of age. There was no significant difference between female C9orf72 and non-transgenic mice at any timepoint (two-way ANOVA with repeated measures, C9orf72 n = 29-32, NT n = 30-35).

4.1.2.12 Subset Data Analysis

An analysis method to identify possible subsets hidden within the data was described in section 2.6.9. Results of this analysis are detailed in Table 4.1. Chi-Square analysis was performed between C9orf72 and NT groups for each test detailed.

Table 4.1: Contingency table counts of C9orf72 and non-transgenic (NT) mice.

Each number is the number of times a score was given in each test. Chi-Square analysis was performed between female C9orf72 and NT groups. None were found to be significantly different. MND-like phenotype = motor neurone disease-compatible score expected in diseased mice, Normal = normal score expected in healthy mice.

Test	C9orf72		Non-transgenic		p-value
	MND-like phenotype	Normal	MND-like phenotype	Normal	
Rotarod	8	24	4	24	0.35
Open field	6	26	9	19	0.25
Marble burying	13	19	13	15	0.79
Balance beam	14	18	12	15	>0.99
Limb hang	13	19	16	12	0.30
Burrowing	15	17	15	13	0.80
Nesting	14	18	13	15	>0.99
CMAP	17	15	15	13	>0.99

4.1.2.13 Running Wheel Test

A subset of C9orf72 (n = 14) and NT (n = 11) mice underwent a running wheel study following conclusion of the 12-month behavioural study to examine the effect of voluntary physical exercise on phenotype. Distance run, max speed, average speed, and time spent running were taken daily for analysis. No significant differences between C9orf72 and NT mice were found in any of the parameters (Figure 4.22 A-D). The study was halted early as it became apparent that both groups of mice were exhibiting stereotypic (circling) behaviour and not engaging with the running wheel.
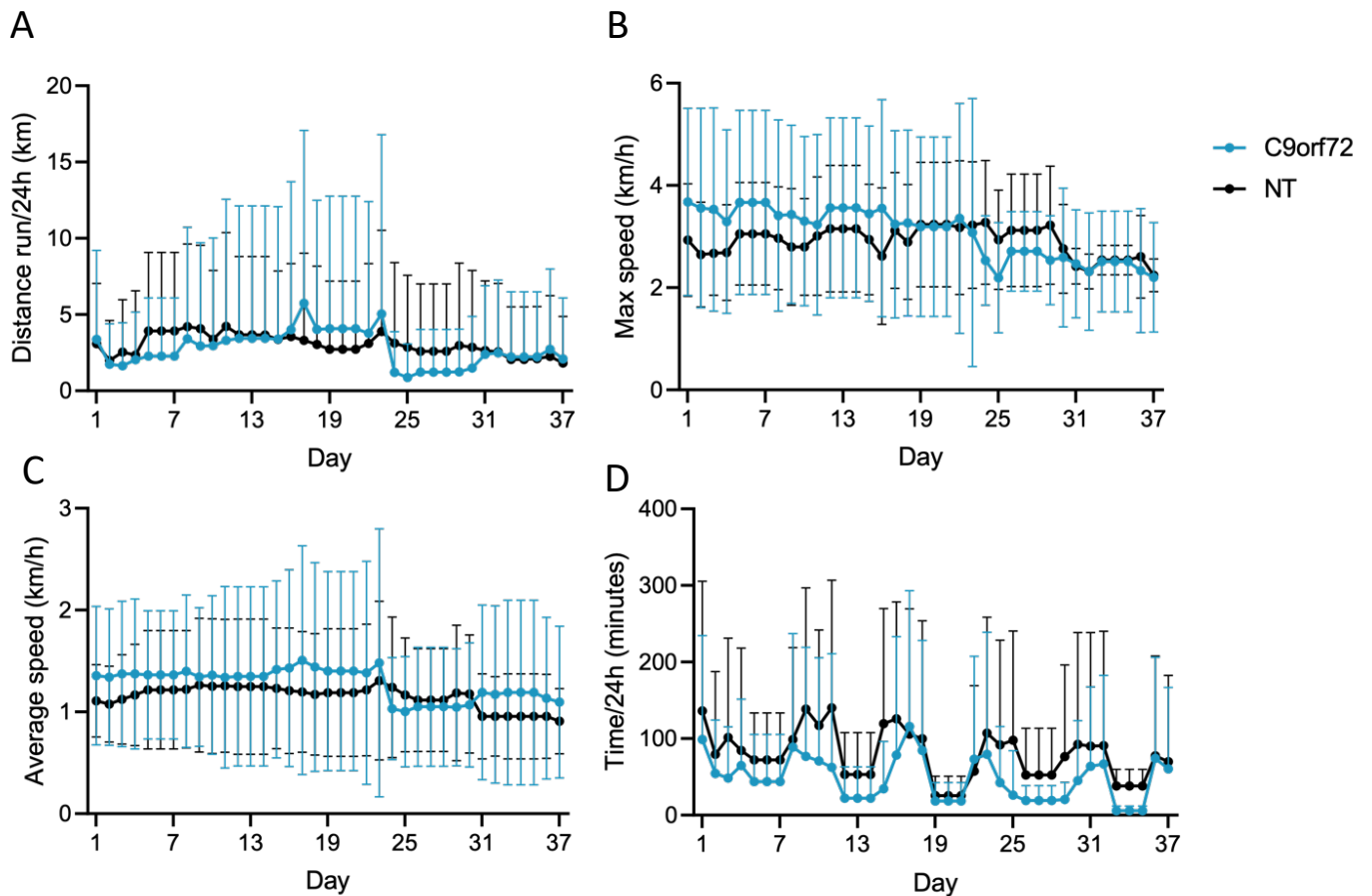
Figure 4.22: Running wheel activity per 24 hours (± SD) in C9orf72 and non-transgenic (NT) mice. There was no significant decrease in (A) distance run, (B) max speed, (C) average speed or (D) time spent running per 24 hours in female C9orf72 mice compared to NT littermates (mean ± SD, two-way ANOVA with repeated measures and Sidak's post-hoc test, C9orf72 n = 4-14, NT n = 4-11).

4.1.2.14 Electrophysiology

There was no significant change in CMAP amplitude in or between either group over time, indicating no loss of motor axons (Figure 4.23 A). Repetitive nerve stimulation revealed no significant decrement in response between repetition 1 and 10 in C9orf72 mice, suggesting a healthy NMJ at all timepoints, as well as no significant difference in response between C9orf72 and NT mice (Figure 4.24 B).

EMG recordings were taken from the gastrocnemius muscle in a small group of mice (C9orf72 n = 4, NT n = 3) at 52 weeks of age by Dr James Alix to examine for spontaneous EMG activity.

No fibrillation potentials, positive sharp waves, or fasciculation potentials were observed in either group (data not shown).
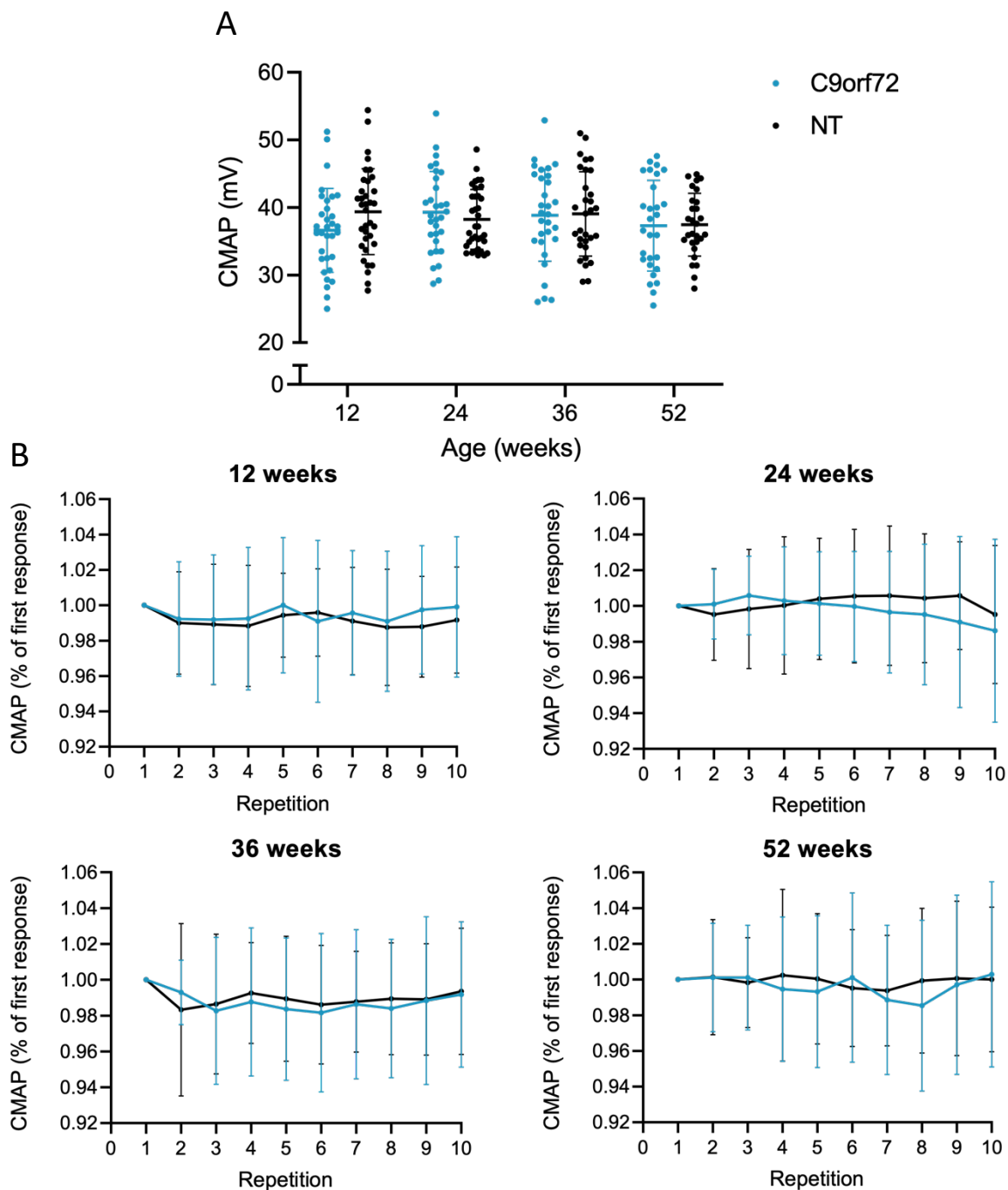
Figure 4.23: Electrophysiology of the hindlimb in C9orf72 and non-transgenic (NT) mice.

(A) There was no significant decrease in CMAP amplitude in female C9orf72 mice compared to NT mice at any timepoint. (B) Repetitive nerve stimulation tests revealed no significant decrement in response (represented as percentage of the first response) in C9orf72 mice compared to NT mice at any timepoint (mean ± SD, two-way ANOVA with repeated measures and Sidak's post-hoc test, C9orf72 n = 28-32, NT n = 28-36).

At 52 weeks of age prior to end of study, a small group of C9orf72 and NT mice underwent additional electrophysiological tests. There was no decrease in plantar interossei CMAP amplitudes in C9orf72 compared to NT mice (Figure 4.24 A). There was also no prolonged F wave latencies and no reduced persistence in C9orf72 mice compared to NT mice, indicating no F wave abnormalities suggestive of peripheral neuropathy (Figure 4.24 B, C).
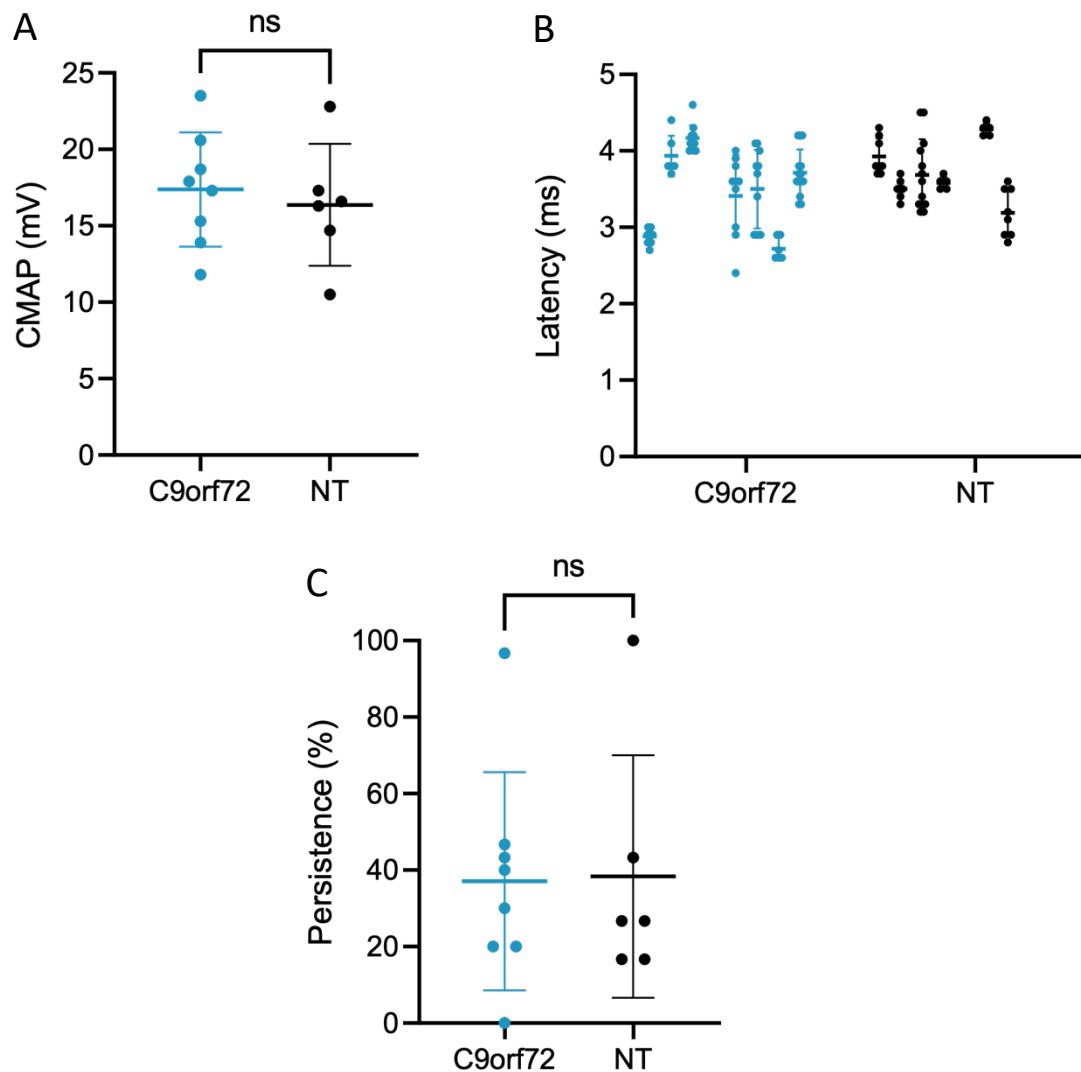
Figure 4.24: Plantar interossei CMAPs and F waves in C9orf72 and non-transgenic (NT) mice.
Plantar interossei CMAPs and F wave recordings were taken from a small group of female C9orf72 and NT mice at 52 weeks of age prior to end of study. (A) There was no reduction in plantar interossei CMAP amplitude in C9orf72 mice compared to NT (unpaired t-test). (B) F wave latencies were not significantly prolonged in C9orf72 mice (nested t-test), (C) and F wave persistence was unchanged in C9orf72 mice (mean ± SD, C9orf72 n = 7-8, NT n = 6).

4.1.2.15 Survival

There was no reduction in survival in C9orf72 mice compared to NT (Figure 4.25). Of the three C9orf72 mice that died during the study, two were found dead in their home cages and one was euthanised on advice of the resident veterinarian due to a severe eye infection. Of the five NT mice that died, three were found dead in their home cages, one was euthanised due to a seizure, and one was euthanised due to substantial distress of unknown cause.

When possible, post-mortems were performed on mice found dead to ascertain cause of death. However, no cause was found. The only characteristic of note was a wet ventral neck present on all C9orf72 and NT mice found dead.
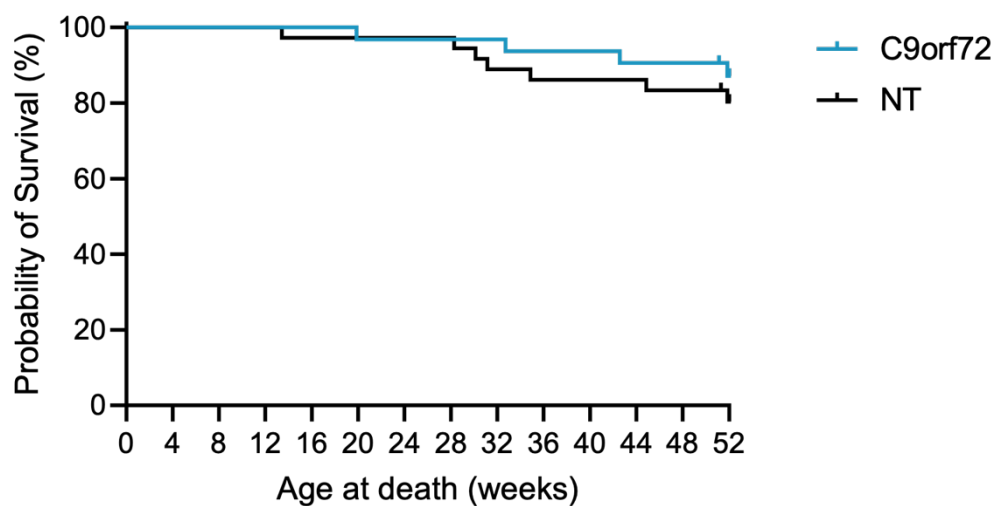
Figure 4.25: Survival curve of C9orf72 and non-transgenic (NT) mice.

Kaplan-Meier survival curve of female C9orf72 mice shows no decreased survival compared to NT mice (Gehan-Breslow-Wilcoxon test, p = 0.8202; C9orf72 n = 32, NT n = 36).

Representative examples of clasping scores were shown in Figure 3.26 A. The proportions of each score given at each timepoint for both groups in this study are shown in Figure 4.26.
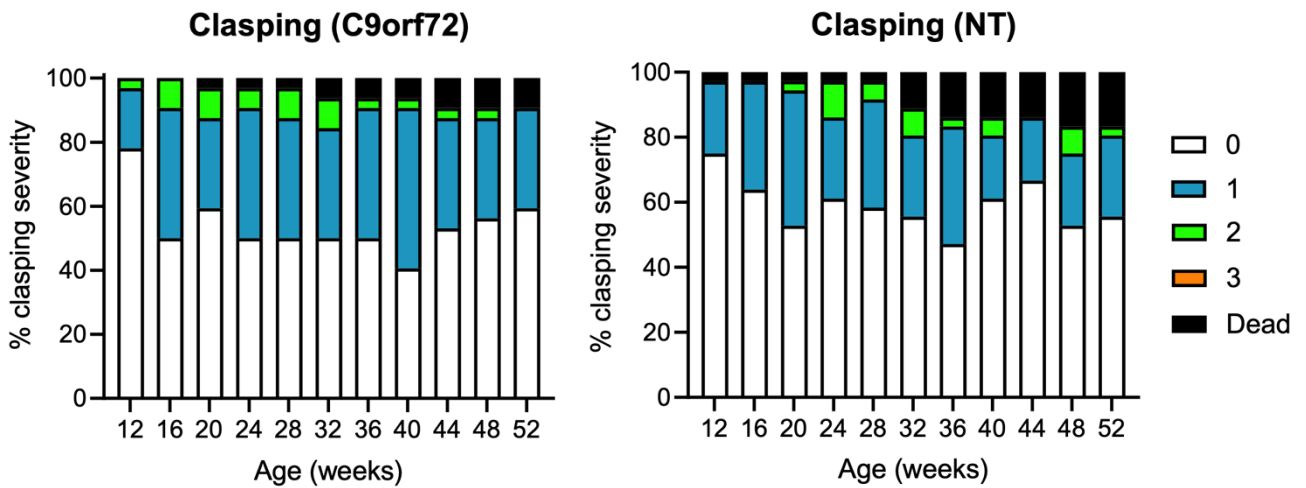
Figure 4.26: Clasping phenotypes of C9orf72 and non-transgenic (NT) mice.

Graphical depiction of female C9orf72 and NT mice displaying clasping phenotypes from 12-52 weeks of age (C9orf72 n = 33, NT n = 36).

4.1.2.16 Stereotypic Behaviour

Stereotypic circling behaviour was observed in both C9orf72 and NT groups (Figure 4.27). At the beginning of the study, over 50% of C9orf72 mice were already exhibiting circling behaviour. Incidence increased over time in both groups.
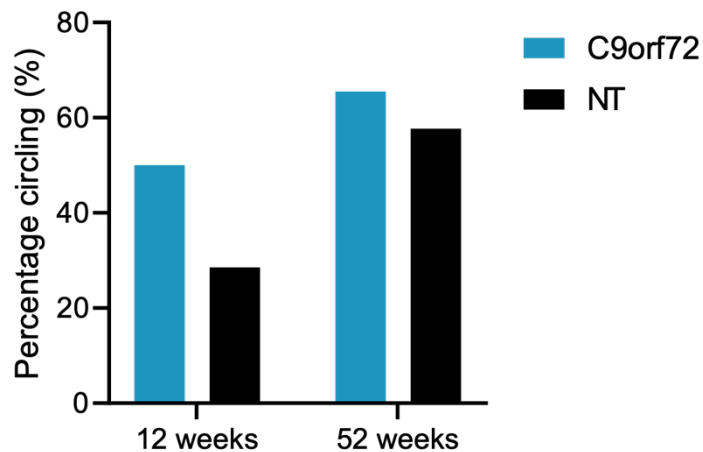
Figure 4.27: Stereotypic circling behaviour in C9orf72 and non-transgenic (NT) mice.

Stereotypic behaviour was observed in both female C9orf72 and non-transgenic mice at 12 weeks of age and increased in incidence over time.

4.1.2.17 Variability of Behavioural Tests

Many of the behavioural tests show substantial variability. To investigate this, the coefficient of variability was calculated for C9orf72 and NT mice in each test and compared (Figure 4.28). As expected, the behavioural tests showed the largest variability, with the balance beam, limb hang, and burrowing tests showing the most. Neither group demonstrated more variability than the other. The electrophysiological tests showed the least variability as they were not reliant on mouse behaviour and demonstrate that the technique has a high level of reproducibility.
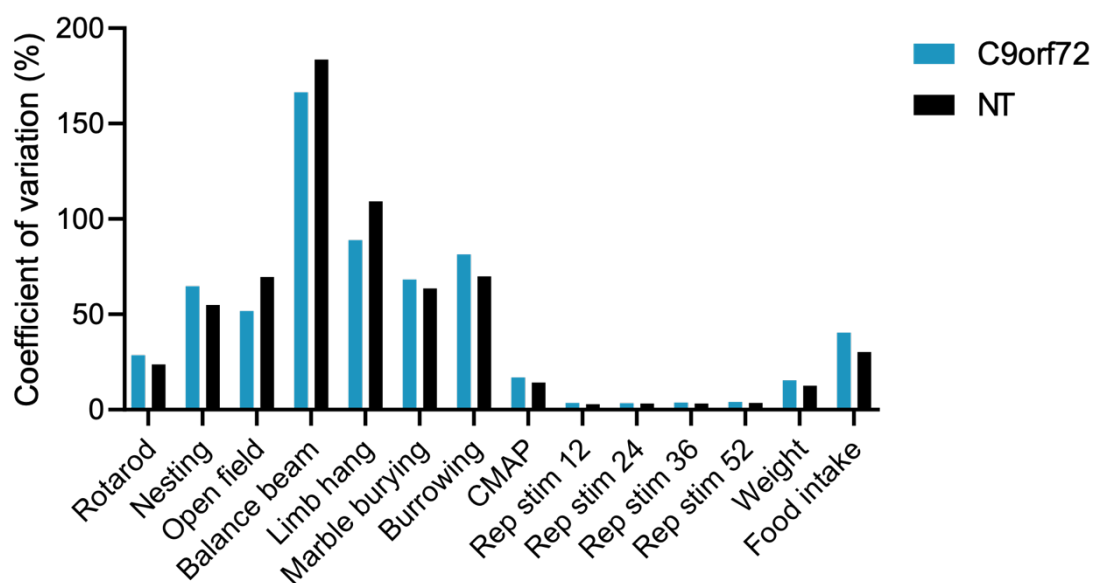
Figure 4.28: Variability of behavioural tests.

Coefficient of variation showed both female C9orf72 and non-transgenic mice were equally variable within each test. Balance beam, limb hang, and burrowing show the largest amount of variability.

4.1.2.18 Seizure Observations

As mentioned in section 3.1.2.15, seizure susceptibility is a well-known phenotype in the FVB/N background strain. Seizures were observed in C9orf72 and non-transgenic mice throughout this study. Seizures were timed at onset or from time of discovery and scored according to the scale from Van Erum et al. (2019). Severe or repetitive seizures, or failure to recover from seizure, resulted in euthanasia. Seven mice were observed seizing in this study, one of which required euthanasia (Table 4.2).

Table 4.2: Seizures observed in C9orf72 and non-transgenic (NT) mice.

Seizures were scored according to Van Erum et al. (2019). Scores 1 to 3 were classed as mild (1, whisker trembling; 2, sudden behavioural arrest; 3, facial jerking). Scores 4 to 6 were classed as moderate (4, neck jerks; 5, clonic seizure (sitting); 6, clonic, clonic-tonic seizure (lying on belly)), 7 and 8 were classed as severe (7, clonic, clonic-tonic seizure (lying on side) and wild jumping; 8, tonic extension, possibly leading to respiratory arrest and death).

Genotype	Age	Score	Euthanasia
C9orf72	10 weeks	2	No
NT	20 weeks	3	No
NT	30 weeks	3	Yes
NT	44 weeks	5	No
NT	45 weeks	5	Yes
NT	49 weeks	4	No
NT	35 weeks	5	Yes

Two NT mice were culled mid-seizure and the hippocampus of each was histopathologically analysed to investigate for neurodegeneration, astrogliosis or neuroinflammation (microgliosis). NeuN staining revealed neurodegeneration in the CA and DG regions of the hippocampus that was not present in a mouse not observed to have seizures (Figure 4.29). Astrogliosis and neuroinflammation were also present in the hippocampus compared to C9orf72 and NT mice not observed to have seizures (Figure 4.30). Quantification showed increased GFAP staining area and slightly increased staining index (a measure of staining intensity) in one mouse, while the other showed increased GFAP staining area but no increased staining index, and increased Iba1 staining area and staining index (Figure 4.30).
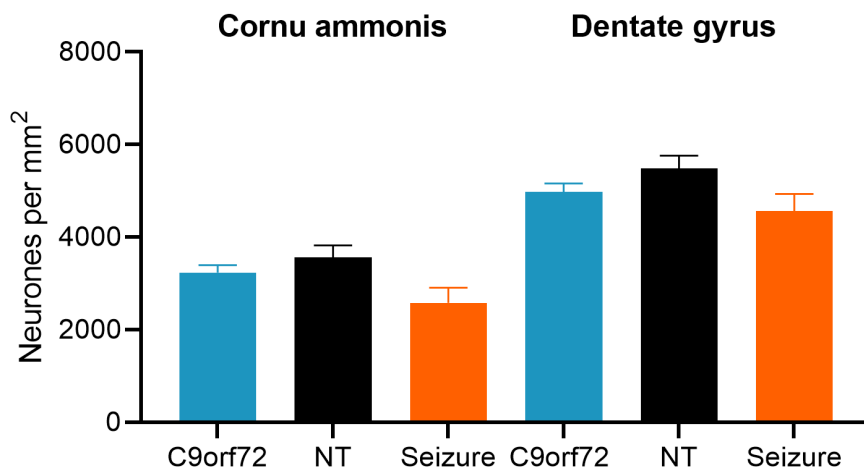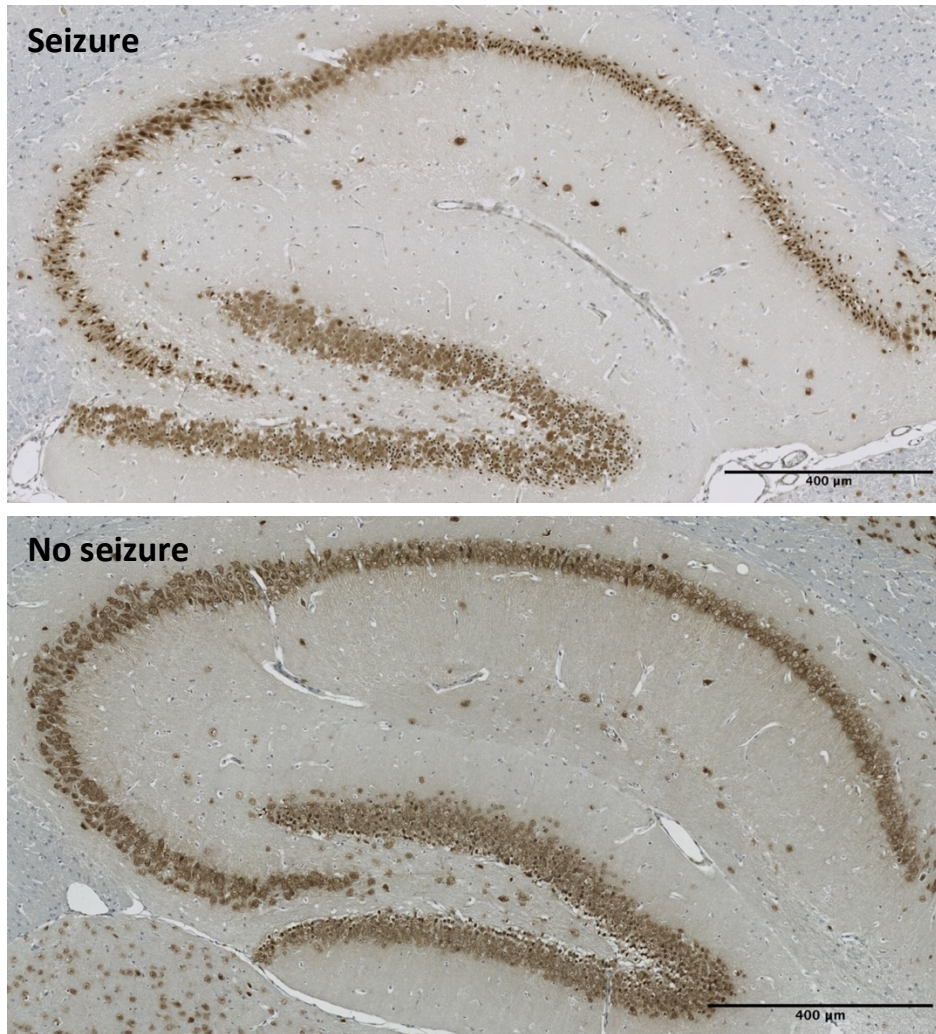
Figure 4.29: Hippocampal neuronal counts in C9orf72 and non-transgenic mice not observed to have seizures compared to non-transgenic mice culled mid-seizure.

NeuN staining shows neurodegeneration in the CA and DG regions of the hippocampus in female non-transgenic mice culled mid-seizure compared to mice not observed to have seizures.
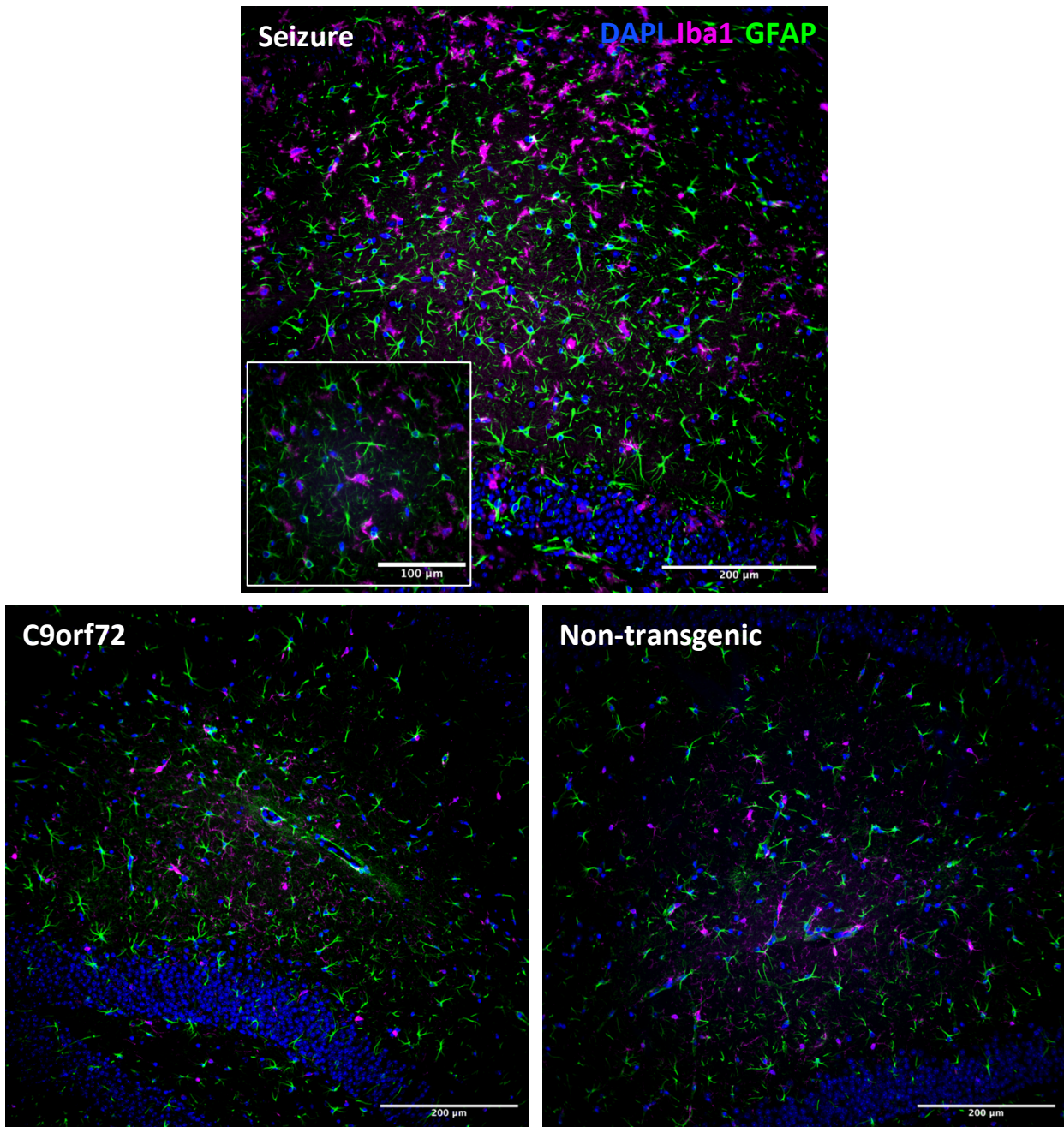
Figure 4.30: Histopathology of mice culled mid-seizure shows astrogliosis and neuroinflammation in the dentate gyrus.

GFAP and Iba1 staining of the dentate gyrus from a NT mouse culled mid-seizure compared to C9orf72 and NT mice with no observed seizures. Inset: x60 magnification.
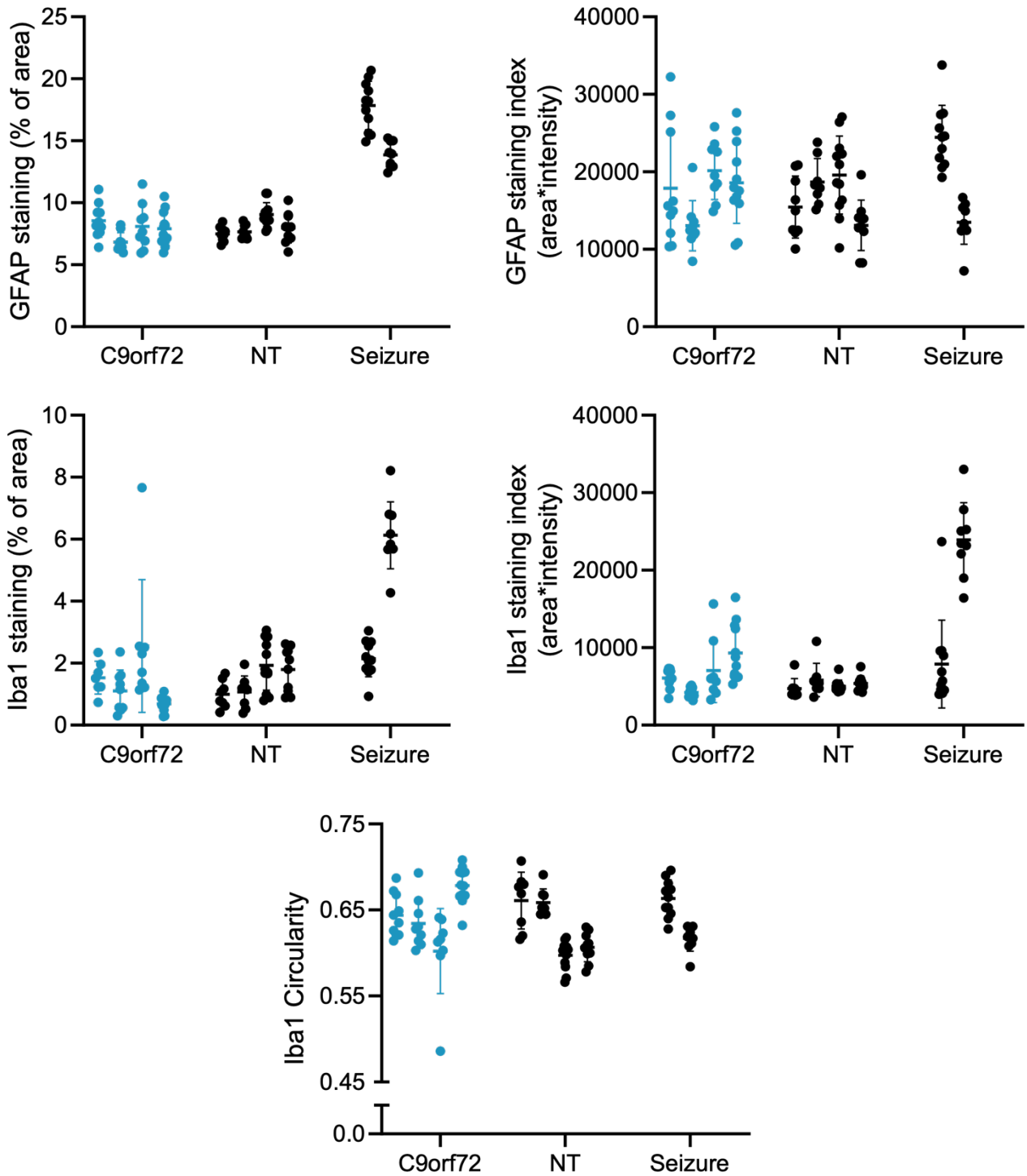
Figure 4.31: Quantification of histopathology of mice culled mid-seizure.

Both female non-transgenic mice culled mid-seizure show increased GFAP staining area compared to mice not observed to have seizures. One of the mice culled mid-seizure also shows increased Iba1 staining area and staining index compared to mice not observed to have seizures.

4.1.3 Tissue Pathology

4.1.3.1 Dipeptide Repeat Protein Quantification

Detection of dipeptide repeat proteins (DPRs) was performed by Meso Scale Discovery (MSD) immunoassay on frontal cortex and gastrocnemius muscle tissue taken at 52 weeks of age. Poly-GP and poly-GA DPRs were both detected in the frontal cortex tissue at significantly elevated levels compared to NT controls (Figure 4.32 A), indicating expression of the *C9ORF72* transgene. The remaining DPRs, poly-GR, poly-PA, and poly-PR, were not detected (data not shown). Only poly-GP was detected in the gastrocnemius muscle (Figure 4.32 B).
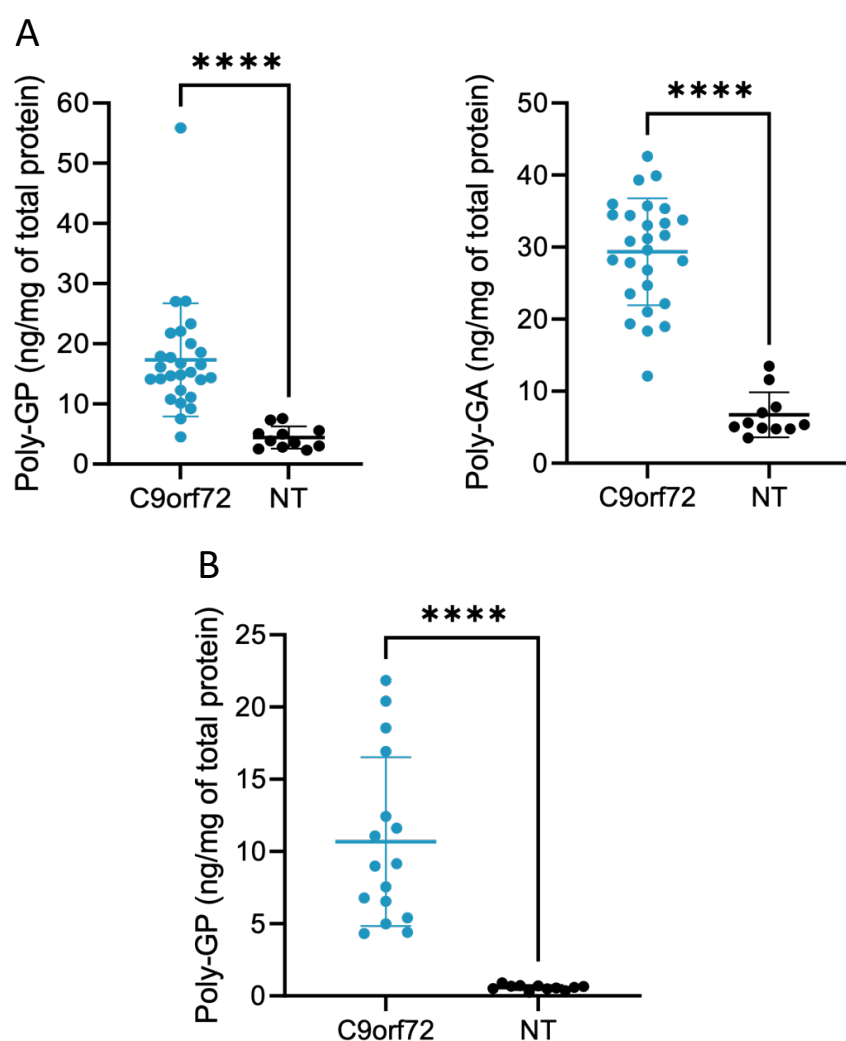
Figure 4.32: Dipeptide repeat protein detected in brain tissue of C9orf72 mice.

Meso scale discovery (MSD) immunoassay for poly-GP and poly-GA dipeptide repeat proteins in (A) frontal cortex and (B) gastrocnemius muscle tissue in female C9orf72 mice compared to non-transgenic controls (unpaired t-test, **** $p < 0.0001$, cortex: C9orf72 n = 28, NT n = 11, muscle: C9orf72 n = 16, NT = 11, mean ± SD).

4.1.3.2 Neurone Counts

Motor neurone counts were performed in ventral horns of the L4-5 region of the spinal cord in 52-week-old mice. There was no significant difference in the number of motor neurones in this region between C9orf72 and NT mice (Figure 4.33).
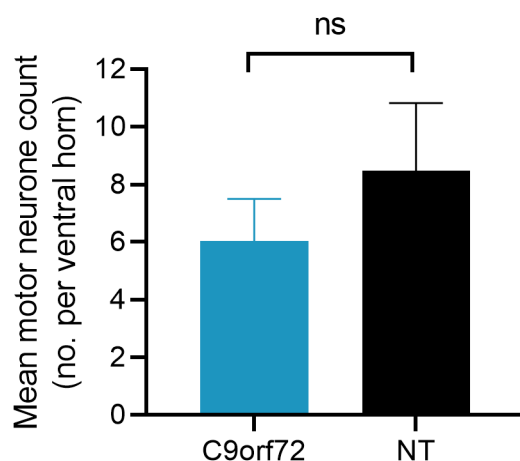
Figure 4.33: Motor neurone count in the lumbar spinal cord.

(A) Nissl staining of motor neurones in the lumbar spinal cord. (B) No significant motor neurone loss in the lumbar spinal cord of female C9orf72 mice compared to non-transgenic controls (mean ± SD, nested t-test, n = 7 per group).

Neuronal counts were performed in the CA and DG regions of the hippocampus (Figure 4.34) and layer V of the motor cortex (Figure 4.33) in 52-week-old mice. There was no significant difference in the number of neurones between C9orf72 and NT mice in any of the hippocampal regions or layer V of the motor cortex.
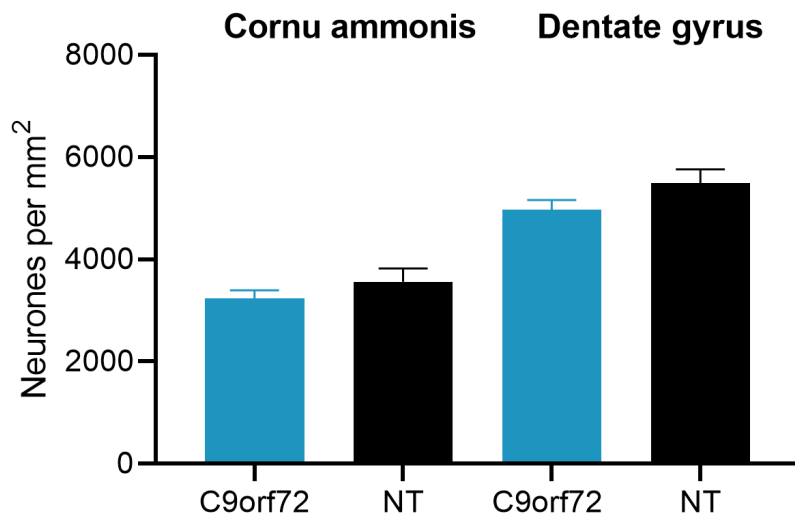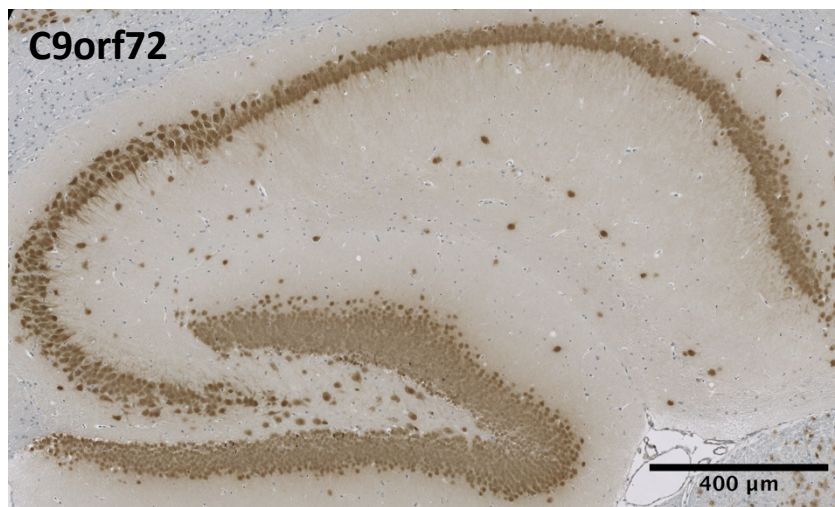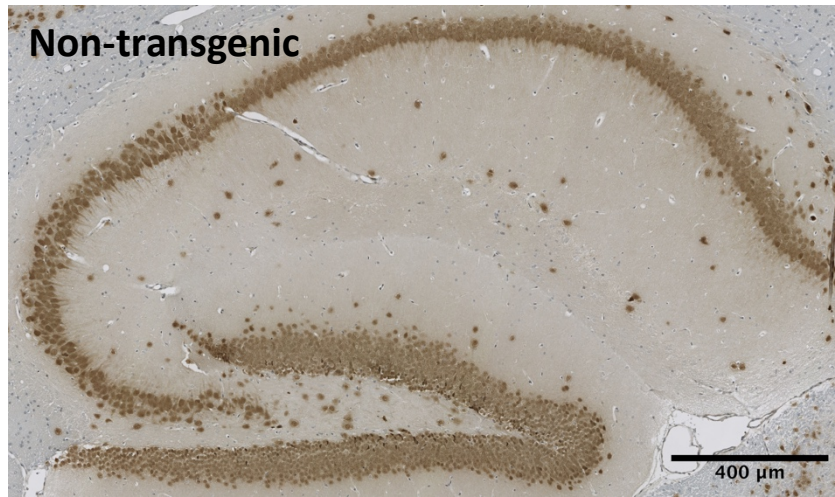
Figure 4.34: Neuronal counts in the hippocampus of C9orf72 and non-transgenic (NT) mice.

There was no significant difference in neuronal counts in the hippocampus between female C9orf72 and NT mice (mean ± SD, nested one-way ANOVA with Bonferroni's multiple comparisons, n = 4 per group).
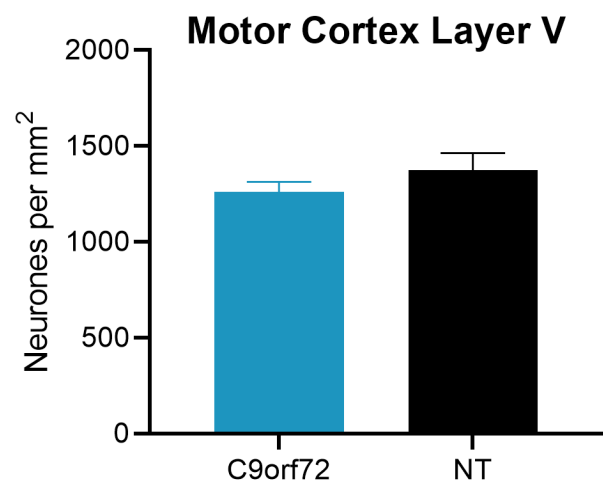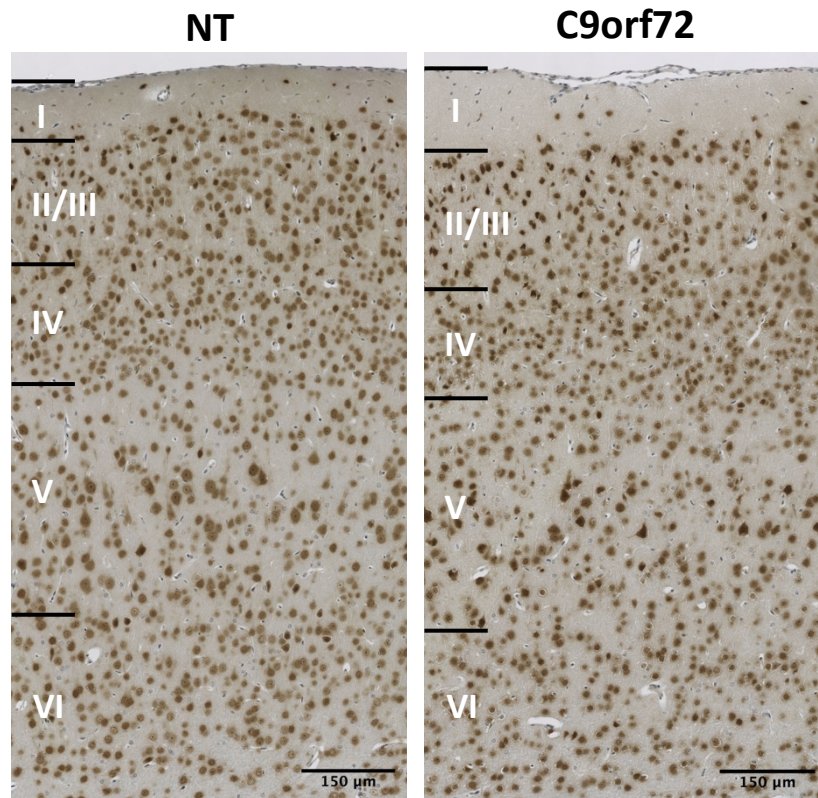
Figure 4.35: Neuronal count in layer V of the motor cortex in C9orf72 and non-transgenic (NT) mice.
There was no significant difference in neurones counted between female C9orf72 and NT mice (mean ± SD, nested t-test, n = 4 per group).

4.1.3.3 Sholl Analysis

Sholl analysis is a method of quantifying the complexity of neuronal dendritic arbours. C9orf72 mice exhibited an increased number of intersections at distances 8-13 µm from the soma, however there were no significant differences at distances further from the soma (Figure 4.36 A). The number of branch points and tips were also analysed, with no significant differences observed (Figure 4.36 B).
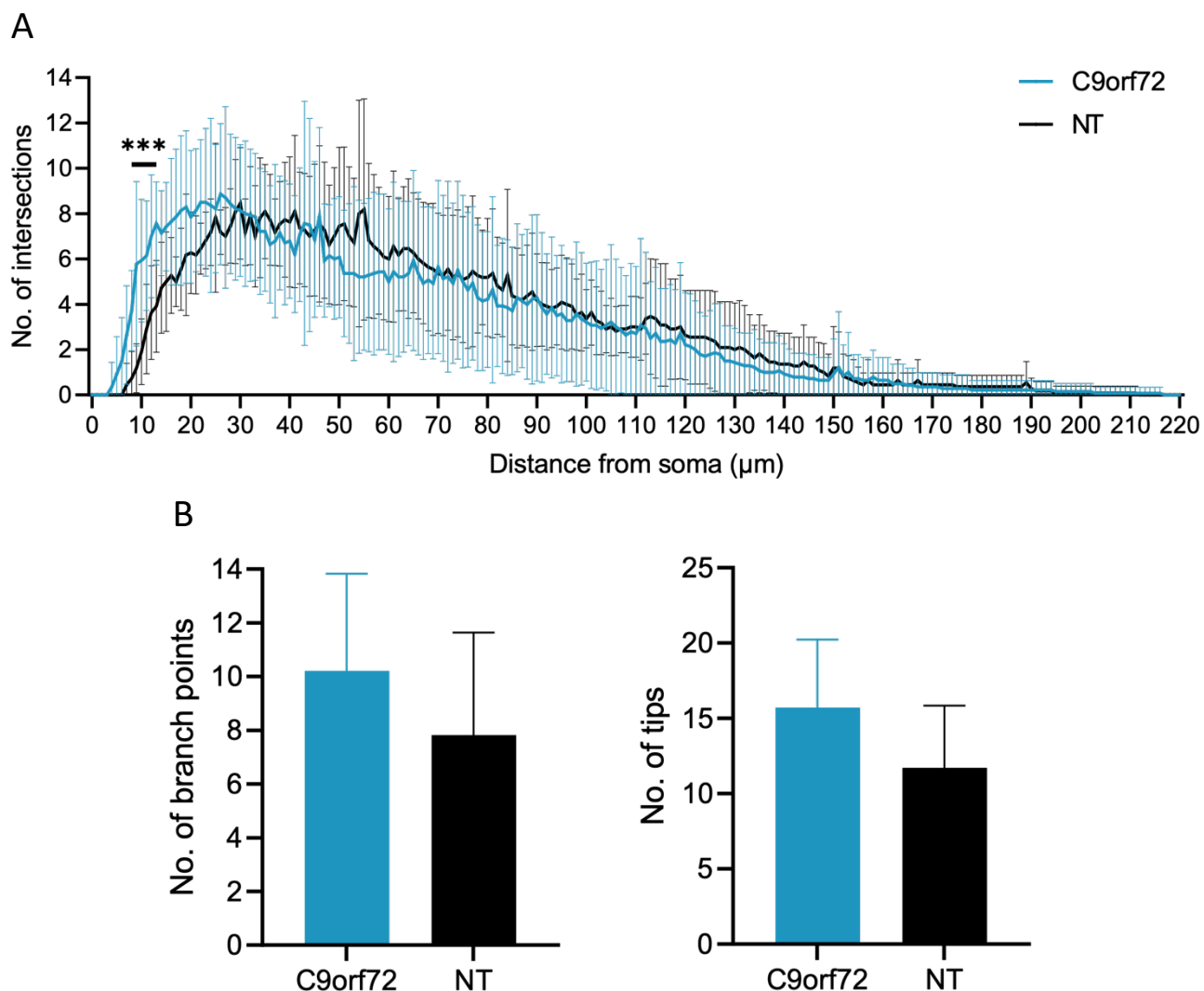
Figure 4.36: Sholl analysis of layer V pyramidal neurones in the motor cortex.

Sholl analysis revealed no significant reduction in pyramidal neurone complexity in layer V of the motor cortex in female C9orf72 mice compared to non-transgenic controls. C9orf72 mice displayed an increase in number of intersections at distances 8-13 µm from cell soma (mean ± SD, mixed model analysis with FDR correction for multiple comparisons, five neurones were analysed per mouse, C9orf72 n = 3, NT n = 2).

4.1.3.4   Immunohistochemical Analysis of Astrogliosis

Hippocampal sections from 52-week-old mice were stained for GFAP and analysed for increased area and intensity of staining, both of which are indicative of astrogliosis. No increased area or intensity of GFAP staining was found in C9orf72 mice compared to NT on a nested t-test (Figure 4.37).
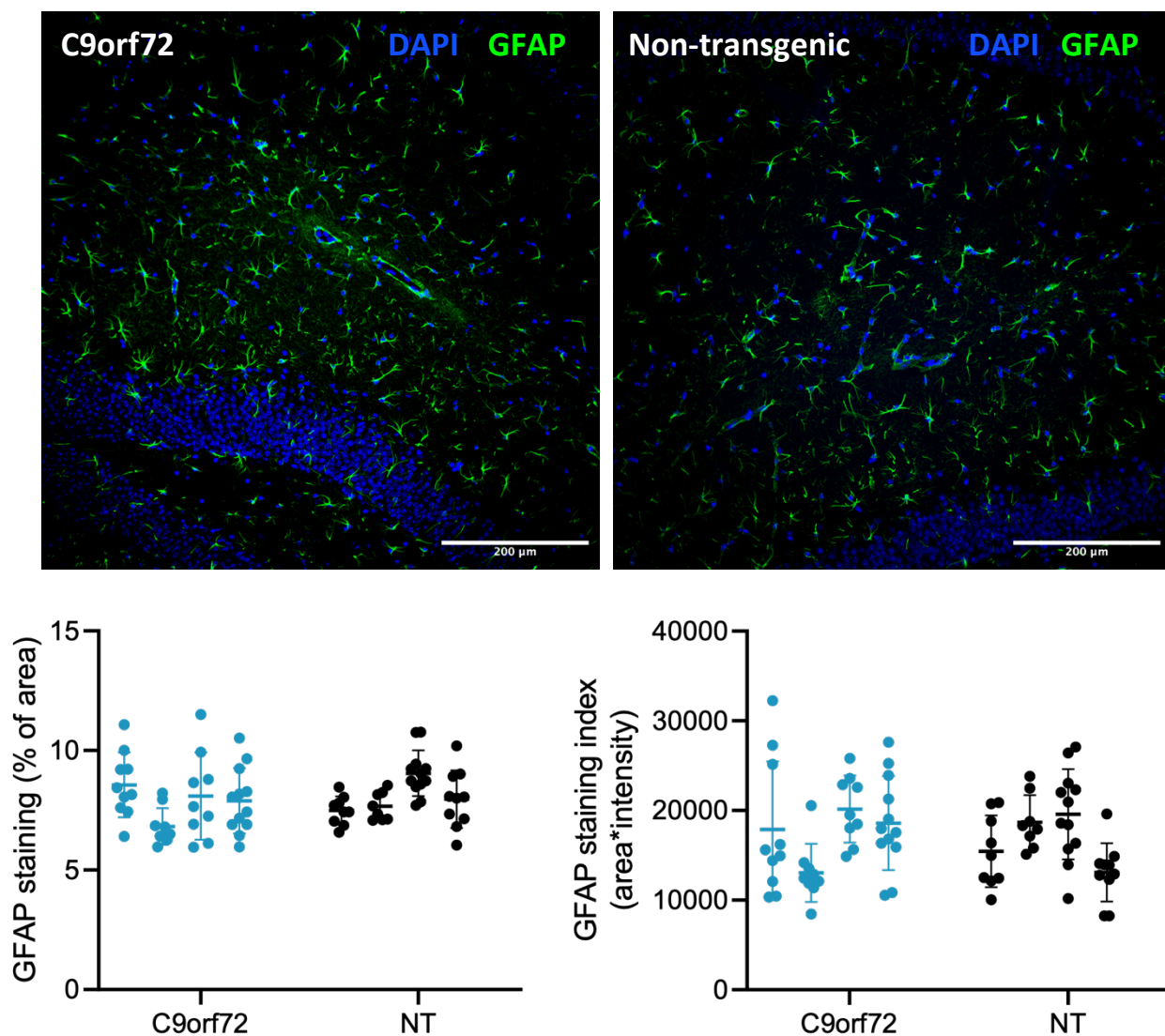
Figure 4.37: Dentate gyrus GFAP staining.

Quantification of GFAP staining in the dentate gyrus of female C9orf72 and non-transgenic mice (n = 4 per group). No significant difference in staining area or staining index (nested t-test).

Motor cortex sections from 52-week-old mice were stained for GFAP and analysed for increased area and intensity of staining. No increased area or intensity of GFAP staining was

found in C9orf72 mice compared to NT on a nested t-test (Figure 4.38). GFAP staining and intensity was variable in both groups. Increased GFAP staining area was seen in one NT mouse, which had previously been observed seizing at 20 weeks of age.
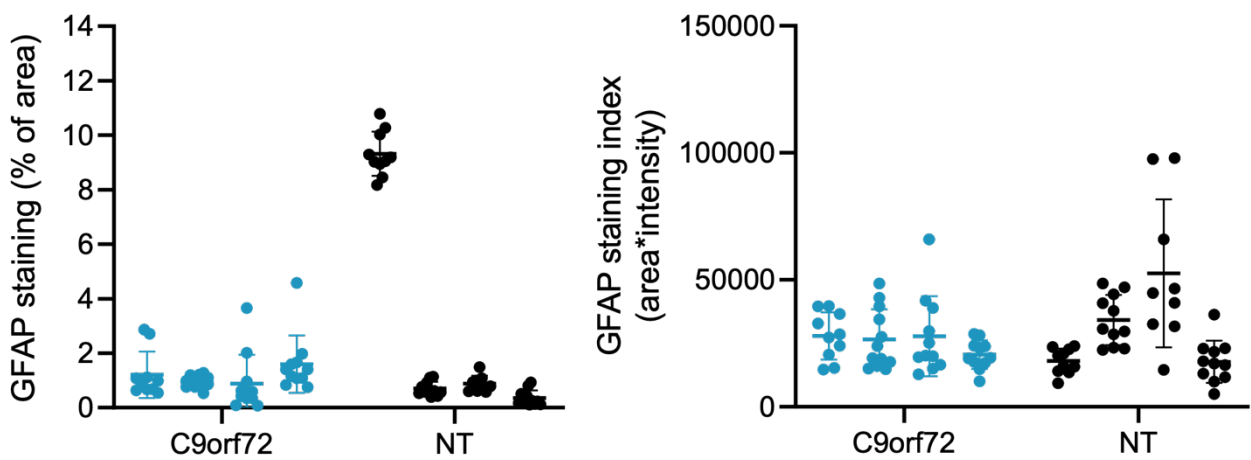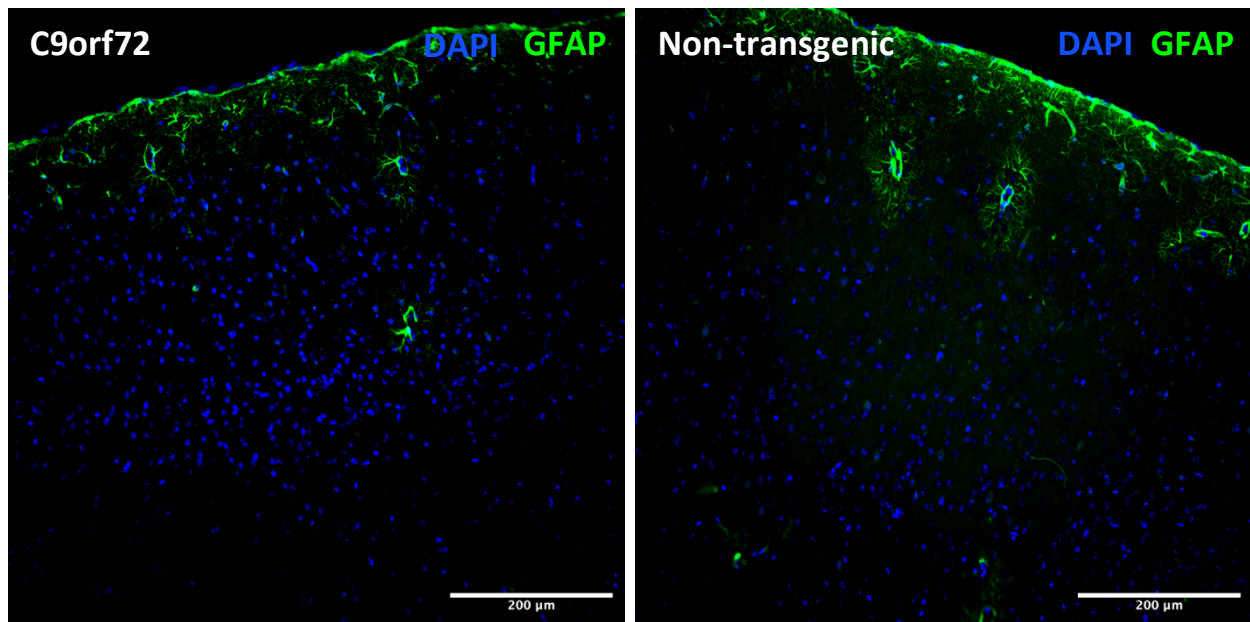
Figure 4.38: GFAP staining of the motor cortex.

Quantification of GFAP staining in the motor cortex of female C9orf72 and non-transgenic mice (n = 4 per group). No significant difference in staining area or staining index (nested t-test).

4.1.3.5 Immunohistochemical Analysis of Microgliosis

Hippocampal sections from 52-week-old mice were stained for Iba1 and analysed for increased area, intensity of staining, and circularity, all of which are indicative of neuroinflammation. No increased area, intensity of Iba1 staining, or increased circularity was found in C9orf72 mice compared to NT on a nested t-test (Figure 4.5).
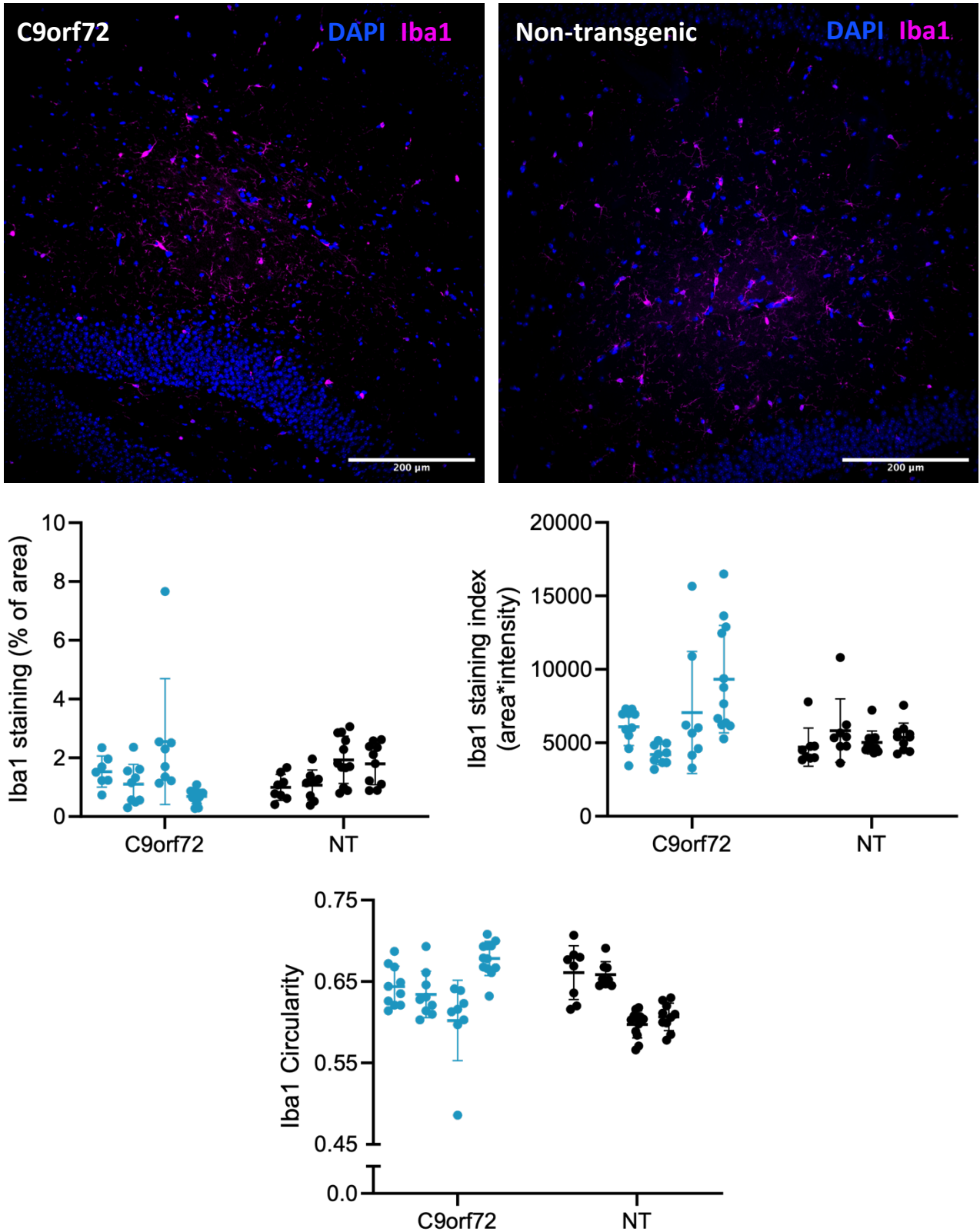
Figure 4.39: Dentate gyrus Iba1 staining.

Quantification of Iba1 staining in the dentate gyrus of female C9orf72 and non-transgenic mice (n = 4 per group). No significant difference on a nested t-test.

Motor cortex sections from 52-week-old mice were stained for Iba1 and analysed for increased area, intensity of staining, and circularity, all of which are indicative of microgliosis. No increased area, intensity of Iba1 staining, or increased circularity was found in C9orf72 mice compared to NT on a nested t-test (Figure 4.40).
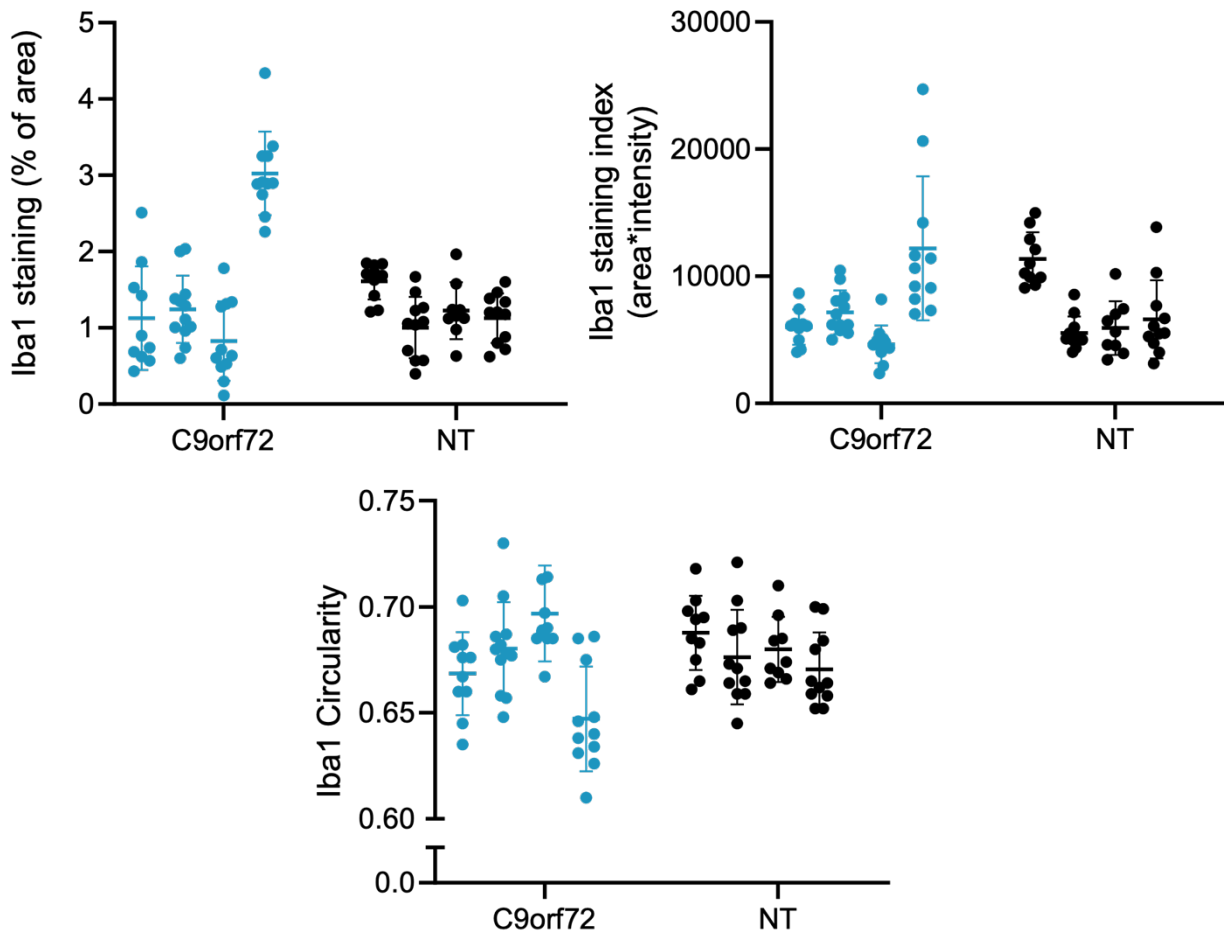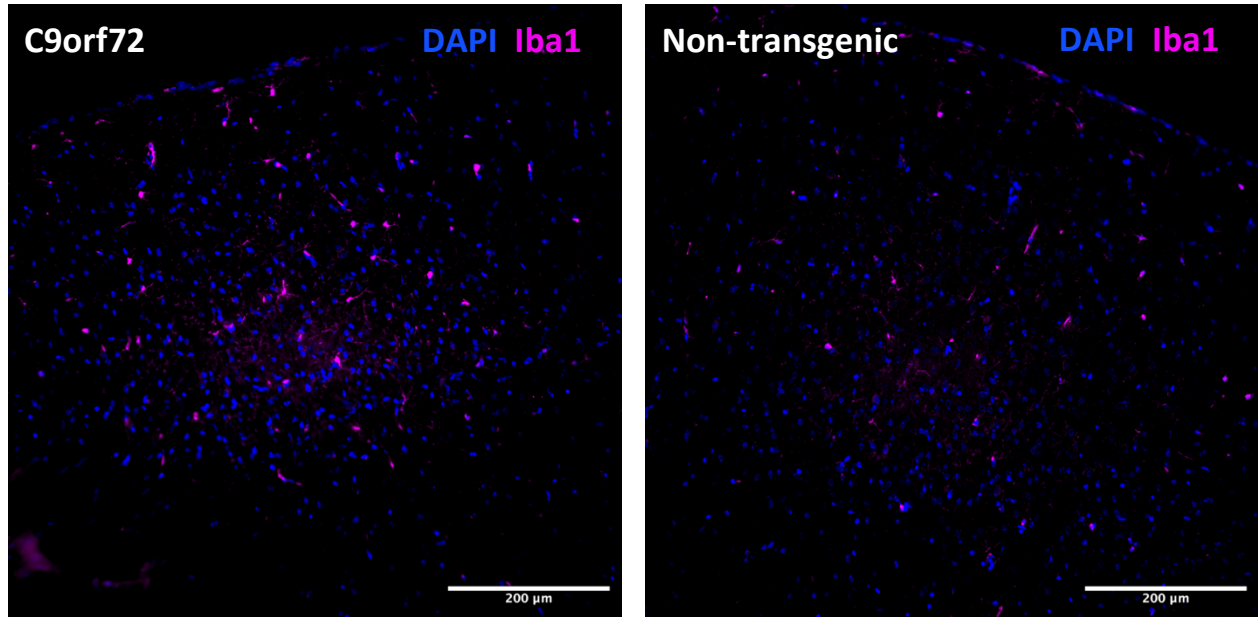
Figure 4.40: Iba1 staining of the motor cortex.

Quantification of Iba1 staining in the motor cortex of female C9orf72 and non-transgenic mice (n = 4 per group). No significant difference on a nested t-test.

5 Discussion

Developing robust and reproducible animal models of ALS is an important aspect of expanding knowledge of the underlying disease mechanisms and, ultimately, to identify potential therapeutics that translate to the clinic. Many therapeutics that have shown promise in an animal model have failed in human clinical trials (Mead et al., 2022), partly attributed to an over-reliance on the SOD1^{G93A} mouse model which represents only a small percentage of ALS cases. ALS is a remarkably heterogeneous disease with a range of genotypes and phenotypic presentations, therefore utilising several disease models to test therapeutics and stratifying patients in clinical trials based on genotype may improve therapeutic translatability. Therefore, there is a need for a range of well-characterised and reproducible models of ALS that consistently develop progressive disease.

To date, there is a distinct lack of C9ALS/FTD BAC mouse models that fully and consistently reproduce the human disease. The most promising model (Liu et al., 2016) has come under scrutiny in recent years after reports of an inconsistent and unreproducible phenotype (Mordes et al., 2020). Therefore, investigation and extensive characterisation of this model is needed to assess its validity and reliability as a preclinical model of C9ALS/FTD. In general, the results of the two studies presented in this thesis demonstrate that this model is unreliable and does not develop the phenotypes reported in the initial publication. These results are discussed in the following sections.

5.1 Behavioural Tests

5.1.1 Accelerating Rotarod Test

The accelerating rotarod test is a commonly used motor test to define disease onset and progression (Mead et al., 2011). There was no significant difference in performance between the C9orf72 and NT groups in both studies, which was consistent with the other BAC models (O'Rourke et al., 2015; Peters et al., 2015; Jiang et al., 2016). However, there was a general decreasing trend in performance in C9orf72 and NT mice which was significant in all groups excluding JAX NT mice. Potential reasons for this decline include weight and age. There was a strong correlation between rotarod performance and weight in all groups. However, when weight was accounted for, the significant decrease in performance remained and was now

present in all groups, suggesting the decline was due to age rather than a disease-related motor dysfunction. There is little information in the literature examining age-related behavioural changes in background strains, but one study on wildtype C57BL/6J mice found a significant decline in rotarod performance with age (Shoji et al., 2016).

A larger proportion of JAX C9orf72 mice performed poorly on the rotarod (<100 seconds) compared to NT mice (Figure 3.2). This could potentially indicate a subset of mice performing poorly over time, however upon closer inspection of the data the poorly performing mice were identified as different mice at each time point. The FVB/N background strain has been identified as one of the more behaviourally variable background strains (Loos et al., 2015), which was highlighted here as there was a large degree of variability in rotarod performance across both studies. Performing the test requires a degree of cooperation from the mouse, and on occasion some mice would refuse to perform the test or would jump off the rotarod mid-test. These incidences were noted and the mice re-tested where possible.

5.1.2 Catwalk Gait Analysis

Gait analysis has been used to evaluate motor deficits in several neurodegenerative diseases (Wooley et al., 2005; Mead et al., 2011; Abada et al., 2013). Decreased hindlimb stride length, increased hindlimb BOS, and reduced time on diagonal paws are the most common reported changes in the SOD1^{G93A} model (Mead et al., 2011). Intensity is a measure of neuropathic pain but can also be used as a measure of limb weakness (e.g., as hindlimb muscles weaken, the mouse may put more weight on their forelimbs, thus reducing the intensity measure of the hindlimbs). Reduced hindlimb swing speed was also reported in a model of Parkinson's disease (Westin et al., 2012).

All gait parameters measured showed no significant differences between C9orf72 and NT groups in both studies, and there were no significant changes over time. This is in line with equivalent parameters reported by Liu et al. (2016), who found no significant differences in stride length and BOS between their C9orf72 and NT mice. Jiang et al. (2016) also found no difference in stride length between their transgenic and control mice at 12 and 18 months of age. Liu et al. (2016) did find a significantly increased swing time in their C9orf72 mice

however this was not observed in either of the cohorts assessed herein. The later timepoints of most parameters in the JAX study showed more variability than the earlier timepoints, but this may be attributed to the reduced n numbers at these timepoints due to the effect of Covid-19 on study organisation.

A number of mice exhibited circling behaviour and were challenging to assess using the catwalk system as several uninterrupted straight runs are required for accurate gait capture. Therefore, a proportion of C9orf72 and NT mice could not be assessed due to this excessive circling. The proportion of circling mice was higher in the Janvier cohort than the JAX cohort (Figure 3.27 and Figure 4.27). This behaviour was also observed in other behavioural tests such as open field and running wheel and highlights a continual issue with the FVB/N strain when used for behavioural studies. The circling behaviour introduces a source of variation in the data and makes FVB/N mice especially challenging to collect behavioural data from. Stereotypic behaviour has not been reported in previous studies with this model (Liu et al., 2016; Mordes et al., 2020; Nguyen et al., 2020a). Stereotypic behaviour can encompass several different behaviours such as circling, backflipping, and bar-mouthing, and may be an indication of stress (Novak et al., 2016). This behaviour has been observed in other strains and correlated with the level of enrichment provided in home-cages (Bailoo et al., 2018). It is possible that facility differences, different handling methods, or enrichment in cages between facilities may lead to different levels of stress and account for the differences in stereotypic behaviour observed between studies. However, there was no difference in handling method between the JAX and Janvier studies and both colonies were kept in the same holding room following recruitment into the study, yet the Janvier study had a significantly higher proportion of stereotypic circling behaviour than the JAX study. It is also possible that the circling behaviour may be attributed to vestibular defects in the inner ear rather than stress (Leduc et al., 2017), however tests such as the swim test or contact-righting test would need to be conducted to assess vestibular function (Hamilton et al., 2011).

5.1.3 Open Field

The open field test is used as a measure of locomotion, anxiety, and willingness to explore a novel environment. The first description of the open field test was in rats in 1932 (Hall and

Ballachey, 1932), but the technique has commonly been used in mice. Several measurements can be made including distance travelled, rearing, time spent at the periphery compared to the centre (thigmotaxis), speed of movement and so on. Distance travelled and time spent in the periphery and centre of the chamber were analysed in both studies as a measure of motor ability and exploratory behaviour. There is debate over whether the open field test can identify anxiety, as anxiety measures are often based on an animal's activity and locomotion, and it is challenging to separate an emotional response from general motor activity (Ramos, 2008). Counting the number of faeces produced during the open field test has been suggested to infer anxiety, with more anxious animals defecating more and moving less, however some studies have suggested the two measures are unrelated (Takahashi et al., 2006; Ramos, 2008). The use of this test along with other measures of motor function, such as rotarod, CMAPs, and catwalk gait analysis, may have enabled us to differentiate between motor dysfunction and anxiety in the open field chamber. For example, changes in open field behaviour may indicate anxiety if motor function remained normal on other tests.

Distance travelled in C9orf72 and NT mice in both studies remained stable over time with no difference between them. However, the Janvier study showed considerably more variability in both groups, and several Janvier NT mice consistently displayed reduced locomotion from 12 weeks of age (Figure 4.8 A).

The JAX and Janvier mice in my studies travelled between 5000-10000 cm, which is slightly increased compared to Liu et al. (2016) and Mordes et al. (2020) who reported similar open field distances of approximately 4000-6000 cm. Interestingly, Liu et al. (2016) and Mordes et al. (2020)'s trials were 30 minutes, while my trials were only 10 minutes. It is unknown why mice in my studies had increased movement in a shorter trial time. It could indicate a more hyperactive phenotype, especially as the FVB/N strain is a hyperactive strain and has been shown to exhibit increased locomotion when compared to other strains (Kim et al., 2002), or increased exploratory behaviour. Chamber sizes were identical between Liu et al. (2016) and my studies. Mordes et al. (2020) did not report their chamber size.

Intriguingly, Liu et al. (2016) split their C9orf72 mice into symptomatic and asymptomatic groups and reported that a subset of their symptomatic mice displayed motor deficits, as

evidenced by their reduced mobility in the open field test. Their data were quite variable, which was also seen in my data as well as Mordes et al. (2020), and the same pattern of reduced mobility in a subset of C9orf72 mice was also seen in my data and Mordes et al. (2020). However, this reduced mobility was also seen in Janvier NT mice and NT mice in Mordes et al. (2020), suggesting it was unrelated to the presence of the *C9ORF72* transgene. Furthermore, Liu et al. (2016) assessed only a small group of C9orf72 and NT mice (NT = 7, asymptomatic C9orf72 = 8, symptomatic C9orf72 = 14) compared to my cohorts (JAX C9orf72 = 14-32, NT = 27-33, Janvier C9orf72 = 29-32, NT = 30-35), and so it is possible that their numbers are too small to detect meaningful differences.

Traditionally, the open field test is performed for 2-10 minutes, however this is more likely to assess exploratory behaviour rather than general activity levels (Blizard et al., 2007). The trials in my studies were 10 minutes, therefore it is possible these trials only assessed exploratory behaviour and did not provide an accurate assessment of baseline activity. Extending the trial to 30 minutes or longer would allow for the novelty factor of the chamber to pass and the general activity levels to be assessed afterwards (Blizard et al., 2007).

The open field chamber was split into centre and periphery zones to measure exploratory behaviour. Ordinarily, mice dislike open and brightly lit areas and will spend most of their time near the walls (thigmotaxis). Unsurprisingly, this behaviour was observed in the JAX and Janvier studies. Both C9orf72 and NT mice spent most of the time in the peripheral part of the open field chamber, with no difference in time spent in the centre between C9orf72 and NT mice. This was also seen in other studies (O'Rourke et al., 2015; Mordes et al., 2020). Liu et al. (2016) reported reduced time in the centre in their symptomatic mice, but not in their asymptomatic mice, which was interpreted as anxiety-like behaviour. Interestingly, these symptomatic mice and the mice in the JAX and Janvier studies spent an equal proportion of time in the centre (~16%), while Mordes et al. (2020) spent 3x less time in the centre. This could be explained by methodological differences, as Mordes et al. (2020) performed their open field test under light conditions while Liu et al. (2016) performed theirs in the dark, and high light conditions have been shown to decrease the time rodents spend in the centre (Bouwknecht et al., 2007). However, in my cohorts the tests were also performed under light conditions. In addition, the FVB/N mice are functionally blind by 30 days due to retinal

degeneration caused by the *Pde6b^{rd1}* mutation and should, in theory, be unaffected by the presence or absence of light (Pugh et al., 2004). Either the FVB/N mice can still detect light/dark, or there are other variables impacting performance such as ambient noise levels, time of test, handling, behavioural test history, and size and shape of the chamber (Gould et al., 2009). This highlights an important issue of standardisation in behavioural tests across facilities to allow accurate comparison of results and evaluate the reproducibility and robustness of not just this model, but others as well.

5.1.4 Social Recognition Test

The social recognition test analyses social memory and relies on the fact that mice spend less time investigating a familiar mouse compared to a novel mouse. Both C9orf72 and NT mice in both studies spent a similar amount of time investigating a familiar mouse as an unfamiliar one and scored >1 on the recognition index. When compared to data from other strains (Kogan et al., 2000; Farley et al., 2011; Chiang et al., 2018), these results indicate an impairment of social memory. As this occurred in all groups, it is highly likely this was due to the FVB/N background strain. The FVB/N strain has traditionally been considered a poor strain for behavioural testing, and in particular learning and memory. They demonstrate poor performance on hippocampal-dependent tests such as the Morris water maze and the radial arm maze (Voikar et al., 2001; Mineur and Crusio, 2002; Pugh et al., 2004). However, the Morris water maze test relies heavily on visual acuity, and the poor vision of FVB/N mice could impact performance. Additionally, the FVB/N strain performs well on other tests that do not rely on visual input, such as conditioned odour preference and fear conditioning (Owen et al., 1997; Brown and Wong, 2007).

Interestingly, studies have found FVB/N mice to have normal learning and memory abilities that are comparable to other strains such as C57BL/6 (Farley et al., 2011; Girard et al., 2016). The only notable difference between the social recognition test in Farley et al. (2011) and this study is the length of time of the initial trial and the interval between the initial and recall trials. Farley et al. (2011) had a 5-minute initial trial and an interval of 3 hours between the initial and recall trials, compared to the 2-minute trial and 72-hour interval in this study. It is possible that the investigation time was too short and the intertrial interval too large to allow

for accurate assessment of social memory in this study. However, previous studies have demonstrated that an initial trial of 2-minutes and an intertrial interval of 7 days still resulted in significantly reduced investigation time of a familiar mouse in the recall trial (Kogan et al., 2000), indicating that a 72-hour interval is not too long to assess social memory. C57BL/6 mice were used in Kogan et al. (2000), so it is possible that FVB/N mice have impaired long-term social memory, and that the 3-hour trial interval in Farley et al. (2011) was not long enough to assess impairments in long-term memory in this strain.

Overall, JAX and Janvier mice in this study exhibited social memory impairment that was not related to the presence of the *C9ORF72* transgene. Further work is needed to assess short- and long-term social memory in the FVB/N strain and identify any impairments therein.

5.1.5 Marble Burying

Behaviour changes such as apathy, reduced motivation, and stereotypies are clinical features of FTD in humans (Piguet et al., 2011). In mice, these types of behavioural changes may be assessed using tests that measure the natural behaviours of mice, such as digging and nesting. Marble burying is one such test that measures motor ability, motivation, and the presence of natural digging behaviour in mice (Deacon, 2006). It was traditionally considered a test of anxiety, with mice burying the marbles due to an aversion to them. However, this interpretation is debated as mice will dig when placed in a new environment whether marbles are present or not, and digging behaviour did not correlate with other anxiety measures (Thomas et al., 2009).

There was no difference in the number of marbles buried between C9orf72 and NT mice in both studies. There was a significant reduction in the number of marbles buried in all groups over time, except in Janvier C9orf72 mice. While this could suggest an increase in FTD-related apathy or lack of motivation, the effect would appear to be independent of the *C9ORF72* transgene, as this decrease was also observed in the NT groups. Additionally, mice that displayed stereotypic behaviour did not actively dig around the cage and thus buried no marbles — although some marbles were inadvertently buried through the action of the mice running around the cage. The Janvier study had a much higher proportion of mice with

stereotypic behaviour than the JAX study, which could explain why the Janvier cohort performed worse on average throughout the study compared to the JAX cohort.

Interestingly, one of the C9ALS/FTD BAC models also assessed marble burying and found a significant increase in burying behaviour of male transgenic mice compared to controls at 18 months old, which they interpreted as increased anxiety (Jiang et al., 2016). This was not present in their female mice; however, interpretation must be taken with caution as a very small number of NT mice were used at this timepoint (n = 4). The mice in my studies were only aged to 12 months, so it is possible that had they been aged further a difference may have become apparent. However, considering the obvious trend of decreasing performance in both cohorts presented here, that is unlikely.

5.1.6 Balance Beam

The balance beam test measures balance and equilibrium, and the ability to perform the test has been shown to decrease in transgenic mice in other ALS models (Wang et al., 2018; Milanese et al., 2021). The cerebellum is heavily involved in balance and cerebellar atrophy has been reported in human C9ALS/FTD patients (Mahoney et al., 2012; Whitwell et al., 2012; Kabiljo et al., 2022). Liu et al. (2016) reported loss of cerebellar Purkinje cells and a decrease in cerebellar molecular layer thickness in their acute C9orf72 mice. However, they did not explicitly test the balance ability of their mice with this test, or another test such as rotarod. In my studies, C9orf72 and NT mice showed no significant differences in balance beam scores. This agrees with the rotarod and catwalk regularity data that show most mice were well coordinated and that carrying the *C9ORF72* transgene had no effect on motor coordination.

5.1.7 Limb Hang Test

The limb hang test has been used as a reliable measure of muscle function and coordination in mice. For example, in a mouse model of muscular dystrophy, dystrophic mice showed a significantly decreased ability to hang compared to controls (Klein et al., 2012). In both studies herein, there was no reduction in limb hang ability in C9orf72 mice compared to NT mice, however the Janvier C9orf72 and NT groups showed significant decreases in hanging ability over time. When the data was normalised to account for the effect of weight on hang time,

the decrease in performance remained significant (Figure 4.16). While this suggests age or strain may be responsible for the decrease, the effect of motivation must also be considered. For the test, the mice were held a certain distance above a cage that was high enough to deter voluntary jumping off the grid but low enough that when they fell, they were uninjured. However, in both studies it was observed at later timepoints that mice in all groups would voluntarily jump from the grid regardless of grid height above the cage. It is possible the mice remembered previous tests and that jumping from the grid would not result in injury. Additionally, this unwillingness to perform the test could also be a measure of apathy, a feature of FTD, however in this case it is unlikely to be a result of the *C9ORF72* transgene as this unwillingness and decrease in performance was also observed in the Janvier NT group. As such, the test proved an unreliable measure of motor ability in this model, and the decrease in performance was most likely due to age or background strain effects.

5.1.8 Burrowing

The burrowing test was first developed on a mouse model of prion disease and was shown to be an exceedingly sensitive measure, detecting differences between diseased and control mice 10 weeks prior to clinical symptoms (Deacon et al., 2001). Since then, the test has been used as a motor function test, as the burrowing material is primarily dug out with the forelimbs, and a cognitive test, as it is a natural mouse behaviour and the mouse must be motivated to voluntarily participate in the test (Pond et al., 2021). Furthermore, the hippocampus has been shown to be heavily involved in burrowing behaviour after hippocampal-lesioned mice showed significantly decreased burrowing compared to controls (Deacon and Rawlins, 2005). Considering the dramatic hippocampal degeneration observed in the initial study with this C9ALS/FTD model (Liu et al., 2016), it could be hypothesised that poor burrowing performance may correlate with this degeneration.

There was no significant difference in burrowing behaviour between C9orf72 and NT mice in both studies, indicating no motor or cognitive impairment. However, the data was remarkably variable in C9orf72 and NT mice, which has been observed previously in female mice when performing the test (Pond et al., 2021). The Janvier mice generally performed more poorly than the JAX mice, regardless of genotype. The reason for this is unknown, however the

Janvier study had a markedly increased number of mice exhibiting stereotypic behaviour compared to the JAX study. These mice were observed to circle the cage and not interact with the burrow, potentially resulting in the reduced weight burrowed in the Janvier study.

5.1.9 Nesting

Like marble burying and burrowing, nesting is an example of a natural mouse behaviour and has previously been shown to be impaired in a model of FTD (Warmus et al., 2014). While primarily considered a cognitive measure of apathy, there is also a motor element to the test. Nest-building ability was comparable between C9orf72 and NT mice in both studies. Interestingly, the longitudinal analysis showed a clear decrease in nesting ability in the JAX study which was likely due to age or strain effects as it was present in both C9orf72 and NT groups. Furthermore, the Janvier study showed decreased nesting ability compared to the JAX study. The reason for this is unknown, however as mentioned previously, the Janvier study had an increased number of mice exhibiting stereotypic behaviour when compared to the JAX study. These mice were observed to circle the cage and not interact with the nestlet, potentially resulting in the overall lower nesting scores across the Janvier study.

5.1.10 Food Intake

Increased appetite and hyperphagia is a clinical feature of FTD (Ikeda et al., 2002; Rascovsky et al., 2011; Snowden et al., 2012). During the JAX study, the increased weight of some C9orf72 mice was noted and food intake was measured from approximately halfway through the study. Due to this, the n numbers for each time point in the JAX study are variable. Food intake was comparable between C9orf72 and NT mice in both studies. A larger proportion of C9orf72 mice in both studies showed higher food intake, however this did not translate into significant weight gain as has been found in previous studies with TDP-43^{Q331K} mice (White et al., 2018).

5.1.11 Weight

Weight increased between 12 and 20 weeks in C9orf72 and NT groups in both studies before plateauing and remaining steady. A small number C9orf72 and NT mice in both studies became overweight with age, exceeding 40 g, but were otherwise healthy. The reason for this

weight gain was unknown, and upon dissection at end of study, it was confirmed the weight gain was due to increased abdominal white fat. This has not been reported previously in this model (Mordes et al., 2020; Nguyen et al., 2020a) or in other C9ALS/FTD BAC models (O'Rourke et al., 2015; Peters et al., 2015; Jiang et al., 2016). Liu et al. (2016) did not report the average weight of the cohorts in their study. Overall, no disease-related weight loss was observed in either study and no mouse required euthanasia due to continued weight loss.

5.1.12 Subset Data Analysis

The data in both studies presented here are extremely variable. As the initial study of this model reported that only a small subset of C9orf72 mice developed an "acute" phenotype (Liu et al., 2016), it is possible that any poorly performing C9orf72 mice may have been obscured within the data. To identify hidden subsets, a simple data analysis method was devised to identify latent patterns within the data (detailed in section 2.6.9). This analysis identified no subsets within the data and showed that approximately equal numbers of C9orf72 and NT mice in both studies demonstrated MND-like phenotype scores in every behavioural test (Table 3.1 and Table 4.1). This is further supported by the survival data of both studies, showing no significantly reduced survival between 20 and 40 weeks of age in the C9orf72 groups as reported in the "acute" mice in Liu et al. (2016).

5.1.13 Running Wheel Test

Evidence is beginning to support the idea that exercise may increase the risk of developing ALS in those with a genetic predisposition to the disease (Zheng et al., 2023). It has been previously shown in *mdx* mice that exercise exacerbates muscle pathology and deterioration in muscle strength (Manning and O'Malley, 2015). Therefore, it was decided to test whether voluntary running wheel exercise in the Janvier mice would trigger a phenotype after none was observed during the 12-month behavioural study.

Initially, the test was to be run for between 3 and 6 months, however it was terminated early as both C9orf72 and NT mice exhibited stereotypic behaviour and were not fully engaging with the running wheel. As such, interpretation of the data from the month-long test is limited. Distance, max speed, average speed, and time spent running were measured every

24 hours, and there was no difference between C9orf72 and NT mice in any of these parameters. Average speed was comparable to previous studies of FVB/N mice on running wheels (Lerman et al., 2002), while running distance and duration were reduced. This is unsurprising considering the observed lack of engagement with the running wheel, however there were a small number of mice in this study that did fully engage with the running wheel and ran comparable distances and durations to the previous study. There were also several mice that did not engage at all, either through lack of interest and motivation, or due to circling the cage rather than running on the running wheel.

There was distinct variation in time spent running that was not present in any of the other parameters. It showed a regular pattern of increasing and decreasing approximately every 5-6 days (Figure 4.22 D). The average length of the oestrus cycle of female mice is 4-5 days (Byers et al., 2012) and it has been suggested to affect the variability of this parameter (De Bono et al., 2006). Therefore, it was most likely the cause of the variation seen.

5.1.14 Electrophysiology

5.1.14.1 CMAP

CMAP amplitude is a measure of the electrophysiological integrity of the distal axon, neuromuscular junction, and muscle. Reduction in this measure is seen as indicative of motor axon degeneration. The CMAP response was measured in the hindlimb, which was shown to be one of the earlier muscles to degenerate in a SOD1 mouse model (Azzouz et al., 1997; Mancuso et al., 2011).

There was no significant difference in CMAP amplitudes between C9orf72 and NT mice in either study at any timepoint, and there was no change over time, indicating no loss of motor axons. It is possible for CMAP amplitude to be maintained via reinnervation despite loss of 50-80% of motor axons (Ibrahem et al., 2021). However, there was no evidence on EMG to suggest active denervation. Similarly, there was no loss of motor neurones in the ventral horns of the lumbar spinal cord in the JAX and Janvier mice. More sensitive techniques, such as motor unit number estimation, could be considered, although these are more technically challenging to perform.

5.1.14.2 Repetitive Nerve Stimulation

Repetitive nerve stimulation is a measure of NMJ function. When a nerve is stimulated, acetylcholine (ACh) is released from the pre-synaptic terminal. This activates post-synaptic ACh receptors and causes an influx of sodium which depolarises the muscle cell and triggers an endplate potential (EPP) if the threshold is reached. When a nerve is repeatedly stimulated, the ACh store is rapidly depleted and a smaller EPP is produced. In a normal NMJ, the EPP will remain above the threshold despite this, and the CMAP amplitude is unaffected. However, in diseases such as ALS, the initial stimuli will result in an EPP that meets the threshold and results in an action potential, but as the stimulus continues the threshold is no longer met in some NMJs, resulting in fewer muscle fibres contracting and a decrease in CMAP amplitude. A steady CMAP response is therefore indicative of a healthy NMJ, while a decrement of >10% is considered abnormal. This decrement can be seen in ALS patients (Iwanami et al., 2011; Sun et al., 2018), and is generally attributed to progressive denervation and reinnervation following motor neurone loss (Sun et al., 2018). Considering no significant decrement was observed in C9orf72 mice of both groups, and all responses were comparable to NT mice, this indicates a healthy NMJ in all mice with no evidence of denervation or motor neurone loss. This is supported by the CMAP data and lumbar spinal cord motor neurone counts.

5.1.14.3 F Waves

F waves are produced by antidromic activation of anterior horn motor neurones following peripheral nerve stimulation (Fisher, 2007). Following this activation, some motor neurones will rebound, sending an orthodromic impulse back towards the muscle fibres innervated by the stimulated nerve and resulting in a small CMAP. F waves can be challenging to interpret and are inherently variable (Fisher, 2007). In ALS, there are reports of increased F wave latencies and amplitudes and decreased F wave frequency due to LMN loss (Argyriou et al., 2006; Wijesekera and Leigh, 2009).

There was no significant difference in F wave latencies or persistence in C9orf72 mice compared to NT. JAX C9orf72 mice had a non-significant decrease in F wave persistence which could indicate LMN loss (Figure 3.24 D), however this is not supported by the JAX lumbar spinal cord motor neurone counts (Figure 3.30 B).

Plantar interossei CMAPs were measured at 52 weeks of age alongside F wave assessment. There was no significant difference detected between C9orf72 and NT mice in both studies. This was unsurprising as more distal muscles, such as the plantar interossei, have been shown to degenerate later than more proximal muscles in the hindlimb (Azzouz et al., 1997; Mancuso et al., 2011), and no reduction in hindlimb CMAPs had been previously observed in the C9orf72 mice.

5.1.15 Survival

There was no reduction in survival in C9orf72 mice in both studies when compared to NT controls, indicating no effect of the *C9ORF72* transgene on mortality. This was also seen in a previous study with this model (Mordes et al., 2020) and in a different BAC model of C9ALS/FTD (Peters et al., 2015). As mentioned in results sections 3.1.2.14 and 4.1.2.15, most mouse deaths observed were due to seizures requiring euthanasia or the mice were found dead in their cages with no prior signs of weight loss or abnormal behaviour or distress scores. This conflicts with previous studies by Liu et al. (2016) and Nguyen et al. (2020a) that reported a mortality rate of 36% and 94% respectively in their C9orf72 mice at 52 weeks. Since differences in repeat lengths and gene expression across studies have been ruled out, it has been suggested that environmental differences could account for this discrepancy. *C9orf72* knockout models show variable mortality rates that are dependent on facility (Burberry et al., 2016; Atanasio et al., 2016; Jiang et al., 2016), which has recently been shown to be a result of different commensal micro-organisms (Burberry et al., 2020). Therefore, it is feasible that a similar effect could be occurring here, thus accounting for the striking increase in mortality in the Saxena laboratory at the University of Bern, and the lack of mortality in this and the Mordes et al. (2020) study. Faeces were collected at 6 and 12 months of age in both the JAX and Janvier study for microbiome analyses, however there was not enough time to obtain appropriate samples from other research sites for comparison and perform the analysis.

Another possible explanation for the mortality differences could be due to the FVB/N background strain. Out of all the C9ALS/FTD BAC mouse models, this model was the only one generated on the FVB/N strain and the only one to report ALS-associated behavioural, pathological, and survival phenotypes. As previously discussed in section 1.3.3, the choice of

background strain when generating a disease model must be carefully considered as it can influence results. In short, FVB/N mice are susceptible to seizures and previous studies have found that approximately 15-20% of FVB/N mice develop chronic seizure activity, known as SCS, that results in gait abnormalities and sudden death, among other neurological pathologies (Hennemann, 2007; Silva-Fernandes et al., 2010). This proportion of 15-20% matches the level of mortality seen in C9orf72 and NT mice in the JAX and Janvier studies, and in Mordes et al. (2020). Due to the phenotypic similarities between SCS, the seizure mice examined in the Janvier study (results section 4.1.2.18), and the acute ALS/FTD phenotype reported by Liu et al. (2016), it is feasible that their phenotype may have been due to seizures and not the *C9ORF72* transgene.

This still raises the question of how the results were later repeated in Nguyen et al. (2020a), as it is unlikely for a chance occurrence such as this to occur twice in succession. Interestingly, a previous study in a transgenic mouse model of Alzheimer's disease that overexpressed the human or mouse amyloid precursor protein also used the FVB/N background. They reported a naturally occurring age-related CNS disorder in the FVB/N mice that was exacerbated by the transgene (Hsiao et al., 1995). It is possible that the presence of the *C9ORF72* transgene may be doing something similar, accelerating onset of this CNS disorder in C9orf72 mice, and thus resulting in the acute phenotypes reported in Liu et al. (2016) and Nguyen et al. (2020a). However, this did not occur in my studies; possibly due to some as yet unidentified environmental factor such as stress. Another potential explanation could be due to transgene expression, as suggested by a recent conditional transgenic mouse model (LaClair et al., 2020). The model expresses high levels of poly-PR on a C57BL/6N background, and the authors found that 40% of their poly-PR expressing mice suffered seizures and ataxia in the absence of neuronal loss. Further investigation revealed that transgene expression was directly responsible for the seizures, with those suffering seizures expressing high levels of the transgene while their unaffected littermates had significantly reduced transgene expression. Seizures have also been observed in DPR-expressing *Drosophila* (West et al., 2020). Therefore, it is possible that in a seizure-prone background such as FVB/N, the level of transgene expression could be impacting seizures or the naturally occurring age-related CNS disorder suggested to occur in the FVB/N mice. Transgene expression was not examined in my studies or in all C9orf72 mice in Liu et al. (2016) or Nguyen et al. (2020a), but it would be

interesting to discover whether the reported asymptomatic and symptomatic C9orf72 mice had differing levels of transgene expression, and thus differing incidences of seizures.

5.2   Tissue Pathology

5.2.1   Dipeptide Repeat Proteins

To check that expression of the *C9ORF72* HRE was occurring, an MSD ELISA immunoassay was performed to evaluate the production of all five DPRs in the frontal cortex and gastrocnemius muscle. All C9orf72 mice in both studies demonstrated significantly increased levels of DPR compared to NT mice, indicating expression of the HRE. Only two of the five DPRs were detected in the cortex, poly-GP and poly-GA, while only poly-GP was detected in the gastrocnemius. DPRs in muscle tissue have been detected in zebrafish (Shaw et al., 2018), *Drosophila* (Freibaum et al., 2015), and, more recently, in ALS patient tissue (Cykowski et al., 2019). The cortex displayed increased levels of DPRs compared to the gastrocnemius, indicating higher expression in the CNS, which is in line with what is seen in humans (Schipper et al., 2016). Poly-GA concentrations were higher than poly-GP in the cortex (approximately 2-fold), which is in line with what is seen in human cortex and one other C9ALS/FTD BAC model (Jiang et al., 2016; Lee et al., 2017).

Poly-GR, one of the more toxic DPRs, was not detected. While not reported in the initial publication for this model, a subsequent publication by the same authors suggested they detected poly-GR in the frontal cortex and hindbrain (Nguyen et al., 2020b). However, the amount detected was very small and at the limit of detection for the MSD ELISA used in my studies. It is possible that while poly-GR was not detected, the mice in these studies may have still expressed it. Attempts were made to improve detection of poly-GR, through testing alternate protein extraction methods and increasing the concentration of protein lysate 2- and 5-fold (data not shown), however no improvement in signal was seen. The possibility that the JAX and Janvier mice do not express poly-GR must not be discounted, however. Mouse poly-GR overexpression models display behavioural abnormalities, neurodegeneration, and microgliosis (Choi et al., 2019), suggesting that poly-GR has a toxic effect *in vivo*. Furthermore, poly-GR has been found to interact with TDP-43 and evidence suggests that it is exclusively responsible for recruiting TDP-43 into inclusions (Cook et al., 2020). As TDP-43 is thought to

be responsible for neurodegeneration, poly-GR could play a vital role in disease pathogenesis. Therefore, the absence of poly-GR in our mice may represent the missing insult required to trigger disease. On the other hand, poly-GR was not detected in mice from the Saxena lab at the University of Bern either (Nguyen et al., 2020a), and yet they reported the same "acute" phenotype as Liu et al. (2016).

There was quite a large degree of variability within C9orf72 mice, with some displaying 4-fold higher levels of DPRs than others. A previous study on the Peters et al. (2015) C9ALS/FTD BAC model investigated epigenetic expression of the HRE in different age groups (Esanov et al., 2017). They found that hypermethylation of the promoter occurred in a subset of C9ALS/FTD mice, which has also been observed in a subset of human C9ALS/FTD patients, which led to decreased poly-GP levels. It is possible something similar occurred in the two studies herein and could provide an explanation for the varying levels of DPRs.

While this model does not appear to develop behavioural or neuromuscular phenotypes akin to ALS/FTD, it may still have value. The expression of DPRs provides a molecular fingerprint that may be useful to test DPR-related therapeutic strategies (Castelli et al., 2023), although amelioration of this pathology is unlikely to be reflected in behavioural or neurodegenerative changes.

5.2.2 Neurone Counts

5.2.2.1 Lumbar Motor Neurone Counts

Both UMNs and LMNs are affected in ALS. To investigate pathological changes in LMNs in the spinal cord of C9orf72 mice, motor neurone counts in the ventral horns of the L4-5 region were performed. Liu et al. (2016) reported significant loss of motor neurones in their "acute" C9orf72 mice in this region. There was no lumbar motor neurone loss in either group in this study, which was also reflected in the behavioural and electrophysiology tests that displayed no deficits. This concurs with the results reported by Mordes et al. (2020) that the C9orf72 mice did not develop motor neurone disease.

5.2.2.2   Brain Neurone Counts

To investigate pathological changes in UMN regions, neurone counts in the CA and DG regions of the hippocampus and layer V of the motor cortex were performed. Liu et al. (2016) reported significant neurodegeneration in the CA and DG hippocampal regions, which was not found by Mordes et al. (2020), and in layers II/III and V of the motor cortex. Both JAX and Janvier C9orf72 mice showed no neurodegeneration in the CA or DG regions or in layer V of the motor cortex compared to NT mice. One of the other BAC models reported mild neurodegeneration in the CA1 and DG regions as well as significant deficits in some tests that rely on working memory, and therefore hippocampal function, such as the Barnes maze and the radial maze (Jiang et al., 2016). The remaining BAC models found no neurodegeneration (Peters et al., 2015; O'Rourke et al., 2015).

The two Janvier NT mice that were culled mid-seizure were also examined for neurodegeneration. While there was no significant decrease compared to C9orf72 and NT neurone counts, there was an obvious decreasing trend of neuronal loss in the CA and DG regions. This is unsurprising as seizures are associated with hippocampal neurodegeneration in humans (Hattiangady and Shetty, 2008), and recurrent seizures due to SCS or kainic-acid treatment in FVB/N mice have been shown to result in hippocampal neurodegeneration also (Goelz et al., 1998; Hennemann, 2007; McCord et al., 2008; Silva-Fernandes et al., 2010). The areas of the CA that display neurodegeneration in these two NT mice, primarily the CA1 and CA3 regions, are also identical to the areas that showed degeneration in C9orf72 mice in Liu et al. (2016) and Nguyen et al. (2020a). This makes it challenging to determine whether the pathology seen was indeed caused by the *C9ORF72* transgene, especially when the background strain itself is susceptible to developing the same pathology, and highlights how the FVB/N strain may be unsuitable for use in modelling neurodegenerative diseases.

5.2.3   Sholl Analysis

In ALS, post-mortem tissue from patients has shown reduced dendritic complexity in both UMNs and LMNs (Hammer et al., 1979; Udaka et al., 1986). This has been suggested to be associated with cortical hyperexcitability (Eisen et al., 1993; Fogarty et al., 2016). These dendritic abnormalities have also been observed in the SOD1^{G93A} mouse model in the motor

cortex, brainstem, and spinal cord (van Zundert et al., 2008; Jara et al., 2012; Martin et al., 2013; Fogarty et al., 2015). Sholl analysis, branch point, and tip point analyses were performed to give a broad picture of the dendritic complexity of layer V pyramidal neurones in the motor cortex of the Janvier model. Sholl analysis revealed that C9orf72 mice had a significantly increased number of intersections closer to the soma, which could be a structural correlate of hyperexcitability. A previous study has shown that hyperexcitability leads to changes such as increased length and ramification of basal dendrites of layer V motor neurones as they receive increased excitatory input (Saba et al., 2016). The authors suggested that this indicated enhanced cortical connectivity in early disease. Hyperexcitability of the motor cortex has been demonstrated in patients (Vucic et al., 2013) and so it is tempting to speculate that this observation provides some preliminary evidence for this in the mice. However, other indices did not demonstrate changes in keeping with this, such as increased tip number and branch points, and these are typically taken together as more robust structural markers of excitability changes. Similarly, there was no evidence of degeneration within the dendritic tree. However, basal dendrites were not analysed separately in this study, so analysis of basal dendrites and other measures of hyperexcitability such as evaluating glutamatergic activity could be investigated in future studies to determine whether hyperexcitability was present and could have been responsible for the subtle changes seen here. It should be noted, however, that caution must be taken in this interpretation of the data due to the relatively few n numbers in this analysis.

5.2.4 Analysis of Astrogliosis

In response to injury and neurodegeneration, astrocytes become reactive and hypertrophic and display increased immunoreactivity for GFAP (Vargas and Johnson, 2010). Abnormal and reactive astrocytes have been documented in ALS since the 1970s (Smith et al., 1975; Stoklund Dittau and Van Den Bosch, 2023) and astrogliosis has been observed in many fALS mouse models (Hall et al., 1998; Stallings et al., 2010; Sunyach et al., 2012). Astrogliosis and hypertrophic astrocytes were reported in the hippocampus and motor cortex of "acute" C9orf72 mice in the initial publication of this C9ALS/FTD model (Liu et al., 2016). No astrogliosis was reported in other C9ALS/FTD BAC models that assessed for it (Peters et al., 2015; Jiang et al., 2016). GFAP staining area and intensity were assessed in the hippocampus

and motor cortex in both the JAX and Janvier cohorts. No differences were found in these parameters in either brain region between C9orf72 and NT mice of both cohorts, indicating no injury or degeneration was present.

One JAX C9orf72 mouse and one Janvier NT mouse had increased GFAP staining area in the hippocampus and motor cortex, respectively, and both had previously been observed seizing at 24 and 20 weeks of age, respectively. As astrogliosis is a common pathological feature of seizures (Sano et al., 2021), it is possible these mice suffered additional seizures to the ones observed that resulted in this increased astrocyte reactivity. Additionally, the two Janvier NT mice that were culled mid-seizure show stark increases in astrocyte reactivity compared to C9orf72 and NT mice. Alongside the overt neurodegeneration and microgliosis also seen in both CA and DG regions of these mice, these phenotypes are directly comparable to the histopathology reported by Liu et al. (2016) and Nguyen et al. (2020a) in these brain regions and to the reported SCS in the FVB/N strain (Mahler et al., 1996; Goelz et al., 1998; Hennemann, 2007). This once again highlights how the FVB/N strain may be unsuitable for use in modelling neurodegenerative diseases.

5.2.5 Analysis of Microgliosis

Like astrocytes, microglia become activated in response to injury or neurodegeneration, leading to morphological changes and altered gene expression (Mathys et al., 2017; Ajami et al., 2018; Clarke and Patani, 2020). Microgliosis has been observed in several mouse models (Chiu et al., 2008; Mitchell et al., 2013; O'Rourke et al., 2016), and was reported in the hippocampus of acute C9orf72 mice in the initial publication of this C9ALS/FTD model (Liu et al., 2016). Iba1 staining area, intensity of staining, and circularity was assessed in the hippocampus and motor cortex in both the JAX and Janvier cohorts. No differences were found in these parameters in either brain region between C9orf72 and NT mice of both cohorts, indicating no microgliosis or neuroinflammation was present.

The two Janvier NT mice that were culled mid-seizure show stark increases in Iba1 staining area and intensity compared to C9orf72 and NT mice, indicating microgliosis and neuroinflammation. Alongside the overt neurodegeneration and astrogliosis also seen in

these mice, it further highlights the issue with using the FVB/N strain to model neurodegenerative diseases.

5.3 Conclusion

To conclude, the two behavioural studies presented here have provided an in-depth characterisation using a battery of tests to thoroughly interrogate the disease phenotype of this C9ALS/FTD BAC model on two FVB/N genetic backgrounds. The data presented appears to show no behavioural phenotypes, neurodegeneration, or neuromuscular impairments associated with the *C9ORF72* transgene like those originally reported by Liu et al. (2016). These results concur with a previous study using this model (Mordes et al., 2020). As such, the model is unreliable and lacks a robust phenotype, and its utility for preclinical research is greatly reduced. However, the model does express DPRs, and may be useful to test DPR-related therapeutic strategies, although amelioration of this pathology is unlikely to be reflected in behavioural or neurodegenerative changes. It also raises questions over the role of toxic gain-of-function mechanisms in the development of C9ALS/FTD, further compounding uncertainties already present in the field. Additionally, these two studies have highlighted issues with the choice of the FVB/N background strain for modelling ALS/FTD, and neurodegenerative diseases in general, and suggest a more suitable and less behaviourally variable strain such as C57BL/6 could be considered instead.

6 Comparison of the Jax and Janvier FVB/N Mouse Background

6.1 Introduction

The two FVB/N background strains used in this study were imported by The Jackson Laboratory and Janvier Labs in 1988 and 1996, respectively, from the National Institutes of Health (NIH), US. How these two groups differ from each other is unknown, and it is possible that sufficient changes may have occurred between the two to influence phenotypes of transgenic models of disease. There are documented differences in behavioural test performance between background strains (Heiman-Patterson et al., 2011; Eltokhi et al., 2020) and even between substrains (Matsuo et al., 2010; Zurita et al., 2011; Simon et al., 2013; Temme et al., 2014). To my knowledge, below is the first direct behavioural comparison of the FVB/N strain from The Jackson Laboratory and Janvier Labs. The data herein are from the non-transgenic mice in the experimental studies in chapters 3 and 4.

6.2 Behavioural Tests

6.2.1 Accelerating Rotarod Test

There was no significantly decreased latency to fall between the two groups at any timpoint (Figure 6.1), however Janvier mice showed a significantly decreased latency to fall at 52 weeks of age compared to 12 weeks (Janvier n = 28-35, 287.3 ± 33.5 vs 242.3 ± 63.6, p = 0.02).
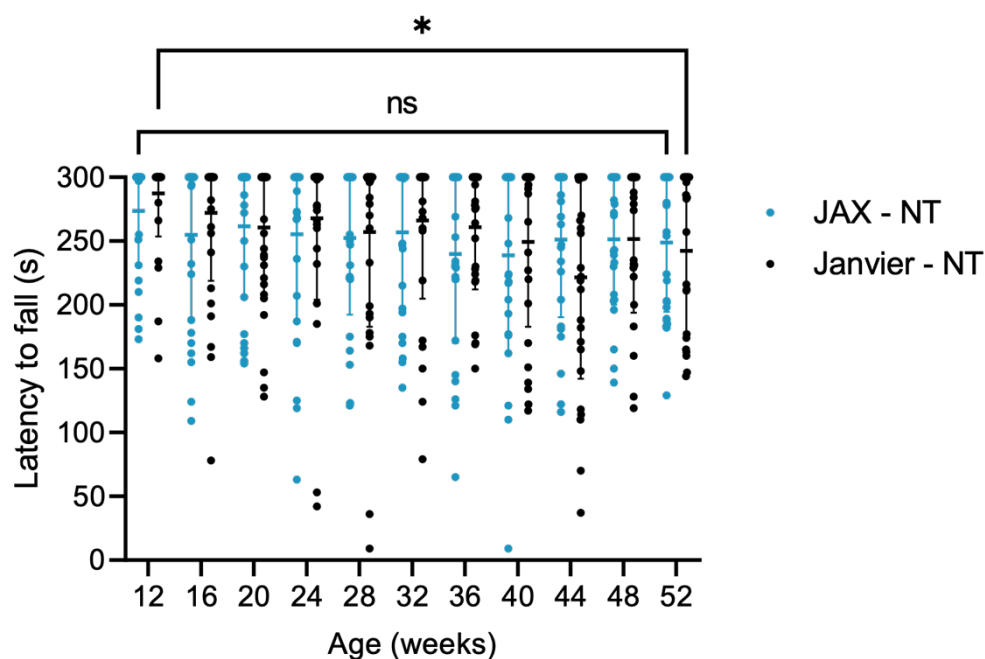
Figure 6.1: Mean latency to fall (± SD) in JAX and Janvier FVB/N mice.

There was no significant difference in latency to fall (± SD) between female JAX and Janvier mice at any timepoint. Janvier mice showed a significantly decreased latency to fall at 52 weeks of age compared to 12 weeks. *p<0.05, two-way ANOVA with repeated measures and Tukey's post-hoc test (JAX n = 27-33, Janvier n = 28-35).

After rotarod performance was normalised to weight, a two-way ANOVA revealed no significant differences between JAX and Janvier FVB/N mice (Figure 6.2). However, there was a significant decrease in performance at 52 weeks of age compared to 12 weeks in both groups.
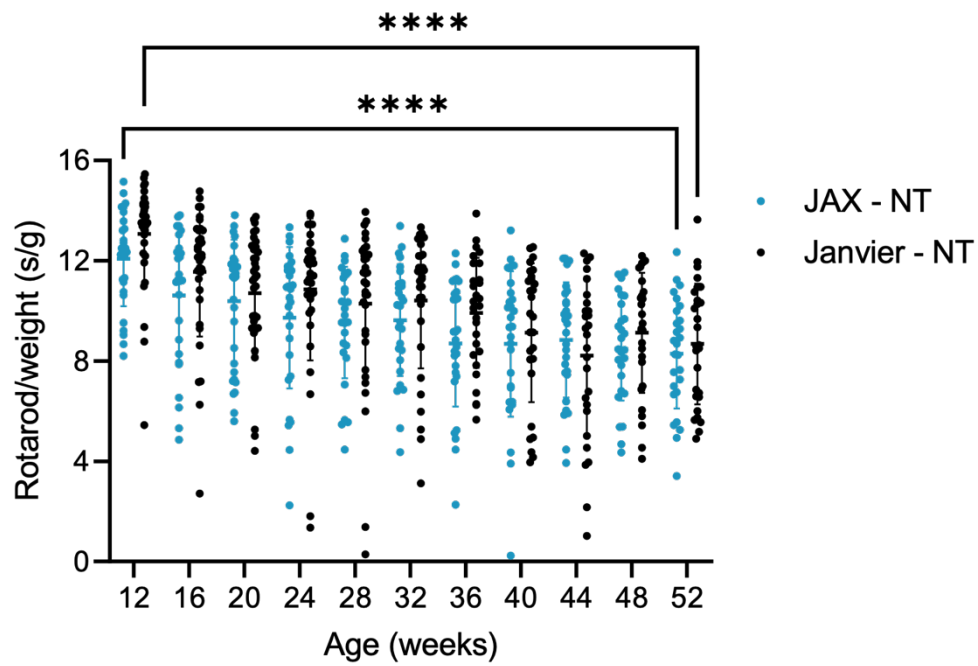
Figure 6.2: Rotarod performance/weight in JAX and Janvier FVB/N mice.

Mean latency to fall normalised to weight (± SD) showed no significant decreased between female JAX and Janvier mice. At 52 weeks of age both groups showed a significant decrease in latency to fall/weight ratio compared to 12 weeks. ****$p<0.0001$, two-way ANOVA with repeated measures and Tukey's post-hoc test (JAX n = 27-33, Janvier n = 28-35).

6.2.2 Catwalk Gait Analysis

Gait analysis was performed at monthly intervals from 12 weeks of age. Descriptions of parameters are detailed in Table 2.3. There were no significant differences in hindlimb stride length of base of support between the two groups at any timepoint (Figure 6.3 A, B). Hindlimb swing time was significantly reduced in JAX mice compared to Janvier at 12 weeks of age (0.07 ± 0.02 vs 0.09 ± 0.02, $p = 0.006$), however this difference was no longer present at 52 weeks (Figure 6.3 C). Janvier mice had significantly reduced hindlimb swing speed compared to JAX mice at 12 weeks (0.71 ± 0.13 vs 0.91 ± 0.23, $p = 0.004$), however this difference was no longer present at 52 weeks of age (Figure 6.3 D).
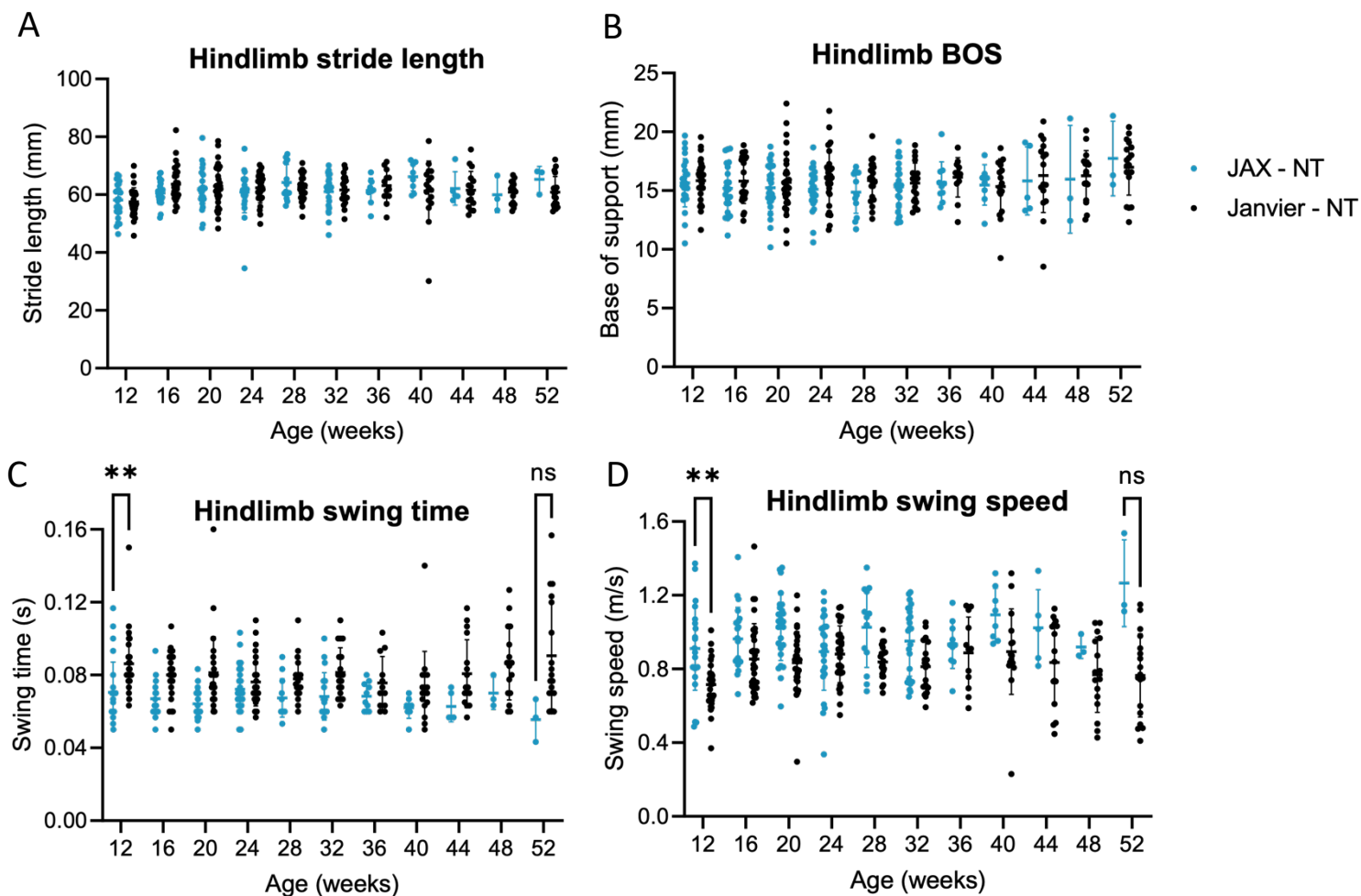
Figure 6.3: Catwalk gait analysis of JAX and Janvier FVB/N hindlimb stride length (A), base of support (B), hindlimb swing time (C), and hindlimb swing speed (D).

Values are presented as the mean (± SD) of left and right paws of each mouse. There were no significant differences between female JAX and Janvier mice in hindlimb stride length or base of support at any timepoint. JAX mice had a significantly decreased hindlimb swing time compared to Janvier mice at 12 weeks of age, however this difference was not present at 52 weeks. Janvier mice had a significantly decreased hindlimb swing speed compared to JAX mice at 12 weeks of age, however this difference was not present at 52 weeks. ns = non-significant, **$p < 0.01$, two-way ANOVA with repeated measures and Bonferroni's post-hoc test (JAX n = 3-28, Janvier n = 12-33).

Hindlimb print length remained stable with age, with no significant differences between the two groups. There was a slight increase in print length in JAX mice at 52 weeks, however this was likely due to the small n number and one outlier at that timepoint (Figure 6.4 A). JAX mice had a significantly larger print width compared to Janvier mice at 12 weeks of age (5.1 ± SD

155

vs 4.4 ± SD, p = 0.03), however this difference was not present at 52 weeks (Figure 6.4 B). Both groups were well-coordinated, with no significant differences in regularity between them at any timepoint (Figure 6.4 C). JAX mice had significantly increased intensity compared to Janvier mice at 12 weeks of age that was still present at 52 weeks (12 weeks, 117 ± SD vs 101 ± SD, p<0.0001; 52 weeks, 127.1 ± SD vs 95.7 ± SD, p<0.0001), indicating that JAX mice supported more weight on the paws than Janvier mice (Figure 6.4 D).
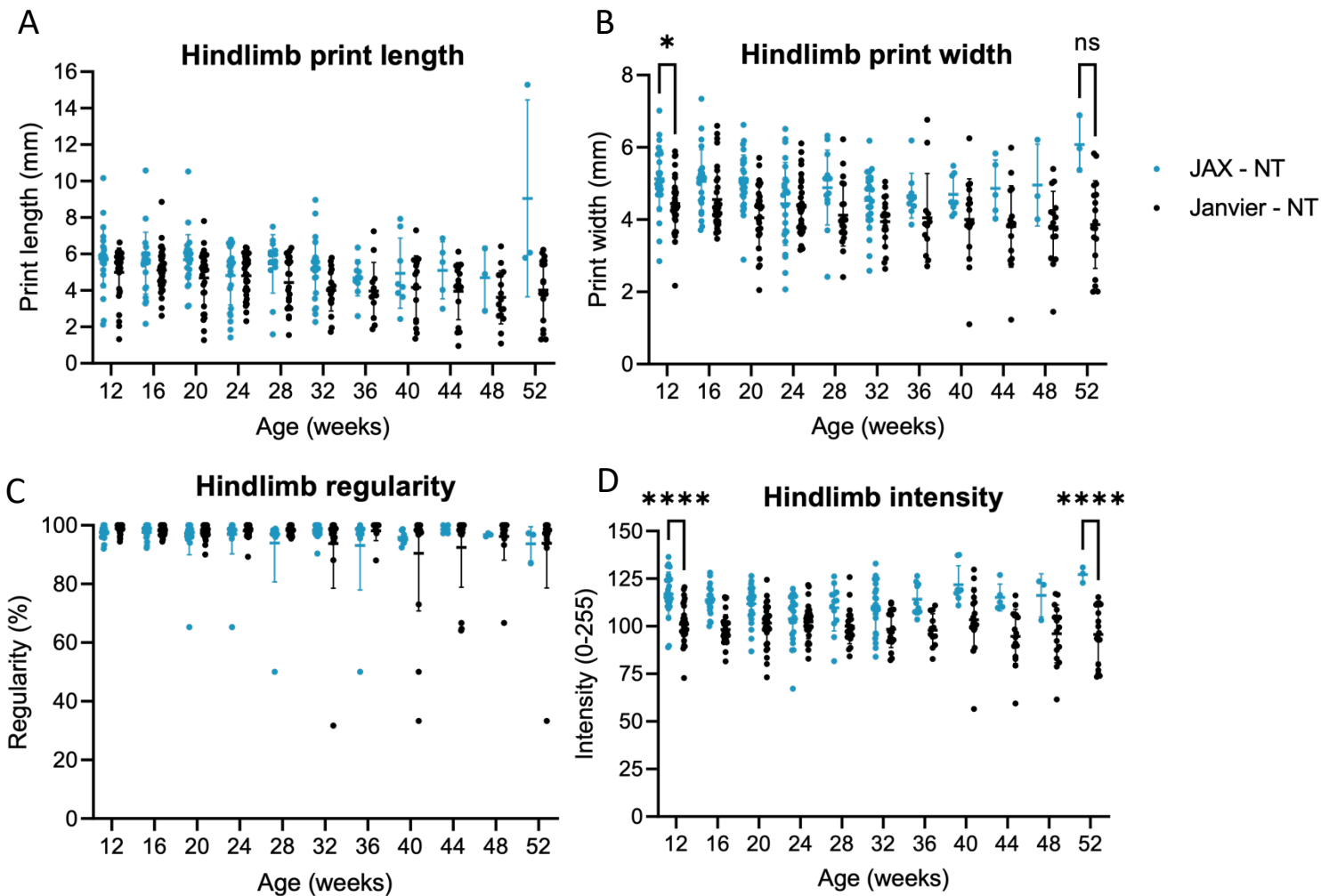
Figure 6.4: Catwalk gait analysis of JAX and Janvier FVB/N hindlimb print length (A), hindlimb print width (B), regularity (C), and intensity (D).

Values are presented as the mean (± SD) of the left and right paws of each mouse. There was no significant difference in print length or regularity between female JAX and Janvier mice at any timepoint. JAX mice had a significantly increased print width compared to Janvier at 12 weeks of age, however this difference was not present at 52 weeks. JAX mice had significantly increased intensity compared to Janvier mice at 12 weeks of age that was still present at 52 weeks. $p<0.05$, $****p<0.0001$, two-way ANOVA with repeated measures and Bonferroni's post-hoc test (JAX n = 3-28, Janvier n = 12-33).

Both groups spent most of the time on diagonal paws at all ages (Figure 6.5 A). The hindlimb duty cycle was significantly increased in JAX FVB/N mice compared to Janvier at 12 weeks of

age (Figure 6.5 B; JAX 61.1 ± 7.3 vs Janvier 55.1 ± 8.8, p = 0.011), however this difference was not present at 52 weeks.

A

B
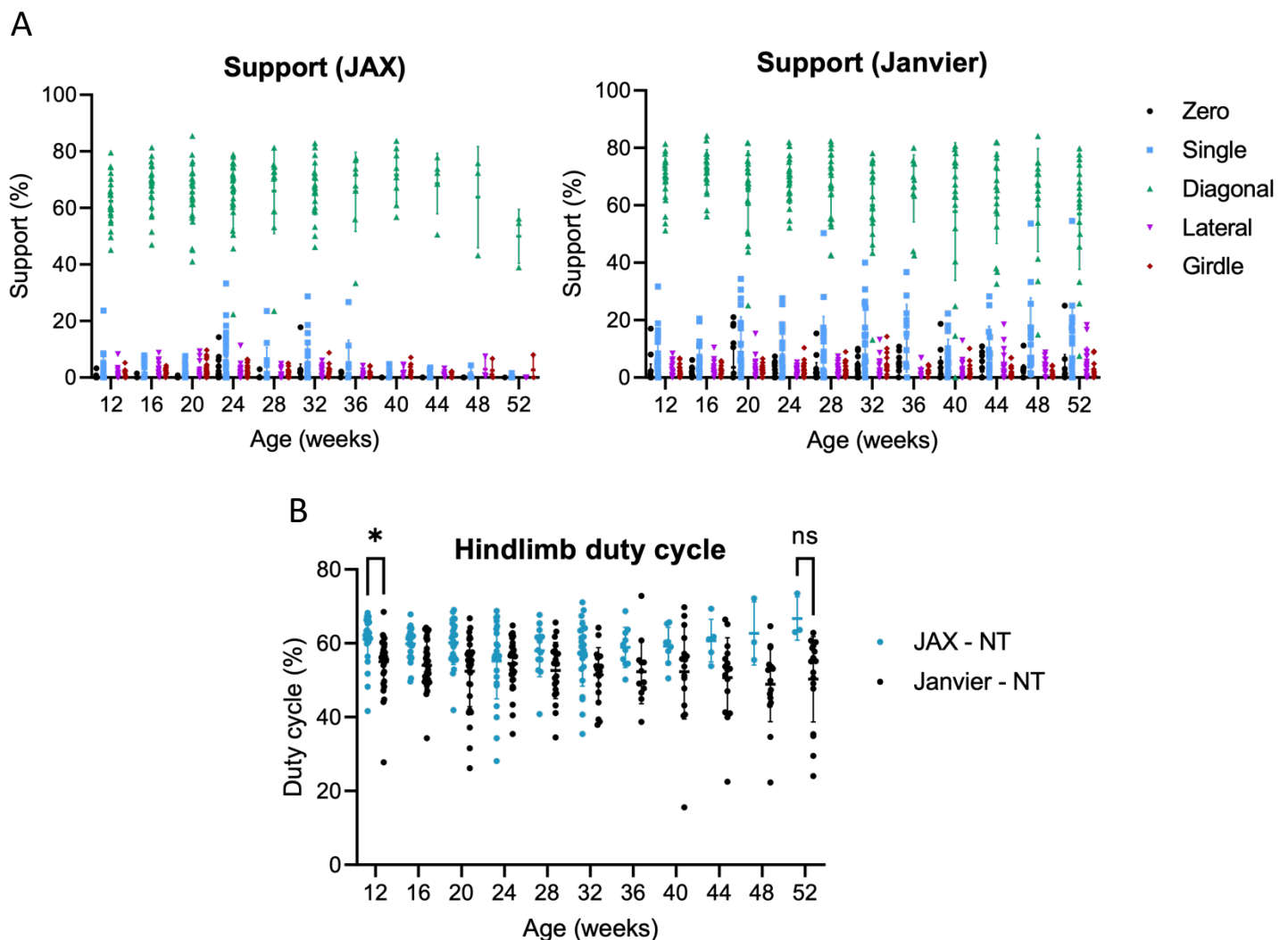
Figure 6.5: Catwalk gait analysis of percentage time spent on paws (A) and hindlimb duty cycle (B) in JAX and Janvier FVB/N mice.

Values are presented as the mean (± SD) of the left and right paws of each mouse. There were no significant differences in support between female JAX and Janvier mice. Mice predominantly displayed the diagonal step pattern. There was a significant difference in hindlimb duty cycle between the two groups at 12 weeks of age that was not present at 52 weeks (*p<0.05, two-way ANOVA with repeated measures and Bonferroni's post-hoc test, JAX n = 3-28, Janvier n = 12-33).

6.2.3 Open Field

Both groups of mice showed a very similar level of movement, with a general trend of increasing distance travelled with age (Figure 6.6). Several mice in both groups showed a large total distance travelled (>15000 cm) compared to all other mice. This was attributed to the development of stereotypic behaviour in these mice, with a higher proportion of Janvier mice developing this behaviour than JAX mice.

The open field chamber was virtually split into centre and periphery zones to analyse exploratory behaviour and anxiety. Neither group spent any more or less time in the centre of the open field chamber than the other (Figure 6.7).
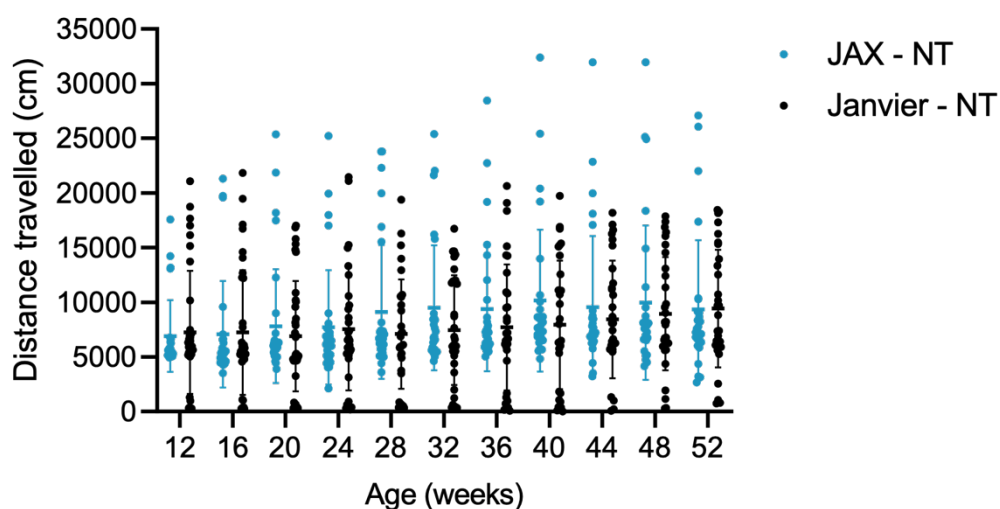
Figure 6.6: Mean distance travelled (± SD) in JAX and Janvier FVB/N mice.

Both female JAX and Janvier mice displayed a similar level of mobility (two-way ANOVA with repeated measures, JAX n = 27-33, Janvier n = 30-35).
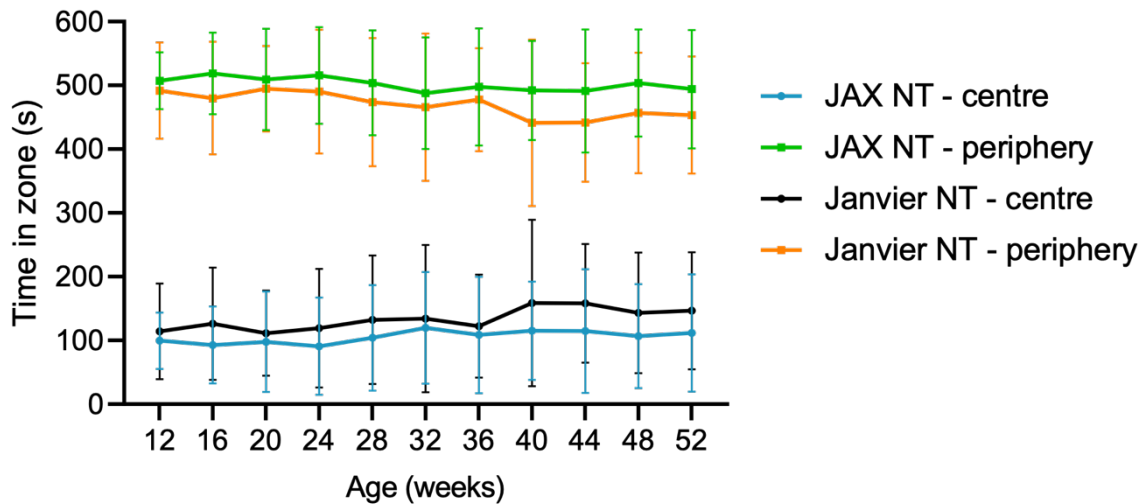
Figure 6.7: Mean time (± SD) in centre and periphery zones of open field chamber in JAX and Janvier FVB/N mice.

Both female JAX and Janvier mice spent equivalent time (± SD) in the centre and periphery zones of the open field chamber at every timepoint (two-way ANOVA with repeated measures, JAX n = 27-33, Janvier n = 30-35).

6.2.4 Social Recognition Test

Janvier FVB/N mice investigated the juvenile mice for a longer duration than the JAX FVB/N mice at later timepoints. Both groups showed no significantly reduced investigation time in the recall session compared to the initial session and spent a similar amount of time investigating novel and familiar individuals, indicating both groups may have impaired social memory (Figure 6.8).

Recognition index (the ratio of recall investigation time relative to initial investigation time) also showed no differences in ability to recognise a familiar individual between JAX and Janvier mice. It revealed that at most timepoints both groups spent equal or more time investigating the familiar mouse than the novel mouse (Figure 6.9), indicating impaired social memory.
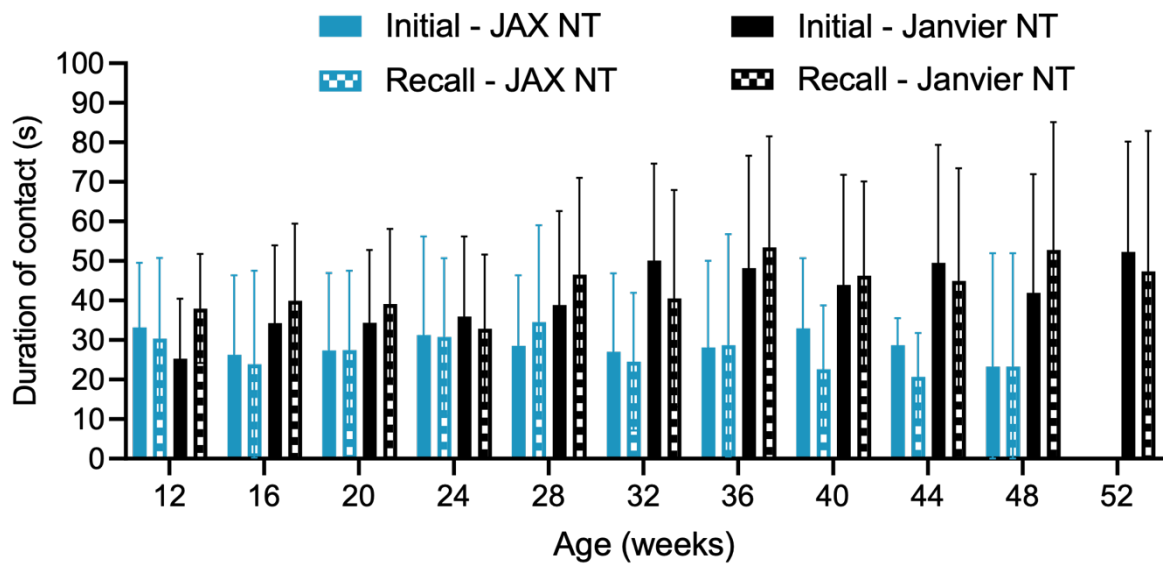
Figure 6.8: Mean duration of contact (± SD) with juvenile female mouse in JAX and Janvier FVB/N mice.

The same female juvenile mouse was used in the initial and recall sessions. Both female JAX and Janvier mice showed no significantly decreased investigation time in the recall session compared to the initial session at any timepoint (two-way ANOVA with repeated measures, JAX n = 2-28, Janvier n = 14-28).
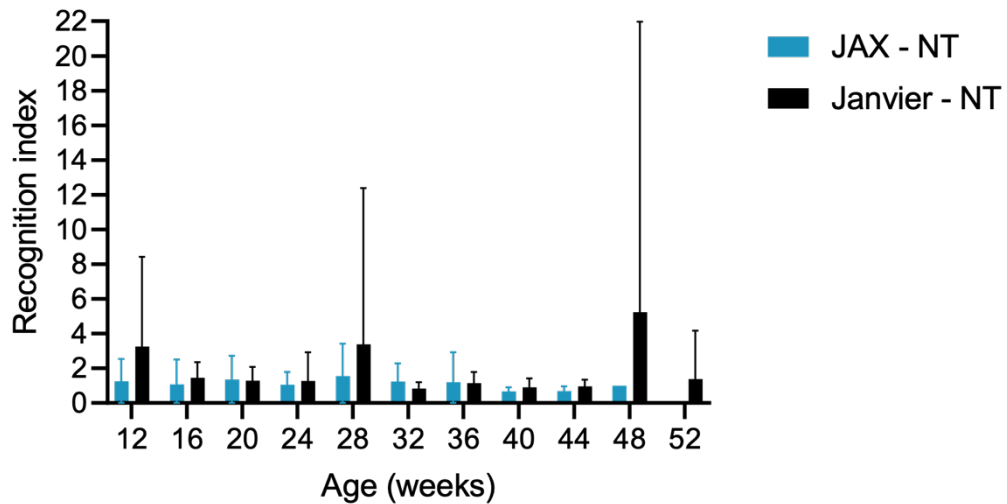
Figure 6.9: Recognition index of JAX and Janvier FVB/N mice.

Recognition index (the ratio of recall investigation time relative to initial investigation time, mean ± SD) showed no differences in ability to recognise a familiar individual between female JAX and Janvier mice (two-way ANOVA with repeated measures, JAX n = 2-28, Janvier n = 14-28). Both groups spent equal or more time investigating the familiar mouse than the novel mouse (index = 1: equal time spent investigating familiar and novel mouse, index > 1: more time spent investigating familiar mouse compared to novel mouse, index < 1: more time spent investigating novel mouse compared to familiar mouse).

6.2.5 Marble Burying

There was no significant difference in the number of marbles buried between JAX and Janvier mice (Figure 6.10). Both groups buried significantly fewer marbles at 52 weeks of age compared to 12 weeks (JAX 8.4 ± 2.6 vs 4.5 ± 2.9, p = 0.0005; Janvier 7.2 ± 2.9 vs 4 ± 3.2, p = 0.001).
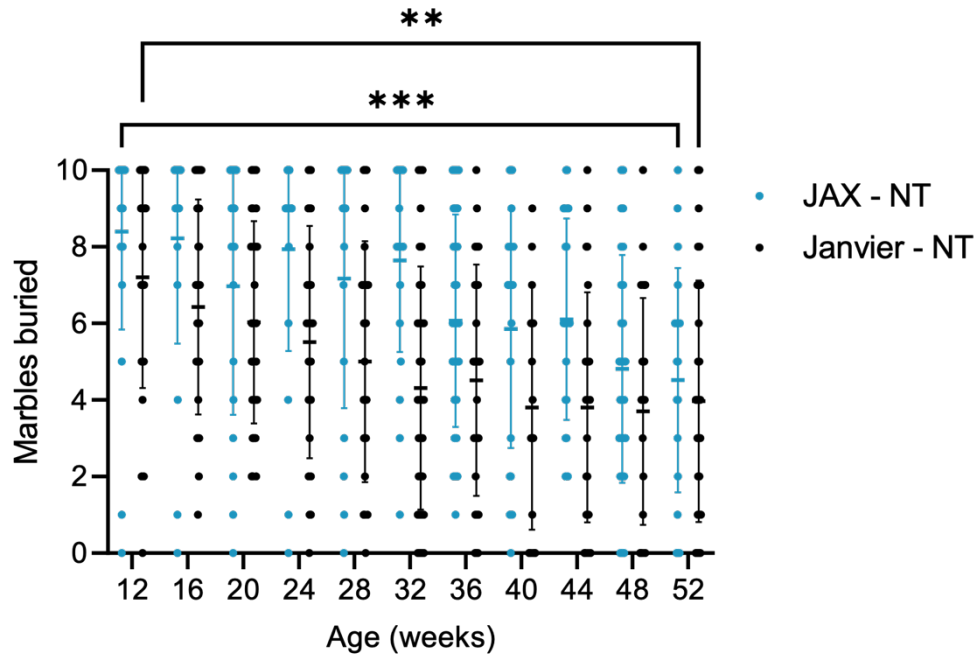
Figure 6.10: Mean number of marbles buried (± SD) in JAX and Janvier FVB/N mice.

Female JAX and Janvier mice buried similar numbers of marbles at all timepoints. Both groups buried significantly fewer marbles at 52 weeks of age compared to 12 weeks. **p<0.01, ***p<0.001, two-way ANOVA with repeated measures and Tukey's post-hoc test (JAX n = 27-33, Janvier n = 30-35).

6.2.6 Balance Beam

Median scores on the balance beam showed no differences in ability between JAX and Janvier FVB/N mice (Figure 6.11).
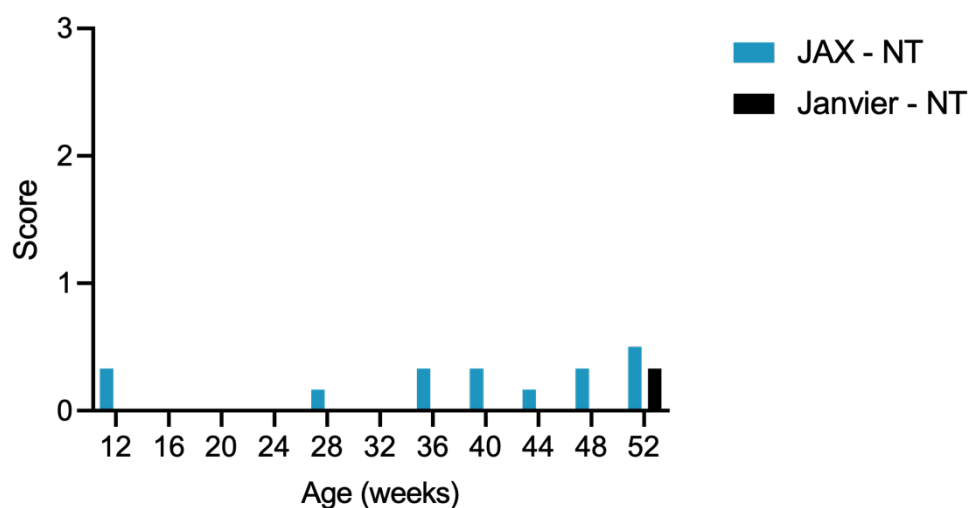
Figure 6.11: Median balance beam score of JAX and Janvier FVB/N mice.
Female JAX and Janvier mice displayed no significantly impaired coordination at any timepoint (JAX n = 27-33, Janvier n = 26-35).

6.2.7 Limb Hang Test

There was no significant difference in latency to fall between JAX and Janvier FVB/N mice (Figure 6.12), however Janvier mice showed a significant decrease in latency to fall at 52 weeks of age compared to 12 weeks (40.6 ± 42.5 vs 97.2 ± 86.1, $p = 0.02$, Figure 6.12). After eliminating the influence of weight on ability to hang, limb hang performance remained the same, with Janvier mice showing a significant decrease in latency to fall at 52 weeks of age compared to 12 weeks.
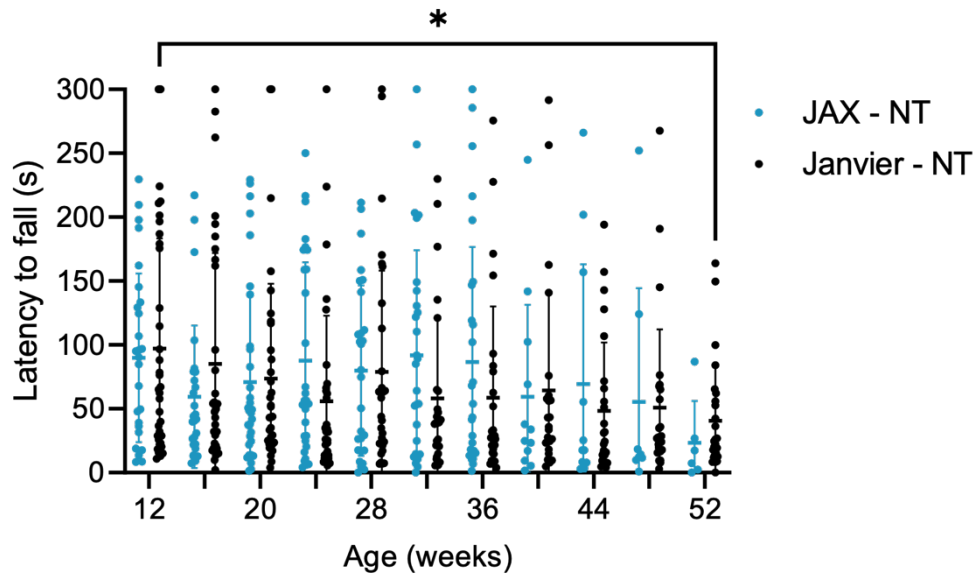
Figure 6.12: Mean hang time (± SD) in JAX and Janvier FVB/N mice.

Female JAX and Janvier mice showed no reduced hanging ability when compared to each other, however Janvier mice showed significantly reduced hanging ability at 52 weeks of age compared to 12 weeks. *$p<0.05$, two-way ANOVA with repeated measures and Tukey's post-hoc test (JAX n = 27-33, Janvier n = 23-35).
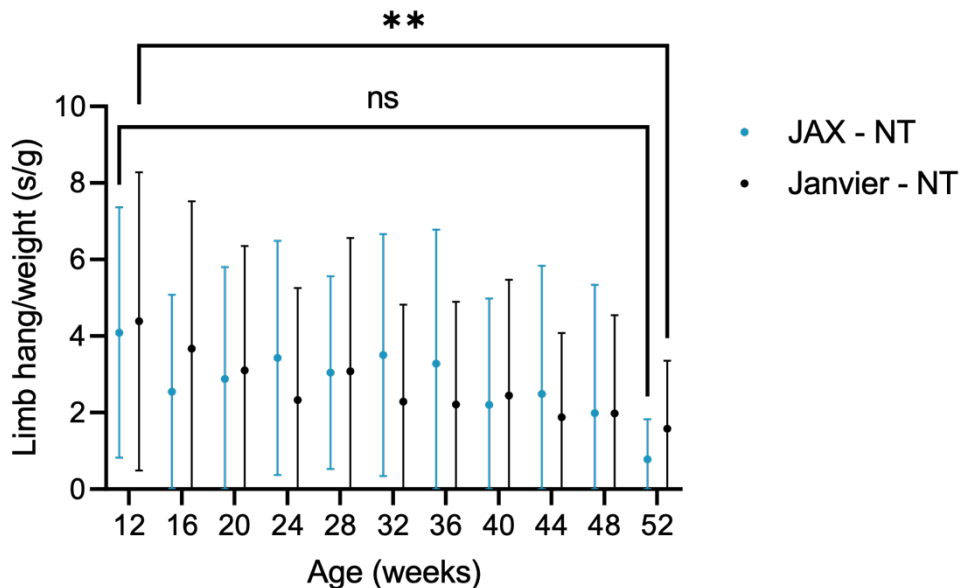
Figure 6.13: Limb hang/weight in JAX and Janvier FVB/N mice.

Mean latency to fall normalised to weight (± SD) showed no significant differences between female JAX and Janvier FVB/N mice. At 52 weeks of age, Janvier mice showed a significantly reduced hanging ability compared to 12 weeks (two-way ANOVA with repeated measures and Tukey's post **$p<0.01$, ns = non-significant, JAX n = 27-33, Janvier n = 23-35).

165

6.2.8 Burrowing

There was no significant difference in weight burrowed between JAX and Janvier FVB/N mice (Figure 6.14).
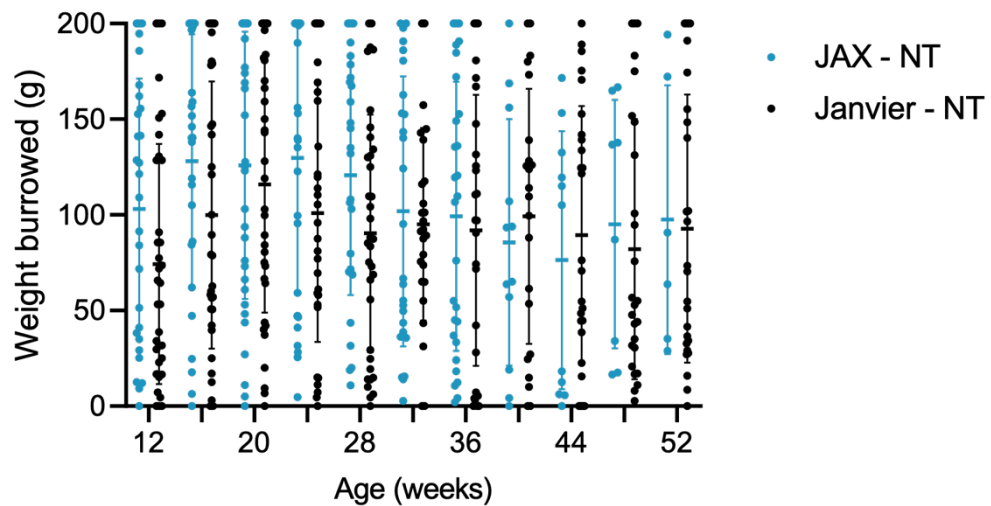
Figure 6.14: Mean weight burrowed (± SD) in JAX and Janvier FVB/N mice.

There was no significant difference in weight burrowed (± SD) between female JAX and Janvier mice at any timepoint (JAX n = 27-33, Janvier n = 22-35).

6.2.9 Nesting

Median nesting scores showed no differences in nest building ability between JAX and Janvier FVB/N mice (Figure 6.15). However, there was a general non-significant decrease in nest building ability in Janvier mice with age.
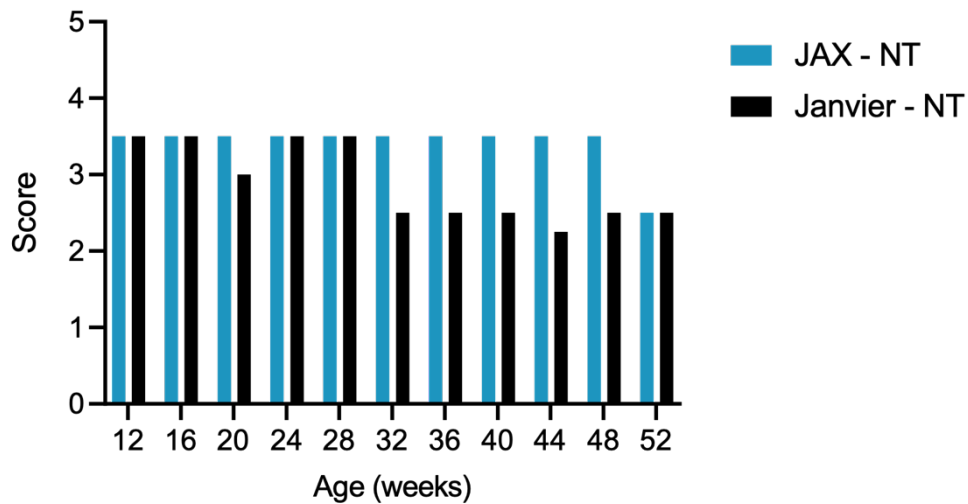
Figure 6.15: Median nesting score in JAX and Janvier FVB/N mice.

Female JAX and Janvier mice displayed no significantly impaired nest building behaviour at any timepoint (JAX n = 27-33, Janvier n = 26-35).

6.2.10 Food Intake

The test was performed overnight (16 hours) once a month alongside the nesting test. There was no significant difference in food intake between the two groups at any timepoint (Figure 6.16).
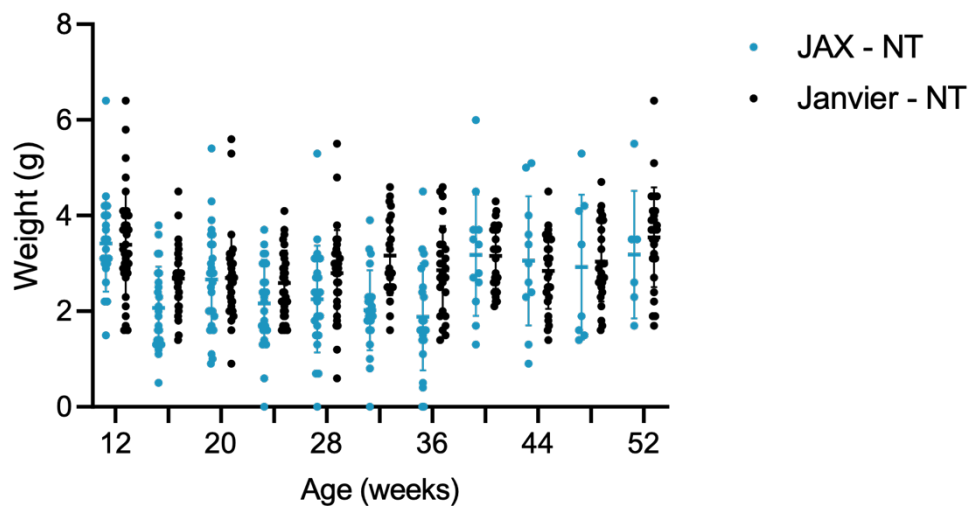
Figure 6.16: Mean food intake (± SD) overnight in JAX and Janvier FVB/N mice.

Test was performed alongside nesting behaviour over a 16-hour period. There was no significant difference in food intake (± SD) between female JAX and Janvier mice at any timepoint (two-way ANOVA with repeated measures, JAX n = 21-28, Janvier n = 26-35).

6.2.11 Weight

Both grouped showed an increase in body weight with age (Figure 6.17). There was no significant difference between JAX and Janvier FVB/N mice at any timepoint. Weight was monitored weekly.
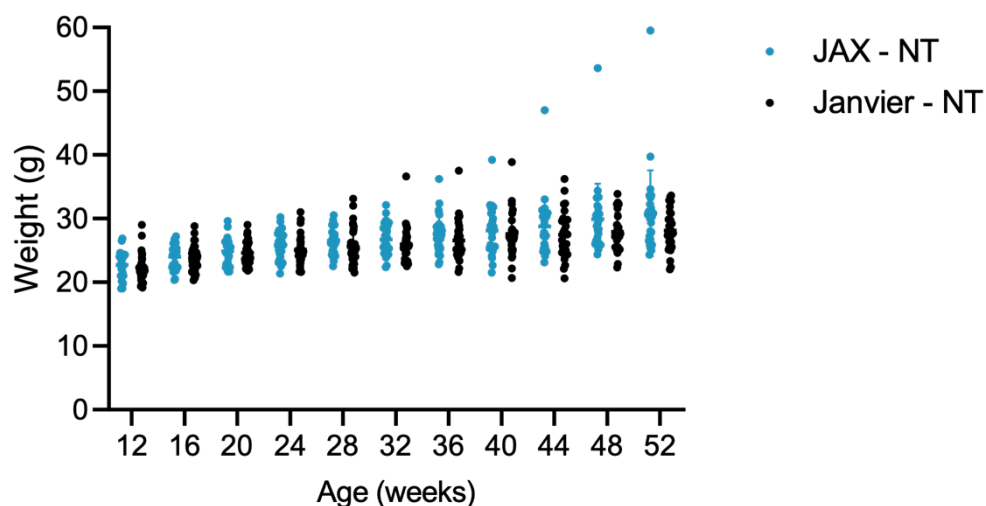
Figure 6.17: Mean weight (± SD) of JAX and Janvier FVB/N mice.

Both groups increased body weight (± SD) from 12-52 weeks of age. There was no significant difference between female JAX and Janvier mice at any timepoint (two-way ANOVA with repeated measures, JAX n = 27-33, Janvier n = 30-35).

6.2.12 Subset Data Analysis

An analysis method to identify subsets hidden within the data was described in methods section 2.6.9. Results of this analysis are detailed in Table 6.1. Chi-Square analysis was performed between JAX and Janvier FVB/N mice for each test detailed, with neither group performing significantly worse than the other.

Table 6.1: Contingency table counts of JAX and Janvier FVB/N mice.

Each number is the number of times a score was given in each test. Chi-square analysis was performed between female JAX and Janvier mice. None were found to be significantly different. MND-like phenotype = motor neurone disease-compatible score expected in diseased mice, Normal = normal score expected in healthy mice.

Test	JAX FVB/N		Janvier FVB/N		p-value
	MND-like phenotype	Normal	MND-like phenotype	Normal	
Rotarod	11	23	4	24	0.14
Open field	9	25	9	19	0.78
Marble burying	18	16	13	15	0.80
Balance beam	18	16	12	15	0.61
Limb hang	13	21	16	12	0.20
Burrowing	14	20	15	13	0.44
Nesting	15	19	13	15	>0.99
CMAP	12	22	15	13	0.20

6.2.13 Electrophysiology

There was no significant change in CMAP amplitude in or between either group over time (Figure 6.18). Repetitive nerve stimulation revealed no significant decrement in response between repetition 1 and 10 in both groups, as expected in healthy mice (Figure 6.19).
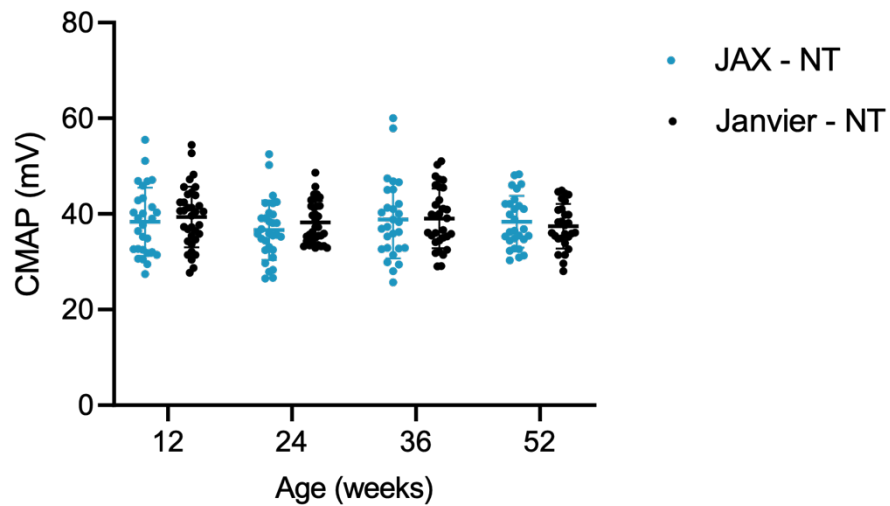
Figure 6.18: CMAP of the hindlimb muscles in JAX and Janvier FVB/N mice.

CMAP amplitudes were equal between female JAX and Janvier mice at all timepoints (mean ± SD, JAX n = 28-30, Janvier n = 28-36).
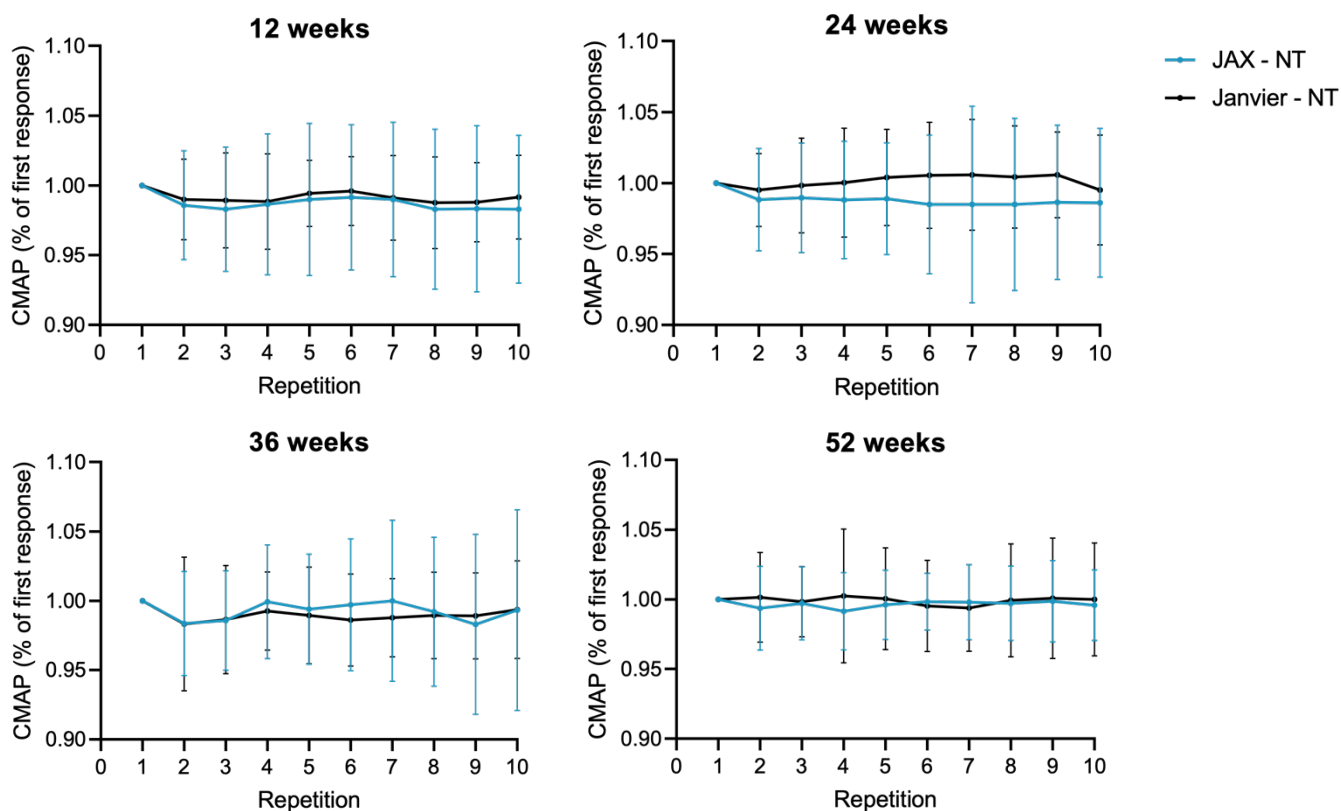
Figure 6.19: Repetitive stimulation of the hindlimb muscles in JAX and Janvier FVB/N mice.

There was no significant decrement in response (represented as percentage of the first response) in female JAX and Janvier mice (mean ± SD, two-way ANOVA with repeated measures and Sidak's post-hoc test, JAX n = 28-30, Janvier n = 28-36).

6.2.14 Survival

There was no difference in survival between JAX and Janvier FVB/N groups. Of the six JAX FVB/N mice that died, four were found dead in their home cages, one was euthanised due to substantial distress of unknown cause, and one was euthanised on advice of the resident veterinarian due to a prolapse. Of the five Janvier FVB/N mice that died, three were found dead in their home cages, one was euthanised due to a seizure, and one was euthanised due to substantial distress of unknown cause.
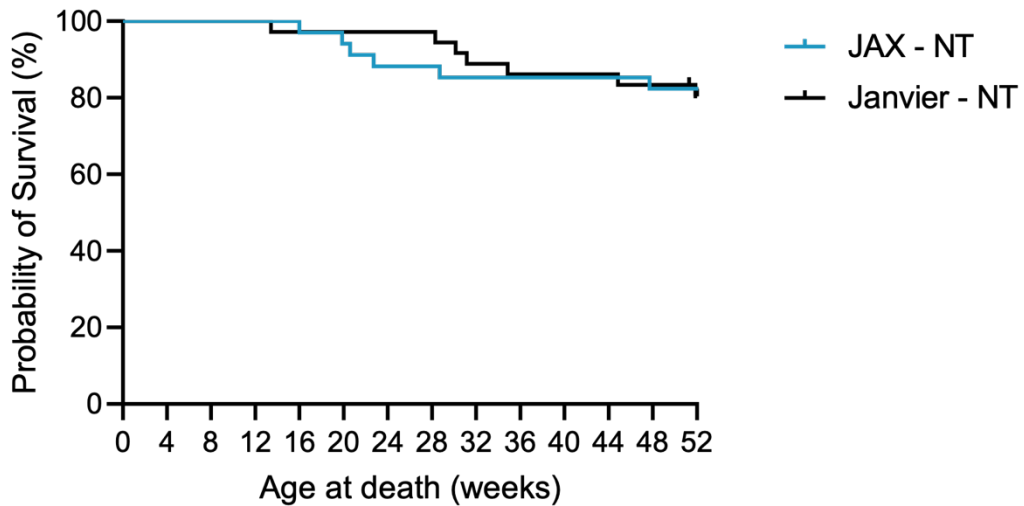
Figure 6.20: Survival curve of JAX and Janvier FVB/N mice.

Kaplan-Meier survival curse of female JAX and Janvier FVB/N mice shows no difference in survival (Gehan-Breslow-Wilcoxon test, p = 0.8252, JAX n = 34, Janvier n = 36).

6.2.15 Clasping

Representative examples of clasping scores were show in Figure 3.26 A. The proportions of each score given at each timepoint for JAX and Janvier FVB/N mice are shown in Figure 6.21.
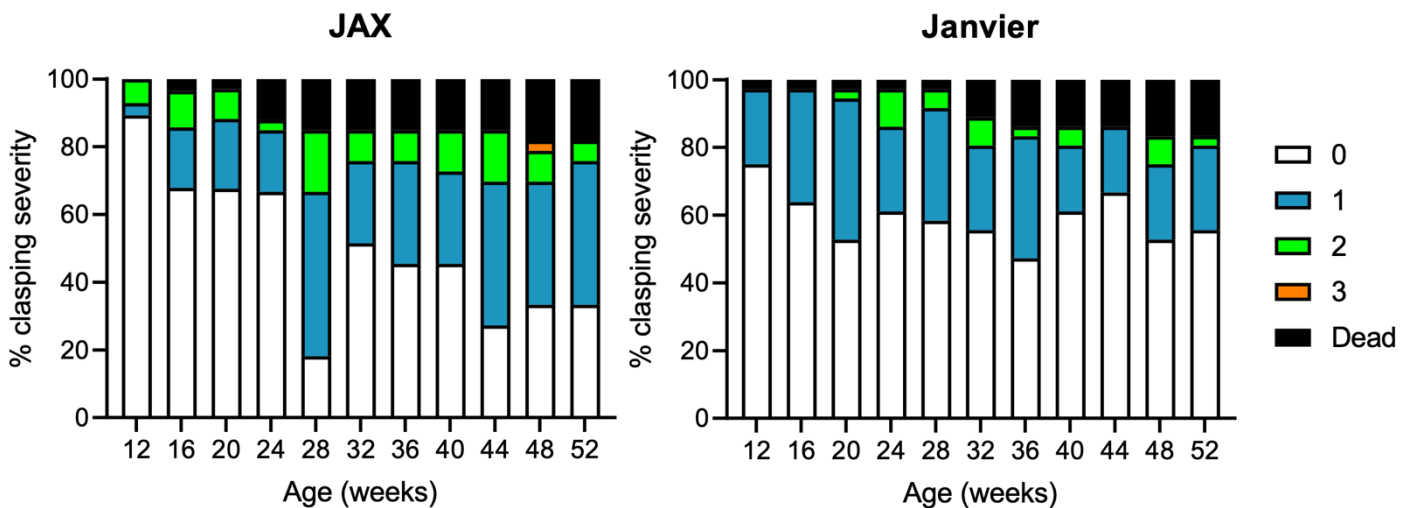
Figure 6.21: Clasping phenotypes of JAX and Janvier FVB/N mice.

Graphical depiction of female JAX and Janvier FVB/N mice displaying clasping phenotypes from 12-52 weeks of age (JAX n = 34, Janvier n = 36).

6.2.16 Stereotypic Behaviour

Stereotypic circling behaviour was observed in both JAX and Janvier FVB/N mice. Incidence increased over time in both groups but was significantly increased in the Janvier FVB/N group compared to JAX at both 12 weeks of age and 52 weeks (Figure 6.22).
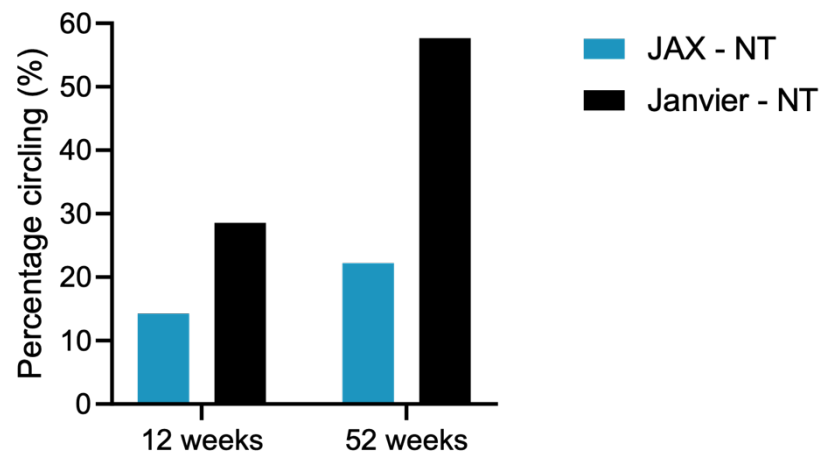
Figure 6.22: Proportion of stereotypic circling behaviour in JAX and Janvier FVB/N mice.
Stereotypic circling behaviour was observed at 12 weeks of age in female JAX and Janvier mice and increased in incidence over time.

6.2.17 Variability of Behavioural Tests

As expected, the behavioural tests showed the largest variability, with the balance beam, limb hang, burrowing and open field showing the most. Neither group demonstrated more variability than the other (Figure 6.23).
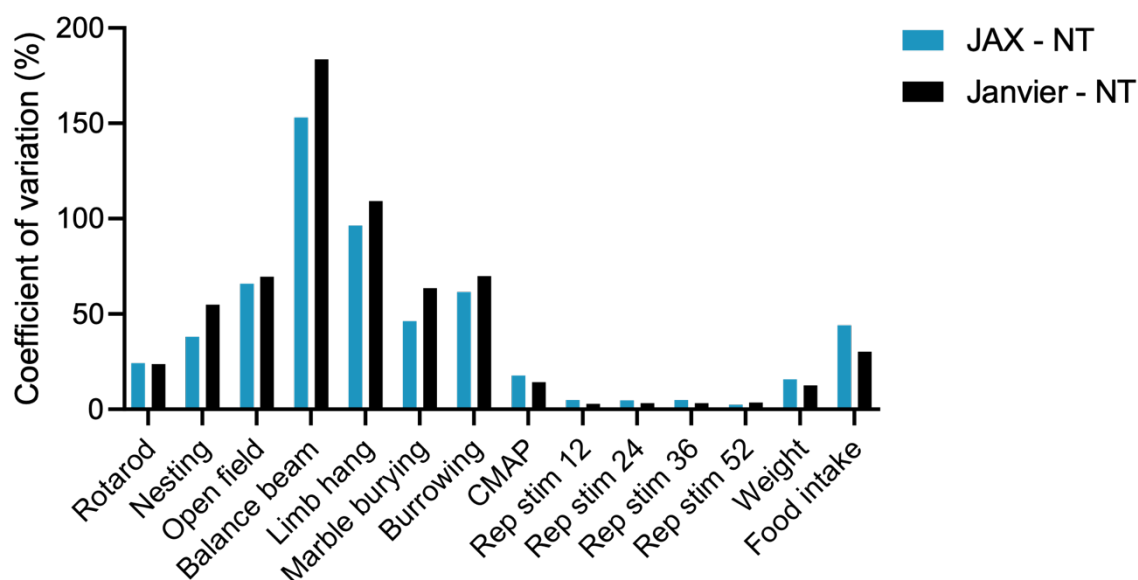
Figure 6.23: Variability of behavioural tests.

Coefficient of variation showed both female JAX and Janvier mice were equally variable within each test. Balance beam, limb hang, and burrowing show the largest amount of variability.

6.2.18 Seizure Observations

Seizures were observed in NT mice in both studies. Seizures were timed at onset or from time of discovery and scored according to the scale from Van Erum et al. (2019). Severe or repetitive seizures, or failure to recover from seizure, resulted in euthanasia. Janvier mice were observed to have more seizures than JAX mice (Table 6.2).

Table 6.2: Seizures observed in JAX and Janvier FVB/N mice.

Seizures were scored according to Van Erum et al. (2019). Scores 1 to 3 were classed as mild (1, whisker trembling; 2, sudden behavioural arrest; 3, facial jerking). Scores 4 to 6 were classed as moderate (4, neck jerks; 5, clonic seizure (sitting); 6, clonic, clonic-tonic seizure (lying on belly)), 7 and 8 were classed as severe (7, clonic, clonic-tonic seizure (lying on side) and wild jumping; 8, tonic extension, possibly leading to respiratory arrest and death).

Strain	Age	Score	Euthanasia
JAX	28 weeks	5	No
JAX	20 weeks	3	No
Janvier	20 weeks	3	No
Janvier	30 weeks	3	Yes
Janvier	44 weeks	5	No
Janvier	45 weeks	5	Yes
Janvier	49 weeks	4	No
Janvier	35 weeks	5	Yes

6.3 Tissue Pathology

6.3.1 Neurone Counts

There was no significant difference in the number of lumbar motor neurones in the spinal cord between JAX and Janvier FVB/N mice at 52 weeks of age (Figure 6.24), but there was a trend in the Janvier mice towards having fewer motor neurones than the JAX mice.
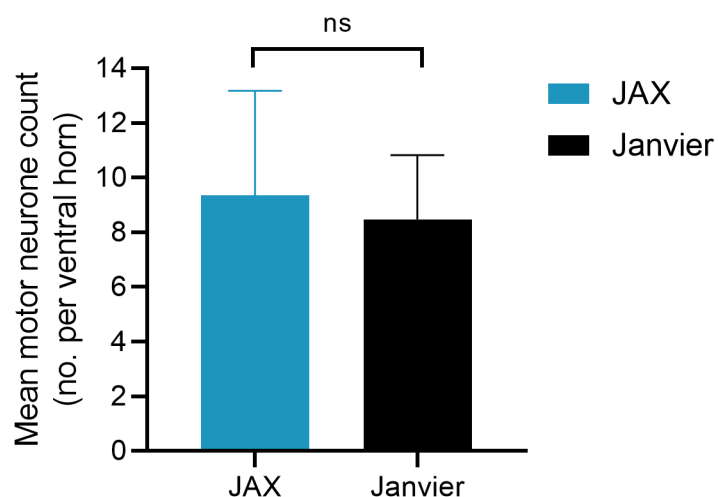
Figure 6.24: Motor neurone count in the lumbar spinal cord.

No significant difference between motor neurone counts in the lumbar spinal cord of female JAX and Janvier FVB/N mice (mean ± SD, nested t-test, JAX n = 5, Janvier n = 7).

Neuronal counts were performed in the CA and DG regions of the hippocampus and layer V of the motor cortex in 52-week-old mice. There were significant differences in the number of neurones between JAX and Janvier FVB/N mice in both hippocampal brain regions (**Error! R eference source not found.**). This was not present in the motor cortex (Figure 6.25).
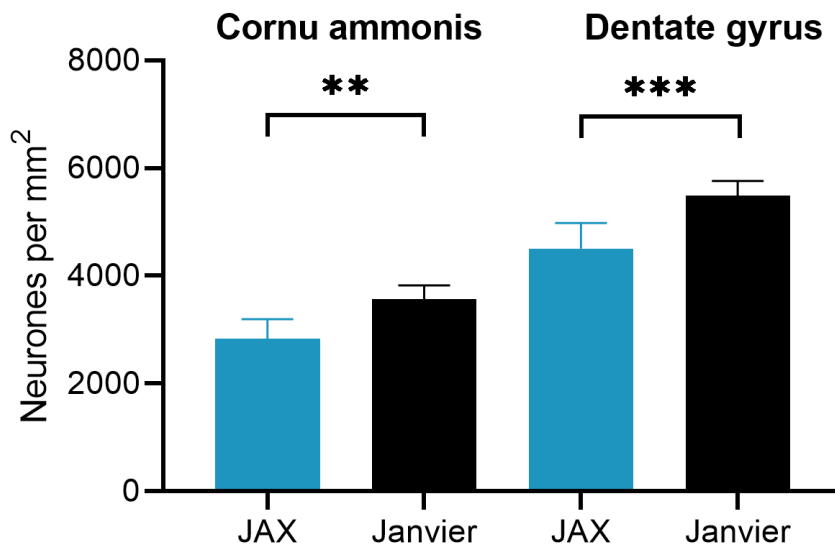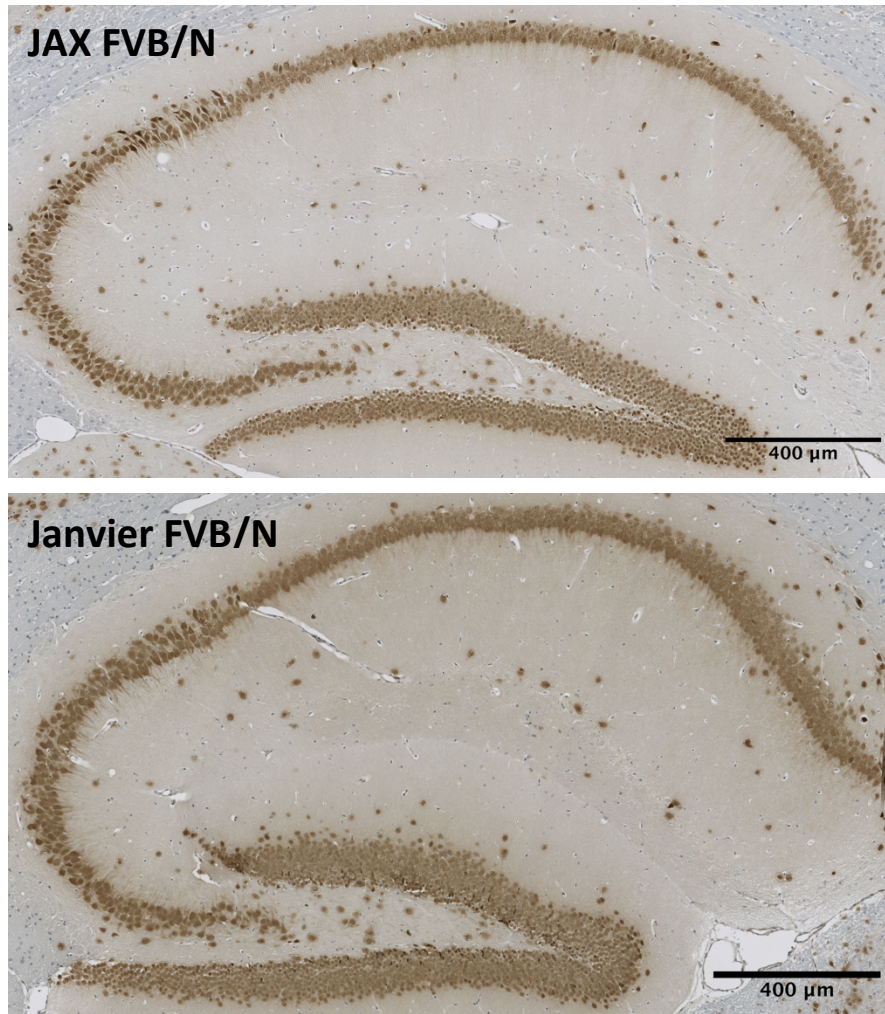
Figure 6.25: Neuronal counts in the hippocampus of JAX and Janvier FVB/N mice.

Neuronal counts in the cornu ammonis (CA) and the dentate gyrus (DG) of the hippocampus showed significant differences between female JAX and Janvier FVB/N mice (mean ± SD, nested one-way ANOVA with Bonferroni's multiple comparisons, JAX n = 5, Janvier n = 4).
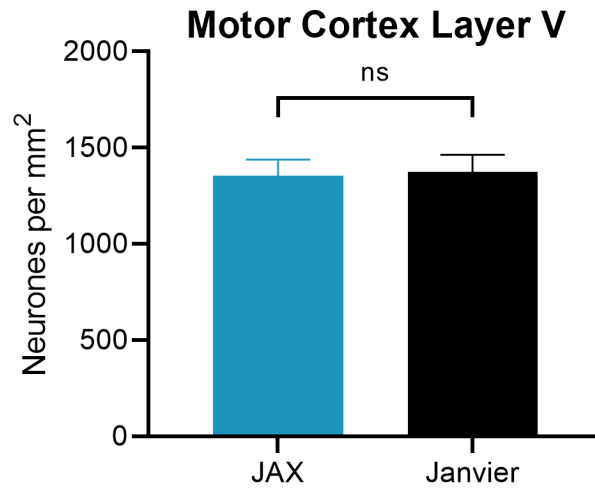
Figure 6.26: Neuronal count in layer V of the motor cortex.

There was no significant difference in neurone counts between female JAX and Janvier FVB/N mice (mean ± SD, nested t-test).

7   Discussion

Different strains, and even substrains, can differ significantly in their performance of behavioural tests (Voikar et al., 2001). These differences are important to identify as they may influence the phenotypes of transgenic mice and affect the results of preclinical studies. The above comparison of the JAX and Janvier FVB/N background strains revealed very few behavioural differences between them despite breeding separation for nearly 30 years. Overall, the most striking aspect of the FVB/N data herein was the variability of both strains in their performance of almost all the behavioural tests. Historically, the FVB/N strain has been considered a poor strain for behavioural studies (Voikar et al., 2001; Mineur and Crusio, 2002; Bothe et al., 2004), and the variability and stereotypic circling behaviour observed in both studies concurs with that assessment.

There were a small number of differences in gait analysis parameters, primarily in hindlimb intensity, which was significantly increased in JAX FVB/N mice at 12 weeks of age and was still present at 52 weeks. Intensity is a measure of weight on the paws, but as the JAX mice were no heavier than the Janvier mice, that was unlikely to be the driving influence behind the difference. The JAX mice also had a significantly quicker hindlimb swing time and swing speed at 12 weeks of age. Both parameters had lost significance by 52 weeks, however this may be due to the reduced n numbers in the JAX group at that timepoint due to Covid-19.

Interestingly, although there were no significant differences in distance travelled in the open field test, several Janvier mice displayed distinctly reduced levels of activity at every timepoint that was not exhibited by the JAX mice. The mice had normal motor function, as assessed by rotarod, gait analysis, and electrophysiology measurements, and so this reduced activity may instead be a feature of the anxiety reported in this strain (Mineur and Crusio, 2002). The social recognition test revealed impaired social memory in both groups and has been previously discussed in section 5, as have the significant reductions in performance that were seen in the marble burying, rotarod, and limb hang tests.

The Janvier mice appeared to exhibit more seizures than the JAX mice, although this could partly be due to chance observations as the mice were not monitored 24/7. However, as both

groups were housed in the same environmental conditions, there is the possibility that the Janvier mice may have developed an increased genetic susceptibility to seizures. A similar occurrence was reported by Nguyen et al. (2020a) in which the original authors of Liu et al. (2016) at the University of Florida observed a sudden increase in seizure activity and aggression in their colony following introduction of fresh female FVB/N breeders. However, these breeders were FVB/N mice from Jackson Laboratories, while the Janvier FVB/N mice in Nguyen et al. (2020a) at the University of Bern did not display this increased seizure activity. This is in opposition to my observations.

Histology analyses revealed that both groups had similar numbers of motor neurones in the lumbar spinal cord. Neuronal counts in layer V of the motor cortex were also similar, however the JAX FVB/N mice had significantly fewer neurones in the CA and DG regions of the hippocampus. Determining baseline neurone counts in background strains may prove informative for cross-strain comparisons.

This study did not compare the two strains on a genome-wide scale, and so genetic differences may still have occurred that have not been identified here. Additionally, while mice within an inbred strain are intended to be genetically identical, it is possible that they may differ in minisatellite regions and short repetitive DNA sequences that could affect gene expression and behaviour (Lathe, 2004; Eltokhi et al., 2020). As such, future studies comparing individuals within and between strains may prove informative.

7.1   Utility of the Mouse Model for Preclinical Research

The two behavioural studies presented here have provided an in-depth characterisation using a battery of tests to thoroughly interrogate the disease phenotype of this C9ALS/FTD BAC model. The data presented appears to show no behavioural phenotypes, neurodegeneration, or neuromuscular impairments associated with the *C9ORF72* transgene. This clearly contrasts with the reports of Liu et al. (2016) and Nguyen et al. (2020a). Rather, the data are in agreement with the two-centre report of Mordes et al. (2020). As such, the lack of a robust and reproducible phenotype and the highly variable behavioural data makes this model unsuitable for preclinical research. However, the model does express DPRs, and so may be

useful to test DPR-related therapeutic strategies (Castelli et al., 2023), although amelioration of this pathology is unlikely to be reflected in behavioural or neurodegenerative changes.

Potential reasons for the disparate findings between the two studies presented in this thesis and the initial publication of this C9ALS/FTD model have been discussed in previous sections. Such discrepancies are an example of the concerns that have been raised in recent years surrounding the reproducibility of mouse model findings both within and between laboratories (Fisher and Bannerman, 2019). Transgenic mouse models allow us to investigate the effect of a gene on a phenotype in a controlled environment, and it has long been considered that using inbred strains in preclinical research reduces variability to allow the identification of differences between transgenic mice and controls (Festing, 1999). However, even within a controlled environment there are several factors that can affect reproducibility. These include experimental design, differences in behavioural protocols, animal husbandry, handling techniques, environmental conditions, choice of genetic background, and sex (Sare et al., 2021). To minimise this variation, it has been suggested to use several background strains within each study, especially as the choice of genetic background can influence the phenotype of the same mutation (Heiman-Patterson et al., 2011).

Using several background strains could also benefit our understanding of disease pathogenesis through the identification of modifier genes. For example, in a mouse model of Huntington's disease, phenotypic variation across three different background strains allowed the identification of genetic modifiers that influenced disease severity (Van Raamsdonk et al., 2007). Therefore, using several genetic backgrounds to study a mutation could help mimic the genetic diversity seen in humans. However, even when genetic backgrounds are identical, an important source of variation across facilities is in behavioural test protocols. Slight changes such as time of day the test is performed, the order of behavioural tests, level of pretraining, or type of equipment used can have a significant effect on results. For example, one study found that the order of behavioural tests significantly influenced the behaviour in certain tests (McIlwain et al., 2001). This highlights the importance of standardising behavioural tests across facilities and including detailed experimental protocols in publications to aid replicability.

On the other hand, there is the argument to keep variability within preclinical studies to mimic the wide genetic diversity of the human population and the potentially informative behavioural artefacts that may occur in a heterogeneous environment (Wurbel, 2000). Mice have been crossbred over many generations to become homogeneous in as many genetic loci as possible, and while this may decrease variability and improve reproducibility of preclinical studies, there still remains the challenge of translating preclinical results into the clinic. Historically, this translation has failed (Mead et al., 2022). Additionally, human clinical trials are multicentre, while preclinical animal studies are often performed in just one. Therefore, it has been suggested to perform mouse studies across several facilities to mimic clinical trials (Fisher and Bannerman, 2019). Thoroughly understanding the variability in preclinical studies and how, why, and where it occurs may prove beneficial in improving the translatability of preclinical studies into human trials.

7.2   Why is there no Phenotype in the C9orf72 ALS/FTD BAC Models?

Three other C9ALS/FTD BAC models were generated around the same time as Liu et al. (2016). All develop DPR and RNA foci pathology, yet the Peters et al. (2015) and O'Rourke et al. (2015) models exhibited no behavioural deficits, neurodegeneration, or TDP-43 pathology, while the Jiang et al. (2016) model displayed mild hippocampal neurodegeneration and spatial and working memory deficits. Why these models developed different phenotypes, or no phenotype at all, remains unclear, but there are several possibilities.

The first possibility is the lack of haploinsufficiency. The *C9ORF72* HRE results in haploinsufficiency of the *C9ORF72* gene and a reduced level of the C9ORF72 protein in humans (Gijselinck et al., 2016; Jackson et al., 2020). While mice have their own endogenous *C9orf72* gene, knockdown or knockouts of this gene do not cause disease (Burberry et al., 2016; Atanasio et al., 2016; Sudria-Lopez et al., 2016). Instead, it has been suggested that haploinsufficiency may sensitise neurons to additional insults and cause disease in combination with toxic gain-of-function mechanisms. The C9ALS/FTD BAC models express DPRs and RNA foci yet do not develop behavioural or neurodegenerative features (Peters et al., 2015; O'Rourke et al., 2015), except the mild neurodegeneration and increased anxiety seen in the Jiang et al. (2016) model. As the mouse *C9orf72* gene is still intact in these models,

haploinsufficiency is not present, and so may be required in combination with DPRs for a phenotype to develop. To investigate this, the authors of the Jiang et al. (2016) model inactivated one or both alleles of the endogenous mouse *C9orf72* gene in their 66- and 450-repeat containing mice (Zhu et al., 2020). They found that reduction or loss of *C9orf72* in 450-repeat mice exacerbated cognitive and motor deficits, although interestingly there was no reduction in grip strength or lumbar motor neurone loss. They also observed increased hippocampal degeneration and glial activation. The mice also displayed premature death; however, this was indistinguishable from purely *C9orf72* knockout mice, indicating that the presence of 450 repeats did not impact survival. Additionally, autophagy was impaired in their *C9orf72* knockout mice, and increased accumulation of poly-GA and poly-GP was observed in the cortex of their 450-repeat *C9orf72* knockout mice. Reduced C9ORF72 levels have been found to increase DPR accumulation (Boivin et al., 2020), therefore it is possible that reduced C9ORF72 leads to interrupted autophagy which impairs the ability of neurons to clear DPRs, leading to neurotoxicity and ultimately neurodegeneration.

In addition to this study, a rat model of C9ALS was generated around the same time to also investigate the effect of reducing endogenous rat *C9orf72* expression on disease (Dong et al., 2020). The authors did this by inserting an 80-repeat human *C9ORF72* HRE into the endogenous *C9orf72* rat locus, reducing expression of the rat C9ORF72 protein by 40%. The rats went on to develop immune system dysregulation, as previously observed in *C9orf72* knockout mouse models (Burberry et al., 2016; Atanasio et al., 2016; Sudria-Lopez et al., 2016), lumbar motor neurone loss, and progressive motor deficits that resulted in hindlimb paralysis. The results of these two studies provide evidence that loss-of-function and toxic gain-of-function mechanisms may synergise to drive disease and is an important step forward in developing a murine model of C9ALS/FTD.

The second possibility as to why the C9ALS/FTD BAC models do not develop a phenotype may be due to the differing lifespans between mice and humans. ALS is a late onset disease, typically developing in middle- or old-age. The average lifespan of a research mouse is approximately 2 years (Yuan et al., 2009), compared to humans who, in the UK for example, have an average life expectancy of 80 years. It may be that the mouse simply does not live long enough to develop a late onset disease for which ageing is a component. Therefore,

integrating ageing into current ALS mouse models may be beneficial. This has already been shown in a SOD1[G93A] mouse model that was crossed onto a telomerase knockout model (Linkus et al., 2016). The results showed an earlier disease onset and an exacerbated phenotype, implicating telomerase dysfunction as an ALS risk factor. Telomeres have been observed to be shorter in ALS patients (De Felice et al., 2014). Furthermore, an overlap between the pathology of ageing and ALS was identified when TDP-43 aggregates were discovered in the cytoplasm of aged mice and SOD1[G93A] mice (Valdez et al., 2012). A model of DNA-repair deficient mice also resulted in age-dependent motor neurone degeneration and neuromuscular deficits (de Waard et al., 2010). DNA damage has been previously implicated in ALS (Martin, 2008) and this model further suggests it may be an age-related risk factor. In combination, these results highlight a link between ageing and ALS and suggests that combining models of ageing and models of ALS may aid recapitulation of the human disease.

In a similar vein, there is the possibility that from an evolutionary perspective, humans and mice are too different to allow faithful recapitulation of ALS. The corticospinal tract is the primary pathway for controlling voluntary movement (Eisen, 2009). In ALS, the 'dying forward' hypothesis supposes that disease originates in the corticomotoneurones, which make direct monosynaptic connections with the anterior horn cells (Baker, 2014). These direct connections are only present in humans and higher primates to allow movement of the digits (Maeda et al., 2016). Mice do not have these direct monosynaptic connections (Bray, 2017), and as ALS is a monosynaptic disease, it could explain why there is no known case of naturally occurring ALS in mice, and non-primate animals in general. This fundamental anatomical difference may make it especially challenging to accurately model ALS in mice and could mean that only non-human primate models would be able to fully recapitulate the human disease.

Lastly, different flanking regions and lengths of the human *C9ORF72* transgene were used in each model. Jiang et al. (2016) and Liu et al. (2016) used a truncated and full-length version, respectively, and both developed a phenotype, suggesting that the full-length gene may not be required for disease. This has been demonstrated in an AAV-mediated C9ALS/FTD model lacking *C9ORF72* gene flanking regions and under the control of an actin promoter that developed DPR, RNA foci, and TDP-43 pathology alongside neurodegeneration and motor and

cognitive deficits (Chew et al., 2015). However, the Peters et al. (2015) and O'Rourke et al. (2015) models also used a truncated and full-length version of the *C9ORF72* transgene, respectively, yet neither developed a phenotype. Therefore, other factors may be at play to account for these differences, and a comparison of these models may aid the identification of the necessary flanking regions and appropriate length of the *C9ORF72* gene required for disease. Additionally, creating genomically humanised mouse models of disease by replacing the mouse ortholog with the human sequence and keeping expression under the control of the mouse promoter may prove beneficial. While technically challenging, this has been done in *SOD1*, *TARDBP*, and *FUS* mouse models, and may represent a novel and more accurate method of human disease modelling in mice (Devoy et al., 2021).

7.3   Future Work

This study has several limitations which could be remedied by future work. These include pathological investigations into the presence of RNA foci and TDP-43 aggregates in neurones. Coupled with investigations comparing expression levels of the HRE to endogenous mouse *C9ORF72* expression, this could help build a broader picture of the molecular profile of this model for comparison with other studies and determine the relevant pathologies required for disease. Moreover, investigating the methylation status of the HRE could help elucidate the reason behind the variable DPR levels observed. Ageing the mice beyond 12 months may also reveal further insights.

Future studies backcrossing this model onto a less variable and less seizure prone genetic background such as C57BL/6 could prove informative and could aid identification of strain and gender effects or the presence of modifier genes and flanking regions of the human gene required for disease. Similarly, crossing the model onto a model of mouse ageing could expand our knowledge of the influence of age and its effect on C9ALS/FTD onset and progression.

7.4   Final Conclusions

Overall, this work has highlighted the difficulties surrounding reproducibility within preclinical studies and demonstrated that the generation of a robust C9ALS/FTD BAC model with a reliable phenotype has yet to be achieved. Both studies presented here do not recapitulate the acute phenotype previously reported in this model by Liu et al. (2016) and Nguyen et al. (2020a). However, the possible neuronal abnormalities observed in the motor cortex of the Janvier model may hint at a slower *C9ORF72* HRE-associated disease progression that may be modulated by background strain. Further work is needed to determine whether presence of the *C9ORF72* HRE is sufficient to cause disease in mice and whether other confounding factors such as genetics or environment may be influencing the development of the more severe phenotype initially reported.

8 Appendix
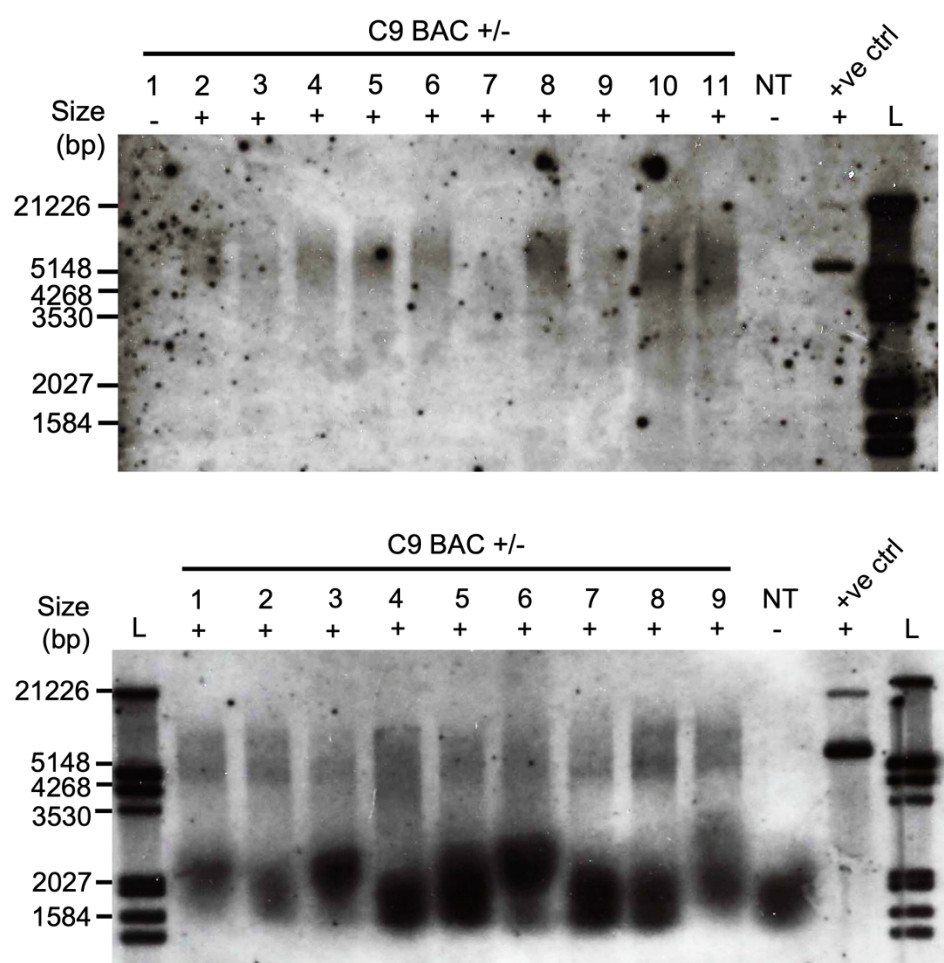
Fig. S 1: Confirmation of transgene with G4C2 repeat expansion in JAX C9orf72 mice.

Southern blots of JAX C9orf72 mice showing repeat expansion size. Repeat size varied from 650-950 repeats. L, DNA ladder; +, transgene present; -, transgene absent; NT, non-transgenic control; +ve ctrl, pcDNA3.1/G4C2x45-3xV5 plasmid with a size of 5,927 bp when linearised.
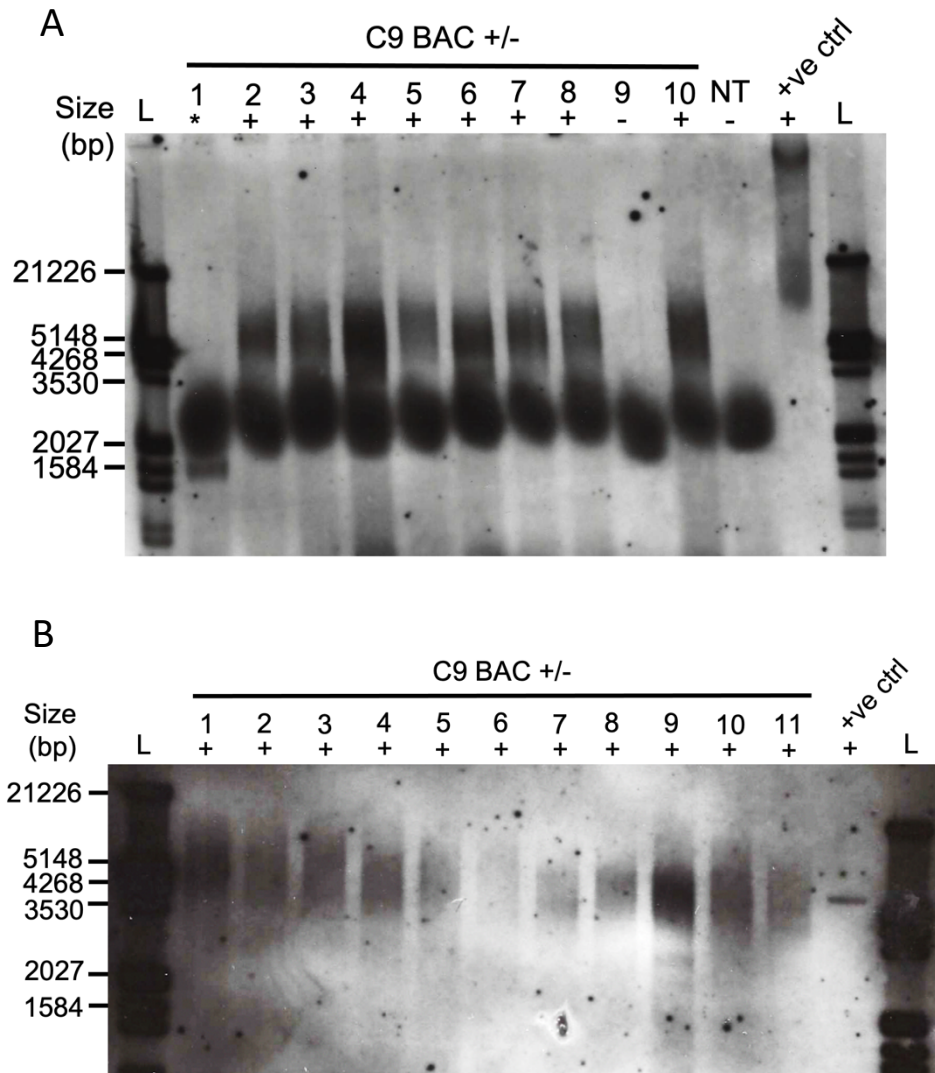
Fig. S 2: Confirmation of transgene with G4C2 repeat expansion in Janvier C9orf72 mice.

Southern blots of Janvier C9orf72 mice showing repeat expansion size. Repeat size varied from 650-950 repeats. L, DNA ladder; +, transgene present; -, transgene absent; *, truncation; NT, non-transgenic control; +ve ctrl, pcDNA3.1/G4C2x45-3xV5 plasmid with a size of 5,927 bp when linearised. (A) Lanes 9 and 10 are re-runs of two C9orf72 mice from the JAX colony.

9 References

Abada, Y. S., Nguyen, H. P., Schreiber, R. & Ellenbroek, B. (2013). Assessment of motor function, sensory motor gating and recognition memory in a novel BACHD transgenic rat model for huntington disease. *PLoS One.* **8**(7)**,** e68584.

Ajami, B., Samusik, N., Wieghofer, P., Ho, P. P., Crotti, A., Bjornson, Z., Prinz, M., Fantl, W. J., Nolan, G. P. & Steinman, L. (2018). Single-cell mass cytometry reveals distinct populations of brain myeloid cells in mouse neuroinflammation and neurodegeneration models. *Nat Neurosci.* **21**(4)**,** 541-551.

Alexander, A., Marfil, V. & Li, C. (2014). Use of Caenorhabditis elegans as a model to study Alzheimer's disease and other neurodegenerative diseases. *Frontiers in Genetics.* **5**.

Aoki, M., Kato, S., Nagai, M. & Itoyama, Y. (2005). Development of a rat model of amyotrophic lateral sclerosis expressing a human SOD1 transgene. *Neuropathology.* **25**(4)**,** 365-70.

Argyriou, A. A., Polychronopoulos, P., Talelli, P. & Chroni, E. (2006). F wave study in amyotrophic lateral sclerosis: assessment of balance between upper and lower motor neuron involvement. *Clin Neurophysiol.* **117**(6)**,** 1260-5.

Arnold, E. S., Ling, S. C., Huelga, S. C., Lagier-Tourenne, C., Polymenidou, M., Ditsworth, D., Kordasiewicz, H. B., McAlonis-Downes, M., Platoshyn, O., Parone, P. A., Da Cruz, S., Clutario, K. M., Swing, D., Tessarollo, L., Marsala, M., Shaw, C. E., Yeo, G. W. & Cleveland, D. W. (2013). ALS-linked TDP-43 mutations produce aberrant RNA splicing and adult-onset motor neuron disease without aggregation or loss of nuclear TDP-43. *Proc Natl Acad Sci U S A.* **110**(8)**,** E736-45.

Arshadi, C., Gunther, U., Eddison, M., Harrington, K. I. S. & Ferreira, T. A. (2021). SNT: a unifying toolbox for quantification of neuronal anatomy. *Nat Methods.* **18**(4)**,** 374-377.

Arthur, K. C., Calvo, A., Price, T. R., Geiger, J. T., Chio, A. & Traynor, B. J. (2016). Projected increase in amyotrophic lateral sclerosis from 2015 to 2040. *Nat Commun.* **7**12408.

Ash, P. E., Bieniek, K. F., Gendron, T. F., Caulfield, T., Lin, W. L., Dejesus-Hernandez, M., van Blitterswijk, M. M., Jansen-West, K., Paul, J. W., 3rd, Rademakers, R., Boylan, K. B., Dickson, D. W. & Petrucelli, L. (2013). Unconventional translation of C9ORF72 GGGGCC expansion generates insoluble polypeptides specific to c9FTD/ALS. *Neuron.* **77**(4)**,** 639-46.

Atanasio, A., et al. (2016). C9orf72 ablation causes immune dysregulation characterized by leukocyte expansion, autoantibody production, and glomerulonephropathy in mice. *Sci Rep.* **6**23204.

Azzouz, M., Leclerc, N., Gurney, M., Warter, J. M., Poindron, P. & Borg, J. (1997). Progressive motor neuron impairment in an animal model of familial amyotrophic lateral sclerosis. *Muscle Nerve.* **20**(1)**,** 45-51.

Babin, P. J., Goizet, C. & Raldua, D. (2014). Zebrafish models of human motor neuron diseases: advantages and limitations. *Prog Neurobiol.* **118**36-58.

Bailoo, J. D., Murphy, E., Boada-Sana, M., Varholick, J. A., Hintze, S., Baussiere, C., Hahn, K. C., Gopfert, C., Palme, R., Voelkl, B. & Wurbel, H. (2018). Effects of Cage Enrichment on Behavior, Welfare and Outcome Variability in Female Mice. *Front Behav Neurosci.* **12**232.

Baker, M. R. (2014). ALS--dying forward, backward or outward? *Nat Rev Neurol.* **10**(11)**,** 660.

Bandres-Ciga, S., Noyce, A. J., Hemani, G., Nicolas, A., Calvo, A., Mora, G., Consortium, I., International, A. L. S. G. C., Tienari, P. J., Stone, D. J., Nalls, M. A., Singleton, A. B., Chio,

A. & Traynor, B. J. (2019). Shared polygenic risk and causal inferences in amyotrophic lateral sclerosis. *Ann Neurol.* **85**(4)**,** 470-481.

Barber, S. C. & Shaw, P. J. (2010). Oxidative stress in ALS: key role in motor neuron injury and therapeutic target. *Free Radic Biol Med.* **48**(5)**,** 629-41.

Beck, J., Lloyd, S., Hafezparast, M., Lennon-Pierce, M., Eppig, J., Festing, M. & Fisher, E. (2000). Genealogies of mouse inbred strains. *Nature Genetics.* **24**23-25.

Benoit, E. & Escande, D. (1991). Riluzole specifically blocks inactivated Na channels in myelinated nerve fibre. *Pflugers Arch.* **419**(6)**,** 603-9.

Bensimon, G., Lacomblez, L. & Meininger, V. (1994). A controlled trial of riluzole in amyotrophic lateral sclerosis. ALS/Riluzole Study Group. *N Engl J Med.* **330**(9)**,** 585-91.

Blacher, E., et al. (2019). Potential roles of gut microbiome and metabolites in modulating ALS in mice. *Nature.* **572**(7770)**,** 474-480.

Blizard, D. A., Takahashi, A., Galsworthy, M. J., Martin, B. & Koide, T. (2007). Test standardization in behavioural neuroscience: a response to Stanford. *J Psychopharmacol.* **21**(2)**,** 136-9.

Boivin, M., Pfister, V., Gaucherot, A., Ruffenach, F., Negroni, L., Sellier, C. & Charlet-Berguerand, N. (2020). Reduced autophagy upon C9ORF72 loss synergizes with dipeptide repeat protein toxicity in G4C2 repeat expansion disorders. *EMBO J.* **39**(4)**,** e100574.

Bothe, G. W., Bolivar, V. J., Vedder, M. J. & Geistfeld, J. G. (2004). Genetic and behavioral differences among five inbred mouse strains commonly used in the production of transgenic and knockout mice. *Genes Brain Behav.* **3**(3)**,** 149-57.

Bouwknecht, J. A., Spiga, F., Staub, D. R., Hale, M. W., Shekhar, A. & Lowry, C. A. (2007). Differential effects of exposure to low-light or high-light open-field on anxiety-related behaviors: relationship to c-Fos expression in serotonergic and non-serotonergic neurons in the dorsal raphe nucleus. *Brain Res Bull.* **72**(1)**,** 32-43.

Bozzo, F., Mirra, A. & Carri, M. T. (2017). Oxidative stress and mitochondrial damage in the pathogenesis of ALS: New perspectives. *Neurosci Lett.* **636**3-8.

Bray, N. (2017). Motor systems: Mice get manual. *Nat Rev Neurosci.* **18**(9)**,** 512.

Brooks, B. R., Berry, J. D., Ciepielewska, M., Liu, Y., Zambrano, G. S., Zhang, J. & Hagan, M. (2022). Intravenous edaravone treatment in ALS and survival: An exploratory, retrospective, administrative claims analysis. *EClinicalMedicine.* **52**101590.

Brooks, B. R., Miller, R. G., Swash, M., Munsat, T. L. & World Federation of Neurology Research Group on Motor Neuron, D. (2000). El Escorial revisited: revised criteria for the diagnosis of amyotrophic lateral sclerosis. *Amyotroph Lateral Scler Other Motor Neuron Disord.* **1**(5)**,** 293-9.

Brown, A. L., et al. (2022). TDP-43 loss and ALS-risk SNPs drive mis-splicing and depletion of UNC13A. *Nature.* **603**(7899)**,** 131-137.

Brown, R. E. & Wong, A. A. (2007). The influence of visual ability on learning and memory performance in 13 strains of mice. *Learn Mem.* **14**(3)**,** 134-44.

Bryda, E. C. (2013). The Mighty Mouse: the impact of rodents on advances in biomedical research. *Mo Med.* **110**(3)**,** 207-11.

Buratti, E. & Baralle, F. E. (2012). TDP-43: gumming up neurons through protein-protein and protein-RNA interactions. *Trends Biochem Sci.* **37**(6)**,** 237-47.

Burberry, A., Suzuki, N., Wang, J. Y., Moccia, R., Mordes, D. A., Stewart, M. H., Suzuki-Uematsu, S., Ghosh, S., Singh, A., Merkle, F. T., Koszka, K., Li, Q. Z., Zon, L., Rossi, D. J., Trowbridge, J. J., Notarangelo, L. D. & Eggan, K. (2016). Loss-of-function mutations in

the C9ORF72 mouse ortholog cause fatal autoimmune disease. *Sci Transl Med.* **8**(347)**,** 347ra93.

Burberry, A., Wells, M. F., Limone, F., Couto, A., Smith, K. S., Keaney, J., Gillet, G., van Gastel, N., Wang, J. Y., Pietilainen, O., Qian, M., Eggan, P., Cantrell, C., Mok, J., Kadiu, I., Scadden, D. T. & Eggan, K. (2020). C9orf72 suppresses systemic and neural inflammation induced by gut bacteria. *Nature.* **582**(7810)**,** 89-94.

Burrell, J. R., Kiernan, M. C., Vucic, S. & Hodges, J. R. (2011). Motor neuron dysfunction in frontotemporal dementia. *Brain.* **134**(Pt 9)**,** 2582-94.

Byers, S. L., Wiles, M. V., Dunn, S. L. & Taft, R. A. (2012). Mouse estrous cycle identification tool and images. *PLoS One.* **7**(4)**,** e35538.

Cao, S., Fisher, D. W., Rodriguez, G., Yu, T. & Dong, H. (2021). Comparisons of neuroinflammation, microglial activation, and degeneration of the locus coeruleus-norepinephrine system in APP/PS1 and aging mice. *J Neuroinflammation.* **18**(1)**,** 10.

Carlson, G. (2011). The use of four limb hanging tests to monitor muscle strength and condition over time. *TREAT-NMD.* DMD_M.2.1.005.

Castelli, L. M., et al. (2023). A cell-penetrant peptide blocking C9ORF72-repeat RNA nuclear export reduces the neurotoxic effects of dipeptide repeat proteins. *Sci Transl Med.* **15**(685)**,** eabo3823.

Chakraborty, R., Vepuri, V., Mhatre, S. D., Paddock, B. E., Miller, S., Michelson, S. J., Delvadia, R., Desai, A., Vinokur, M., Melicharek, D. J., Utreja, S., Khandelwal, P., Ansaloni, S., Goldstein, L. E., Moir, R. D., Lee, J. C., Tabb, L. P., Saunders, A. J. & Marenda, D. R. (2011). Characterization of a Drosophila Alzheimer's disease model: pharmacological rescue of cognitive defects. *PLoS One.* **6**(6)**,** e20799.

Chang, Y. J., Jeng, U. S., Chiang, Y. L., Hwang, I. S. & Chen, Y. R. (2016). The Glycine-Alanine Dipeptide Repeat from C9orf72 Hexanucleotide Expansions Forms Toxic Amyloids Possessing Cell-to-Cell Transmission Properties. *J Biol Chem.* **291**(10)**,** 4903-11.

Chebib, J., Jackson, B. C., Lopez-Cortegano, E., Tautz, D. & Keightley, P. D. (2021). Inbred lab mice are not isogenic: genetic variation within inbred strains used to infer the mutation rate per nucleotide site. *Heredity (Edinb).* **126**(1)**,** 107-116.

Chew, J., Cook, C., Gendron, T. F., Jansen-West, K., Del Rosso, G., Daughrity, L. M., Castanedes-Casey, M., Kurti, A., Stankowski, J. N., Disney, M. D., Rothstein, J. D., Dickson, D. W., Fryer, J. D., Zhang, Y. J. & Petrucelli, L. (2019). Aberrant deposition of stress granule-resident proteins linked to C9orf72-associated TDP-43 proteinopathy. *Mol Neurodegener.* **14**(1)**,** 9.

Chew, J., et al. (2015). C9ORF72 repeat expansions in mice cause TDP-43 pathology, neuronal loss, and behavioral deficits. *Science.* **348**(6239)**,** 1151-4.

Chiang, M. C., Huang, A. J. Y., Wintzer, M. E., Ohshima, T. & McHugh, T. J. (2018). A role for CA3 in social recognition memory. *Behav Brain Res.* **354**22-30.

Chiang, P. M., Ling, J., Jeong, Y. H., Price, D. L., Aja, S. M. & Wong, P. C. (2010). Deletion of TDP-43 down-regulates Tbc1d1, a gene linked to obesity, and alters body fat metabolism. *Proc Natl Acad Sci U S A.* **107**(37)**,** 16320-4.

Chio, A., Calvo, A., Mazzini, L., Cantello, R., Mora, G., Moglia, C., Corrado, L., D'Alfonso, S., Majounie, E., Renton, A., Pisano, F., Ossola, I., Brunetti, M., Traynor, B. J., Restagno, G. & Parals (2012). Extensive genetics of ALS: a population-based study in Italy. *Neurology.* **79**(19)**,** 1983-9.

Chio, A., Calvo, A., Moglia, C., Restagno, G., Ossola, I., Brunetti, M., Montuschi, A., Cistaro, A., Ticca, A., Traynor, B. J., Schymick, J. C., Mutani, R., Marrosu, M. G., Murru, M. R. &

Borghero, G. (2010). Amyotrophic lateral sclerosis-frontotemporal lobar dementia in 3 families with p.Ala382Thr TARDBP mutations. *Arch Neurol.* **67**(8)**,** 1002-9.

Chio, A., et al. (2018). The multistep hypothesis of ALS revisited: The role of genetic mutations. *Neurology.* **91**(7)**,** e635-e642.

Chiu, I. M., Chen, A., Zheng, Y., Kosaras, B., Tsiftsoglou, S. A., Vartanian, T. K., Brown, R. H., Jr. & Carroll, M. C. (2008). T lymphocytes potentiate endogenous neuroprotective inflammation in a mouse model of ALS. *Proc Natl Acad Sci U S A.* **105**(46)**,** 17913-8.

Choi, S. Y., Lopez-Gonzalez, R., Krishnan, G., Phillips, H. L., Li, A. N., Seeley, W. W., Yao, W. D., Almeida, S. & Gao, F. B. (2019). C9ORF72-ALS/FTD-associated poly(GR) binds Atp5a1 and compromises mitochondrial function in vivo. *Nat Neurosci.* **22**(6)**,** 851-862.

Chou, C. C., et al. (2018). TDP-43 pathology disrupts nuclear pore complexes and nucleocytoplasmic transport in ALS/FTD. *Nat Neurosci.* **21**(2)**,** 228-239.

Cirulli, E. T., et al. (2015). Exome sequencing in amyotrophic lateral sclerosis identifies risk genes and pathways. *Science.* **347**(6229)**,** 1436-41.

Ciura, S., Lattante, S., Le Ber, I., Latouche, M., Tostivint, H., Brice, A. & Kabashi, E. (2013). Loss of function of C9orf72 causes motor deficits in a zebrafish model of amyotrophic lateral sclerosis. *Ann Neurol.* **74**(2)**,** 180-7.

Cividini, C., Basaia, S., Spinelli, E. G., Canu, E., Castelnovo, V., Riva, N., Cecchetti, G., Caso, F., Magnani, G., Falini, A., Filippi, M. & Agosta, F. (2021). Amyotrophic Lateral Sclerosis-Frontotemporal Dementia: Shared and Divergent Neural Correlates Across the Clinical Spectrum. *Neurology.* **98**(4)**,** e402-15.

Clarke, B. E. & Patani, R. (2020). The microglial component of amyotrophic lateral sclerosis. *Brain.* **143**(12)**,** 3526-3539.

Cook, C. N., et al. (2020). C9orf72 poly(GR) aggregation induces TDP-43 proteinopathy. *Sci Transl Med.* **12**(559).

Cooper-Knock, J., et al. (2012). Clinico-pathological features in amyotrophic lateral sclerosis with expansions in C9ORF72. *Brain.* **135**(Pt 3)**,** 751-64.

Cykowski, M. D., Dickson, D. W., Powell, S. Z., Arumanayagam, A. S., Rivera, A. L. & Appel, S. H. (2019). Dipeptide repeat (DPR) pathology in the skeletal muscle of ALS patients with C9ORF72 repeat expansion. *Acta Neuropathol.* **138**(4)**,** 667-670.

De Bono, J. P., Adlam, D., Paterson, D. J. & Channon, K. M. (2006). Novel quantitative phenotypes of exercise training in mouse models. *Am J Physiol Regul Integr Comp Physiol.* **290**(4)**,** R926-34.

de Carvalho, M., Dengler, R., Eisen, A., England, J. D., Kaji, R., Kimura, J., Mills, K., Mitsumoto, H., Nodera, H., Shefner, J. & Swash, M. (2008). Electrodiagnostic criteria for diagnosis of ALS. *Clin Neurophysiol.* **119**(3)**,** 497-503.

De Felice, B., Annunziata, A., Fiorentino, G., Manfellotto, F., D'Alessandro, R., Marino, R., Borra, M. & Biffali, E. (2014). Telomerase expression in amyotrophic lateral sclerosis (ALS) patients. *J Hum Genet.* **59**(10)**,** 555-61.

De Schaepdryver, M., Goossens, J., De Meyer, S., Jeromin, A., Masrori, P., Brix, B., Claeys, K. G., Schaeverbeke, J., Adamczuk, K., Vandenberghe, R., Van Damme, P. & Poesen, K. (2019). Serum neurofilament heavy chains as early marker of motor neuron degeneration. *Ann Clin Transl Neurol.* **6**(10)**,** 1971-1979.

de Waard, M. C., van der Pluijm, I., Zuiderveen Borgesius, N., Comley, L. H., Haasdijk, E. D., Rijksen, Y., Ridwan, Y., Zondag, G., Hoeijmakers, J. H., Elgersma, Y., Gillingwater, T. H. & Jaarsma, D. (2010). Age-related motor neuron degeneration in DNA repair-deficient Ercc1 mice. *Acta Neuropathol.* **120**(4)**,** 461-75.

Deacon, R. (2012). Assessing burrowing, nest construction, and hoarding in mice. *J Vis Exp.* 10.3791/2607(59)**,** e2607.

Deacon, R. M. (2006). Digging and marble burying in mice: simple methods for in vivo identification of biological impacts. *Nat Protoc.* **1**(1)**,** 122-4.

Deacon, R. M., Raley, J. M., Perry, V. H. & Rawlins, J. N. (2001). Burrowing into prion disease. *Neuroreport.* **12**(9)**,** 2053-7.

Deacon, R. M. & Rawlins, J. N. (2005). Hippocampal lesions, species-typical behaviours and anxiety in mice. *Behav Brain Res.* **156**(2)**,** 241-9.

DeJesus-Hernandez, M., et al. (2011). Expanded GGGGCC hexanucleotide repeat in noncoding region of C9ORF72 causes chromosome 9p-linked FTD and ALS. *Neuron.* **72**(2)**,** 245-56.

Deng, H. X., Hentati, A., Tainer, J. A., Iqbal, Z., Cayabyab, A., Hung, W. Y., Getzoff, E. D., Hu, P., Herzfeldt, B., Roos, R. P. & et al. (1993). Amyotrophic lateral sclerosis and structural defects in Cu,Zn superoxide dismutase. *Science.* **261**(5124)**,** 1047-51.

Devoy, A., et al. (2021). Generation and analysis of innovative genomically humanized knockin SOD1, TARDBP (TDP-43), and FUS mouse models. *iScience.* **24**(12)**,** 103463.

Dong, W., Ma, Y., Guan, F., Zhang, X., Chen, W., Zhang, L. & Zhang, L. (2021). Ablation of C9orf72 together with excitotoxicity induces ALS in rats. *FEBS J.* **288**(5)**,** 1712-1723.

Dong, W., Zhang, L., Sun, C., Gao, X., Guan, F., Li, J., Chen, W., Ma, Y. & Zhang, L. (2020). Knock in of a hexanucleotide repeat expansion in the C9orf72 gene induces ALS in rats. *Animal Model Exp Med.* **3**(3)**,** 237-244.

Eisen, A. (2009). Amyotrophic lateral sclerosis-Evolutionary and other perspectives. *Muscle Nerve.* **40**(2)**,** 297-304.

Eisen, A., Pant, B. & Stewart, H. (1993). Cortical excitability in amyotrophic lateral sclerosis: a clue to pathogenesis. *Can J Neurol Sci.* **20**(1)**,** 11-6.

Elston, T. W., Pandian, A., Smith, G. D., Holley, A. J., Gao, N. & Lugo, J. N. (2014). Aniracetam does not alter cognitive and affective behavior in adult C57BL/6J mice. *PLoS One.* **9**(8)**,** e104443.

Eltokhi, A., Kurpiers, B. & Pitzer, C. (2020). Behavioral tests assessing neuropsychiatric phenotypes in adolescent mice reveal strain- and sex-specific effects. *Sci Rep.* **10**(1)**,** 11263.

Esanov, R., Cabrera, G. T., Andrade, N. S., Gendron, T. F., Brown, R. H., Jr., Benatar, M., Wahlestedt, C., Mueller, C. & Zeier, Z. (2017). A C9ORF72 BAC mouse model recapitulates key epigenetic perturbations of ALS/FTD. *Mol Neurodegener.* **12**(1)**,** 46.

Farg, M. A., Sundaramoorthy, V., Sultana, J. M., Yang, S., Atkinson, R. A., Levina, V., Halloran, M. A., Gleeson, P. A., Blair, I. P., Soo, K. Y., King, A. E. & Atkin, J. D. (2014). C9ORF72, implicated in amytrophic lateral sclerosis and frontotemporal dementia, regulates endosomal trafficking. *Hum Mol Genet.* **23**(13)**,** 3579-95.

Farley, S. J., McKay, B. M., Disterhoft, J. F. & Weiss, C. (2011). Reevaluating hippocampus-dependent learning in FVB/N mice. *Behav Neurosci.* **125**(6)**,** 871-8.

Feigin, V. L., et al. (2021). Burden of Neurological Disorders Across the US From 1990-2017: A Global Burden of Disease Study. *JAMA Neurol.* **78**(2)**,** 165-176.

Feldman, E. L., Goutman, S. A., Petri, S., Mazzini, L., Savelieff, M. G., Shaw, P. J. & Sobue, G. (2022). Amyotrophic lateral sclerosis. *Lancet.* **400**(10360)**,** 1363-1380.

Ferraiuolo, L., Kirby, J., Grierson, A. J., Sendtner, M. & Shaw, P. J. (2011). Molecular pathways of motor neuron injury in amyotrophic lateral sclerosis. *Nat Rev Neurol.* **7**(11)**,** 616-30.

Festing, M. F. (1999). Warning: the use of heterogeneous mice may seriously damage your research. *Neurobiol Aging.* **20**(2)**,** 237-44; discussion 245-6.

Fisher, E. M. C. & Bannerman, D. M. (2019). Mouse models of neurodegeneration: Know your question, know your mouse. *Sci Transl Med.* **11**(493).

Fisher, M. A. (2007). F-waves--physiology and clinical uses. *ScientificWorldJournal.* **7**144-60.

Fogarty, M. J., Klenowski, P. M., Lee, J. D., Drieberg-Thompson, J. R., Bartlett, S. E., Ngo, S. T., Hilliard, M. A., Bellingham, M. C. & Noakes, P. G. (2016). Cortical synaptic and dendritic spine abnormalities in a presymptomatic TDP-43 model of amyotrophic lateral sclerosis. *Sci Rep.* **6**37968.

Fogarty, M. J., Noakes, P. G. & Bellingham, M. C. (2015). Motor cortex layer V pyramidal neurons exhibit dendritic regression, spine loss, and increased synaptic excitation in the presymptomatic hSOD1(G93A) mouse model of amyotrophic lateral sclerosis. *J Neurosci.* **35**(2)**,** 643-7.

Freibaum, B. D., Lu, Y., Lopez-Gonzalez, R., Kim, N. C., Almeida, S., Lee, K. H., Badders, N., Valentine, M., Miller, B. L., Wong, P. C., Petrucelli, L., Kim, H. J., Gao, F. B. & Taylor, J. P. (2015). GGGGCC repeat expansion in C9orf72 compromises nucleocytoplasmic transport. *Nature.* **525**(7567)**,** 129-33.

Gijselinck, I., et al. (2016). The C9orf72 repeat size correlates with onset age of disease, DNA methylation and transcriptional downregulation of the promoter. *Mol Psychiatry.* **21**(8)**,** 1112-24.

Girard, S. D., Escoffier, G., Khrestchatisky, M. & Roman, F. S. (2016). The FVB/N mice: A well suited strain to study learning and memory processes using olfactory cues. *Behav Brain Res.* **296**254-259.

Goelz, M. F., Mahler, J., Harry, J., Myers, P., Clark, J., Thigpen, J. E. & Forsythe, D. B. (1998). Neuropathologic findings associated with seizures in FVB mice. *Lab Anim Sci.* **48**(1)**,** 34-7.

Goodwin, L. O., Splinter, E., Davis, T. L., Urban, R., He, H., Braun, R. E., Chesler, E. J., Kumar, V., van Min, M., Ndukum, J., Philip, V. M., Reinholdt, L. G., Svenson, K., White, J. K., Sasner, M., Lutz, C. & Murray, S. A. (2019). Large-scale discovery of mouse transgenic integration sites reveals frequent structural variation and insertional mutagenesis. *Genome Res.* **29**(3)**,** 494-505.

Gould, T. D., Dao, D. T. & Kovacsics, C. E. 2009. *The Open Field Test*, Springer Protocols.

Guyenet, S. J., Furrer, S. A., Damian, V. M., Baughan, T. D., La Spada, A. R. & Garden, G. A. (2010). A simple composite phenotype scoring system for evaluating mouse models of cerebellar ataxia. *J Vis Exp.* 10.3791/1787(39).

Hall, C. & Ballachey, E. L. (1932). A study of the rat's behavior in a field. A contribution to method in comparative psychology. *University of California Publications in Psychology.* **6**1-12.

Hall, E. D., Oostveen, J. A. & Gurney, M. E. (1998). Relationship of microglial and astrocytic activation to disease onset and progression in a transgenic model of familial ALS. *Glia.* **23**(3)**,** 249-56.

Hamilton, S. M., Spencer, C. M., Harrison, W. R., Yuva-Paylor, L. A., Graham, D. F., Daza, R. A., Hevner, R. F., Overbeek, P. A. & Paylor, R. (2011). Multiple autism-like behaviors in a novel transgenic mouse model. *Behav Brain Res.* **218**(1)**,** 29-41.

Hammer, R. P., Jr., Tomiyasu, U. & Scheibel, A. B. (1979). Degeneration of the human Betz cell due to amyotrophic lateral sclerosis. *Exp Neurol.* **63**(2)**,** 336-46.

Hardiman, O., Al-Chalabi, A., Chio, A., Corr, E. M., Logroscino, G., Robberecht, W., Shaw, P. J., Simmons, Z. & van den Berg, L. H. (2017). Amyotrophic lateral sclerosis. *Nat Rev Dis Primers.* **3** 17071.

Harwood, C. A., McDermott, C. J. & Shaw, P. J. (2009). Physical activity as an exogenous risk factor in motor neuron disease (MND): a review of the evidence. *Amyotroph Lateral Scler.* **10**(4)**,** 191-204.

Hattiangady, B. & Shetty, A. K. (2008). Implications of decreased hippocampal neurogenesis in chronic temporal lobe epilepsy. *Epilepsia.* **49 Suppl 5**(0 5)**,** 26-41.

Hausmann, O. N. (2003). Post-traumatic inflammation following spinal cord injury. *Spinal Cord.* **41**(7)**,** 369-78.

Heiman-Patterson, T. D., Sher, R. B., Blankenhorn, E. A., Alexander, G., Deitch, J. S., Kunst, C. B., Maragakis, N. & Cox, G. (2011). Effect of genetic background on phenotype variability in transgenic mouse models of amyotrophic lateral sclerosis: a window of opportunity in the search for genetic modifiers. *Amyotroph Lateral Scler.* **12**(2)**,** 79-86.

Hennemann (2007). Space cadet syndrome of female FVB/N mice.

Herranz-Martin, S., Chandran, J., Lewis, K., Mulcahy, P., Higginbottom, A., Walker, C., Valenzuela, I. M. Y., Jones, R. A., Coldicott, I., Iannitti, T., Akaaboune, M., El-Khamisy, S. F., Gillingwater, T. H., Shaw, P. J. & Azzouz, M. (2017). Viral delivery of C9orf72 hexanucleotide repeat expansions in mice leads to repeat-length-dependent neuropathology and behavioural deficits. *Dis Model Mech.* **10**(7)**,** 859-868.

Hobson, E. V., Harwood, C. A., MCDermott, C. J. & Shaw, P. J. (2016). Clinical aspects of motor neurone disease. *Medicine.* **44**(9)**,** 552-556.

Hoppitt, T., Pall, H., Calvert, M., Gill, P., Yao, G., Ramsay, J., James, G., Conduit, J. & Sackley, C. (2011). A systematic review of the incidence and prevalence of long-term neurological conditions in the UK. *Neuroepidemiology.* **36**(1)**,** 19-28.

Hsiao, K. K., Borchelt, D. R., Olson, K., Johannsdottir, R., Kitt, C., Yunis, W., Xu, S., Eckman, C., Younkin, S., Price, D. & et al. (1995). Age-related CNS disorder and early death in transgenic FVB/N mice overexpressing Alzheimer amyloid precursor proteins. *Neuron.* **15**(5)**,** 1203-18.

Iacoangeli, A., Al Khleifat, A., Jones, A. R., Sproviero, W., Shatunov, A., Opie-Martin, S., Alzheimer's Disease Neuroimaging, I., Morrison, K. E., Shaw, P. J., Shaw, C. E., Fogh, I., Dobson, R. J., Newhouse, S. J. & Al-Chalabi, A. (2019). C9orf72 intermediate expansions of 24-30 repeats are associated with ALS. *Acta Neuropathol Commun.* **7**(1)**,** 115.

Ibrahem, A. K., Al-Mahdawi, A. M. & Hamdan, F. B. (2021). Motor unit number estimation versus compound muscle action potential in the evaluation of motor unit loss in amyotrophic lateral sclerosis. *The Egyptian Journal of Neurology, Psychiatry and Neurosurgery.* **57**.

Iguchi, Y., Katsuno, M., Niwa, J., Takagi, S., Ishigaki, S., Ikenaka, K., Kawai, K., Watanabe, H., Yamanaka, K., Takahashi, R., Misawa, H., Sasaki, S., Tanaka, F. & Sobue, G. (2013). Loss of TDP-43 causes age-dependent progressive motor neuron degeneration. *Brain.* **136**(Pt 5)**,** 1371-82.

Ikeda, M., Brown, J., Holland, A. J., Fukuhara, R. & Hodges, J. R. (2002). Changes in appetite, food preference, and eating habits in frontotemporal dementia and Alzheimer's disease. *J Neurol Neurosurg Psychiatry.* **73**(4)**,** 371-6.

Iwanami, T., Sonoo, M., Hatanaka, Y., Hokkoku, K., Oishi, C. & Shimizu, T. (2011). Decremental responses to repetitive nerve stimulation (RNS) in motor neuron disease. *Clin Neurophysiol.* **122**(12)**,** 2530-6.

Iyer, S., Acharya, K. R. & Subramanian, V. (2018). A comparative bioinformatic analysis of C9orf72. *PeerJ.* **6**e4391.

Jackson, J. L., Finch, N. A., Baker, M. C., Kachergus, J. M., DeJesus-Hernandez, M., Pereira, K., Christopher, E., Prudencio, M., Heckman, M. G., Thompson, E. A., Dickson, D. W., Shah, J., Oskarsson, B., Petrucelli, L., Rademakers, R. & van Blitterswijk, M. (2020). Elevated methylation levels, reduced expression levels, and frequent contractions in a clinical cohort of C9orf72 expansion carriers. *Mol Neurodegener.* **15**(1)**,** 7.

Jacobs, S. A., Huang, F., Tsien, J. Z. & Wei, W. (2016). Social Recognition Test in Rodents. *bio-protocol.*

Jara, J. H., Villa, S. R., Khan, N. A., Bohn, M. C. & Ozdinler, P. H. (2012). AAV2 mediated retrograde transduction of corticospinal motor neurons reveals initial and selective apical dendrite degeneration in ALS. *Neurobiol Dis.* **47**(2)**,** 174-83.

Jiang, J., et al. (2016). Gain of Toxicity from ALS/FTD-Linked Repeat Expansions in C9ORF72 Is Alleviated by Antisense Oligonucleotides Targeting GGGGCC-Containing RNAs. *Neuron.* **90**(3)**,** 535-50.

Kabiljo, R., Iacoangeli, A., Al-Chalabi, A. & Rosenzweig, I. (2022). Amyotrophic lateral sclerosis and cerebellum. *Sci Rep.* **12**(1)**,** 12586.

Kaur, S. J., McKeown, S. R. & Rashid, S. (2016). Mutant SOD1 mediated pathogenesis of Amyotrophic Lateral Sclerosis. *Gene.* **577**(2)**,** 109-18.

Kiernan, M. C., Vucic, S., Cheah, B. C., Turner, M. R., Eisen, A., Hardiman, O., Burrell, J. R. & Zoing, M. C. (2011). Amyotrophic lateral sclerosis. *The Lancet.* **377**(9769)**,** 942-955.

Kim, S., Lee, S., Ryu, S., Suk, J. & Park, C. (2002). Comparative analysis of the anxiety-related behaviors in four inbred mice. *Behav Processes.* **60**(2)**,** 181-190.

Klein, S. M., Vykoukal, J., Lechler, P., Zeitler, K., Gehmert, S., Schreml, S., Alt, E., Bogdahn, U. & Prantl, L. (2012). Noninvasive in vivo assessment of muscle impairment in the mdx mouse model--a comparison of two common wire hanging methods with two different results. *J Neurosci Methods.* **203**(2)**,** 292-7.

Kogan, J. H., Frankland, P. W. & Silva, A. J. (2000). Long-term memory underlying hippocampus-dependent social recognition in mice. *Hippocampus.* **10**(1)**,** 47-56.

Kohnken, R. A. & Schwahn, D. J. (2016). Lack of Chronic Histologic Lesions Supportive of Sublethal Spontaneous Seizures in FVB/N Mice. *Comp Med.* **66**(2)**,** 105-11.

Koppers, M., Blokhuis, A. M., Westeneng, H. J., Terpstra, M. L., Zundel, C. A., Vieira de Sa, R., Schellevis, R. D., Waite, A. J., Blake, D. J., Veldink, J. H., van den Berg, L. H. & Pasterkamp, R. J. (2015). C9orf72 ablation in mice does not cause motor neuron degeneration or motor deficits. *Ann Neurol.* **78**(3)**,** 426-38.

LaClair, K. D., Zhou, Q., Michaelsen, M., Wefers, B., Brill, M. S., Janjic, A., Rathkolb, B., Farny, D., Cygan, M., de Angelis, M. H., Wurst, W., Neumann, M., Enard, W., Misgeld, T., Arzberger, T. & Edbauer, D. (2020). Congenic expression of poly-GA but not poly-PR in mice triggers selective neuron loss and interferon responses found in C9orf72 ALS. *Acta Neuropathol.* **140**(2)**,** 121-142.

Lathe, R. (2004). The individuality of mice. *Genes Brain Behav.* **3**(6)**,** 317-27.

Leduc, R. Y., Rauw, G., Baker, G. B. & McDermid, H. E. (2017). What Goes Around Can Come Around: An Unexpected Deleterious Effect of Using Mouse Running Wheels for Environmental Enrichment. *J Am Assoc Lab Anim Sci.* **56**(2)**,** 194-201.

Lee, Y. B., Baskaran, P., Gomez-Deza, J., Chen, H. J., Nishimura, A. L., Smith, B. N., Troakes, C., Adachi, Y., Stepto, A., Petrucelli, L., Gallo, J. M., Hirth, F., Rogelj, B., Guthrie, S. & Shaw, C. E. (2017). C9orf72 poly GA RAN-translated protein plays a key role in amyotrophic lateral sclerosis via aggregation and toxicity. *Hum Mol Genet.* **26**(24)**,** 4765-4777.

Lee, Y. B., et al. (2013). Hexanucleotide repeats in ALS/FTD form length-dependent RNA foci, sequester RNA binding proteins, and are neurotoxic. *Cell Rep.* **5**(5)**,** 1178-86.

Lerman, I., Harrison, B. C., Freeman, K., Hewett, T. E., Allen, D. L., Robbins, J. & Leinwand, L. A. (2002). Genetic variability in forced and voluntary endurance exercise performance in seven inbred mouse strains. *J Appl Physiol (1985).* **92**(6)**,** 2245-55.

Levine, T. P., Daniels, R. D., Gatta, A. T., Wong, L. H. & Hayes, M. J. (2013). The product of C9orf72, a gene strongly implicated in neurodegeneration, is structurally related to DENN Rab-GEFs. *Bioinformatics.* **29**(4)**,** 499-503.

Ling, S. C., Polymenidou, M. & Cleveland, D. W. (2013). Converging mechanisms in ALS and FTD: disrupted RNA and protein homeostasis. *Neuron.* **79**(3)**,** 416-38.

Linkus, B., Wiesner, D., Messner, M., Karabatsiakis, A., Scheffold, A., Rudolph, K. L., Thal, D. R., Weishaupt, J. H., Ludolph, A. C. & Danzer, K. M. (2016). Telomere shortening leads to earlier age of onset in ALS mice. *Aging (Albany NY).* **8**(2)**,** 382-93.

Liu, Y., Pattamatta, A., Zu, T., Reid, T., Bardhi, O., Borchelt, D. R., Yachnis, A. T. & Ranum, L. P. (2016). C9orf72 BAC Mouse Model with Motor Deficits and Neurodegenerative Features of ALS/FTD. *Neuron.* **90**(3)**,** 521-34.

Longinetti, E. & Fang, F. (2019). Epidemiology of amyotrophic lateral sclerosis: an update of recent literature. *Curr Opin Neurol.* **32**(5)**,** 771-776.

Loos, M., Koopmans, B., Aarts, E., Maroteaux, G., van der Sluis, S., Neuro, B. M. P. C., Verhage, M. & Smit, A. B. (2015). Within-strain variation in behavior differs consistently between common inbred strains of mice. *Mamm Genome.* **26**(7-8)**,** 348-54.

Lu, C. H., Macdonald-Wallis, C., Gray, E., Pearce, N., Petzold, A., Norgren, N., Giovannoni, G., Fratta, P., Sidle, K., Fish, M., Orrell, R., Howard, R., Talbot, K., Greensmith, L., Kuhle, J., Turner, M. R. & Malaspina, A. (2015). Neurofilament light chain: A prognostic biomarker in amyotrophic lateral sclerosis. *Neurology.* **84**(22)**,** 2247-57.

Lunetta, C., Moglia, C., Lizio, A., Caponnetto, C., Dubbioso, R., Giannini, F., Mata, S., Mazzini, L., Sabatelli, M., Siciliano, G., Simone, I. L., Soraru, G., Toriello, A., Trojsi, F., Vedovello, M., D'Ovidio, F., Filippi, M., Calvo, A. & and, E. S. G. (2020). The Italian multicenter experience with edaravone in amyotrophic lateral sclerosis. *J Neurol.* **267**(11)**,** 3258-3267.

Mackenzie, I. R., et al. (2007). Pathological TDP-43 distinguishes sporadic amyotrophic lateral sclerosis from amyotrophic lateral sclerosis with SOD1 mutations. *Ann Neurol.* **61**(5)**,** 427-34.

Maeda, H., Fukuda, S., Kameda, H., Murabe, N., Isoo, N., Mizukami, H., Ozawa, K. & Sakurai, M. (2016). Corticospinal axons make direct synaptic connections with spinal motoneurons innervating forearm muscles early during postnatal development in the rat. *J Physiol.* **594**(1)**,** 189-205.

Mahler, J. F., Stokes, W., Mann, P. C., Takaoka, M. & Maronpot, R. R. (1996). Spontaneous lesions in aging FVB/N mice. *Toxicol Pathol.* **24**(6)**,** 710-6.

Mahoney, C. J., Beck, J., Rohrer, J. D., Lashley, T., Mok, K., Shakespeare, T., Yeatman, T., Warrington, E. K., Schott, J. M., Fox, N. C., Rossor, M. N., Hardy, J., Collinge, J., Revesz, T., Mead, S. & Warren, J. D. (2012). Frontotemporal dementia with the C9ORF72

hexanucleotide repeat expansion: clinical, neuroanatomical and neuropathological features. *Brain.* **135**(Pt 3)**,** 736-50.

Majounie, E., et al. (2012). Frequency of the C9orf72 hexanucleotide repeat expansion in patients with amyotrophic lateral sclerosis and frontotemporal dementia: a cross-sectional study. *Lancet Neurol.* **11**(4)**,** 323-30.

Mancuso, R., Santos-Nogueira, E., Osta, R. & Navarro, X. (2011). Electrophysiological analysis of a murine model of motoneuron disease. *Clin Neurophysiol.* **122**(8)**,** 1660-70.

Manning, J. & O'Malley, D. (2015). What has the mdx mouse model of Duchenne muscular dystrophy contributed to our understanding of this disease? *J Muscle Res Cell Motil.* **36**(2)**,** 155-67.

Marat, A. L., Dokainish, H. & McPherson, P. S. (2011). DENN domain proteins: regulators of Rab GTPases. *J Biol Chem.* **286**(16)**,** 13791-800.

Martin, E., Cazenave, W., Cattaert, D. & Branchereau, P. (2013). Embryonic alteration of motoneuronal morphology induces hyperexcitability in the mouse model of amyotrophic lateral sclerosis. *Neurobiol Dis.* **54**116-26.

Martin, L. J. (2008). DNA damage and repair: relevance to mechanisms of neurodegeneration. *J Neuropathol Exp Neurol.* **67**(5)**,** 377-87.

Mathys, H., Adaikkan, C., Gao, F., Young, J. Z., Manet, E., Hemberg, M., De Jager, P. L., Ransohoff, R. M., Regev, A. & Tsai, L. H. (2017). Temporal Tracking of Microglia Activation in Neurodegeneration at Single-Cell Resolution. *Cell Rep.* **21**(2)**,** 366-380.

Matsuo, N., Takao, K., Nakanishi, K., Yamasaki, N., Tanda, K. & Miyakawa, T. (2010). Behavioral profiles of three C57BL/6 substrains. *Front Behav Neurosci.* **4**29.

May, S., Hornburg, D., Schludi, M. H., Arzberger, T., Rentzsch, K., Schwenk, B. M., Grasser, F. A., Mori, K., Kremmer, E., Banzhaf-Strathmann, J., Mann, M., Meissner, F. & Edbauer, D. (2014). C9orf72 FTLD/ALS-associated Gly-Ala dipeptide repeat proteins cause neuronal toxicity and Unc119 sequestration. *Acta Neuropathol.* **128**(4)**,** 485-503.

McCauley, M. E., O'Rourke, J. G., Yanez, A., Markman, J. L., Ho, R., Wang, X., Chen, S., Lall, D., Jin, M., Muhammad, A., Bell, S., Landeros, J., Valencia, V., Harms, M., Arditi, M., Jefferies, C. & Baloh, R. H. (2020). C9orf72 in myeloid cells suppresses STING-induced inflammation. *Nature.* **585**(7823)**,** 96-101.

McCord, M. C., Lorenzana, A., Bloom, C. S., Chancer, Z. O. & Schauwecker, P. E. (2008). Effect of age on kainate-induced seizure severity and cell death. *Neuroscience.* **154**(3)**,** 1143-53.

McIlwain, K. L., Merriweather, M. Y., Yuva-Paylor, L. A. & Paylor, R. (2001). The use of behavioral test batteries: effects of training history. *Physiol Behav.* **73**(5)**,** 705-17.

Mead, R. J., Bennett, E. J., Kennerley, A. J., Sharp, P., Sunyach, C., Kasher, P., Berwick, J., Pettmann, B., Battaglia, G., Azzouz, M., Grierson, A. & Shaw, P. J. (2011). Optimised and rapid pre-clinical screening in the SOD1(G93A) transgenic mouse model of amyotrophic lateral sclerosis (ALS). *PLoS One.* **6**(8)**,** e23244.

Mead, R. J., Shan, N., Reiser, H. J., Marshall, F. & Shaw, P. J. (2022). Amyotrophic lateral sclerosis: a neurodegenerative disorder poised for successful therapeutic translation. *Nat Rev Drug Discov.* 10.1038/s41573-022-00612-21-28.

Mehta, P. R., Brown, A. L., Ward, M. E. & Fratta, P. (2023). The era of cryptic exons: implications for ALS-FTD. *Mol Neurodegener.* **18**(1)**,** 16.

Milanese, M., Bonifacino, T., Torazza, C., Provenzano, F., Kumar, M., Ravera, S., Zerbo, A. R., Frumento, G., Balbi, M., Nguyen, T. P. N., Bertola, N., Ferrando, S., Viale, M., Profumo, A. & Bonanno, G. (2021). Blocking glutamate mGlu(5) receptors with the negative

allosteric modulator CTEP improves disease course in SOD1(G93A) mouse model of amyotrophic lateral sclerosis. *Br J Pharmacol.* **178**(18)**,** 3747-3764.

Miller, T. M., et al. (2022). Trial of Antisense Oligonucleotide Tofersen for SOD1 ALS. *N Engl J Med.* **387**(12)**,** 1099-1110.

Mineur, Y. S. & Crusio, W. E. (2002). Behavioral and neuroanatomical characterization of FVB/N inbred mice. *Brain Res Bull.* **57**(1)**,** 41-7.

Mitchell, J. C., McGoldrick, P., Vance, C., Hortobagyi, T., Sreedharan, J., Rogelj, B., Tudor, E. L., Smith, B. N., Klasen, C., Miller, C. C., Cooper, J. D., Greensmith, L. & Shaw, C. E. (2013). Overexpression of human wild-type FUS causes progressive motor neuron degeneration in an age- and dose-dependent fashion. *Acta Neuropathol.* **125**(2)**,** 273-88.

Mitchell, J. D., Callagher, P., Gardham, J., Mitchell, C., Dixon, M., Addison-Jones, R., Bennett, W. & O'Brien, M. R. (2010). Timelines in the diagnostic evaluation of people with suspected amyotrophic lateral sclerosis (ALS)/motor neuron disease (MND)--a 20-year review: can we do better? *Amyotroph Lateral Scler.* **11**(6)**,** 537-41.

Mitra, J., Guerrero, E. N., Hegde, P. M., Liachko, N. F., Wang, H., Vasquez, V., Gao, J., Pandey, A., Taylor, J. P., Kraemer, B. C., Wu, P., Boldogh, I., Garruto, R. M., Mitra, S., Rao, K. S. & Hegde, M. L. (2019). Motor neuron disease-associated loss of nuclear TDP-43 is linked to DNA double-strand break repair defects. *Proc Natl Acad Sci U S A.* **116**(10)**,** 4696-4705.

Mizielinska, S., et al. (2014). C9orf72 repeat expansions cause neurodegeneration in Drosophila through arginine-rich proteins. *Science.* **345**(6201)**,** 1192-1194.

Mizielinska, S., Lashley, T., Norona, F. E., Clayton, E. L., Ridler, C. E., Fratta, P. & Isaacs, A. M. (2013). C9orf72 frontotemporal lobar degeneration is characterised by frequent neuronal sense and antisense RNA foci. *Acta Neuropathol.* **126**(6)**,** 845-57.

Moens, T. G., Mizielinska, S., Niccoli, T., Mitchell, J. S., Thoeng, A., Ridler, C. E., Gronke, S., Esser, J., Heslegrave, A., Zetterberg, H., Partridge, L. & Isaacs, A. M. (2018). Sense and antisense RNA are not toxic in Drosophila models of C9orf72-associated ALS/FTD. *Acta Neuropathol.* **135**(3)**,** 445-457.

Mordes, D. A., Morrison, B. M., Ament, X. H., Cantrell, C., Mok, J., Eggan, P., Xue, C., Wang, J. Y., Eggan, K. & Rothstein, J. D. (2020). Absence of Survival and Motor Deficits in 500 Repeat C9ORF72 BAC Mice. *Neuron.* **108**(4)**,** 775-783 e4.

Mullard, A. (2022). Amylyx's ALS therapy secures FDA approval, as regulatory flexibility trumps underwhelming data. *Nat Rev Drug Discov.* **21**(11)**,** 786.

Neumann, M., Sampathu, D. M., Kwong, L. K., Truax, A. C., Micsenyi, M. C., Chou, T. T., Bruce, J., Schuck, T., Grossman, M., Clark, C. M., McCluskey, L. F., Miller, B. L., Masliah, E., Mackenzie, I. R., Feldman, H., Feiden, W., Kretzschmar, H. A., Trojanowski, J. Q. & Lee, V. M. (2006). Ubiquitinated TDP-43 in frontotemporal lobar degeneration and amyotrophic lateral sclerosis. *Science.* **314**(5796)**,** 130-3.

Neuwirth, C., Barkhaus, P. E., Burkhardt, C., Castro, J., Czell, D., de Carvalho, M., Nandedkar, S., Stalberg, E. & Weber, M. (2015). Tracking motor neuron loss in a set of six muscles in amyotrophic lateral sclerosis using the Motor Unit Number Index (MUNIX): a 15-month longitudinal multicentre trial. *J Neurol Neurosurg Psychiatry.* **86**(11)**,** 1172-9.

Nguyen, H. P., Van Broeckhoven, C. & van der Zee, J. (2018). ALS Genes in the Genomic Era and their Implications for FTD. *Trends Genet.* **34**(6)**,** 404-423.

Nguyen, L., Laboissonniere, L. A., Guo, S., Pilotto, F., Scheidegger, O., Oestmann, A., Hammond, J. W., Li, H., Hyysalo, A., Peltola, R., Pattamatta, A., Zu, T., Voutilainen, M.

H., Gelbard, H. A., Saxena, S. & Ranum, L. P. W. (2020a). Survival and Motor Phenotypes in FVB C9-500 ALS/FTD BAC Transgenic Mice Reproduced by Multiple Labs. *Neuron.* **108**(4)**,** 784-796 e3.

Nguyen, L., et al. (2020b). Antibody Therapy Targeting RAN Proteins Rescues C9 ALS/FTD Phenotypes in C9orf72 Mouse Model. *Neuron.* **105**(4)**,** 645-662 e11.

Nordin, A., Akimoto, C., Wuolikainen, A., Alstermark, H., Jonsson, P., Birve, A., Marklund, S. L., Graffmo, K. S., Forsberg, K., Brannstrom, T. & Andersen, P. M. (2015). Extensive size variability of the GGGGCC expansion in C9orf72 in both neuronal and non-neuronal tissues in 18 patients with ALS or FTD. *Hum Mol Genet.* **24**(11)**,** 3133-42.

Novak, J., Bailoo, J. D., Melotti, L. & Wurbel, H. (2016). Effect of Cage-Induced Stereotypies on Measures of Affective State and Recurrent Perseveration in CD-1 and C57BL/6 Mice. *PLoS One.* **11**(5)**,** e0153203.

O'Rourke, J. G., et al. (2015). C9orf72 BAC Transgenic Mice Display Typical Pathologic Features of ALS/FTD. *Neuron.* **88**(5)**,** 892-901.

O'Rourke, J. G., Bogdanik, L., Yanez, A., Lall, D., Wolf, A. J., Muhammad, A. K., Ho, R., Carmona, S., Vit, J. P., Zarrow, J., Kim, K. J., Bell, S., Harms, M. B., Miller, T. M., Dangler, C. A., Underhill, D. M., Goodridge, H. S., Lutz, C. M. & Baloh, R. H. (2016). C9orf72 is required for proper macrophage and microglial function in mice. *Science.* **351**(6279)**,** 1324-9.

Owen, E. H., Logue, S. F., Rasmussen, D. L. & Wehner, J. M. (1997). Assessment of learning by the Morris water task and fear conditioning in inbred mouse strains and F1 hybrids: implications of genetic background for single gene mutations and quantitative trait loci analyses. *Neuroscience.* **80**(4)**,** 1087-99.

Paganoni, S., et al. (2021). Long-term survival of participants in the CENTAUR trial of sodium phenylbutyrate-taurursodiol in amyotrophic lateral sclerosis. *Muscle Nerve.* **63**(1)**,** 31-39.

Peters, O. M., et al. (2015). Human C9ORF72 Hexanucleotide Expansion Reproduces RNA Foci and Dipeptide Repeat Proteins but Not Neurodegeneration in BAC Transgenic Mice. *Neuron.* **88**(5)**,** 902-909.

Phukan, J., Elamin, M., Bede, P., Jordan, N., Gallagher, L., Byrne, S., Lynch, C., Pender, N. & Hardiman, O. (2012). The syndrome of cognitive impairment in amyotrophic lateral sclerosis: a population-based study. *J Neurol Neurosurg Psychiatry.* **83**(1)**,** 102-8.

Piguet, O., Hornberger, M., Mioshi, E. & Hodges, J. R. (2011). Behavioural-variant frontotemporal dementia: diagnosis, clinical staging, and management. *Lancet Neurol.* **10**(2)**,** 162-72.

Pond, H. L., Heller, A. T., Gural, B. M., McKissick, O. P., Wilkinson, M. K. & Manzini, M. C. (2021). Digging behavior discrimination test to probe burrowing and exploratory digging in male and female mice. *J Neurosci Res.* **99**(9)**,** 2046-2058.

Pugh, P. L., Ahmed, S. F., Smith, M. I., Upton, N. & Hunter, A. J. (2004). A behavioural characterisation of the FVB/N mouse strain. *Behav Brain Res.* **155**(2)**,** 283-9.

Ramos, A. (2008). Animal models of anxiety: do I need multiple tests? *Trends Pharmacol Sci.* **29**(10)**,** 493-8.

Ranganathan, R., Haque, S., Coley, K., Shepheard, S., Cooper-Knock, J. & Kirby, J. (2020). Multifaceted Genes in Amyotrophic Lateral Sclerosis-Frontotemporal Dementia. *Front Neurosci.* **14**684.

Rascovsky, K., et al. (2011). Sensitivity of revised diagnostic criteria for the behavioural variant of frontotemporal dementia. *Brain.* **134**(Pt 9)**,** 2456-77.

Regal, L., Vanopdenbosch, L., Tilkin, P., Van den Bosch, L., Thijs, V., Sciot, R. & Robberecht, W. (2006). The G93C mutation in superoxide dismutase 1: clinicopathologic phenotype and prognosis. *Arch Neurol.* **63**(2)**,** 262-7.

Renton, A. E., Chio, A. & Traynor, B. J. (2014). State of play in amyotrophic lateral sclerosis genetics. *Nat Neurosci.* **17**(1)**,** 17-23.

Renton, A. E., et al. (2011). A hexanucleotide repeat expansion in C9ORF72 is the cause of chromosome 9p21-linked ALS-FTD. *Neuron.* **72**(2)**,** 257-68.

Ricketts, T., McGoldrick, P., Fratta, P., de Oliveira, H. M., Kent, R., Phatak, V., Brandner, S., Blanco, G., Greensmith, L., Acevedo-Arozena, A. & Fisher, E. M. (2014). A nonsense mutation in mouse Tardbp affects TDP43 alternative splicing activity and causes limb-clasping and body tone defects. *PLoS One.* **9**(1)**,** e85962.

Riemslagh, F. W., van der Toorn, E. C., Verhagen, R. F. M., Maas, A., Bosman, L. W. J., Hukema, R. K. & Willemsen, R. (2021). Inducible expression of human C9ORF72 36x G(4)C(2) hexanucleotide repeats is sufficient to cause RAN translation and rapid muscular atrophy in mice. *Dis Model Mech.* **14**(2).

Rosen, D. R., Siddique, T., Patterson, D., Figlewicz, D. A., Sapp, P., Hentati, A., Donaldson, D., Goto, J., O'Regan, J. P., Deng, H. X. & et al. (1993). Mutations in Cu/Zn superoxide dismutase gene are associated with familial amyotrophic lateral sclerosis. *Nature.* **362**(6415)**,** 59-62.

Rosenfeld, J. & Strong, M. J. (2015). Challenges in the Understanding and Treatment of Amyotrophic Lateral Sclerosis/Motor Neuron Disease. *Neurotherapeutics.* **12**(2)**,** 317-25.

Royle, S. J., Collins, F. C., Rupniak, H. T., Barnes, J. C. & Anderson, R. (1999). Behavioural analysis and susceptibility to CNS injury of four inbred strains of mice. *Brain Res.* **816**(2)**,** 337-49.

Ryan, M., Heverin, M., McLaughlin, R. L. & Hardiman, O. (2019). Lifetime Risk and Heritability of Amyotrophic Lateral Sclerosis. *JAMA Neurol.* **76**(11)**,** 1367-1374.

Saba, L., Viscomi, M. T., Caioli, S., Pignataro, A., Bisicchia, E., Pieri, M., Molinari, M., Ammassari-Teule, M. & Zona, C. (2016). Altered Functionality, Morphology, and Vesicular Glutamate Transporter Expression of Cortical Motor Neurons from a Presymptomatic Mouse Model of Amyotrophic Lateral Sclerosis. *Cereb Cortex.* **26**(4)**,** 1512-28.

Sano, F., Shigetomi, E., Shinozaki, Y., Tsuzukiyama, H., Saito, K., Mikoshiba, K., Horiuchi, H., Cheung, D. L., Nabekura, J., Sugita, K., Aihara, M. & Koizumi, S. (2021). Reactive astrocyte-driven epileptogenesis is induced by microglia initially activated following status epilepticus. *JCI Insight.* **6**(9).

Sare, R. M., Lemons, A. & Smith, C. B. (2021). Behavior Testing in Rodents: Highlighting Potential Confounds Affecting Variability and Reproducibility. *Brain Sci.* **11**(4).

Schipper, L. J., Raaphorst, J., Aronica, E., Baas, F., de Haan, R., de Visser, M. & Troost, D. (2016). Prevalence of brain and spinal cord inclusions, including dipeptide repeat proteins, in patients with the C9ORF72 hexanucleotide repeat expansion: a systematic neuropathological review. *Neuropathol Appl Neurobiol.* **42**(6)**,** 547-60.

Sellier, C., Campanari, M. L., Julie Corbier, C., Gaucherot, A., Kolb-Cheynel, I., Oulad-Abdelghani, M., Ruffenach, F., Page, A., Ciura, S., Kabashi, E. & Charlet-Berguerand, N. (2016). Loss of C9ORF72 impairs autophagy and synergizes with polyQ Ataxin-2 to induce motor neuron dysfunction and cell death. *EMBO J.* **35**(12)**,** 1276-97.

Shao, Q., Liang, C., Chang, Q., Zhang, W., Yang, M. & Chen, J. F. (2019). C9orf72 deficiency promotes motor deficits of a C9ALS/FTD mouse model in a dose-dependent manner. *Acta Neuropathol Commun.* **7**(1)**,** 32.

Sharpe, J. L., Harper, N. S., Garner, D. R. & West, R. J. H. (2021). Modeling C9orf72-Related Frontotemporal Dementia and Amyotrophic Lateral Sclerosis in Drosophila. *Front Cell Neurosci.* **15**770937.

Shaw, M. P., Higginbottom, A., McGown, A., Castelli, L. M., James, E., Hautbergue, G. M., Shaw, P. J. & Ramesh, T. M. (2018). Stable transgenic C9orf72 zebrafish model key aspects of the ALS/FTD phenotype and reveal novel pathological features. *Acta Neuropathol Commun.* **6**(1)**,** 125.

Shefner, J. M., et al. (2020). A proposal for new diagnostic criteria for ALS. *Clin Neurophysiol.* **131**(8)**,** 1975-1978.

Shoji, H., Takao, K., Hattori, S. & Miyakawa, T. (2016). Age-related changes in behavior in C57BL/6J mice from young adulthood to middle age. *Mol Brain.* **9**11.

Silva-Fernandes, A., Oliveira, P., Sousa, N. & Maciel, P. (2010). Motor and Behavioural Abnormalities Associated with Persistent Spontaneous Epilepsy in the fvb/n Mouse Strain. *Scand. J. Lab. Anim. Sci.* **37**(3).

Simon, M. M., et al. (2013). A comparative phenotypic and genomic analysis of C57BL/6J and C57BL/6N mouse strains. *Genome Biol.* **14**(7)**,** R82.

Smith, T. W., Tyler, H. R. & Schoene, W. C. (1975). Atypical astrocytes and Rosenthal fibers in a case of amyotrophic lateral sclerosis associated with a cerebral glioblastoma multiforme. *Acta Neuropathol.* **31**(1)**,** 29-34.

Snowden, J. S., Rollinson, S., Thompson, J. C., Harris, J. M., Stopford, C. L., Richardson, A. M., Jones, M., Gerhard, A., Davidson, Y. S., Robinson, A., Gibbons, L., Hu, Q., DuPlessis, D., Neary, D., Mann, D. M. & Pickering-Brown, S. M. (2012). Distinct clinical and pathological characteristics of frontotemporal dementia associated with C9ORF72 mutations. *Brain.* **135**(Pt 3)**,** 693-708.

Sreedharan, J., Blair, I. P., Tripathi, V. B., Hu, X., Vance, C., Rogelj, B., Ackerley, S., Durnall, J. C., Williams, K. L., Buratti, E., Baralle, F., de Belleroche, J., Mitchell, J. D., Leigh, P. N., Al-Chalabi, A., Miller, C. C., Nicholson, G. & Shaw, C. E. (2008). TDP-43 mutations in familial and sporadic amyotrophic lateral sclerosis. *Science.* **319**(5870)**,** 1668-72.

Stallings, N. R., Puttaparthi, K., Luther, C. M., Burns, D. K. & Elliott, J. L. (2010). Progressive motor weakness in transgenic mice expressing human TDP-43. *Neurobiol Dis.* **40**(2)**,** 404-14.

Stoklund Dittau, K. & Van Den Bosch, L. (2023). Why should we care about astrocytes in a motor neuron disease? *Frontiers in Molecular Medicine.* **3**.

Sudria-Lopez, E., Koppers, M., de Wit, M., van der Meer, C., Westeneng, H. J., Zundel, C. A., Youssef, S. A., Harkema, L., de Bruin, A., Veldink, J. H., van den Berg, L. H. & Pasterkamp, R. J. (2016). Full ablation of C9orf72 in mice causes immune system-related pathology and neoplastic events but no motor neuron defects. *Acta Neuropathol.* **132**(1)**,** 145-7.

Sullivan, P. M., Zhou, X., Robins, A. M., Paushter, D. H., Kim, D., Smolka, M. B. & Hu, F. (2016). The ALS/FTLD associated protein C9orf72 associates with SMCR8 and WDR41 to regulate the autophagy-lysosome pathway. *Acta Neuropathol Commun.* **4**(1)**,** 51.

Sun, X. S., Liu, W. X., Chen, Z. H., Ling, L., Yang, F., Wang, H. F., Cui, F. & Huang, X. S. (2018). Repetitive Nerve Stimulation in Amyotrophic Lateral Sclerosis. *Chin Med J (Engl).* **131**(18)**,** 2146-2151.

Sunyach, C., Michaud, M., Arnoux, T., Bernard-Marissal, N., Aebischer, J., Latyszenok, V., Gouarne, C., Raoul, C., Pruss, R. M., Bordet, T. & Pettmann, B. (2012). Olesoxime delays muscle denervation, astrogliosis, microglial activation and motoneuron death in an ALS mouse model. *Neuropharmacology.* **62**(7)**,** 2346-52.

Swaminathan, A., Bouffard, M., Liao, M., Ryan, S., Callister, J. B., Pickering-Brown, S. M., Armstrong, G. A. B. & Drapeau, P. (2018). Expression of C9orf72-related dipeptides impairs motor function in a vertebrate model. *Hum Mol Genet.* **27**(10)**,** 1754-1762.

Takahashi, A., Kato, K., Makino, J., Shiroishi, T. & Koide, T. (2006). Multivariate analysis of temporal descriptions of open-field behavior in wild-derived mouse strains. *Behav Genet.* **36**(5)**,** 763-74.

Taketo, M., Schroeder, A. C., Mobraaten, L. E., Gunning, K. B., Hanten, G., Fox, R. R., Roderick, T. H., Stewart, C. L., Lilly, F., Hansen, C. T. & et al. (1991). FVB/N: an inbred mouse strain preferable for transgenic analyses. *Proc Natl Acad Sci U S A.* **88**(6)**,** 2065-9.

Temme, S. J., Bell, R. Z., Pahumi, R. & Murphy, G. G. (2014). Comparison of inbred mouse substrains reveals segregation of maladaptive fear phenotypes. *Front Behav Neurosci.* **8**282.

Therrien, M., Rouleau, G. A., Dion, P. A. & Parker, J. A. (2013). Deletion of C9ORF72 results in motor neuron degeneration and stress sensitivity in C. elegans. *PLoS One.* **8**(12)**,** e83450.

Thomas, A., Burant, A., Bui, N., Graham, D., Yuva-Paylor, L. A. & Paylor, R. (2009). Marble burying reflects a repetitive and perseverative behavior more than novelty-induced anxiety. *Psychopharmacology (Berl).* **204**(2)**,** 361-73.

Turner, M. R., Bowser, R., Bruijn, L., Dupuis, L., Ludolph, A., McGrath, M., Manfredi, G., Maragakis, N., Miller, R. G., Pullman, S. L., Rutkove, S. B., Shaw, P. J., Shefner, J. & Fischbeck, K. H. (2013). Mechanisms, models and biomarkers in amyotrophic lateral sclerosis. *Amyotroph Lateral Scler Frontotemporal Degener.* **14 Suppl 1**19-32.

Uchimura, A., Higuchi, M., Minakuchi, Y., Ohno, M., Toyoda, A., Fujiyama, A., Miura, I., Wakana, S., Nishino, J. & Yagi, T. (2015). Germline mutation rates and the long-term phenotypic effects of mutation accumulation in wild-type laboratory mice and mutator mice. *Genome Res.* **25**(8)**,** 1125-34.

Udaka, F., Kameyama, M. & Tomonaga, M. (1986). Degeneration of Betz cells in motor neuron disease. A Golgi study. *Acta Neuropathol.* **70**(3-4)**,** 289-95.

Valdez, G., Tapia, J. C., Lichtman, J. W., Fox, M. A. & Sanes, J. R. (2012). Shared resistance to aging and ALS in neuromuscular junctions of specific muscles. *PLoS One.* **7**(4)**,** e34640.

van Blitterswijk, M., et al. (2013). Association between repeat sizes and clinical and pathological characteristics in carriers of C9ORF72 repeat expansions (Xpansize-72): a cross-sectional cohort study. *Lancet Neurol.* **12**(10)**,** 978-88.

Van Erum, J., Van Dam, D. & De Deyn, P. P. (2019). PTZ-induced seizures in mice require a revised Racine scale. *Epilepsy Behav.* **95**51-55.

Van Raamsdonk, J. M., Metzler, M., Slow, E., Pearson, J., Schwab, C., Carroll, J., Graham, R. K., Leavitt, B. R. & Hayden, M. R. (2007). Phenotypic abnormalities in the YAC128 mouse model of Huntington disease are penetrant on multiple genetic backgrounds and modulated by strain. *Neurobiol Dis.* **26**(1)**,** 189-200.

van Zundert, B., Peuscher, M. H., Hynynen, M., Chen, A., Neve, R. L., Brown, R. H., Jr., Constantine-Paton, M. & Bellingham, M. C. (2008). Neonatal neuronal circuitry shows hyperexcitable disturbance in a mouse model of the adult-onset neurodegenerative disease amyotrophic lateral sclerosis. *J Neurosci.* **28**(43)**,** 10864-74.

Vargas, M. R. & Johnson, J. A. (2010). Astrogliosis in amyotrophic lateral sclerosis: role and therapeutic potential of astrocytes. *Neurotherapeutics.* **7**(4)**,** 471-81.

Voikar, V., Koks, S., Vasar, E. & Rauvala, H. (2001). Strain and gender differences in the behavior of mouse lines commonly used in transgenic studies. *Physiol Behav.* **72**(1-2)**,** 271-81.

Vucic, S., Ziemann, U., Eisen, A., Hallett, M. & Kiernan, M. C. (2013). Transcranial magnetic stimulation and amyotrophic lateral sclerosis: pathophysiological insights. *J Neurol Neurosurg Psychiatry.* **84**(10)**,** 1161-70.

Wang, J., Ho, W. Y., Lim, K., Feng, J., Tucker-Kellogg, G., Nave, K. A. & Ling, S. C. (2018). Cell-autonomous requirement of TDP-43, an ALS/FTD signature protein, for oligodendrocyte survival and myelination. *Proc Natl Acad Sci U S A.* **115**(46)**,** E10941-E10950.

Warmus, B. A., Sekar, D. R., McCutchen, E., Schellenberg, G. D., Roberts, R. C., McMahon, L. L. & Roberson, E. D. (2014). Tau-mediated NMDA receptor impairment underlies dysfunction of a selectively vulnerable network in a mouse model of frontotemporal dementia. *J Neurosci.* **34**(49)**,** 16482-95.

Webster, C. P., Smith, E. F., Bauer, C. S., Moller, A., Hautbergue, G. M., Ferraiuolo, L., Myszczynska, M. A., Higginbottom, A., Walsh, M. J., Whitworth, A. J., Kaspar, B. K., Meyer, K., Shaw, P. J., Grierson, A. J. & De Vos, K. J. (2016). The C9orf72 protein interacts with Rab1a and the ULK1 complex to regulate initiation of autophagy. *EMBO J.* **35**(15)**,** 1656-76.

Wen, X., Tan, W., Westergard, T., Krishnamurthy, K., Markandaiah, S. S., Shi, Y., Lin, S., Shneider, N. A., Monaghan, J., Pandey, U. B., Pasinelli, P., Ichida, J. K. & Trotti, D. (2014). Antisense proline-arginine RAN dipeptides linked to C9ORF72-ALS/FTD form toxic nuclear aggregates that initiate in vitro and in vivo neuronal death. *Neuron.* **84**(6)**,** 1213-25.

West, R. J., Elliott, C. J. & Wade, A. R. (2015). Classification of Parkinson's Disease Genotypes in Drosophila Using Spatiotemporal Profiling of Vision. *Sci Rep.* **5**16933.

West, R. J. H., Sharpe, J. L., Voelzmann, A., Munro, A. L., Hahn, I., Baines, R. A. & Pickering-Brown, S. (2020). Co-expression of C9orf72 related dipeptide-repeats over 1000 repeat units reveals age- and combination-specific phenotypic profiles in Drosophila. *Acta Neuropathol Commun.* **8**(1)**,** 158.

Westin, J. E., Janssen, M. L., Sager, T. N. & Temel, Y. (2012). Automated gait analysis in bilateral parkinsonian rats and the role of L-DOPA therapy. *Behav Brain Res.* **226**(2)**,** 519-28.

White, M. A., et al. (2018). TDP-43 gains function due to perturbed autoregulation in a Tardbp knock-in mouse model of ALS-FTD. *Nat Neurosci.* **21**(4)**,** 552-563.

Whitwell, J. L., Weigand, S. D., Boeve, B. F., Senjem, M. L., Gunter, J. L., DeJesus-Hernandez, M., Rutherford, N. J., Baker, M., Knopman, D. S., Wszolek, Z. K., Parisi, J. E., Dickson, D. W., Petersen, R. C., Rademakers, R., Jack, C. R., Jr. & Josephs, K. A. (2012). Neuroimaging signatures of frontotemporal dementia genetics: C9ORF72, tau, progranulin and sporadics. *Brain.* **135**(Pt 3)**,** 794-806.

Wijesekera, L. C. & Leigh, P. N. (2009). Amyotrophic lateral sclerosis. *Orphanet J Rare Dis.* **4**3.

Wilson, M. D., Sethi, S., Lein, P. J. & Keil, K. P. (2017). Valid statistical approaches for analyzing sholl data: Mixed effects versus simple linear models. *J Neurosci Methods.* **279**33-43.

Witzel, S., et al. (2022). Safety and Effectiveness of Long-term Intravenous Administration of Edaravone for Treatment of Patients With Amyotrophic Lateral Sclerosis. *JAMA Neurol.* **79**(2)**,** 121-130.

Wooley, C. M., Sher, R. B., Kale, A., Frankel, W. N., Cox, G. A. & Seburn, K. L. (2005). Gait analysis detects early changes in transgenic SOD1(G93A) mice. *Muscle Nerve.* **32**(1)**,** 43-50.

Writing Group & Edaravone, A. L. S. S. G. (2017). Safety and efficacy of edaravone in well defined patients with amyotrophic lateral sclerosis: a randomised, double-blind, placebo-controlled trial. *Lancet Neurol.* **16**(7)**,** 505-512.

Wurbel, H. (2000). Behaviour and the standardization fallacy. *Nat Genet.* **26**(3)**,** 263.

Xi, Z., et al. (2015). Jump from pre-mutation to pathologic expansion in C9orf72. *Am J Hum Genet.* **96**(6)**,** 962-70.

Xu, L., Liu, T., Liu, L., Yao, X., Chen, L., Fan, D., Zhan, S. & Wang, S. (2020). Global variation in prevalence and incidence of amyotrophic lateral sclerosis: a systematic review and meta-analysis. *J Neurol.* **267**(4)**,** 944-953.

Xu, Z., Poidevin, M., Li, X., Li, Y., Shu, L., Nelson, D. L., Li, H., Hales, C. M., Gearing, M., Wingo, T. S. & Jin, P. (2013). Expanded GGGGCC repeat RNA associated with amyotrophic lateral sclerosis and frontotemporal dementia causes neurodegeneration. *Proc Natl Acad Sci U S A.* **110**(19)**,** 7778-83.

Yuan, R., Tsaih, S. W., Petkova, S. B., Marin de Evsikova, C., Xing, S., Marion, M. A., Bogue, M. A., Mills, K. D., Peters, L. L., Bult, C. J., Rosen, C. J., Sundberg, J. P., Harrison, D. E., Churchill, G. A. & Paigen, B. (2009). Aging in inbred strains of mice: study design and interim report on median lifespans and circulating IGF1 levels. *Aging Cell.* **8**(3)**,** 277-87.

Zhang, K., et al. (2015). The C9orf72 repeat expansion disrupts nucleocytoplasmic transport. *Nature.* **525**(7567)**,** 56-61.

Zhang, Y. J., et al. (2016). C9ORF72 poly(GA) aggregates sequester and impair HR23 and nucleocytoplasmic transport proteins. *Nat Neurosci.* **19**(5)**,** 668-677.

Zhang, Y. J., et al. (2014). Aggregation-prone c9FTD/ALS poly(GA) RAN-translated proteins cause neurotoxicity by inducing ER stress. *Acta Neuropathol.* **128**(4)**,** 505-24.

Zheng, X., Wang, S., Huang, J., Lin, J., Yang, T., Xiao, Y., Jiang, Q., Huang, R., Li, C. & Shang, H. (2023). Physical activity as risk factor in amyotrophic lateral sclerosis: a systematic review and meta-analysis. *J Neurol.* 10.1007/s00415-022-11555-4.

Zhou, H., Huang, C., Chen, H., Wang, D., Landel, C. P., Xia, P. Y., Bowser, R., Liu, Y. J. & Xia, X. G. (2010). Transgenic rat model of neurodegeneration caused by mutation in the TDP gene. *PLoS Genet.* **6**(3)**,** e1000887.

Zhu, Q., Jiang, J., Gendron, T. F., McAlonis-Downes, M., Jiang, L., Taylor, A., Diaz Garcia, S., Ghosh Dastidar, S., Rodriguez, M. J., King, P., Zhang, Y., La Spada, A. R., Xu, H., Petrucelli, L., Ravits, J., Da Cruz, S., Lagier-Tourenne, C. & Cleveland, D. W. (2020). Reduced C9ORF72 function exacerbates gain of toxicity from ALS/FTD-causing repeat expansion in C9orf72. *Nat Neurosci.* **23**(5)**,** 615-624.

Zou, Z. Y., Zhou, Z. R., Che, C. H., Liu, C. Y., He, R. L. & Huang, H. P. (2017). Genetic epidemiology of amyotrophic lateral sclerosis: a systematic review and meta-analysis. *J Neurol Neurosurg Psychiatry.* **88**(7)**,** 540-549.

Zurita, E., Chagoyen, M., Cantero, M., Alonso, R., Gonzalez-Neira, A., Lopez-Jimenez, A., Lopez-Moreno, J. A., Landel, C. P., Benitez, J., Pazos, F. & Montoliu, L. (2011). Genetic polymorphisms among C57BL/6 mouse inbred strains. *Transgenic Res.* **20**(3)**,** 481-9.